Dissertation ETH Nr. 17967

A New Method for Evaluating Two-Loop Feynman Integrals and its Application To Higgs Production

A dissertation submitted to the

Swiss Federal Institute of Technology Zürich

for the degree of

Dr. Sc. ETH Zürich

presented by

Stefan Beerli

Dipl.-Phys. ETH

born February 11th, 1977

citizen of Bischofszell, TG

Switzerland

accepted on the recommendation of

Prof. Z. Kunszt	examiner
Prof. Ch. Anastasiou	co-examiner
Prof. F. Petriello	co-examiner

–2008–

Pro Vendulku utěšitelku.

Contents

Abstract

A complete set of master integrals for describing the gluon fusion process $gg \to h$ at two-loop order in the Standard Model, SM, is identified. All master integrals are computed as Laurent series in the dimensional regularization parameter ϵ in terms of harmonic polylogarithms. The $gg \to h$ amplitude in the SM is reduced to the master integrals, leading to a closed analytic formula for the amplitude, which is in agreement with the known result.

The reduction procedure is repeated for the SM-like amplitude, where a heavy scalar instead of the quark is running in the loops. This yields a new result.

The complete set of master integrals also allows automated computation of $gg \to h$ contributions in any extension of the SM, as long as only a single mass parameter occurs in the loops, as well as other processes with similar kinematics.

Then it is shown how to use the technique of contour deformation for handling thresholds within the framework of sector decomposition. This leads to the first known numerical method capable of evaluating in principle arbitrary tensor Feynman diagrams with UV, IR and threshold singularities in arbitrary kinematic regions.

The power of this method is demonstrated by computing the full virtual supersymmetric QCD amplitude for $gg \to h, H$ at two-loop order in the Minimal Supersymmetric Standard Model, MSSM. This includes two-loop diagrams containing up to five different kinematic invariants, which are clearly beyond the scope of any known analytic technique. The integration succeeds even in the numerically challenging case, where the kinematic invariants have extremely disparate values, reaching ratios of 10^4.

It is reasonable to assume, that the numerical method presented is capable of evaluating the two-loop $gg \to h$ amplitude in any conceivable extension of the SM. It thus eliminates the awkward situation, that the important NLO QCD corrections to the basic LHC process $gg \to h$ were not computable in viable extensions of the SM, like the MSSM.

The method is clearly not limited to $2 \to 1$ kinematics and yields a flexible tool for checking analytic results as well as for direct numerical computations in perturbative quantum field theory.

Zusammenfassung

Es wird ein vollständiger Satz von Masterintegralen für den Gluon-Fusionsprozess $gg \to h$ in der Zweischleifennäherung im Standard Modell, SM, identifiziert. Alle Masterintegrale werden als Laurentreihen im dimensionellen Regularisierungsparameter ϵ berechnet und durch harmonische Polylogarithmen ausgedrückt. Die $gg \to h$ Amplitude im SM wird auf Masterintegrale reduziert. Auf diese Weise wird ein geschlossener analytischer Ausdruck für die Amplitude gewonnen, welcher mit dem bekannten Resultat übereinstimmt.

Die Reduktionsprozedur wird wiederholt für den SM-ähnlichen Beitrag, in welchem die Schleifenkorrektur nicht von einem Quark, sondern von einem schweren Skalarteilchen herrührt. Dies führt zu einem neuen Resultat.

Der vollständige Satz von Masterintegralen ermöglicht auch die automatisierte Berechnung von $gg \to h$ Beiträgen in beliebigen Erweiterungen des SM, sofern jeweils nur ein einziger Massenparameter in den Schleifen erscheint. Auch andere Prozesse mit ähnlicher Kinematik können auf gleiche Weise behandelt werden.

Danach wird eine Möglichkeit aufgezeigt, wie die Technik des deformierten Integrationswegs zum Behandeln von Thresholds im Rahmen der Sektorzerlegungstechnik verwendet werden kann. Dies liefert erstmals eine numerische Methode, welche im Prinzip die Integration von beliebigen Tensor-Feynmandiagrammen mit UV-, IR- und Thresholdsingularitäten in beliebigen kinematischen Gebieten erlaubt.

Das Potential dieser Methode wird durch die Berechnung der vollständigen, virtuellen, supersymmetrischen QCD Amplitude für den Prozess $gg \to h, H$ in der Zweischleifennäherung im Minimalen Sypersymmetrischen Standardmodell, MSSM, veranschaulicht. Dies beinhaltet die Auswertung von Diagrammen, welche von bis zu fünf verschiedenen kinematischen Invarianten abhängen. Die Integration gelingt auch im numerisch problematischen Fall, wo die kinematischen Invarianten extrem unterschiedliche Werte annehmen. Verhältnisse bis zu 10^4 wurden erfolgreich getestet.

Die beschriebene numerische Methode kann allem Anschein nach dazu benutzt werden, die Zweischleifenkorrektur zur $gg \to h$ Amplitude in jeder denkbaren Erweiterung des SM zu berechnen. Sie bietet daher einen Ausweg aus der unhaltbaren Situation, dass die wichtige QCD Korrektur der ersten Ordnung (next-to-leading order) zum fundamentalen LHC Prozess $gg \to h$ nicht in allen realistischen Erweiterungen des SM, etwa dem MSSM, berechenbar war.

Die Anwendbarkeit der beschriebenen Methode beschränkt sich keinesfalls auf $2 \to 1$ Prozesse. Sie stellt daher ein flexibles Werkzeug dar, das sowohl zur Überprüfung analytischer Resultate, wie auch für direkte numerische Berechnungen im Rahmen der störungstheoretischen Quantenfeldtheorie benutzt werden kann.

Chapter 1

Introduction

Coulomb determined the electric force law measuring the repulsion between two charged balls. Cavendish measured the gravitational force between two lead weights. In the microscopic world of elementary particles there is no such direct way of probing interactions. Information can only be collected from indirect evidence, mainly from scattering experiments. Determining the interaction laws becomes a much harder task under these circumstances. The classical scattering experiment is the Rutherford experiment, measuring the deflection of alpha particles fired at a very thin gold foil. The large deflection angles observed for a small fraction of particles could not be explained by the "plum pudding model" of the atom, assuming that the positive charge is smeared out over the whole atom. Rutherford concluded, that the charge has to be localized in a very small volume.

In the 1920 successful field theoretical descriptions of the known interactions existed. Maxwell's theory of electromagnetism and Einstein's theory of general relativity. When quantum mechanics was born, the question arose, how these theories should be quantized. The case of gravity is still a puzzle today. But the effort to quantize electromagnetism led to the development of a relativistic quantum field theory, called quantum electrodynamics or short QED, describing the interaction of light and matter. Relativistic quantum field theories turned out to be the framework of choice for describing elementary particle interactions. Their ability to deal with changing particle numbers is crucial.

A serious difficulty, that plagued quantum field theories was the "divergence problem". As a consequence of the continuum description having uncountably many degrees of freedom, nonsensical infinite results arose for many quantities of interest. This problem was solved through a procedure called renormalization. It relies on the insight, that the infinities, originating from phenomena at very high momenta or equivalently very small distances, can in fact be absorbed into a redefinition of the input parameters of the theory. What is ill-defined in continuous space-time is the shift between the physical, renormalized masses and couplings and their unobservable, bare counterparts appearing in the Lagrangian defining the theory. One can say, that phenomena at shortest distances, where we lack both, a theoretical model as well as experimental evidence, miraculously affect physics at much lower energies only through the values of certain parameters. The values of these parameters cannot be computed in the low energy theory, they have to be extracted from experiments. A similar thing can be observed in hydrodynamics, where physics at the atomic scale only enters through the value of the viscosity parameter.

QED yielded one of the most precise predictions seen in physics. A key feature of QED

is its local $U(1)$ symmetry: The global $U(1)$ symmetry of the free matter Lagrangian, i.e. the fact, that there is always the freedom of choosing a phase when defining a quantum mechanical state, is promoted to a *local* symmetry. This means a phase can be chosen independently for each space-time point. The kinetic term of the matter Lagrangian, containing space-time derivatives, can only be made gauge invariant, that is invariant under local phase transformations, by introducing a new massless vector particle, the gauge boson. The gauge boson couples to particles carrying the corresponding Noether charge in a way fixed by the requirements of gauge invariance. In QED the gauge boson is of course the photon and the $U(1)$ charge is the electric charge.

It was realized by Yang and Mills, that the principle of promoting a global symmetry to a gauge symmetry, allowing independent action of the symmetry group at every space-time point could be extended from the $U(1)$ case to more complicated Lie groups. When non-abelian groups like $SU(2)$ or $SU(3)$ are used, several gauge bosons, associated with the generators of the group, appear. Unlike in the $U(1)$ case, these non-abelian gauge bosons themselves carry the more complicated group charges and thus exhibit self-interactions. As a consequence these theories can have a virtue known as asymptotic freedom; the strong coupling at low energies becomes weaker at higher energies, contrary to the situation in QED.

Gauge invariance became the most important guiding principle for constructing theories of elementary particle interactions. However, something was clearly missing. Gauge invariance does not allow mass terms for gauge bosons in the Lagrangian. As a consequence, the forces mediated by gauge bosons are all long range, just as the electromagnetic force in QED. Therefore gauge theories were unable to model the observed short ranged nature of the weak and strong forces, calling for massive force carriers.

A solution to this problem is provided by spontaneous symmetry breaking. This term denotes the situation, that a symmetry present in the Lagrangian is not respected by the ground state of the theory. Goldstone showed, that whenever a global symmetry is not respected by the ground state, a massless particle, a goldstone boson, appears for every broken symmetry generator. The simplest example is an $SO(2)$ multiplet of scalars in a potential shaped like a "Mexican hat". The ground state is a constant but nonzero field corresponding to an arbitrarily chosen point in the trough of the potential. Thus the scalar field acquires a nonzero vacuum expectation value, VEV. The massless Goldstone boson corresponds to excitations along the flat trough of the potential. The second degree of freedom is a scalar with a mass given by the positive curvature in axial direction. Spontaneous symmetry breaking was thought to be of no use for the construction of realistic models, since there are no massless Goldstone bosons in nature. This view was proven wrong by a crucial observation by Higgs, Brout, Englert, Guralnik, Hagen and Kibble. If a *gauge* symmetry is spontaneously broken, the gauge bosons can acquire a mass. Moreover the massless Goldstone bosons do not appear in the spectrum. They are "eaten" by the gauge bosons and supply the third degree of freedom inherent to a massive vector particle. If the spontaneous symmetry breaking is caused by a scalar gauge multiplet acquiring a nonzero VEV, the radial excitation in the "Mexican hat" remains in the spectrum; a massive particle called the Higgs boson.

Glashow, Weinberg and Salam proposed a model for the interactions of elementary particles based on spontaneously broken gauge invariance. It unifies the weak and electromagnetic force using $SU(2) \times U(1)$ gauge invariance, which is spontaneously broken down to the observed electromagnetic $U(1)$. The strong force is described by an unbroken local $SU(3)$ "color" symmetry. In this model, called the Standard Model of elementary particles, the

Higgs mechanism is not only needed to give mass to vector bosons. The chiral nature of the weak force, acting only on left handed fermions, calls for left and right handed fermions carrying different $SU(2) \times U(1)$ charges. Therefore gauge symmetry does not allow ordinary Dirac mass terms in the Lagrangian. Fermion mass terms have to be generated by couplings to the Higgs boson similar like gauge boson masses. So the Higgs boson is in fact responsible for the masses of all Standard Model particles. The full $SU(3) \times SU(2) \times U(1)$ theory is more than the sum of its parts, since a miracle called cancellation of anomalies happens, preventing the chiral symmetry of the Lagrangian from being spoiled through quantum corrections.

The Standard Model is the description of elementary particle interaction we have been living with and proud of for the last three decades. Its superb successes were the prediction of weak neutral currents measured at CERN and SLAC and the prediction of the masses of the Z and $W^{\pm}$ bosons mediating the weak force, discovered at CERN in 1983. Thorough tests of the Standard Model could be performed with electroweak precision data from LEP and until today, although there is some tension in the data, no measurement is in real disagreement with the Standard Model. A key point of the Standard Model is the prediction of the Higgs boson. The Standard Model is sometimes presented as a jigsaw puzzle with the Higgs boson as the last missing piece.

There are, however, several issues with the Standard Model. First of course the predicted Higgs boson has not been found so far. Thereby the mass region, where it should be accommodated with highest probability according to electroweak precision data, is already excluded by direct search. This is no support for the Standard Model, but it should not be overstated, since only the logarithm of the Higgs mass enters these considerations. But concerns arise from the theoretical side as well. The Standard Model is clearly not complete, since it does not include gravity. At the same time, the mass of the Higgs boson is not stable against addition of new sectors. It will naturally assume a value comparable to the highest mass scale of the theory. This is known as the gauge hierarchy problem. A new sector containing very heavy particles should therefore be supplemented by a mechanism protecting the Higgs mass from large corrections.

The Higgs mechanism realized in the Standard Model is just the simplest phenomenological model of electroweak symmetry breaking, providing a triplet of Goldstone bosons, that can be eaten by the $W^{\pm}$ and the Z boson. Nature might have chosen a more complicated solution. It is very well possible, that the ongoing LHC experiment will reveal so-called new physics beyond the Standard Model, forcing us to revise the latter, rather than just find the elusive Standard Model Higgs boson. However, there is more truth in the Standard Model Higgs sector, than it might first seem. Theorists have found it is extremely difficult to extend the Standard Model without getting into conflict with electroweak precision data. The ρ parameter related to the $W^{\pm}$ and Z masses plays a key role in this respect. Custodial symmetry, an accidental global $SO(4)$ symmetry of the Higgs sector fixes $\rho = 1$. It is broken only by the large mass differences of the third quark generation. For alternative models it is virtually impossible to be consistent with data, if they do not respect custodial symmetry.

One very well known extension of the Standard Model is the introduction of supersymmetry. Supersymmetry is an extension of Lorentz symmetry of space-time, which transforms bosons into fermions and vice versa. Therefore every particle has a superpartner with opposite statistics. The Minimal Supersymmetric Standard Model, MSSM, is the simplest possible, phenomenologically viable supersymmetrization of the Standard Model. It introduces new particles as superpartners for all known Standard Model particles. Whereas the Standard Model Higgs sector is made of a single scalar $SU(2)$ doublet, in the MSSM for technical

reasons two $SU(2)$ doublets with opposite $U(1)$ hypercharge are required. They both come with fermionic superpartners. Electroweak symmetry breaking has to produce three Goldstone bosons, which are eaten just like in the Standard Model. Therefore five real degrees of freedom remain in the spectrum: two CP even neutral Higgs bosons called the light and the heavy Higgs, one CP odd neutral Higgs boson and two charged Higgs bosons. Contrary to the Standard Model, the MSSM itself, not data, provides an upper bound for the mass of the light Higgs. At leading order this bound is $m_h < m_Z$, so the light Higgs would have to be in the region searched by LEP, but radiative corrections can weaken it considerably. Note, that also in the Standard Model a further Higgs doublet can be added. Doing so introduces many unwanted new parameters, however. It is remarkable, that supersymmetry requires the introduction of a second doublet, and at the same time allows to do so without proliferation of parameters.

A main virtue of supersymmetry is the arrangement of a cancellation in the quantum corrections to the Higgs mass. The bothersome quadratic divergence cancels between contributions from quarks and from their superpartners, the scalar quarks or squarks. This cancellation is not just a neat coincidence. It happens, because the Higgs can be rotated into its fermionic superpartner by a symmetry of the theory, and fermions, unlike scalars, only receive logarithmically divergent quantum corrections to their masses. The idea of supersymmetry also gets support for other reasons. The Standard Model gauge group can be embedded into a larger $SU(5)$ or $SO(10)$. The matter content of the Standard Model neatly fits into anomaly free representations of these groups. Such a grand unified theory would explain the fractional charges of quarks. Further it fixes the strength of the three gauge couplings of $SU(3) \times SU(2) \times U(1)$ in terms of a single unified gauge coupling. When the three gauge couplings are evolved to very high energies using the renormalization group equation, their values come close to each other at a certain point. Thereby the normalization of the $U(1)$ hypercharge given by the embedding is important. If the evolution is done taking into account the doubled particle spectrum of the MSSM, the three couplings actually meet in a single point somewhere above 10^{16} GeV. This fact can be considered a smoking gun hinting at the existence of supersymmetry. Also its conceptual beauty and its crucial role in string theories are often put forward in the prospect of supersymmetry.

There is clearly no exact supersymmetry in nature, since particles do not group into pairs with opposite statistics but otherwise equal quantum numbers and masses. Thus if supersymmetry indeed exists, it has to be supplemented by a mechanism of so-called soft SUSY breaking, which disguises supersymmetry at low energy and allows superpartners to obtain masses around the TeV scale, but without ruining the highly welcome cancellation occurring in the corrections to the Higgs mass. Various such mechanisms have been proposed. For us it will be sufficient just to parametrize their possible effects by directly including effective soft SUSY breaking terms into the Lagrangian. It cannot remain unmentioned here, that soft SUSY breaking is a delicate issue, which introduces many problems. Some of them are actually of a similar type like the gauge hierarchy problem, which supersymmetry solves. Still, among the proposed extensions of the Standard Model, the MSSM is arguably the most solid and best analyzed one. In any case it is a very predictive model, postulating many new particles as well as intricately related couplings.

Testing the Higgs sector at colliders is a difficult task. While the Higgs gives rise to quantum corrections to many measurable quantities, these indirect effects are very small. The challenge is to produce real Higgs bosons and to detect telltale decay products. Assuming the existence of a Higgs, the fact, that we have not seen it so far neither at LEP2 nor at the

Tevatron clearly tells us, that it is difficult to produce. And it is difficult to produce for a reason. The list of particles we can collide at accelerators is very limited. It is essentially electrons and protons. Due to asymptotic freedom, colliding protons in fact means colliding its constituents; gluons, as well as up and down quarks. The problem is, that all these particles have zero or very small masses. Therefore, their coupling to the Higgs is zero or very small. The only viable way to produce a Higgs is thus to produce other heavy particles first, particles to which the Higgs "talks more" than to light quarks or electrons. The only known particles with strong enough couplings to the Higgs are the top quark and the heavy vector bosons $W^{\pm}$ and Z.

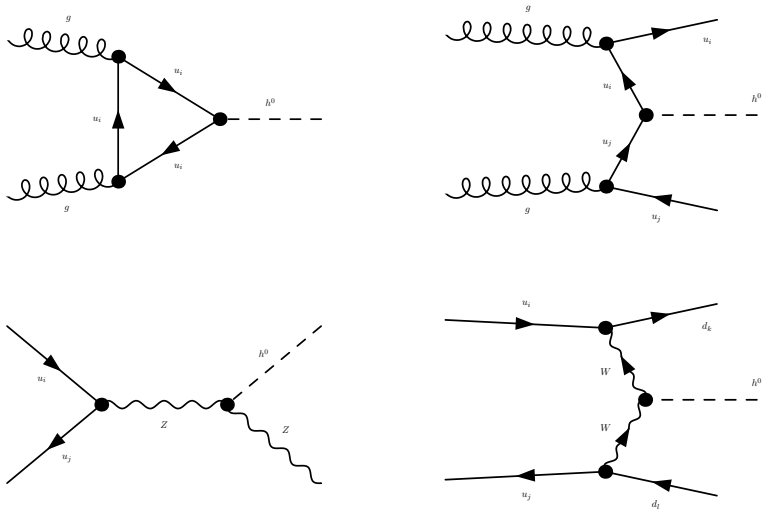

Figure 1.1: Relevant processes for Higgs production at hadron colliders: Gluon fusion, associated production, Higgs strahlung and vector boson fusion.

Figure 1.1 shows the relevant Higgs production channels at hadron colliders in terms of Feynman diagrams, the language of perturbative quantum field theory. In the second diagram, the vector boson fusion process, a pair of heavy vector bosons, mostly $W^{\pm}$ is produced from energetic quarks and annihilates into a Higgs boson. In the following diagrams a heavy state, either a vector boson or a top quark pair is produced from energetic quarks and subsequently radiates off a higgs boson. Diagrams 2-4 are tree diagrams, i.e. classical approximations. Each of these processes receives quantum corrections from many diagrams containing loops. The first diagram, the gluon fusion channel, is special. The diagram shown, containing a loop, is the leading contribution. There is no corresponding tree diagram; the Higgs does not talk directly to gluons, since they are massless. This is a genuine quantum effect. It is instructive to view this process in the following way. Rather than actually producing the heavy particles, which the Higgs talks to, we let the vacuum do this demanding task for us. According to the energy-time uncertainty $\Delta E\,\Delta t \gtrsim \hbar$ nature can lend the energy for producing a very heavy particle. Clearly, this energy will be claimed back after a very short time, so a top-antitop pair arising this way cannot appear as real particles in a final state. But if we feed in two gluons for the sake of energy and momentum conservation, the virtual quark can emit a real Higgs boson, that can appear in the final state. We can read off figure 1.2, that exactly this process is the most important production channel at hadron colliders. The reason is, that in this process, the Higgs is alone in the final state. Therefore the available phase space is not reduced by other heavy particles. At the same time, the loop suppression is moderate, since

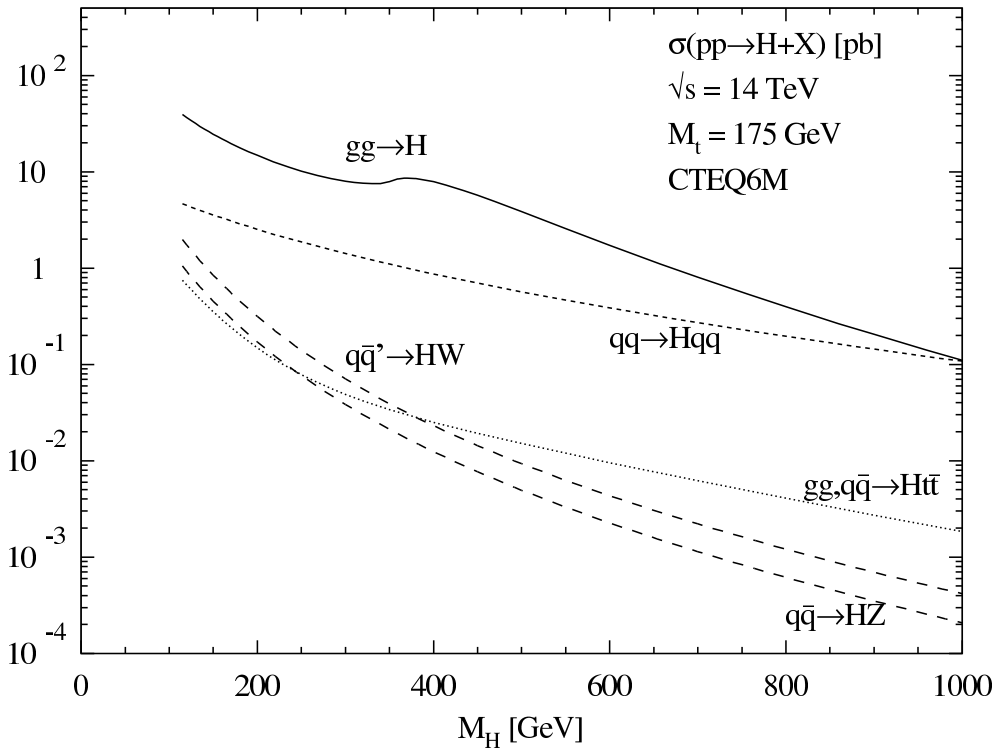

Figure 1.2: Cross sections for various channels of Standard Model Higgs production at the LHC. Gluon fusion is the dominant channel over the whole mass range.

the coupling of the gluon to the quarks is strong.

An important detail is, that in the limit, where the top quark is made infinitely heavy, the cross section of the gluon fusion process does not go to zero, it rather approaches a constant. Actually, provided the Higgs is somewhat lighter than the top quark, this so called heavy top limit yields a decent approximation of the exact gluon fusion process. Since the Standard Model is presumabley not the last word in particle physics, this non-decoupling could have an important impact. It is well possible that additional colored particles exist. Prime examples could be squarks and gluinos, the superpartners of quarks and gluons. Each such heavy colored particle would most likely give rise to a contribution to the gluon fusion cross section. Note, that this is true even if the new particles are so heavy, that they cannot be produced at the collider. In such a case, processes where the heavy particles also appear in the final state are of course not possible, but the gluon fusion process just does not care. The collider only has to supply enough energy to pay for the Higgs, whereas the heavy particle loop is borrowed from the vacuum for free.

Imagine the LHC finds deviations from the Standard Model. It should have become clear by now, that the ability to accurately predict the gluon fusion cross section in any extension of the Standard Model physicists might come up with, becomes very important then. Unfortunately, this can be a rather difficult task. The production of colored particles from gluons happens via the strong force or Quantum Chromodynamics, QCD. For electroweak processes the leading order diagrams usually give a viable approximation and the next order gives precision results. In QCD the situation is very different. The leading order usually

contains large scale dependencies and is very unreliable. To get an acceptable approximation, the next-to-leading order, NLO, is mandatory and for precision, one has to go further in the perturbative expansion. The gluon fusion process $gg \to h$ is no exception here. In the Standard Model it is known, that NLO corrections increase the leading order cross section by more than 70% at the LHC [1]. The next-to-next-to-leading order, computed in the heavy top approximation only, gives another 30% [10]. Since $gg \to h$ is a loop induced process, the mandatory next-to-leading order correction is a two-loop amplitude.

The evaluation of amplitudes or single Feynman diagrams containing loops is a general unresolved problem of quantum field theory. At one-loop order, the problem was in principle solved long time ago by the reduction to scalar integrals according to Passarino and Veltman. However, this representation is not well behaved and not useful in practice, if the process under consideration has many legs. Only recently improved reduction methods have emerged [72]. At two-loop order nothing comparable exists. Important progress has been achieved over the last years for certain classes of diagrams. But despite of that, even for a process like $gg \to h$, having only three legs, one can easily run into diagrams, which are hopeless cases with today's analytic technology. Where analytic integration is not feasible, it is natural to resort to numerical techniques. But until now in many cases not even numerical evaluation of loop integrals is possible, at least not in the relevant kinematic region. The reasons for this unpleasant situation are ultraviolet and infrared singularities of Feynman diagrams calling for regulators, and the appearance of thresholds.

The above statements are reflected in the status of the $gg \to h$ computation as follows: In the Standard Model, the NLO corrections were computed already in 1993 by Spira, Djouadi, Graudenz and Zerwas [1]. The result was given in a somewhat impractical one-dimensional integral representation. Recently this result was put into a more useful form by matching a carefully chosen ansatz to the result of [1]. Analytic calculation techniques developed over the last years are expected to provide a direct path to a closed analytic solution for the Standard Model case. Such a computation is of considerable interest, since it also provides the basis for automated computations of $gg \to h$ in arbitrary extensions of the Standard Model, as long as only a single mass parameter appears in the loops. For more complicated extensions of the Standard Model, leading to two-loop diagrams with several mass parameters, only effective field theory solutions could be obtained. These are approximations analogous to the heavy top limit, where all massive particles appearing in the loops are assumed to be infinitely heavy. For the MSSM this calculation was accomplished in [25] and very recently repeated in [26]. However, the very example of the MSSM also shows, that this is not an acceptable situation for two reasons. First the MSSM also predicts a heavy Higgs boson. Since it is expected to be heavier than the top quark, the effective theory solution is meaningless for the heavy Higgs case. Second, due to the more complicated structure of the Higgs sector, for certain parameter regions, the contribution from bottom quarks can be enhanced so much, that they are no longer negligible despite their small mass of only 5 GeV. Since they spoil the mass hierarchy, contributions containing bottom quarks are not calculable in an effective theory approach. The bottom line is clear. In the MSSM and probably also in other viable extensions of the Standard Model, the mandatory NLO corrections to $gg \to h, H$, the most important LHC process, require the evaluation of two-loop Feynman diagrams with many different masses in the loops. The evaluation of these diagrams is not feasible with any known technique. The presence of several kinematic invariants virtually disqualifies analytic techniques. Ultraviolet, infrared and threshold singularities in Feynman diagrams impede numerical integration.

This thesis remedies this awkward situation. It is organized as follows:

Chapter 2 deals with the analytic computation of $gg \to h$ in the Standard Model and closely related processes. We make use of modern analytic techniques, that allow us to re-compute the $gg \to h$ amplitude in a more general framework. The Laporta algorithm [15] allows for automated reduction of multi-loop integrals to a small number of master integrals. The differential equation method [3] yields robust technology for computing master integrals. Many of the master integrals required for the $gg \to h$ process were indeed known in the literature [18, 19, 20, 21, 22, 23, 24]. We present here for the first time the full set of master integrals for the $gg \to h$ process via a heavy quark at two-loop order. We compute all master integrals using the method of differential equations. Our expressions are given as an expansion in the dimensional regularization parameter $\epsilon = (4-d)/2$ in terms of harmonic polylogarithms. HPLs with transcedentalities up to four appear. Our result for the two-loop $gg \to h$ amplitude in terms of master integrals fully agrees with [28]. This presents the first independent check of [1]. But this is not the main impact of a full set of master integrals. The more important consequence is, that it allows for automated computation of processes with similar distributions of masses in the loops. We illustrate this by computing the two-loop amplitude for $gg \to h$ via a heavy scalar particle. The scalar particle can be considered a scalar quark for instance. So, with adequate couplings, this result is a partial contribution to the full two-loop SUSY-QCD amplitude for $gg \to h, H$ in the MSSM. Our set of master integrals may prove equally useful for the computation of $gg \to h$ in other extensions of the Standard Model. It is also a subset of the master integrals, that enter the two-loop amplitudes of more complicated $2 \to 2$ processes, such as heavy quark production.

In chapter 3 we show a way of using contour deformation [54, 55, 57, 58] for dealing with thresholds within the framework of sector decomposition [4, 5, 8, 12]. Together with a simple program for Feynman parametrizing tensor integrals this yields a flexible tool, which in principle allows numerical evaluation of arbitrary loop integrals in arbitrary kinematic regions. The method described here has been developed contemporeanously and applied to five leg processes at one-loop order by Lazopoulos, Melnikov and Petriello [61, 60, 59]. At the moment of this writing, this is the only viable method for evaluating multi-loop integrals with several mass parameters in the presence of thresholds.

Finally, in chapter 4 we demonstrate the power of our method by computing the full SUSY-QCD two-loop amplitude for $gg \to h, H$ in the MSSM. This includes the numerically challenging contribution from diagrams containing bottom (s)quarks and gluinos, and thus extremely disparate mass parameters.

Chapter 2

Analytic calculation of the $gg \to h$ Amplitude at $\mathcal{O}(\alpha_s^2)$ in the Standard Model

In this chapter we study the virtual contribution to the $gg \to h$ amplitude at $\mathcal{O}(\alpha_s^2)$ in the Standard Model. As it comes at almost no additional cost, we also consider the case, where the ggh interaction is mediated via a massive scalar instead of the massive quark. With adequate couplings both pieces are partial contributions to the full SUSY QCD $gg \to h, H$ amplitude in the Minimal Supersymmetric Standard Model, which will be computed in chapter 4. We neglect the contributions of the first and the second generation due to the smallness of their masses. In the Standard Model, also the contribution of the bottom quark is negligible. In the MSSM this is not true, as the bottom-higgs-coupling is enhanced by $\tan\beta$.

2.1 Reduction of Amplitudes to Master Integrals

The leading order contribution to $gg \to h$ in the Standard Model is given by two triangle diagrams, where two gluons create a Higgs boson via a top quark loop. One of them is shown in figure 2.1, labeled $\frac{1}{2}$ BORN1. The second diagram is obtained by reverting the direction of particle flow in the loop. One finds, that the two diagrams lead to the same integrand. This can be understood as follows. The color factor is simply $\mathrm{tr}(T^a T^b) = \frac{1}{2}\delta^{ab}$ and thus the same for both direction of the arrows. The Lorentz parts of the two diagrams differ in the order of the γ-matrices in the trace. But this order can be reversed using $C\gamma^\mu C^\dagger = -(\gamma^\mu)^T$, where C is the charge conjugation operator. Alternatively the equality can be explained with bose symmetry.

The contribution with a scalar running in the loop has three diagrams. Two of them again differ only by the direction of particle flow in the loop and turn out to be equal. One representative together with the third diagram is shown in figure 2.1.

The two-loop QCD contribution to $gg \to h$ in the Standard Model consists of 21 Feynman diagrams. The SM-like contribution containing only gluons and a massive scalar particle counts 56 diagrams, 16 of which vanish. As in the one-loop case we find that diagrams related by reversion of arrows are equal. It is easy to check, that color factors do not depend on the arrow direction and the insertion of an internal gluon does not spoil the equality of the Lorentz parts. Unlike in the leading order case, some diagrams are not symmetric

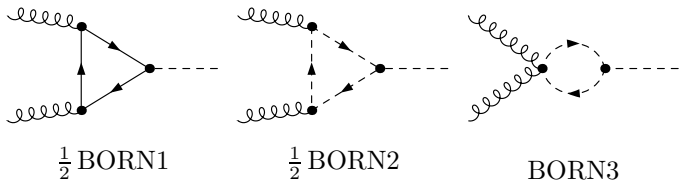

Figure 2.1: Leading order contribution to $gg \to h$ in the Standard Model, as well as the SM-like contribution, where the gluons couple to the Higgs via a heavy scalar. Both triangle diagrams appear with reversed arrows of particle flow as well. Reversing the arrows in the bubble diagram would give a topologically equivalent diagram.

under permutation of the two gluons even if we ignore arrows. Action of bose symmetry, i.e. swapping $p_1, \mu, a \leftrightarrow p_2, \nu, b$ is thus not equivalent to reversing the arrows. This means, that these diagrams actually come in four rather than two variants. In figures 2.2 and 2.3 we show the nonzero diagrams for the quark and the scalar case, respectively. Where equivalent diagrams exist, only one representative is shown. The full set of diagrams is given in

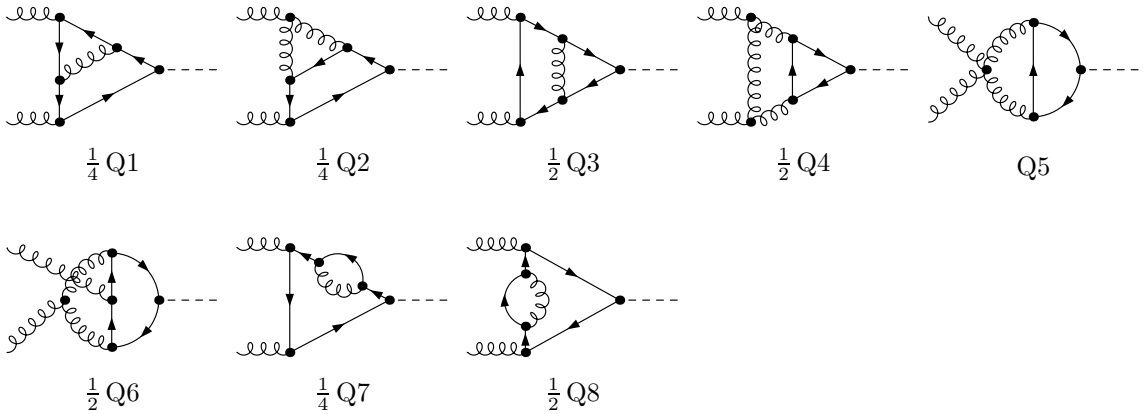

Figure 2.2: $\mathcal{O}({\alpha_s}^2)$ contributions to $gg \to h$ in the Standard Model. Note that we give a name to the sum of equivalent diagrams. For instance, Q1 refers to the sum of four equivalent diagrams. Therefore the representative drawn is labled by $\frac{1}{4}$ Q1. The whole two-loop amplitude is given by Q1+Q2+...+Q8.

appendix A.

The color structure of the $gg \to h$ amplitude is trivial. The only invariant $SU(N_c)$ tensor that can be constructed from the two external gluons is δ_{ab}. It is handy to drop the factor δ_{ab} at the very beginning. We just have to remember to put back a factor $\delta_{ab}\delta^{ab} = N_c^2 - 1$ when computing an $|\mathcal{M}|^2$ summed over color.

In the amplitude the polarization vectors of the external gluons are contracted with a tensor expression

$$\mathcal{M} = \varepsilon_1^\mu(p_1)\, \varepsilon_2^\nu(p_2)\, \mathcal{M}_{\mu\nu}. \tag{2.1}$$

It is convenient to project $\mathcal{M}_{\mu\nu}$ onto scalar form factors. The only vectors $\mathcal{M}_{\mu\nu}$ can contain are p_1 and p_2. Bose symmetry further tells us, that $\mathcal{M}_{\mu\nu}$ has to be symmetric under $p_1, \mu \leftrightarrow p_2, \nu$. Therefore $\mathcal{M}_{\mu\nu}$ can be written as the linear combination

$$\mathcal{M}^{\mu\nu} = a\,(p_1 \cdot p_2) g^{\mu\nu} + b\, p_2^\mu p_1^\nu + c\, p_1^\mu p_2^\nu + d\,(p_1^\mu p_1^\nu + p_2^\mu p_2^\nu). \tag{2.2}$$

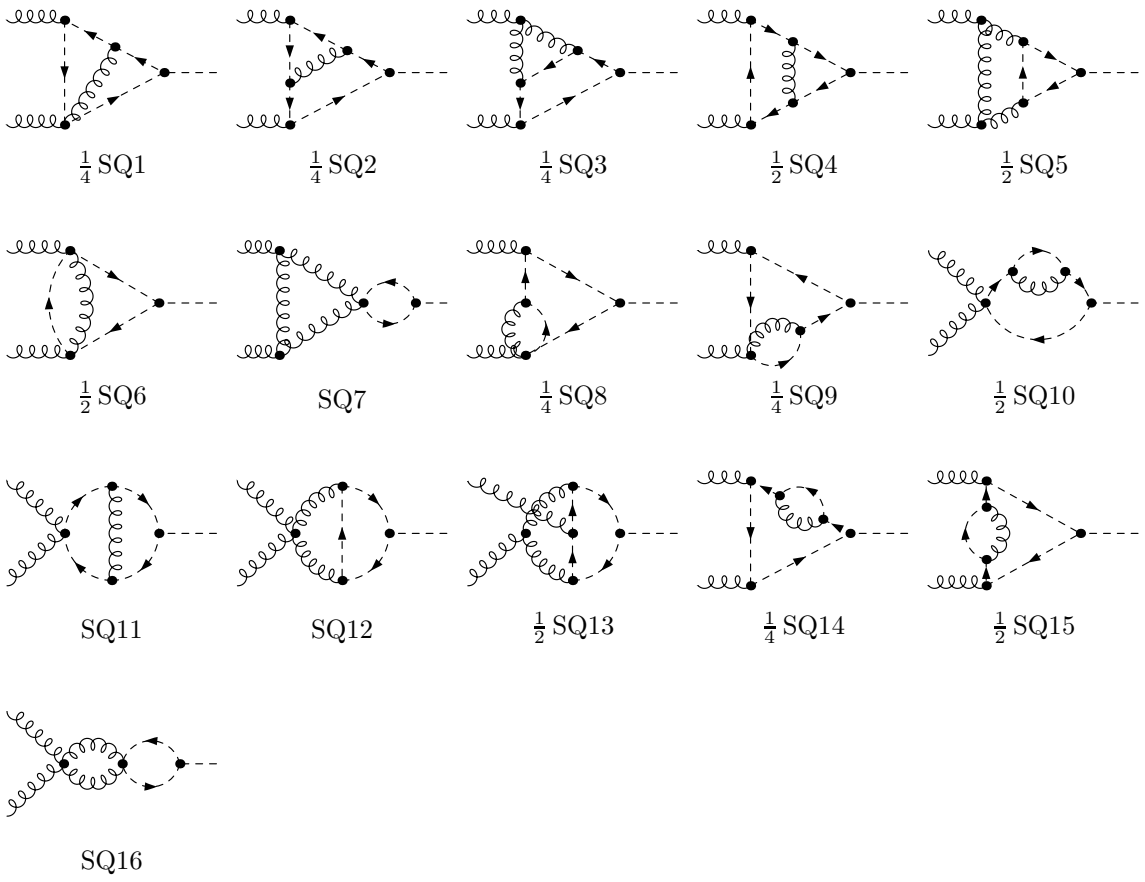

Figure 2.3: SM-like contributions to $gg \to h$ from scalars at $\mathcal{O}({\alpha_s}^2)$.

Gauge invariance requires $p_{1\mu}\,\mathcal{M}^{\mu\nu} = 0$. So

$$0 = p_{1\mu}\,\mathcal{M}^{\mu\nu} = (a+b)(p_1\cdot p_2)\,p_1^\nu + d(p_1\cdot p_2)\,p_2^\nu, \tag{2.3}$$

what requires $b = -a$ and $d = 0$. The condition $p_{2\nu}\,\mathcal{M}^{\mu\nu} = 0$ does not lead to further constraints, as we have already used bose symmetry in eq. (2.2). The lesson is, that $\mathcal{M}^{\mu\nu}$ is described by only two scalar form factors

$$\mathcal{M}^{\mu\nu} = [(p_1\cdot p_2)g^{\mu\nu} - p_2^\mu p_1^\nu]\cdot\mathcal{A} + [p_1^\mu p_2^\nu]\cdot\mathcal{B}. \tag{2.4}$$

And even better, as $p_1^\mu p_2^\nu$ vanishes when contracted with physical polarization vectors, it suffices to compute $\mathcal{A}$. In order to extract $\mathcal{A}$ it is useful to define

$$P^{\mu\nu} = g^{\mu\nu} - \frac{p_2^\mu\,p_1^\nu}{(p_1\cdot p_2)} \tag{2.5}$$

$$P_s^{\mu\nu} = g^{\mu\nu} - \frac{p_2^\mu\,p_1^\nu + p_1^\mu\,p_2^\nu}{(p_1\cdot p_2)}. \tag{2.6}$$

One easily verifies that $P^{\mu\nu'}{P_{\nu'}}^\nu = P^{\mu\nu}$ and $P_s^{\mu\nu'}{P_{s\,\nu'}}^\nu = P_s^{\mu\nu}$, so $P^{\mu\nu}$ and $P_s^{\mu\nu}$ are both

projectors. Further

$$P_s^{\mu\nu'} P_{\nu'}{}^{\nu} = P_s^{\mu\nu} \tag{2.7}$$

$$P^{\mu\nu'} P_{s\nu'}{}^{\nu} = P_s^{\mu\nu}, \tag{2.8}$$

meaning that $P_s^{\mu\nu} \subset P^{\mu\nu}$. The projector $P^{\mu\nu}$ has to be handled with care, as it is not symmetric in $\mu\nu$. We have

$$\begin{aligned} P_{\mu\nu} P^{\nu\mu} = P_\mu{}^\mu &= d-1 \qquad \text{but} \\ P_{\mu\nu} P^{\mu\nu} &= d-2 \qquad \text{and} \\ P_{s\mu\nu} P_s^{\mu\nu} = P_{s\mu\nu} P_s^{\nu\mu} = P_{s\mu}{}^{\mu} &= d-2. \end{aligned} \tag{2.9}$$

Equipped with this notation we can rewrite eq. (2.4) as

$$\mathcal{M}^{\mu\nu} = (p_1 \cdot p_2)\, P^{\mu\nu}\, \mathcal{A} + (p_1 \cdot p_2)\, [P^{\mu\nu} - P_s^{\mu\nu}] \cdot \mathcal{B}. \tag{2.10}$$

Clearly, contracting this equation with either $P^{\mu\nu}$ or $P_s^{\mu\nu}$ projects out $\mathcal{A}$ in the same way,

$$(d-2)(p_1 \cdot p_2)\, \mathcal{A} = P^{\mu\nu} \mathcal{M}_{\mu\nu} = P_s^{\mu\nu} \mathcal{M}_{\mu\nu}. \tag{2.11}$$

What is the difference between using $P_s^{\mu\nu}$ and $P^{\mu\nu}$? Note that our discussion relies on gauge invariance. If in a single diagram we replace the polarization vectors $\varepsilon_1^\mu(p_1)\varepsilon_2^\nu(p_2)$ by a projector, it makes a difference whether we put $P_s^{\mu\nu}$ or $P^{\mu\nu}$. The diagram may for instance contain a $(p_1 \cdot p_2) g^{\mu\nu}$ not balanced by a $-p_2^\mu p_1^\nu$. So single diagrams contracted with $P_s^{\mu\nu}$ or $P^{\mu\nu}$ will differ in general. The difference of course disappears, when summing over a gauge invariant set of diagrams.

Instead of replacing $\varepsilon_1^\mu(p_1)\varepsilon_2^\nu(p_2)$ by a projector $P_s^{\mu\nu}$ or $P^{\mu\nu}$ in the amplitude or single diagrams, one might want to keep the the polarization vectors, multiply by the helicity structure of $\mathcal{M}^*$, namely

$$\left(\varepsilon_1 \cdot \varepsilon_2 - \frac{(\varepsilon_1 \cdot p_2)(\varepsilon_2 \cdot p_1)}{p_1 \cdot p_2} \right)^* = \left(\varepsilon_1^{\mu'} \varepsilon_2^{\nu'} \right)^* P_{\mu'\nu'}, \tag{2.12}$$

and sum over polarizations. Choosing p_2 and p_1 as reference vectors for $\varepsilon_1(p_1)$ and $\varepsilon_2(p_2)$ we get

$$\sum_{\varepsilon_1} \varepsilon_1^\mu \varepsilon_1^{*\mu'} = -g^{\mu\mu'} + \frac{p_1^\mu p_2^{\mu'} + p_2^\mu p_1^{\mu'}}{p_1 \cdot p_2} = -P_s^{\mu\mu'} \tag{2.13}$$

and dito for ε_2. Then

$$\sum_{\varepsilon_1, \varepsilon_2} \left(\varepsilon_1 \cdot \varepsilon_2 - \frac{(\varepsilon_1 \cdot p_2)(\varepsilon_2 \cdot p_1)}{p_1 \cdot p_2} \right)^* \varepsilon_1^\mu \varepsilon_2^\nu X_{\mu\nu} = P_{\mu'\nu'} P_s^{\mu\mu'} P_s^{\nu\nu'} X_{\mu\nu} = P_s^{\mu\nu} X_{\mu\nu}. \tag{2.14}$$

So, with the given choice of reference vectors, this procedure is equivalent to replacing the polarization vectors by $P_s^{\mu\nu}$.

We have generated the amplitudes described by the diagrams in figures 2.2 and 2.3 using FeynArts and FormCalc [68]. FeynArts contains all necessary Feynman rules and is able to produce expressions for the amplitudes out of the box. FormCalc tries to process these expressions further, carrying out color and spinor algebra and reducing integrals into

Passarino-Veltman functions. Due to the reduction step FormCalc works for one-loop amplitudes only. With some tampering, essentially patching the output from FeynArts to pretend we are dealing with tree diagrams, FormCalc could be persuaded to carry out numerator algebra without attempting to reduce loop integrals. The expressions obtained this way were checked against an independent derivation of the amplitude using QGRAF and private scripts implementing the Feynman rules and numerator algebra.

The scalar form factors are given by the projected amplitude and thus by projected Feynman diagrams. This means we have to compute loop integrals with scalar products of momenta in the numerator. These integrals can be classified into topologies according to their propagators. The diagrams in figures 2.2 and 2.3 contain at most six propagators, of which five can be massive. In the numerators, however, one can find seven independent scalar products. In each topology, the irreducible scalar product can be dealt with by introducing an additional propagator, which can be raised to negative powers. This way, all integrals belong to sub-topologies of the three master topologies shown in figure 2.4. The propagators appearing in each topology are

$$
\begin{array}{lcl|lcl|lcl}
 & & \mathrm{TP}_1 & & & \mathrm{TP}_2 & & & \mathrm{TP}_3 \\
D_{11} &=& k^2 & D_{21} &=& k^2 - m^2 & D_{31} &=& k^2 - m^2 \\
D_{12} &=& (k+p_1)^2 & D_{22} &=& (k+p_2)^2 - m^2 & D_{32} &=& (k-l-p_1)^2 \\
D_{13} &=& (k+p_{12})^2 & D_{23} &=& (k+p_{12})^2 - m^2 & D_{33} &=& (k+p_{12})^2 - m^2 \\
D_{14} &=& (l+p_{12})^2 - m^2 & D_{24} &=& (l+p_{12})^2 - m^2 & D_{34} &=& (l+p_{12})^2 - m^2 \\
D_{15} &=& (l+p_1)^2 - m^2 & D_{25} &=& (l+p_2)^2 - m^2 & D_{35} &=& (l+p_1)^2 - m^2 \\
D_{16} &=& l^2 - m^2 & D_{26} &=& l^2 - m^2 & D_{36} &=& (k+p_1)^2 - m^2 \\
D_{17} &=& (k-l)^2 - m^2 & D_{27} &=& (k-l)^2 & D_{37} &=& (k-l)^2\,,
\end{array}
\tag{2.15}
$$

The reduction to master integrals is done using integration by part identities [13, 14] combined with the Laporta algorithm [15] in [16, 17]. We found 17 master integrals, which are shown in Figure 2.5. It is possible to choose a different basis of master integrals; the basis we choose is particularly convenient for the method of differential equations.

We write the amplitude $\mathcal{M}$ in terms of the form factor $\mathcal{A}$

$$
\mathcal{M}_i = \left[(\varepsilon_1 \cdot \varepsilon_2)\,(p_1 \cdot p_2) - (p_2 \cdot \varepsilon_1)\,(p_1 \cdot \varepsilon_2)\right] \mathcal{A}_i \qquad i \in \{\mathrm{f}, \mathrm{s}\} \tag{2.16}
$$

and expand $\mathcal{A}_i$ in the bare coupling α_s^0,

$$
\mathcal{A}_i = \left(\frac{\alpha_s^0 S_\epsilon}{4\pi}\right) \mathcal{C}_i^{(0)} + \left(\frac{\alpha_s^0 S_\epsilon}{4\pi}\right)^2 \mathcal{C}_i^{(1)} + \mathcal{O}\left((\alpha_s^0)^3\right) \qquad i \in \{\mathrm{f}, \mathrm{s}\}. \tag{2.17}
$$

The subscript $i \in \{\mathrm{f}, \mathrm{s}\}$ serves to distinguish the cases of a fermion and a scalar running in the loop, respectively. Renormalization will only be discussed in chapter 4. Still, in order to simplify the renormalized expressions later, we have extracted a factor

$$
S_\epsilon = (4\pi)^\epsilon\, e^{-\gamma_E \epsilon} \tag{2.18}
$$

from the expansion coefficients $\mathcal{C}^{(0)}$ and $\mathcal{C}^{(1)}$ together with every power of α_s^0.

The coefficients $\mathcal{C}_i^{(o)}$ can now be written in terms of master integrals. It will prove useful

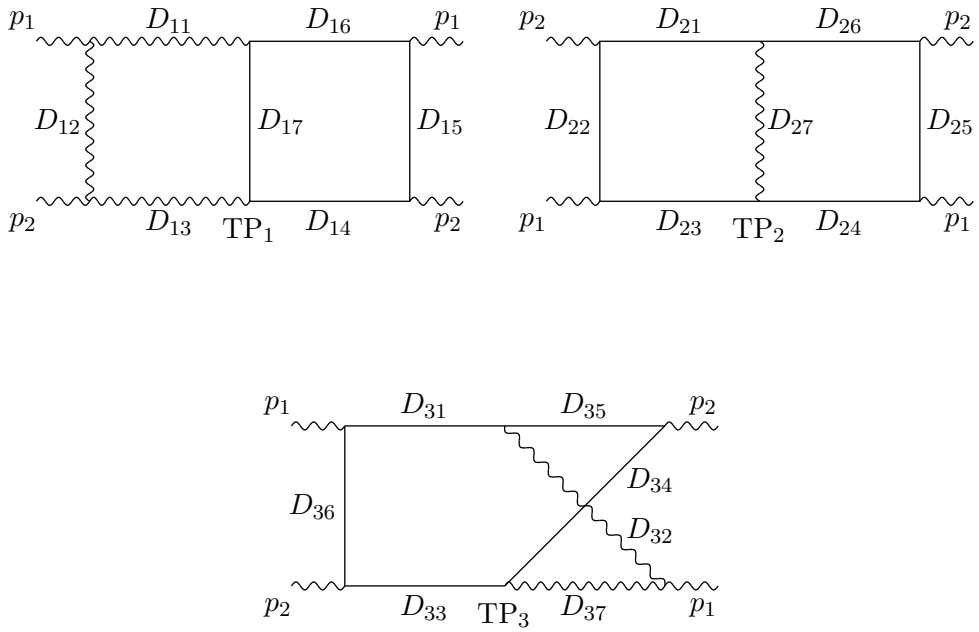

Figure 2.4: Master topologies. Wavy lines denote massless particles, both internal and external. Straight lines denote the massive particle running in the loops. The massive external line belonging to the Higgs boson is not present, as the Higgs vertex has been "opened up" by the insertion of an auxiliary propagator. Therefore, the momentum of the Higgs, $p_1 + p_2$, flows out split into massless p_1 and p_2.

not to do so directly, but to write

$$\mathcal{C}_{\mathrm{f}}^{(0)} = \Lambda_{\mathrm{f}} \, \frac{1}{m^{2\epsilon}} \, c_{\mathrm{f}}^{(0)} \qquad \mathcal{C}_{\mathrm{f}}^{(1)} = \Lambda_{\mathrm{f}} \, \frac{1}{m^{4\epsilon}} \, c_{\mathrm{f}}^{(1)} \tag{2.19}$$

$$\mathcal{C}_{\mathrm{s}}^{(0)} = \Lambda_{\mathrm{s}} \, \frac{1}{m^{2\epsilon}} \, c_{\mathrm{s}}^{(0)} \qquad \mathcal{C}_{\mathrm{s}}^{(1)} = \Lambda_{\mathrm{s}} \, \frac{1}{m^{4\epsilon}} \, c_{\mathrm{s}}^{(1)}. \tag{2.20}$$

Here we have factored out the couplings of the Higgs boson to the fermion and the scalar particle, given by $\mathcal{L}_{hqq} = -m \, \Lambda_{\mathrm{f}} \, h\bar{q}q$ and $\mathcal{L}_{hss} = -m^2 \, \Lambda_{\mathrm{s}} \, hs^*s$, respectively. In the Standard Model, only the fermionic contribution exists and we have $\Lambda_{\mathrm{f}} = 1/v$, where v is the vacuum expectation value of the Higgs boson. We have also pulled out a mass factor in order to make the coefficients $c_i^{(o)}$ dimensionless. Therefore they can be written as functions of a dimensionless variable instead of s and m^2. A convenient choice of this dimensionless variable

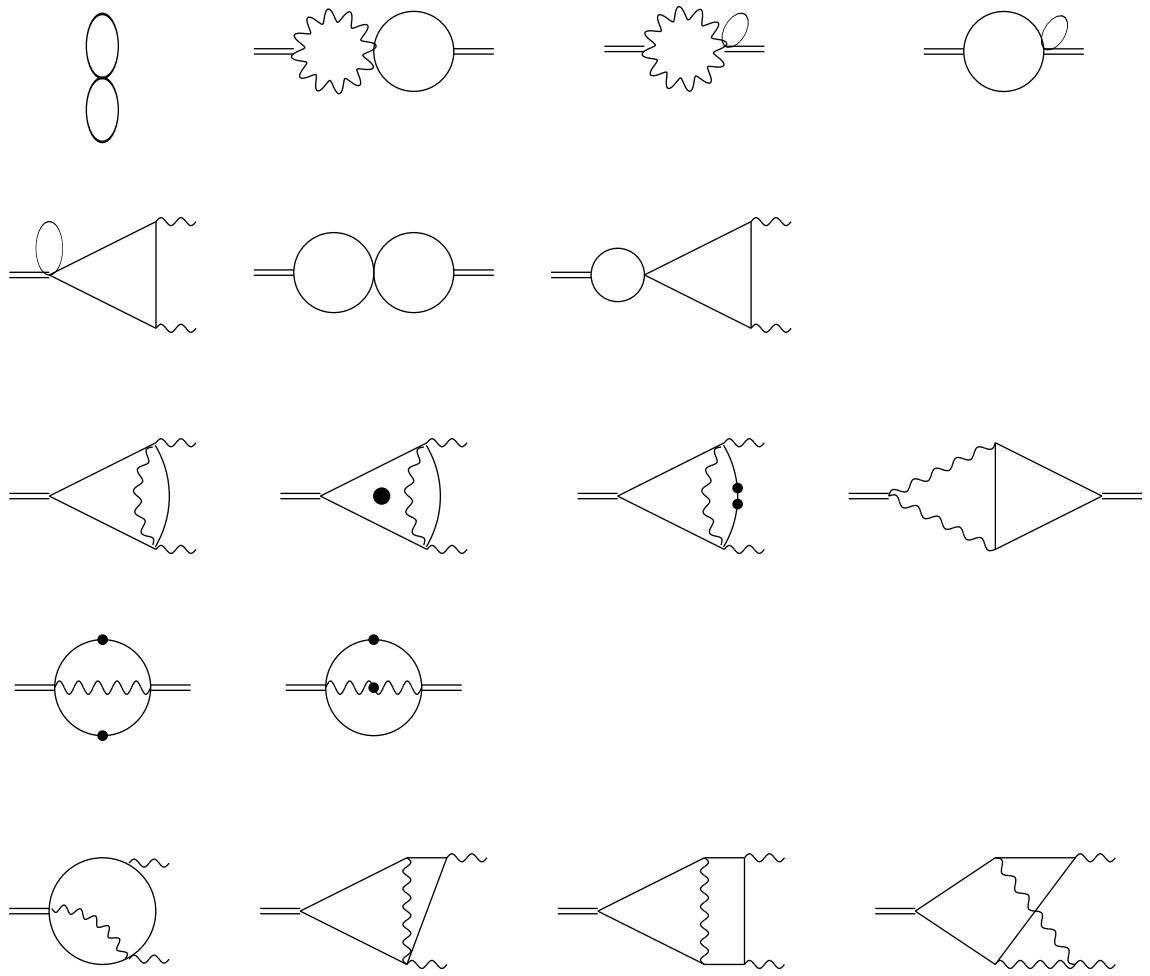

Figure 2.5: Set of master integrals for $gg \to h$ in the Standard Model. Again, wavy lines denote massless particles, straight lines the massive loop particle. The double straight line stands for the external Higgs boson. Each dot on a propagator line denotes an additional power of the propagator in the denominator. The big dot in the middle of a diagram stands for a numerator made of scalar products of loop momenta. The precise form of the numerator is given later, as it depends on the routing.

will be defined in section 2.2.1. For the leading order coefficients we get[1]

$$c_{\mathrm{f}}^{(0)} = m^{2\epsilon} e^{\gamma_E \epsilon} \left\{ -\frac{4m^2}{s} \frac{2\epsilon}{(1-\epsilon)} \right.$$
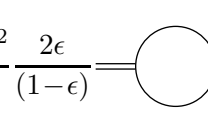
$$\left. + \frac{4}{(1-\epsilon)} \left(1 - \frac{4m^2}{s} - \epsilon\right) m^2 \right.$$
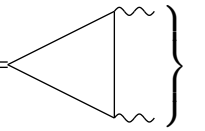
$$\left. \right\} \tag{2.21}$$

[1]The expression inside the curly bracket corresponds to $\bar{\mathcal{M}}_{\mathrm{f}}^{(0)}$ in [44]. Compared to expression (A.2) in [44], we have written the coefficient of the triangle diagram in terms of x and m^2, rather than x and s, as also the master integrals are given in these variables. Further, eq. (2.21) is not expanded in ϵ and thus valid at all orders. The factors $1-\epsilon$ in the denominators have their origin in the projector norm $P_{\mu\nu}P^{\mu\nu} = d-2$. In [44], eq. (A.2), this factor was expanded for no good reason and a mistake was introduced by doing so: The expansion should be $(1+\epsilon+\epsilon^2)$, not just $(1+\epsilon)$, as the overall factor ϵ gets cancelled by the UV-pole of the massive bubble. Eq. (A.1) in [44] also attempts to make the color factor δ_{ab} explicit in a slightly unfortunate way.

for the case of a fermion running in the loop and

$$c_{\rm s}^{(0)} = m^{2\epsilon} e^{\gamma_E \epsilon} \left\{ \frac{4m^2}{s} \frac{\epsilon}{2(1-\epsilon)} \right.$$ 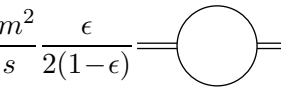 $$+ \frac{4m^2}{s} \frac{1}{(1-\epsilon)} m^2$$ 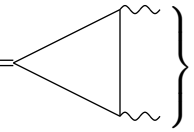 $$\left. \right\} \qquad (2.22)$$

for the case of a scalar particle running in the loop. Note that these expressions are indeed dimensionless. Factors of m^2 not divided by s cancel with the corresponding factors carrying the dimensions of the master integrals. The NLO expressions $c_{\rm f}^{(1)}$ and $c_{\rm s}^{(1)}$ are given in appendix B, as they are rather lengthy.

The leading order contributions $c_{\rm f}^{(0)}$ and $c_{\rm s}^{(0)}$ are UV and IR finite. In eq. (2.21) and (2.22) they are expressed in terms of two master integrals, a massive scalar bubble and a massive scalar triangle. Both masters are IR finite due to the massive propagators. The triangle is also UV finite, whereas the bubble has a logarithmic UV divergence, leading to a single pole in ϵ. In the expressions for $c_{\rm f}^{(0)}$ and $c_{\rm s}^{(0)}$ this pole is cancelled by the overall ϵ in the coefficient. When computing $c_{\rm f}^{(0)}$ directly from the Feynman diagram BORN1 in figure 2.1 it is easy to get confused about the fact, that the fermionic triangle seems to be UV divergent by power counting. But the dangerous part of the numerator actually comes with a factor ϵ. In the scalar triangle BORN2, the vertices also produce two powers of the loop momentum in the numerator. This diagram really has a UV divergence, which cancels against BORN3.

2.2 Computing the Master Integrals

The 17 master integrals for $gg \to h$ are shown in figure 2.5. Those in the first two lines are products of known one-loop integrals [18, 20]. The integrals in the third, fourth and fifth line are non-factorizable. Integrals in the third and fourth line were calculated already in [19][2] and [23, 22, 20]. respectively. The double triangle, last diagram in the third line was calculated in [23, 24, 22]. Also the six propagator triangle - the third diagram in the last line - was calculated in [21].

2.2.1 Differential Equations

We computed all master integrals using the differential equation method [3, 33, 34, 35, 36, 37]. Differentiating a master integral with respect to m^2, the squared mass of the loop particle, and interchanging the order of the differential operator and the loop integrations gives representations of the derivatives in terms of integrals with increased powers of propagators. These integrals can again be reduced to master integrals. Applying this procedure to the whole set of masters leads to a closed system of differential equations, describing the master integrals's m^2 dependence. This indeed fixes the entire dependence on kinematics, as, up to a dimensional factor, which can be fixed by power counting, the integrals only depend on the dimensionless ratio m^2/s. It is useful to parametrize this ratio as

$$\frac{m^2}{s} = -\frac{x}{(1-x)^2}, \qquad (2.23)$$

[2]Our results fully agree with the results quoted in this reference taken from the electronic file in `http://pheno.physik.uni-freiburg.de/bonciani/`. The printed version contains several typographical mistakes.

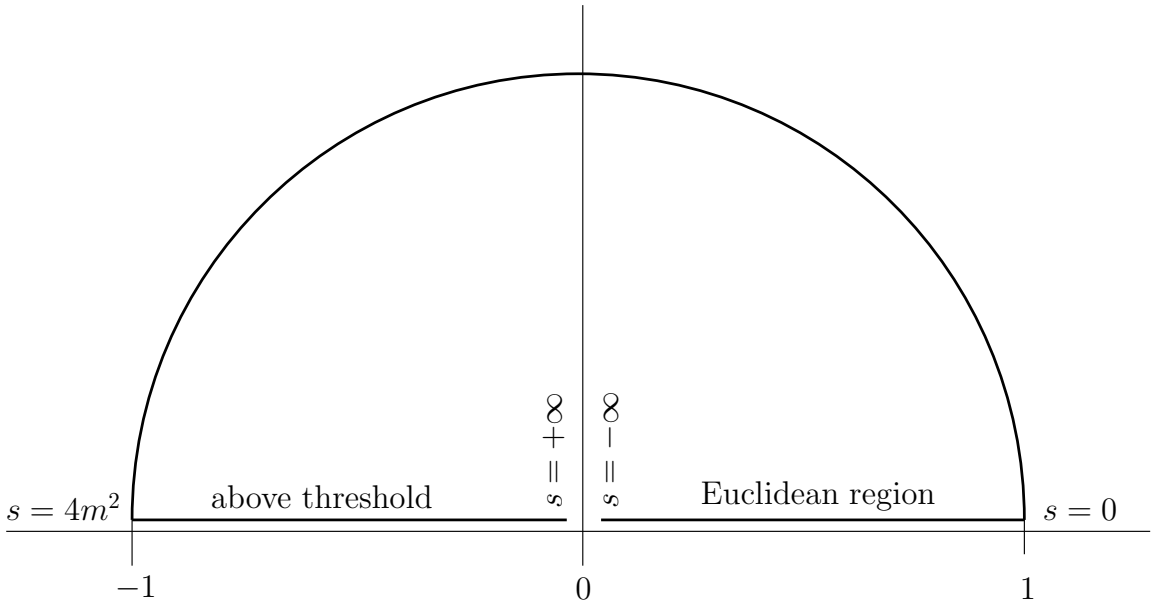

Figure 2.6: Values of x in the complex plane depending on s/m^2. For unphysical negative s, x lies $i\delta$ above the real axis, reaching $x = 1 + i\delta$ for $s = 0$. For physical s x then travels along the unit circle through the complex plane, returning to real axis at $-1 + i\delta$ when the threshold value $s = 4m^2$ is reached. For growing s above threshold, x then again moves along the real axis, approaching $0 + i\delta$ from the left for $s \to +\infty$.

and to eliminate s, using x and m^2 as independent variables. For the m^2 derivative of master integrals, the chain rule gives

$$\frac{\partial}{\partial m^2} \operatorname{MI}(m^2, s) = \frac{d}{dm^2} \operatorname{MI}(m^2, x(m^2, s)) = \frac{\partial}{\partial m^2} \operatorname{MI}(m^2, x) + \left(\frac{\partial x}{\partial m^2}\right) \frac{\partial}{\partial x} \operatorname{MI}(m^2, x). \quad (2.24)$$

For dimensional reasons

$$\operatorname{MI}(m^2, x) = (m^2)^{2n_L - n_P - n_L \epsilon} \operatorname{mi}(x), \quad (2.25)$$

where n_P is the number of propagators and n_L the number of loops. So the $\partial \operatorname{MI}(m^2, x)/\partial m^2$ derivative can be carried out and we are left with an ordinary differential equation in x. For convenience we give

$$\frac{\partial x}{\partial m^2} = \frac{x}{m^2} \frac{1 - x}{1 + x} \quad (2.26)$$

and solve eq. (2.23) for x

$$x = \frac{\sqrt{1 - \tau} - 1}{\sqrt{1 - \tau} + 1} + i0 \qquad \text{where} \qquad \tau = \frac{4m^2}{s}. \quad (2.27)$$

The values of x in the complex plane are sketched in figure 2.6.

The way the differential equations arise suggests they should not form a fully coupled system, connecting the 17 master integrals in the most general way. The system should rather be triangular, so that the derivative of a given master $\partial \operatorname{mi}_k / \partial x$ is expressed through

mi_k and an inhomogeneity, which is a combination of diagrams belonging to sub-topologies of mi_k. I.e. assuming suitable ordering of the masters, we should have

$$\frac{\partial}{\partial x}\,\mathrm{mi}_k(x) = A_k(x)\;\mathrm{mi}_k(x) + \sum_{l<k} B_{kl}(x)\,\mathrm{mi}_l(x), \tag{2.28}$$

allowing us to compute the mi_k one after the other. This is almost true. However, if a topology happens to have more than one master integral, their differential equations are usually coupled. In our case, the first three diagrams in the third line of figure 2.5 give rise to a triple coupled system. Also the equations for the two sunset diagrams in the fourth line are coupled. But this is less severe a complication than it might seem. Note that the $\mathrm{mi}_k(x)$ as well as the coefficients $A_k(x)$ and $B_{kl}(x)$ actually depend on the dimensional regularization parameter ϵ, although we did not write so explicitly. We do not attempt to solve the differential equations to all orders in ϵ, but rather series expand them in ϵ, making a Laurent series ansatz

$$\mathrm{mi}_k(x) = \sum_{i=i_0}^{i_{\max}} \mathrm{mi}_k^i(x)\epsilon^i \tag{2.29}$$

for the master integrals. We then solve the resulting differential equations for the coefficients $\mathrm{mi}_k^i(x)$ up to the required order. For the topologies with more than one master integrals mentioned above, we chose the basis integrals such, that their Laurent series start at different orders i_0. To be more explicit, the triangle diagram containing a propagator raised to the third power starts at ϵ^0, whereas the other two have double poles ϵ^{-2}. The sunset diagram in which both massive propagators are squared is finite, the other has a single pole ϵ^{-1}. We find, that for this choice of basis integrals, the system of equations for the coefficients $\mathrm{mi}_k^i(x)$ actually becomes triangular. The only reminder from the coupled system is, that we have to compute the expansion coefficients of the coupled integrals by turns, rather than computing all required orders of one integral before proceeding to the next one. The order of the deepest pole i_0 is given by the initial condition: To fix the integration constant in the solution of our first order differential equation, we need to know the solution for a specific value of x. It is described below, how to obtain this. Clearly, we can also read off there, at what order the Laurent series starts.

For every order of every master integral, we have to solve a linear first order differential equation

$$f'(x) = \alpha(x)f(x) + \beta(x), \tag{2.30}$$

where $f(x)$ is the $\mathrm{mi}_k^i(x)$ under consideration and $\alpha(x) = A_k^0(x)$ is the order ϵ^0 term arising in the expansion of $A_k(x)$. The inhomogeneity

$$\beta(x) = \left[\sum_{l<k} B_{kl}(x)\,\mathrm{mi}_l(x)\right]_{\text{order }\epsilon^i} + \sum_{j=1}^{\infty} A_k^j\,\mathrm{mi}_k^{i-j}(x) \tag{2.31}$$

receives contributions from simpler master integrals as well as from lower ordersof $\mathrm{mi}_k(x)$, both already computed. Solving the homogeneous equation $\omega'(x) = \alpha(x)\omega(x)$ is straightforward in all cases encountered. The ansatz $f(x) = \omega(x)\,g(x)$, sometimes called variation of constant

method, then leads to the integral representation

$$f(x) = \omega(x) \int_1^x dy \, \frac{\beta(y)}{\omega(y)} + C\omega(x). \tag{2.32}$$

The lower integration limit 1 can of course by replaced by an arbitrary value, as this corresponds to a change of the integration constant C. In practice, however, 1 was a very convenient choice, usually leading to a vanishing integration constant $C = 0$. On the other hand, the obvious choice of setting the integration limit to 0 is impractical, since the integral will often diverge at 0, requiring the use of a regulator until the divergence is cancelled by a divergent integration constant C.

The key point is now, that it was always possible to write the integrations occurring in eq. (2.32) as integrations against a kernel $1/x$, $1/(1-x)$ or $1/(1+x)$. Therefore the solutions can be written in terms of harmonic polylogarithms. A definition of HPLs is given in appendix C

Integration could be accomplished as follows. We prepare the integrand in three steps:

1. Get rid of possible products of HPLs in the inhomogeneity $\beta(x)$. They can be expressed as sums of HPLs of higher weight using the HPL product algebra eq. (C.10). The Mathematica package HPL [38] provides the function `HPLProductExpand` for this purpose.

2. Use partial fractioning to simplify the rational functions appearing in $\beta(y)/\omega(y)$ and make a list of all partial fractions.

3. Last, every element of the obtained list, i.e. every partial fraction, possibly accompanied by a single HPL is wrapped into symbol `int[1,x][expr]`, signaling that it has to be integrated from 1 to x.

Then we repeatedly apply the following transformation rules

1. In cases where the integrand contains no HPL, we let Mathematica perform the integration, and wrap the result into a symbol `done`, signaling, that this part needs no further treatment i.e.
   `int[1,x][expr_] :> done[Integrate[expr,{y,1,x}]]/;FreeQ[expr,HPL[__]]`.

2. HPLs over a y^2 denominator can be integrated by parts

$$\int_1^x dy \frac{\mathrm{HPL}(a_1, \vec{a}; y)}{y^2} = -\frac{\mathrm{HPL}(a_1, \vec{a}; x)}{x} + \mathrm{HPL}(a_1, \vec{a}; 1) + \int_1^x dy \frac{\mathrm{HPL}'(a_1, \vec{a}; y)}{y}, \tag{2.33}$$

   where we have split the indices into a_1 and the remaining indices $\vec{a}$. The derivative of the HPL on the right hand side of course produces a HPL of lower weight $\mathrm{HPL}(\vec{a}, y)$ times a kernel $\frac{1}{y}$, $\frac{1}{1+y}$ or $\frac{1}{1-y}$ for $a_1 = 0$, -1 or 1 respectively. So, for $a_1 = 0$, the kernel $\frac{1}{y}$ combines with the already factor $\frac{1}{y}$ already present to give $\frac{1}{y^2}$ again. But since the weight of the HPL has reduced, we have moved one step forward anyway. For $a_1 = \pm 1$

we can use partial fractioning to get linear denominators. So

$$\int_1^x dy \frac{\mathrm{HPL}'(0,\vec{a};y)}{y} = \int_1^x dy \frac{\mathrm{HPL}(\vec{a};y)}{y^2} \tag{2.34}$$

$$\int_1^x dy \frac{\mathrm{HPL}'(-1,\vec{a};y)}{y} = \int_1^x dy \frac{\mathrm{HPL}(\vec{a};y)}{y} + \int_1^x dy \frac{-\mathrm{HPL}(\vec{a};y)}{1+y} \tag{2.35}$$

$$\int_1^x dy \frac{\mathrm{HPL}'(1,\vec{a};y)}{y} = \int_1^x dy \frac{\mathrm{HPL}(\vec{a};y)}{y} + \int_1^x dy \frac{\mathrm{HPL}(\vec{a};y)}{1-y} \tag{2.36}$$

The boundary terms are integrated, so we flag them with `done`[].

3. HPLs with all indices zero do not fit into the general recursive definition scheme, using integrations from zero

$$\mathrm{HPL}(a_1,\vec{a};x) = \int_0^x dy\; g_{a_1}(y)\,\mathrm{HPL}(\vec{a};y). \tag{2.37}$$

Instead

$$\mathrm{HPL}(\,^n0;x) = \tfrac{1}{n!}\log^n x, \tag{2.38}$$

where $^n0$ denotes a sequence of n zeros, and thus, mind the integration limits,

$$\int_1^x dy\; \frac{\mathrm{HPL}(\,^n0;y)}{y} = \mathrm{HPL}(\,^{n+1}0;x). \tag{2.39}$$

We should exploit this before moving to integration limit zero in rule 4 in order not to produce singular objects. Thus[3]
`int[1, x][c_. HPL[{w : (0)..}, y]/y] :> done[c HPL[{0, w}, x]]/; FreeQ[c, y]`

4. Now we rewrite integrals with lower integration limits 1 as a sum of integrals with lower integration boundary 0
`int[1, x_][f_] :> Sequence[int[0, x][f], int[0, 1][-f]]`

5. Pure integrals of HPLs can again be integrated by parts.

$$\int_0^x dy\; \mathrm{HPL}(a_1,\vec{a};y) = x\,\mathrm{HPL}(a_1,\vec{a};x) - \int_0^x dy\; y\,\mathrm{HPL}'(a_1,\vec{a};y) \tag{2.40}$$

The factor y on the right hand side combines with the kernel produced by the derivative to give

$$\frac{y}{y} = 1 \qquad \frac{y}{1+y} = 1 - \frac{1}{1+y} \quad \text{or} \quad \frac{y}{1-y} = -1 + \frac{1}{1-y},$$

depending on a_1. We can catch all three cases with the compact notation

$$\int_0^x dy\; \mathrm{HPL}(a_1,\vec{a};y) = (x-a_1)\,\mathrm{HPL}(a_1,\vec{a};x) + \mathrm{sgn}(a_1-\tfrac{1}{2}) \int_0^x dy\; \mathrm{HPL}(\vec{a};y). \tag{2.41}$$

[3]The expression `w : obj` represents the pattern object `obj`, assigned the name `w`. The two dots stand for "repeated". I.e. the given pattern will match any sequence of zeros and assign it the name `w`
`c_.` matches an optional factor. The form `c : _.` is equivalent

6. Finally, we need the very definition of HPLs of higher weights
   `int[0,x][c_. HPL[{w__},y]/(y)] :> done[c HPL[{0,w},x]]/;FreeQ[c,y]`
   `int[0,x][c_. HPL[{w__},y]/(1+y)] :> done[c HPL[{-1,w},x]]/;FreeQ[c,y]`
   `int[0,x][c_. HPL[{w__},y]/(y-1)] :> done[c(-1) HPL[{1,w},x]]/;FreeQ[c,y]`

At every step, the above rules are tried in the given order. The first rule, that matches, gets applied. With this, the step finishes; no further rules are tried. In the next step, rules are again tried starting from the first one. This way of of applying rules is precisely what one gets by application of the `ReplaceRepeated` operator[4] //. in Mathematica, i.e. `ListOfExpressions //. ListOfRules`

The above rules were almost sufficient to integrate the differential equations for all master integrals in figure 2.5. A minor complication arising for some integrals is the occurrence of logarithmic divergences. Such divergences always come in combinations, that eventually cancel. However, if they are contained in HPLs with different indices, the cancellation is not necessarily explicit. To fix this we use a regulator instead of a plain 1 as the lower integration limit in eq. (2.32) and thus in the above integration rules. After integration we extract the singular behavior of HPLs and collect the singular pieces to make the cancellation explicit. After that, the regulator can be removed. HPLs whose index vector contains n zeros at the right end behave like $\sim \log^n(x)$. Such with n ones at the left end like $\sim \log^n(1-x)$. A factor $\log(1-x)$, or $-\,\mathrm{HPL}(1;x)$ in terms of HPLs, can be extracted from $\mathrm{HPL}(1, a_1, \ldots a_k; x)$ by using the product relation (C.10)

$$\begin{aligned}\mathrm{HPL}(1;x)\,\mathrm{HPL}(a_1,\ldots a_k;x) = \\ \mathrm{HPL}(1,a_1,\ldots a_k;x) + \mathrm{HPL}(a_1,1,a_2,\ldots a_k;x) + \ldots + \mathrm{HPL}(a_1,\ldots a_k,1;x)\end{aligned} \quad (2.42)$$

and solving for $\mathrm{HPL}(1, a_1, \ldots a_k; x)$. Clearly, by recursive application of this procedure, every HPL can be expressed in terms of explicit $\mathrm{HPL}(1;x)$ and $\mathrm{HPL}(0,x)$ as well as HPLs without left ones and right zeros. Such HPLs are regular at 0 and 1. The Mathematica package `HPL` provides the function `HPLLogExtract` precisely for this purpose.

In general the application dictates to what order in ϵ the master integrals are required. $\mathcal{O}(\epsilon^0)$ is not always sufficient. Some limits are already given by the system of differential equations, in the sense that $B_{kl}(x)$ in eq. (2.28) can contain negative powers of ϵ, meaning that in order to compute a master integral to a given order, knowledge of some of the simpler ones to higher order may be necessary. We took a pragmatic approach and just computed all master integrals up to the order, at which HPLs with weight four appeared. For the most complicated diagrams this was $\mathcal{O}(\epsilon^0)$.

2.2.2 Boundary Conditions

To fully determine the solution of the differential equations we have to fix the integration constant C. This requires the value of the master integrals at a certain kinematic point. The $x \to 1$ limit is especially easy to obtain, as it corresponds to vanishing external momenta or $s \to 0$. The answer can always be written in terms of Γ functions. Instead of calculating

[4]The `ReplaceRepeated` operator //. just applies the `ReplaceAll` operator /. repeatedly, until a fixed point is reached. `ReplaceAll`, when used with a list of rules, i.e. `expr /. ListOfRules`, it transforms the first part of `expr` by applying the first rule, that matches. It then moves on to the next part of `expr`. Thus a part of `expr` gets transformed only once by a single application of /. `ListOfRules`. In our case, `expr` is a list and "part" is equivalent to list entry, as all our rules are formulated to match whole list entries only.

it for each case separately, one can observe, that for vanishing external momenta all non-factorizable master integrals $\mathrm{MI}^{(\mathrm{NF})}$ collapse to a vacuum sunset diagram with extra powers of propagators:

$$\lim_{x\to 1} \mathrm{MI}^{(\mathrm{NF})} = \quad .$$

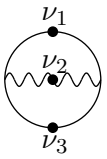

(2.43)

The exponent ν_2 corresponds to the number of massless propagators in the integral whereas $\nu_1 + \nu_3$ is the number of massive propagators. The diagram can be evaluated for arbitrary powers ν_1, ν_2, ν_3, one finds

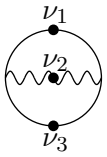

$$= (-1)^{\nu_{123}}\, m^{2\,(d-\nu_{123})} \frac{\Gamma\left(\nu_{123}-d\right)\Gamma\left(\nu_{12}-\frac{d}{2}\right)\Gamma\left(\nu_{23}-\frac{d}{2}\right)\Gamma\left(\frac{d}{2}-\nu_2\right)}{\Gamma(\nu_1)\Gamma(\nu_3)\Gamma\left(\frac{d}{2}\right)\Gamma\left(\nu_{13}+2\,\nu_2-d\right)} \,. \tag{2.44}$$

We have observed, that the homogeneous solutions of the differential equations usually diverge for $x \to 1$. Therefore, the information, taken for instance from (2.44), that the full solution should be finite, is already sufficient to fix the integration constant. It is then an additional consistency check, that the actual finite value obtained by fixing the constant this way is indeed the one required by eq. (2.44).

In one master integral the $x \to 1$ limit does not commute with the expansion around $\epsilon = 0$ due to a collinear singularity as s vanishes. For this master integral we have used the massless limit $x \to 0$, which is well behaved:

$$\lim_{x\to 0} \quad = \quad , \tag{2.45}$$

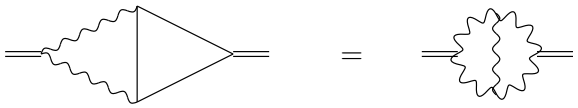

with

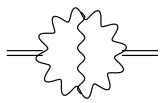

$$= (-s)^{-1-2\,\epsilon} \left(\frac{\Gamma(1+\epsilon)}{(1-\epsilon)}\right)^2 \left(-6\,\zeta(3) - \epsilon\,\frac{\pi^4}{10} + \mathcal{O}\left(\epsilon^2\right)\right) \tag{2.46}$$

2.2.3 Results for Master Integrals

In this section we give results for the most complicated master integrals. Eq. (2.50ff) and eq. (2.57ff) are new results. Expressions for the rest of the master integrals are given in appendix D, as they are rather lengthy.

The results are given in terms of HPLs with argument x. Without worrying about analytic continuation they can therefore be evaluated for $x \in (0, 1]$, what corresponds to the Euclidean region. Analytic continuation to $x \in [-1, 0)$, that is to the physical region above threshold, through the upper half plane is simple. For HPLs, whose rightmost index is nonzero, there is

no cut and the relation

$$\mathrm{HPL}(\vec{a};-x) = (-1)^{n_1+n_{-1}}\,\mathrm{HPL}(-\vec{a};x) \tag{2.47}$$

holds[5] . Here n_1 is the number of 1, and n_{-1} is the number of -1 in the index vector $\vec{a}$. For HPLs with zeros at the right end of the index vector one has to extract all factors of $\mathrm{HPL}(0;x)$ using the product algebra and use the fact, that $\mathrm{HPL}(0;x) = \log x$, so

$$\mathrm{HPL}(0,-x+i\delta) = \mathrm{HPL}(0;x) + i\pi. \tag{2.49}$$

Again, the Mathematica package `HPL` provides a routine for this:
`HPLAnalyticContinuation[expr, AnalyticContinuationRegion->m1to0,`
`AnalyticContinuationSign->1]` . For the Standard Model $gg \to h$ amplitude, assuming a Higgs boson mass smaller than $2\,m_{\rm top}$, we need the physical region below threshold. In this region x is a complex phase as shown in figure 2.6. In [44] we gave expressions for all 17 master integrals in this kinematical region in terms of Cl_1, $\mathrm{Ls}_j^{(k)}$, $\mathrm{Lsc}_{i,j}$, and $\mathrm{LsLsc}_{n,i,j}$ functions [20, 43, 42]. However, this is no longer necessary, as in the meantime implementations of HPLs for arbitrary complex arguments became available[6] for Mathematica in `HPL 2.0`, see [39], and C++ within the GiNaC framework [41].

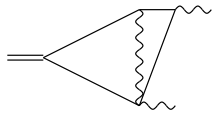

$$\begin{aligned} &= \int\frac{d^dk}{i\pi^{d/2}}\int\frac{d^dl}{i\pi^{d/2}}\frac{1}{D_{22}D_{23}D_{24}D_{26}D_{27}} \\ &= \left(\frac{\Gamma(1+\epsilon)}{1-\epsilon}\right)^2 (m^2)^{-2\epsilon-1}F_7^0(x) + \mathcal{O}(\epsilon^1) \end{aligned} \tag{2.50}$$

$$\begin{aligned} F_7^0(x) \;=\; & \frac{1}{(1-x)^2}\Big\{ -\frac{1}{6}\pi^2 H(0,0;x)x - \frac{1}{3}\pi^2 H(1,0;x)x - \frac{\pi^4 x}{36} \\ & - xH(0,0,1,0;x) - 2xH(1,0,1,0;x) - 2xH(0,1,0,0;x) - 3xH(1,0,0,0;x) \\ & - 4xH(1,1,0,0;x)\Big\} \end{aligned} \tag{2.51}$$

[5] In the abbreviated "m"-notation, this formula reads

$$\mathrm{HPL}(\{m_1,\ldots m_k\};-x) = (-1)^k\,\mathrm{HPL}(\{-m_1,\ldots -m_k\};x). \tag{2.48}$$

[6] The GiNaC implementation [41] appeared already in 2004, however it contained bugs, that were fixed with the appearance of [39] only.

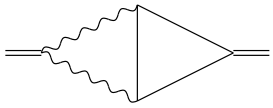

$$= \int \frac{d^dk}{i\pi^{d/2}} \int \frac{d^dl}{i\pi^{d/2}} \frac{1}{D_{11}D_{13}D_{14}D_{16}D_{17}}$$
$$= \left(\frac{\Gamma(1+\epsilon)}{1-\epsilon}\right)^2 (m^2)^{-2\epsilon-1} \sum_{i=0}^{1} \epsilon^i F_8^i(x) + \mathcal{O}(\epsilon^2) \tag{2.52}$$

$$F_8^0(x) = \frac{x}{(1-x)^2}\Big\{ -2H(0,0,1;x) - 2H(0,1,0;x) + 4H(1,0,0;x) - 6\zeta(3)\Big\} \tag{2.53}$$

$$\begin{aligned} F_8^1(x) = \frac{x}{(1-x)^2}\Big\{ & -12\zeta(3)H(0;x) + \frac{1}{3}\pi^2 H(0,1;x) - 24H(1;x)\zeta(3) - \frac{\pi^4}{10} \\ & - 8H(0,0,0,1;x) - 10H(0,0,-1,0;x) + 4H(0,-1,0,1;x) - \frac{2}{3}\pi^2 H(1,0;x) \\ & - 4H(1,0,0,1;x) - 4H(0,1,0,1;x) - 4H(0,0,1,0;x) - 4H(0,0,1,1;x) + 4H(0,-1,0,0;x) \\ & + 4H(0,-1,1,0;x) - 24H(1,0,-1,0;x) + 4H(1,0,1,0;x) + 4H(0,1,-1,0;x) \\ & - 6H(0,1,0,0;x) - 4H(0,1,1,0;x) + 12H(1,0,0,0;x)\Big\} \end{aligned} \tag{2.54}$$

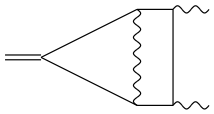

$$= \int \frac{d^dk}{i\pi^{d/2}} \int \frac{d^dl}{i\pi^{d/2}} \frac{1}{D_{21}D_{23}D_{24}D_{25}D_{26}D_{27}}$$
$$= \left(\frac{\Gamma(1+\epsilon)}{1-\epsilon}\right)^2 (m^2)^{-2\epsilon-2} F_9^0(x) + \mathcal{O}(\epsilon^1) \tag{2.55}$$

$$\begin{aligned} F_9^0(x) = \frac{x^2}{(1-x)^3(x+1)}\Big\{ & 8\zeta(3)H(0;x) + 16H(0,0,-1,0;x) + \frac{\pi^4}{10} \\ & + \frac{2}{3}\pi^2 H(0,0;x) - 4H(0,0,1,0;x) - 8H(0,-1,0,0;x) + 14H(0,1,0,0;x) \\ & + H(0,0,0,0;x)\Big\} \end{aligned} \tag{2.56}$$

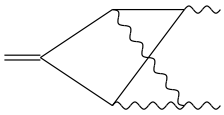

$$= \int \frac{d^dk}{i\pi^{d/2}} \int \frac{d^dl}{i\pi^{d/2}} \frac{1}{D_{31}D_{32}D_{33}D_{34}D_{35}D_{37}}$$
$$= \left(\frac{\Gamma(1+\epsilon)}{1-\epsilon}\right)^2 (m^2)^{-2\epsilon-2} \sum_{i=-1}^{0} \epsilon^i F_{10}^i(x) + \mathcal{O}(\epsilon^1) \tag{2.57}$$

$$F_{10}^{-1}(x) = \frac{x^2}{(1-x)^4}\Big\{ -\frac{2}{3}\pi^2 H(0;x) - 8H(0,-1,0;x) + 4H(0,0,0;x) - 12\zeta(3)\Big\} \qquad (2.58)$$

$$\begin{aligned} F_{10}^{0}(x) = {} & \frac{x^2}{(1-x)^4}\Big\{\frac{8}{3}\pi^2 H(0,-1;x) + 24\zeta(3) - \frac{16\pi^4}{45} \\ & + \frac{4}{3}\left(\pi^2 - 33\zeta(3)\right) H(0;x) - \frac{4}{3}\pi^2 H(0,1;x) - 48H(1;x)\zeta(3) \\ & - 56H(0,0,-1,0;x) + 16H(0,-1,0;x) - \frac{10}{3}\pi^2 H(0,0;x) - \frac{8}{3}\pi^2 H(1,0;x) \\ & + 8H(0,0,1,0;x) + 64H(0,-1,-1,0;x) - 40H(0,-1,0,0;x) - 16H(0,-1,1,0;x) \\ & - 8H(0,0,0;x) - 32H(1,0,-1,0;x) - 16H(0,1,-1,0;x) + 8H(0,1,0,0;x) \\ & + 12H(0,0,0,0;x) + 16H(1,0,0,0;x)\Big\} \end{aligned} \qquad (2.59)$$

2.2.4 Amplitudes in terms of HPLs

The dimensionless functions $c^{(i)}(x)$ are

$$\begin{aligned} c_{\rm f}^{(0)}(x) = & -\frac{2x\left((x+1)^2 H(0,x)^2 - 4(x-1)^2\right)}{(x-1)^4} + \\ & \frac{1}{(1-x)^4}\Bigg[-\frac{2}{3}x\Big((x+1)^2 H(0,x)^3 + 12xH(0,x)^2 \\ & - (x+1)\Big(\pi^2 x - 12x + 12(x+1)H(0,-1,x) + \pi^2 + 12\Big)H(0,x) \\ & + 6\left(4(x+1)^2 H(0,0,-1,x) - 3\left((2+\zeta(3))x^2 + 2(-2+\zeta(3))x + \zeta(3) + 2\right)\right)\Bigg]\epsilon \\ & + \frac{1}{18(1-x)^4}\Bigg[x\Big(-3(x+1)^2 H(0,x)^4 - 48xH(0,x)^3 + 3\Big(24H(0,-1,x)(x+1)^2 + \\ & \pi^2(x+1)^2 - 24\Big(x^2+2x-1\Big)\Big)H(0,x)^2 + 48\Big(-6H(0,-1,-1,x)x^2 - \\ & 3H(0,0,-1,x)x^2 + 3\zeta(3)x^2 - 9x^2 + 12H(0,-1,x)x - 12H(0,-1,-1,x)x - \\ & 6H(0,0,-1,x)x + 6\zeta(3)x + \pi^2 x + 6\Big(x^2-1\Big)H(-1,x) - 6H(0,-1,-1,x) - \\ & 3H(0,0,-1,x) + 3\zeta(3) + 9\Big)H(0,x) + \pi^4 x^2 + 36\pi^2 x^2 + 1008x^2 + \\ & 144(x+1)^2 H(0,-1,x)^2 + 2\pi^4 x - 24\pi^2 x - 2016x - \\ & 24(x+1)\Big(12(x-1) + \pi^2(x+1)\Big)H(0,-1,x) - 1152xH(0,0,-1,x) + 864x\zeta(3) + \\ & \pi^4 - 12\pi^2 + 1008\Big)\Bigg]\epsilon^2 + \mathcal{O}(\epsilon^3) \end{aligned}$$

$$
\begin{aligned}
c_{\rm s}^{(0)}(x) =& -\frac{2x\Big((x-1)^2 - xH(0,x)^2\Big)}{(x-1)^4} \\
&\frac{1}{(1-x)^4}\Bigg[\frac{2}{3}x\Big(xH(0,x)^3 + 3xH(0,x)^2 - \Big(-3x^2+\pi^2x+3\Big)H(0,x) \\
&- 3\Big(3x^2 + 4H(0,-1,0,x)x + 6\zeta(3)x - 6x + 3\Big)\Big)\Bigg]\epsilon \\
&- \frac{x}{18(1-x)^4}\Bigg[-3xH(0,x)^4 - 12xH(0,x)^3 + 3\Big(-6x^2 + \Big(-12+\pi^2\Big)x \\
&+ 6\Big)H(0,x)^2 + 12\Big(-9x^2 + 12\zeta(3)x + \pi^2x + 6\Big(x^2-1\Big)H(-1,x) + 9\Big)H(0,x) \\
&+ 9\pi^2x^2 + 252x^2 + \pi^4x - 6\pi^2x - 504x - 24\Big(3x^2 + \pi^2x - 3\Big)H(0,-1,x) \\
&+ 144xH(0,-1,0,x) - 288xH(0,-1,-1,0,x) \\
&+ 144xH(0,-1,0,0,x) + 144xH(0,0,-1,0,x) + 216x\zeta(3) - 3\pi^2 + 252\Bigg]\epsilon^2 + \mathcal{O}(\epsilon^3)
\end{aligned}
$$

$$
\begin{aligned}
c_{\rm f}^{(1)}(x) =& \frac{24x\left((x+1)^2H(0,0,x) - 2(x-1)^2\right)}{(x-1)^4}\frac{1}{\epsilon^2} \\
&+ \frac{1}{(1-x)^4}\Bigg[-4x\Big(-24H(0,0,-1,x)(x+1)^2 + H(0,x)\Big(12H(0,-1,x)(x+1)^2 \\
&+ \pi^2(x+1)^2 - 8\Big(x^2+3x-4\Big)\Big) + 2\Big(-12H(0,0,0,x)x^2 + 9\zeta(3)x^2 + 10x^2 \\
&- 24H(0,0,0,x)x + 18\zeta(3)x - 20x + 4\Big(x^2+3x+1\Big)H(0,0,x) \\
&- 6H(1,x)\Big((x+1)^2H(0,0,x) - 2(x-1)^2\Big) - 12H(0,0,0,x) + 9\zeta(3) + 10\Big)\Big)\Bigg]\frac{1}{\epsilon} \\
&+ \frac{1}{45(x-1)^5}\Bigg[x\Big(-8640H(1,1,x)(x-1)^3 - 7200(x+1)H(-1,0,x)(x-1)^2 \\
&+ 1080(x+1)^2H(0,0,x)^2(x-1) + 360(x+1)^2\Big(-6H(0,x)^2 - 12H(1,x)H(0,x) \\
&+ \pi^2\Big)H(0,-1,x)(x-1) - 180(x+1)H(0,x)^2\Big(-20(x-1) + \pi^2(x+1) \\
&+ 6(x+1)H(0,0,x)\Big)(x-1) + 720\Big(3(x+1)^2H(0,0,x) - 2\Big(5x^2-6x+1\Big)\Big) \\
&\times H(0,1,x)(x-1) - 720\Big(\pi^2(x+1)^2 + 2\Big(5x^2-6x+1\Big)\Big)H(1,0,x)(x-1) \\
&+ 960\Big(7x^2+17x+7\Big)H(0,-1,0,x)(x-1) + 8640(x+1)^2H(1,x)H(0,0,-1,x) \\
&\times (x-1) + 2880\Big(x^2+6x+1\Big)H(0,0,1,x)(x-1) + 1920\Big(x^2+8x+1\Big)H(0,1,0,x)
\end{aligned}
$$

$$
\begin{aligned}
&\times (x-1) + 240\Big(59x^2 + 138x + 59\Big)H(1,0,0,x)(x-1) + 4320(x+1)^2 \\
&\times H(0,-1,-1,0,x)(x-1) + 8640(x+1)^2 H(0,-1,0,1,x)(x-1) \\
&+ 8640(x+1)^2 H(0,-1,1,0,x)(x-1) + 8640(x+1)^2 H(0,1,-1,0,x)(x-1) \\
&+ 4320(x+1)^2 H(1,0,0,0,x)(x-1) - 720H(1,x)\Big(12H(0,-1,0,x)(x+1)^2 \\
&+ 4\Big(x^2 + 3x + 1\Big)H(0,0,x) - 3\Big(4(x+1)^2 H(0,0,0,x) - 3\Big((2+3\zeta(3))x^2 \\
&+ (-4+6\zeta(3))x + 3\zeta(3) + 2\Big)\Big)\Big)(x-1) + 20H(0,0,x)\Big(-150x^3 - 822x^2 \\
&+ 750x - \pi^2\Big(43x^3 + 43x^2 - 11x - 11\Big) + 108(x-1)(x+1)^2 H(1,0,x) \\
&+ 216(x-1)(x+1)^2 H(1,1,x) + 222\Big) + 240\Big(45x^3 + 136x^2 - 19x - 6\Big)H(0,0,0,x) \\
&+ 240\Big(7x^3 + 7x^2 + 25x + 25\Big)H(0,-1,0,0,x) + 480\Big(7x^3 + 7x^2 + 25x + 25\Big) \\
&\times H(0,0,-1,0,x) + 720\Big(73x^3 + 73x^2 + 55x + 55\Big)H(0,0,0,-1,x) \\
&- 480\Big(x^3 + x^2 + x + 1\Big)H(0,0,0,0,x) + 1920\Big(x^3 + x^2 + x + 1\Big)H(0,0,1,0,x) \\
&- 6720\Big(x^3 + x^2 + x + 1\Big)H(0,1,0,0,x) - 3\Big(200\pi^2(x+1)(x-1)^2 \\
&+ 80\Big((-36+13\zeta(3))x^2 + (72-20\zeta(3))x + 13\zeta(3) - 36\Big)(x-1) + \pi^4\Big(53x^3 \\
&+ 53x^2 - 21x - 21\Big)\Big) + 40H(0,x)\Big(108(x-1)H(0,0,0,x)(x+1)^2 - 9(x-1) \\
&\times H(1,x)\Big(-20(x-1) + \pi^2(x+1) + 6(x+1)H(0,0,x)\Big)(x+1) + 2\pi^2\Big(5x^3 \\
&+ 8x^2 - 8x - 5\Big) - 36(x-1)\Big(x^2 + 3x + 1\Big)H(0,0,x) - 6\Big(55x^3 + 55x^2 + 73x \\
&+ 73\Big)H(0,0,-1,x) + 3\Big(-(32+131\zeta(3))x^3 + (140-131\zeta(3))x^2 + (-184 \\
&+ 67\zeta(3))x + 67\zeta(3) + 76\Big)\Big)\Big)\Big] + \mathcal{O}(\epsilon)
\end{aligned}
$$

$$
\begin{aligned}
c_{\rm s}^{(1)}(x) =& \frac{12x\left((x-1)^2 - 2xH(0,0,x)\right)}{(x-1)^4}\frac{1}{\epsilon^2} \\
&+ \frac{1}{(x-1)^4(x+1)}\Bigg[4x\Big(H(0,x)\Big(\pi^2x^2 - 10x^2 - 36(x+1)H(0,-1,x)x \\
&+ 24(x+1)H(0,1,x)x + \pi^2x + 4x + 6\Big) + 72x(x+1)H(0,0,-1,x) + (x+1) \\
&\times \Big(7x^2 + 2H(0,0,x)x + 48H(0,-1,0,x)x - 24H(0,0,0,x)x - 48H(0,0,1,x)x \\
&- 24H(0,1,0,x)x + 18\zeta(3)x - 14x + 6H(1,x)\Big((x-1)^2 - 2xH(0,0,x)\Big) + 7\Big)\Big)\Bigg]\frac{1}{\epsilon} \\
&+ \frac{1}{45(x-1)^5}\Bigg[x\Big(2160H(1,1,x)(x-1)^3 + 8640xH(0,1,x)^2(x-1) + 1080
\end{aligned}
$$

$$\times \Big(\Big(-2+\pi^2\Big)x+2\Big)H(1,0,x)(x-1)-360xH(0,-1,x)\Big(36H(0,0,x)$$
$$+36H(0,1,x)+36H(1,0,x)+\pi^2\Big)(x-1)+360H(0,1,x)\Big(6H(0,0,x)x$$
$$+24H(1,0,x)x+\pi^2x-6x+6\Big)(x-1)-4560xH(0,-1,0,x)(x-1)$$
$$-2160xH(0,0,1,x)(x-1)-1200xH(0,1,0,x)(x-1)-11760xH(1,0,0,x)(x-1)$$
$$-4320xH(0,-1,-1,0,x)(x-1)+17280xH(0,-1,0,1,x)(x-1)+17280x$$
$$\times H(0,-1,1,0,x)(x-1)+25920xH(0,0,-1,1,x)(x-1)+38880x$$
$$\times H(0,0,0,-1,x)(x-1)-15120xH(0,0,0,1,x)(x-1)+25920xH(0,0,1,-1,x)$$
$$\times (x-1)-38880xH(0,0,1,1,x)(x-1)+17280xH(0,1,-1,0,x)(x-1)+25920x$$
$$\times H(0,1,0,-1,x)(x-1)-30240xH(0,1,0,1,x)(x-1)-21600xH(0,1,1,0,x)$$
$$\times (x-1)+25920xH(1,0,-1,0,x)(x-1)+25920xH(1,0,0,-1,x)(x-1)$$
$$-19440xH(1,0,0,0,x)(x-1)-21600xH(1,0,0,1,x)(x-1)-12960x$$
$$\times H(1,0,1,0,x)(x-1)-4320xH(1,1,0,0,x)(x-1)+3240H(1,x)\Big(x^2+(-2$$
$$+6\zeta(3))x+1\Big)(x-1)-120x(65x-23)H(0,0,0,x)\Big)$$
$$+\frac{1}{x+1}\Bigg[x\Big(360\Big(3x^2+10x+3\Big)H(-1,0,x)(x-1)^2-20H(0,0,x)\Big(54x^4-\Big(150$$
$$+61\pi^2\Big)x^3-234x^2-108\Big(x^2-1\Big)H(1,0,x)x+\Big(222+29\pi^2\Big)x+108\Big)+240x$$
$$\times \Big(65x^2-97\Big)H(0,-1,0,0,x)+240x\Big(185x^2-121\Big)H(0,0,-1,0,x)-240x$$
$$\times \Big(43x^2-47\Big)H(0,0,0,0,x)-240x\Big(71x^2-55\Big)H(0,0,1,0,x)-1680x\Big(5x^2-13\Big)$$
$$\times H(0,1,0,0,x)+20H(0,x)\Big(36x^4+\Big(-246-11\pi^2+786\zeta(3)\Big)x^3+258x^2+\Big(78$$
$$+11\pi^2-402\zeta(3)\Big)x-126\Big)+3\Big(10\pi^2\Big(3x^2+10x+3\Big)(x-1)^2+\pi^4x\Big(53x^2-21\Big)$$
$$-40\Big(x^2-1\Big)\Big(5x^2-(10+39\zeta(3))x+5\Big)\Big)\Big)\Bigg]\Bigg]+\mathcal{O}(\epsilon).$$

Chapter 3

Numerical Approach

3.1 Overview of the Problem

A main challenge in computing Feynman diagrams is the evaluation of integrals over loop momenta. For multi-loop diagrams containing several mass scales we cannot realistically hope for an analytic solution; we are forced to resort to numerical integration.

Two main main issues usually impede straightforward numerical integration:

3.1.1 IR and UV singularities

Feynman diagrams are often plagued by ultraviolet and infrared divergences. The former can be absorbed into an unobservable shift in the parameters of the theory – a procedure known as renormalization. The latter cancel against divergences occurring in the integration over unobserved soft radiation processes, which have to be considered when calculating physical observables.

In analytical calculations it is common practice to introduce regulators that render integrals finite. After assembling all pieces of a physical quantity the singular dependence on the regulator cancels out and so the regulator can be dropped.

The above procedure relies on knowing the regulator dependence analytically (to a certain extent). So it might seem, that it is not applicable in the context of numerical integration. Numerical approaches use local subtractions in order to render loop diagrams finite.

For IR singularities those subtractions were usually designed such, that summing up all subtractions applied in the calculation of a whole amplitude resulted in a simple function, allowing analytic integration.

The UV behavior of one loop diagrams gets captured in Γ functions when the integration over the loop momentum is carried out in a Feynman parameter representation. Alternatively subtractions equivalent to counter-terms appearing in the renormalization procedure have been suggested. For multi loop diagrams, the situation is more complicated, as UV divergences find their way into Feynman parameter representations.

There exists, however, a far more flexible way of dealing with divergences: The sector decomposition algorithm [4, 5, 12] discussed below allows to isolate and extract singularities in Feynman parameter integrals. It is a mathematical tool that works without caring about the physical origin of divergences. It produces a Laurent series in the dimensional regularization parameter ϵ. The coefficients of this expansion are finite integrals. They can be computed up

to the order required by the problem. As one goes to higher orders in ϵ, the integrals usually become more involved[1].

3.1.2 Thresholds

For physical values of the kinematical invariants there may be values of four momenta flowing in the loops, that put virtual particles onto their mass shell. In this case, the "$i\delta$-prescription" appearing in propagators,

$$\frac{1}{p^2 - m^2 + i\delta},$$

tells us, how the integration should circumvent the pole. Quantum field theory instructs us to carry out integrations over loop momenta keeping $\delta > 0$ and to take the limit $\delta \to 0^+$ afterwards. It is important to note, that unlike in the IR problem, we are not dealing with a divergence here. While the integral might have a *discontinuity* in the imaginary part at $\delta = 0$, the limit $\delta \to 0^+$ is finite. As an illustration, we can consider the simple example of a scalar bubble diagram with equal masses and one propagator squared:

$$\lim_{\delta\to 0^+} \int \frac{d^4\ell}{(2\pi)^4} \frac{1}{[\ell^2 - m^2 + i\delta]^2[(\ell+q)^2 - m^2 + i\delta]}.$$

The integral is free of UV and IR divergences and can therefor be evaluated in four dimensions. Introducing a Feynman parameter and carrying out the loop momentum leads to (dropping prefactors)

$$\lim_{\delta\to 0^+} \int_0^1 dx \frac{x}{x(1-x)q^2 - m^2 + i\delta}. \tag{3.1}$$

Close to the zeros of the denominator we are roughly dealing with an integration of the form

$$\lim_{\delta\to 0^+} \int_{-1}^1 dx \frac{f(x)}{x + i\delta}.$$

For analytic functions $f(x)$ this is the same as

$$\int_{C(r)} dz \frac{f(z)}{z}$$

along the contour $C(r)$ depicted in figure 3.1. By virtue of Cauchy's theorem the radius r is arbitrary. In the limit $r \to 0$ the integral over the half circle contributes $-i\pi f(0)$, whereas the rest of the contour gives a principle value. With fewer words

$$\frac{1}{x + i0} = \mathrm{PV}\frac{1}{x} - i\pi\delta(x). \tag{3.2}$$

In analytic calculations one usually evaluates integrals in parameter regions, where the denominator has a definite sign, e.g. $q^2 < 0$ and $m^2 > 0$ in the above example. After integrations one can analytically continue the result to physical values of the parameters. In the above

[1]Note, that also with traditional subtraction methods terms of order ϵ^n, $n > 0$ do not come for free: While the integrated sum of subtractions is usually known to all orders in ϵ, in the subtracted integral one has to set $\epsilon = 0$ before integration. To compute higher order terms one would have to do a series expansion under the integral.

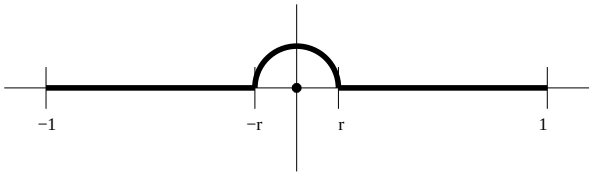

Figure 3.1: Integration contour $C(r)$.

example a discontinuity appears for $q^2 > 4m^2$. We can read off the denominator of expression (3.1), that the pole is circumvented in the correct way, if we integrate along the real axis, but shift the kinematical invariants $q^2 \to q^2 + i\delta$ or $m^2 \to m^2 - i\delta$. This tells us, to which side of the cut we have to analytically continue our answer.

In a numerical calculation analytic continuation is not possible. Nagy and Soper [57] suggested to deform the integration contour into the complex domain. This way the pole can be circumvented at a finite distance and stable numerical integration can be achieved for physical values of the kinematic parameters.

The details of the deformation will be discussed later. One interesting thing can already be observed here, however: Let us denote the integrand occurring in expression (3.1) by $\mathcal{I}$. (Replace $+i\delta$ by $+i0$, a reminder, that the poles should be circumvented via the upper half plane.) The analyticity properties of $\mathcal{I}$ make sure we can deform the integration contour into the upper half plane in whatever form we wish without changing the value of

$$\int_C \mathcal{I} dz \quad \text{and thus} \quad \int_C \mathrm{Re}\left\{\mathcal{I} dz\right\} \quad \text{and} \quad \int_C \mathrm{Im}\left\{\mathcal{I} dz\right\}.$$

On the other hand, the values of

$$\int_C |\,\mathrm{Re}\left\{\mathcal{I} dz\right\}\,| \quad \text{and} \quad \int_C |\,\mathrm{Im}\left\{\mathcal{I} dz\right\}\,|$$

do in general depend on the contour, as the modulus is not an analytic function[2]. The meaning of this is, that the contour independent value of the integral arises as the difference between positive and negative contributions, which do depend on the contour. Thus by tuning the contour we have a handle on the amount of cancellation occurring in the calculation of the integral. Or stated differently, the integral of the modulus measures the quality of the deformation. In the limit where the contour approaches the real axis, the integral approaches the case, where it is only defined as a principle value. Needless to say, that the amount of cancellation has a huge impact on the stability of numerical integration.

3.2 Feynman Parameters

Raw Feynman diagrams have a difficult singularity structure. It is hard to construct an integration contour, that correctly treats the intersecting surfaces on which propagators van-

[2]The weird notation with dz inside Re or Im can of course be avoided by parametrizing the contour over the real interval [0,1], leading to

$$\int_0^1 \mathrm{Re}\left\{\mathcal{I}(z(x))\frac{\partial z}{\partial x}\right\} dx.$$

ish. Soper managed to compute the $e^+e^- \to 3$ jets cross section at NLO by combining real and virtual contributions at the integrand level and performing direct numerical integration [54, 55]. But in general it seems that Feynman parameters do a good job casting the singularity structure into a form that eases its treatment. They proved useful even in case without the intention of integrating out the loop momentum analytically [58].

The method described here heavily depends on Feynman parametrization. We give some details here as, at least for the multi loop case, there are several viable ways of parametrizing a diagram.

3.2.1 Standard Parametrization at one-loop

Feynman parametrization relies on the well known formula

$$\frac{1}{d_1^{\nu_1} d_2^{\nu_2} \cdots d_n^{\nu_n}} = B(\{\nu_i\}) \int_0^1 d\vec{x}\, \delta\left(1 - \sum x_i\right) \frac{\prod x_i^{\nu_i - 1}}{\left[\sum x_i d_i\right]^{\nu_1 + \cdots + \nu_n}}, \tag{3.3}$$

with

$$B(\{\nu_i\}) = \frac{\Gamma(\nu_1 + \cdots + \nu_n)}{\Gamma(\nu_1) \cdots \Gamma(\nu_n)}$$

which is valid also for non-integer ν_i.

For a one-loop diagram

$$I_{\text{1-loop}} = \int \frac{d^d k}{(2\pi)^d} \frac{\mathcal{N}(k)}{[(k+q_1)^2 - m_1^2 + i0]^{\nu_1} \cdots [(k+q_n)^2 - m_n^2 + i0]^{\nu_n}}, \tag{3.4}$$

there is not much to discuss. As every denominator D_i contains the one and only loop momentum k with coefficient one and $\sum x_i = 1$, the combined denominator has the form $k^2 + 2k \cdot P - \tilde{\Lambda}$. By completing the square and then introducing a shifted integration variable $K = k + P$, one arrives at

$$I_{\text{1-loop}} = B(\{\nu_i\}) \int_0^1 d\vec{x}\, \delta\left(1 - \sum x_i\right) \prod x_i^{\nu_i - 1} \int \frac{d^d K}{(2\pi)^d} \frac{\mathcal{N}(k = K - P)}{[K^2 - \Lambda(\vec{x}) + i0]^{\sigma}}, \tag{3.5}$$

with

$$P = \sum_i x_i q_i$$

and

$$\sigma = \sum_i \nu_i.$$

The form of $\Lambda(\vec{x})$ is not unique. The constraint $\sum x_i = 1$ allows us write it as a homogeneous polynomial of second order in x. A convenient representation is

$$\Lambda(\vec{x}) = -\frac{1}{2} \sum_{i,j} x_i x_j S_{ij} \tag{3.6}$$

with

$$S_{ij} = (q_i - q_j)^2 - m_i^2 - m_j^2. \tag{3.7}$$

The denominator in eq. (3.5) depends on K only through K^2. For symmetry reasons, the

numerator $\mathcal{N}(K-P)$ can be replaced by an equivalent one, that only depends K^2 rather than K. The details of this replacement are discussed in section 3.2.3. After this simplification the K integrand can be evaluated using the well known formula from dimensional regularization:

$$\begin{aligned}\int \frac{d^dK}{i\pi^{d/2}} \frac{(K)^m}{[K^2-M^2+i\delta]^\sigma} &= \frac{\Gamma(\frac{d}{2}+\frac{m}{2})}{\Gamma(\frac{d}{2})} \cdot \frac{\Gamma(\sigma-\frac{m}{2}-\frac{d}{2})}{\Gamma(\sigma)} \cdot \frac{(-1+i\delta)^{-\frac{d}{2}}}{[-M^2+i0]^{\sigma-m/2-d/2}} \\ &= \frac{\Gamma(\frac{d}{2}+\frac{m}{2})}{\Gamma(\frac{d}{2})} \cdot \frac{\Gamma(\sigma-\frac{m}{2}-\frac{d}{2})}{\Gamma(\sigma)} \cdot \frac{(-1)^{m/2}(-1+i\delta)^{-\sigma}}{[M^2-i0]^{\sigma-m/2-d/2}},\end{aligned} \tag{3.8}$$

valid for even m. It is derived by performing a Wick rotation and, introducing spherical coordinates and performing the substitution $K^2 = -M^2/(1-t)$. The right hand side is analytic in d. It develops poles at integer values of $d/2$ where the integral diverges, but is meaningful for non-integer dimension like $d = 4-2\epsilon$. In the last expression, a minus sign has been factored out of the denominator. This trades the $(-1+i\delta)^{-d/2}$ for a $(-1+i\delta)^{-\sigma}$, which is convenient, as σ is usually integer and thus one does not have to care about the $i\delta$ there.

3.2.2 Parametrizations at two-loops

A two-loop integral has to form

$$I_{\text{2-loop}} = \int \frac{d^dk}{(2\pi)^d} \frac{d^d\ell}{(2\pi)^d} \frac{\mathcal{N}(k,\ell)}{d_1^{\nu_1} d_2^{\nu_2} \cdots d_n^{\nu_n}} \tag{3.9}$$

with propagators of the form

$$d_i = (\chi_i^k k + \chi_i^\ell \ell + q_i)^2 - m_i^2 \qquad \chi_i^k, \chi_i^\ell \in \{0,1\}, \tag{3.10}$$

or more explicitly (we will use both notations below)

$$\begin{aligned}I_{\text{2-loop}} = \int \frac{d^dk}{(2\pi)^d} \frac{d^d\ell}{(2\pi)^d}\, \mathcal{N}(k,\ell) \prod_{a_i} \frac{1}{[(k+q_{a_i})^2 - m_{a_i}^2]^{\nu_{a_i}}} \times \\ \prod_{b_i} \frac{1}{[(\ell+q_{b_i})^2 - m_{b_i}^2]^{\nu_{b_i}}} \prod_{c_i} \frac{1}{[(k+\ell+q_{c_i})^2 - m_{c_i}^2]^{\nu_{c_i}}}.\end{aligned} \tag{3.11}$$

There is more than one valid strategy for combining all propagators. We spell out two possibilities here. In any case one eventually has to face the complication, that in the combined denominator, squares of loop-momenta no longer appear with coefficient one. Instead, their coefficient is a combination of Feynman parameters. People often just pull the bothersome factor in front k^2 out of the denominator, integrate out k and then proceed the same way with the second loop momentum ℓ. Here we avoid integrating out loop momenta at intermediate steps and rather rescale them. This way the integral is cast into a standard form and the three steps

1. Feynman parametrizing

2. Replacing $K^{\mu_1} \cdots K^{\mu_{2k}}$ tensors by K^{2k} times a combination of metric tensors (see section 3.2.3)

3. Integrating out the loop momenta

are disentangled.

Strategy "at once"

Here we combine all propagators using a single set of Feynman parameters. Then we shift and rescale the loop momenta to reach the standard form of the denominator. The parametrization of eq. (3.9) is then

$$I_{\text{2-loop}}=B(\{\nu_i\})\int_0^1 d\vec{x}\;\delta\,(1-\textstyle\sum x_i)\prod x_i^{\nu_i-1}\;\beta^{\sigma-3d/2}\displaystyle\int\frac{d^dK}{(2\pi)^d}\frac{d^dL}{(2\pi)^d}\frac{\mathcal{N}(k,l)}{[K^2+L^2-\Lambda(\vec{x})]^\sigma}, \tag{3.12}$$

with

$$\begin{aligned}\beta &= ab-c^2\\ \Lambda(\vec{x}) &= ae^2-2c\;d\cdot e-\beta f+bd^2\\ k &= a^{-1/2}\beta^{-1/2}K-a^{-1}P_k\\ \ell &= \beta^{-1}(a^{1/2}L-P_\ell)\\ P_k &= d+c\ell\\ P_\ell &= ae-cd,\end{aligned}$$

where the a, b, c, d, e, f are coefficients of various terms in the combined denominator:

$$\sum_i x_i d_i = ak^2+b\ell^2+2c\;k\cdot\ell+2d\cdot k+2e\cdot\ell+f. \tag{3.13}$$

The parametrization eq. (3.12) remains valid even if we allow for coefficients

$$\chi_i^k,\chi_i^\ell\in\{-1,0,1\}$$

in eq. (3.10). That means we allow propagators like

$$d_i=(k-\ell+q_i)^2-m_i^2 \quad\text{instead of}\quad (k+\ell+q_i)^2-m_i^2.$$

Note that β is a second order polynomial in the Feynman parameters, which does not depend on kinematics. The $\beta^{\sigma-3d/2}$ term can contain UV divergences. The negative powers, that arise when the original loop momenta k and ℓ are expressed through K and L can also contribute to UV divergences. Later we will apply sector decomposition to Feynman parametrized integrals. It will be convenient to divide an integral into a "scalar" part containing all divergences and a regular numerator function, which we call tensor. The tensor is what remains from $\mathcal{N}(k,\ell)$, when k and ℓ are expressed through K and L and the mentioned negative powers are included into the "scalar" part. So keep in mind, that scalar part here does not exactly denote the integral with $\mathcal{N}$ set to one.

Strategy "sunset"

Alternatively we use three independent sets of Feynman parameters to combine propagators containing the same combination of loop momenta. Thus we use x_{a_i} to combine all propaga-

tors containing only k, x_{b_i} to combine those containing only ℓ and finally x_{c_i} for those that contain $k+\ell$. This gives an effective sunset diagram with propagators

$$\frac{1}{[(k+q_A)^2-Q_A^2]^{\sigma_A}}\,\frac{1}{[(\ell+q_B)^2-Q_B^2]^{\sigma_B}}\,\frac{1}{[(k+\ell+q_C)^2-Q_C^2]^{\sigma_C}}, \tag{3.14}$$

with

$$\begin{aligned}
q_A &= \sum_{a_i} x_{a_i} q_{a_i}, \qquad q_B = \sum_{b_i} x_{b_i} q_{b_i}, \qquad q_C = \sum_{c_i} x_{c_i} q_{c_i},\\
Q_A^2 &= \sum_{a_i} x_{a_i} m_{a_i}^2 - \sum_{a_i} \sum_{a_j<a_i} x_{a_i} x_{a_j} (q_{a_i}-q_{a_j})^2,\\
Q_B^2 &= \sum_{b_i} x_{b_i} m_{b_i}^2 - \sum_{b_i} \sum_{b_j<b_i} x_{b_i} x_{b_j} (q_{b_i}-q_{b_j})^2,\\
Q_C^2 &= \sum_{c_i} x_{c_i} m_{c_i}^2 - \sum_{c_i} \sum_{c_j<c_i} x_{c_i} x_{c_j} (q_{c_i}-q_{c_j})^2,\\
\sigma_A &= \sum_{a_i} \nu_{a_i}, \quad \sigma_B = \sum_{b_i} \nu_{b_i}, \quad \sigma_C = \sum_{c_i} \nu_{c_i}.
\end{aligned}$$

After shifting away q_A and q_B, we combine the two effective propagators depending on ℓ using the Feynman parameters $y_B + y_C = 1$. Finally, after a further shift in ℓ, we combine the two effective propagators using Feynman parameters $z_A + z_F = 1$. Putting everything together, some of the Γ functions arising in the various steps cancel and we are only left with the combination, that appeared also in the "at once" strategy, namely $B(\{\nu_i\}) = B(\{\nu_{a_i}, \nu_{b_i}\nu_{c_i}\})$. The net result is

$$\begin{aligned}
I_{\text{2-loop}} = B(\{\nu_{a_i}, \nu_{b_i}\nu_{c_i}\}) &\int \frac{d^dK}{(2\pi)^d}\frac{d^dL}{(2\pi)^d} \\
&\int_0^1 d\{x_{a_i},\nu_{a_i}\}\int_0^1 d\{x_{b_i},\nu_{b_i}\}\int_0^1 d\{x_{c_i},\nu_{c_i}\} \\
&\int_0^1 dy_B dy_C\; y_B^{\sigma_A+\sigma_B-d/2-1} y_C^{\sigma_A+\sigma_C-d/2-1}\delta(1-y_A-y_C) \\
&\int_0^1 dz_A dz_F\; z_A^{\sigma_A-1} z_F^{\sigma_B+\sigma_C-d/2-1}\delta(1-z_A-z_F) \\
&\frac{\mathcal{N}(k,\ell)}{[K^2+L^2+z_Az_Fy_By_CP^2 - z_Fy_BQ_B^2 - z_Fy_CQ_C^2 - z_Ay_By_CQ_A^2]^{\sigma_A+\sigma_B+\sigma_C}},
\end{aligned} \tag{3.15}$$

where we have introduced the shorthand

$$d\{x_i,\nu_i\} = d\vec{x}_i\;\delta(1-\textstyle\sum_i x_i)\;\displaystyle\prod_i x_i^{\nu_i-1}, \tag{3.16}$$

and

$$P = q_C - q_A - q_C. \tag{3.17}$$

The original loop-momenta are given by

$$k = K y_B^{-1/2} y_C^{-1/2} - z_F P - q_A \tag{3.18}$$
$$\ell = L z_F^{-1/2} - K y_B^{-1/2} y_C^{1/2} - y_C z_A P - q_B.$$

3.2.3 Tensor Integrals

We return to the postponed question of nontrivial numerators. The simplest example is the following:

$$\int d^d K \frac{K^{\mu_1} K^{\mu_2}}{[K^2 - \Lambda]^\sigma} = \frac{g^{\mu_1\mu_2}}{c(2)} \int d^d K \frac{K^2}{[K^2 - \Lambda]^\sigma}. \tag{3.19}$$

As the denominator does not depend on the direction of K^μ, the integral must be proportional to the metric tensor $g^{\mu_1\mu_2}$. Contracting both sides of the above equation with $g_{\mu_1\mu_2}$ is a cheap way to fix the constant $c(2) = d$.

An integral with numerator $K^{\mu_1} \dots K^{\mu_{2k}}$ will be proportional to the totally symmetric combination of metric tensors $g^{\mu_i\mu_j}$. We define

$$G^{\mu_1\mu_2} = g^{\mu_1\mu_2} \tag{3.20}$$
$$G^{\mu_1\mu_2\mu_3\mu_4} = g^{\mu_1\mu_2} g^{\mu_3\mu_4} + g^{\mu_1\mu_3} g^{\mu_2\mu_4} + g^{\mu_1\mu_4} g^{\mu_2\mu_3} \tag{3.21}$$
$$G^{\mu_1\dots\mu_{2k}} = \frac{1}{k!\, 2^k} \sum_{\sigma \in S_{2k}} g^{\mu_{\sigma(1)}\mu_{\sigma(2)}} \dots g^{\mu_{\sigma(2k-1)}\mu_{\sigma(2k)}}. \tag{3.22}$$

The normalization factor in the last line takes care of the fact, that the sum always produces $k!\, 2^k$ equivalent terms.

A handy recursive characterization is

$$G^{\mu_1\dots\mu_{2k}} = \sum_{i=2\dots 2k} g^{\mu_1\mu_i} G^{\not{\mu}_1\mu_2\dots\not{\mu}_i\dots\mu_{2k}}, \tag{3.23}$$

where on the right hand side, the crossed out indices μ_1 and μ_i are absent. This reproduces the expression. This is equivalent to eq. (3.22) because

1. There are no equivalent summands: $g^{\mu_1\mu_i}$ does not appear in any of the $G^{\not{\mu}_1\mu_2\dots\not{\mu}_j\dots\mu_{2k}}$, $j = 2 \dots 2k$ as these do not contain μ_1
2. Sorting all products appearing eq. (3.22) such, that the metric containing the index μ_1 always comes first, it becomes clear, that we have written down all the terms.

With the symbol $G^{\mu_1\dots\mu_{2k}}$ at hand, we can now express the rank $2k$ tensor integral:

$$\int d^d K \frac{K^{\mu_1} \dots K^{\mu_{2k}}}{[K^2 - \Lambda]^\sigma} = \frac{G^{\mu_1\dots\mu_{2k}}}{c(2k)} \int d^d K \frac{K^{2k}}{[K^2 - \Lambda]^\sigma}. \tag{3.24}$$

To compute the constant $c(2k)$ we contract both sides of this equation with

$$g_{\mu_1\mu_2}\, g_{\mu_3\mu_4} \cdots g_{\mu_{2k-1}\mu_{2k}}. \tag{3.25}$$

The representation in eq. (3.23) makes it easy to see, what happens if we contract $G^{\mu_1\dots\mu_{2k}}$ with a single metric tensor $g_{\mu_1\mu_2}$: In the summand $i = 2$, $g_{\mu_1\mu_2}$ is contracted with $g^{\mu_1\mu_2}$,

giving d times a G tensor of the remaining indices. In all other summands, the contraction just replaces the index μ_2 by μ_i and thus leaves us with a G tensor of (a permutation of) the remaining indices. Thus

$$g_{\mu_1\mu_2} G^{\mu_1\mu_2\ldots\ldots\mu_{2k}} = g_{\mu_1\mu_2} \sum_{i=2\ldots 2k} g^{\mu_1\mu_i} G^{\mu_1\mu_2\ldots\not{\mu}_i\ldots\mu_{2k}} = (d+2k-2) G^{\mu_3\mu_4\ldots\ldots\mu_{2k}}. \tag{3.26}$$

Iterating this procedure gives allows us to fix the constant $c(2k)$

$$c(2k+2) = (d+2k)c(2k). \tag{3.27}$$

Integrals with an odd power of K in the numerator are of course zero.

We can make another observation, that will come in handy for implementation in a computer algebra system: As we might want to work with dot products rather than with open indices, we might encounter numerators containing dot products of the K with constant vectors as well as (K,K), for instance

$$(K,K)^5\ (K,p_1)(K,p_2)(K,p_3)(K,p_4). \tag{3.28}$$

It is now easy to see, that in this situation just replacing the last four dot products by $(K,K)^2\ G(p_1,p_2,p_3,p_4)/c(4)$ is equivalent to replacing $K^{\mu_1}\ldots K^{\mu_{14}}$ by $G^{\mu_1\cdots\mu_{14}}(K,K)^7/c(14)$ and then contracting with 5 metric tensors originating from $(K,K)^5$. It is understood, that $G(p_1,p_2,p_3,p_4)$ denotes the contraction $G_{\mu_1\mu_2\mu_3\mu_4}\ p_1^{\mu_1} p_2^{\mu_2} p_3^{\mu_3} p_4^{\mu_4}$.

Note, that in principle eq. (3.24) is nothing but the heart of the well known Davydychev formula. The difference is, that we only give an expression for an integral with a tensor written in terms of the shifted loop momentum K^μ, what is simple. The Davydychev formula [48] on the other hand gives an explicit expression for an integral with a tensor written in terms of the original, unshifted loop momentum k^μ. When k^μ is expressed in terms of the shifted momentum, $k^\mu = K^\mu + P^\mu$, a tensor $k^{\mu_1}\ldots k^{\mu_n}$ decomposes into 2^n terms, as every index μ_i can be carried either by a K or by a P. This leads to a daunting formula containing tensors made of different numbers of metric tensors g and external momenta. Clearly, if we treat a tensor integral by introducing Feynman parameters, shifting the loop momentum, expanding the tensor and applying eq. (3.24) to every piece, all these terms will be produced as well. But this is work for the computer algebra system only. It is not necessary to program the complicated formula, which does everything in one step.

Recall, that we have brought our two-loop integrals into a standard form with denominator $[K^2+L^2-\Lambda(\vec{x})]^\sigma$. Since the presence of L^2 does not interfere with anything said in this section, our treatment of tensors trivially extends to the two-loop case. Explicitly we can write

$$\int d^dK d^dL \frac{K^{\mu_1}\ldots K^{\mu_{2k}}\ L^{\nu_1}\ldots L^{\nu_{2l}}}{[K^2+L^2-\Lambda]^\sigma} = \frac{G^{\mu_1\ldots\mu_{2k}} G^{\nu_1\ldots\nu_{2l}}}{c(2k)c(2l)} \int d^dK d^dL \frac{K^{2k} L^{2l}}{[K^2+L^2-\Lambda]^\sigma}, \tag{3.29}$$

but that is not even necessary, in an implementation we can just call the routine, that does the replacement eq. (3.24), once for every loop momentum.

3.2.4 Mapping Feynman Parameters to the Hypercube

Feynman parameters sum up to one, as can be seen from the δ-functions appearing in the above formulae. Thus they lie on a n-dimensional standard simplex S_n. The sector decomposition method discussed in the next in section 3.3 deals with functions defined on a hypercube. Also contour deformation is far less cumbersome if done on a hypercube, rather than on a simplex.

Thus we have to parametrize S_n over $[0,1]^{n-1}$. A straightforward way to do so is to just eliminate one variable

$$x_n = 1 - x_1 - x_2 - \ldots - x_{n-1} \tag{3.30}$$

and to rescale the remaining ones as follows

$$\begin{aligned}
x_{n-1} &= (1 - x_1 - x_2 - \ldots - x_{n-2})\, r_{n-1} && (3.31)\\
x_{n-2} &= (1 - x_1 - x_2 - \ldots - x_{n-3})\, r_{n-2} && (3.32)\\
&\vdots && (3.33)\\
x_2 &= (1 - x_1)\, r_2 && (3.34)\\
x_1 &= r_1 && (3.35)
\end{aligned}$$

The jacobian of this transformation is

$$\left|\frac{\partial x_k}{\partial r_l}\right| = \prod_{j=2}^{n-1} \left(1 - \sum_{i=1}^{j-1} x_i\right) \tag{3.36}$$

The disadvantage of this transformation is, that the x_i become polynomials of order up to $n-1$ in the r_j and that the simplex is parametrized in a very non-uniform way. In the $gg \to h$ computation at two-loop discussed in chapter 4 this did not really hurt, as the diagrams parametrized with the "sunset" strategy had always two simplices of modest dimensionality (plus two trivial S_2) instead of a single high dimensional one. However, for two-loop diagrams parametrized according to the "at once" strategy, as well as for one-loop diagrams with many legs, is is most probably better to use the so called primary sector decomposition. This means, that the simplex S_n – very much like the hypercube in the next section – is split into n regions R_i, each one characterized by one variable being larger than all the others. These regions can then be parametrized like

$$R_i = \{(r_1, \ldots, r_{i-1}, 1, r_{i+1}, \ldots, r_{n-1})^T / (1 + r_1 + r_2 + \ldots + r_{n-1}) \mid r_i \in [0,1]\}. \tag{3.37}$$

The fact, that β and Λ are homogeneous polynomials can be used to get rid of the normalization factors.

3.3 Sector Decomposition

3.3.1 Basic idea

IR and partially also UV divergences appear as endpoint singularities in Feynman parameter integrals. In the context of dimensional regularization such a singularity might look like

$$\int_0^1 dx\; x^{-1+s\epsilon} f(x), \tag{3.38}$$

where $f(x)$ does not vanish on $[0,1]$. Obviously, switching off the regulator $\epsilon \to 0$ leaves us with a logarithmically divergent integral. Usually one tries to obtain a series expansion in ϵ. Expanding the integrand in a Taylor series in ϵ is clearly not helpful. Such a series would start at $\mathcal{O}(\epsilon^0)$ and its coefficient would be $x^{-1}f(x)$, the divergent integrand with the regulator switched off. Fortunately the divergence can easily be subtracted:

$$\int_0^1 dx\; x^{-1+s\epsilon} f(x) = \int_0^1 dx\; x^{-1+s\epsilon}[f(x) - f(0)] + f(0) \int_0^1 dx\; x^{-1+s\epsilon}. \tag{3.39}$$

The first integral is free of divergences, as $f(x) - f(0)$ behaves like $x\; f'(0)$ for $x \to 0$. We can safely Taylor expand the subtracted integrand in ϵ. The second integral now contains the singularity. But since it contains only the singularity, analytic integration is trivial, yielding $\frac{1}{s\epsilon} f(0)$. Stronger singularities can be handled as well. We just have to write a subtraction term, that approximates $f(x)$ to a higher degree:

$$\int_0^1 dx\; x^{-n+s\epsilon} f(x) = \int_0^1 dx\; x^{s\epsilon}\; \frac{f(x) - \sum_{k=0}^{n-1} x^k \frac{f^{(k)}(0)}{k!}}{x^n} + \sum_{k=0}^{n-1} \frac{f^{(k)}(0)}{k!(k+1-n+s\epsilon)}. \tag{3.40}$$

Isolated singularities occurring in more than one variable, e.g.

$$\int_0^1 d\vec{x}\, x_1^{-1+s_1\epsilon}\, x_2^{-1+s_2\epsilon}\, f(x_1, x_2), \tag{3.41}$$

can be treated by iterated application of eq. (3.40). A common complication is, that overlapping singularities occur. We talk about an overlapping singularity, if our integrand becomes infinite due to simultaneous vanishing of more than one variable. In the following simple example, this happens at $x = y = 0$:

$$\int_0^1 dx \int_0^1 dy \frac{1}{x+y}. \tag{3.42}$$

Sector decomposition is a simple, yet powerful method to isolate overlapping singularities. As shown in fig. 3.3.1, we can split the integration region into two triangular sectors given by

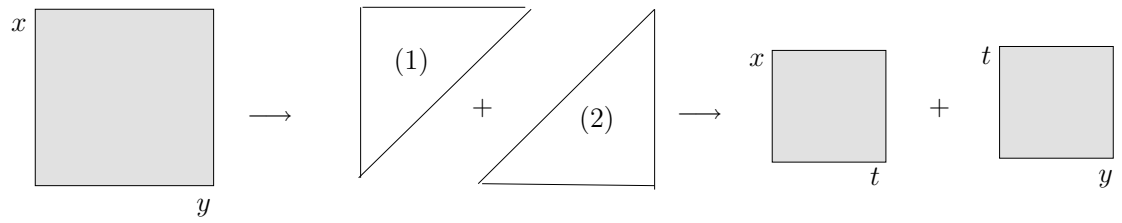

Figure 3.2: The basic step of sector decomposition.

$x > y$ and $y > x$. Then we rescale the dominated variable by the dominating one.

$$\int_0^1 dx \int_0^1 dy \frac{1}{x+y} = \int_0^1 dx \int_0^x dy \frac{1}{x+y} + \int_0^1 dy \int_0^y dx \frac{1}{x+y} \tag{3.43}$$

$$\downarrow y = x\tilde{y} \qquad \downarrow x = y\tilde{x} \tag{3.44}$$

$$= \int_0^1 dx \int_0^1 d\tilde{y} \frac{x}{x+x\tilde{y}} + \int_0^1 dy \int_0^1 d\tilde{x} \frac{y}{y\tilde{x}+y} \tag{3.45}$$

This not only brings us back to a quadratic integration domain, but it mainly produces a common factor of x or y in the denominator. This is a bit like introducing polar coordinates, the rescaling factor playing the role of the radius. Here the singularity is then actually cancelled by the jacobian, as it was an integrable one. In general it will just stay in the "radius" variable. The case of a non integrable singularity in the context of dimensional regularization might look as follows:

$$\int_0^1 dx \int_0^1 dy \frac{1}{[x+y]^{2-\epsilon}} = \int_0^1 dx \int_0^1 d\tilde{y} \frac{x^{-1+\epsilon}}{[1+\tilde{y}]^{2-\epsilon}} + \int_0^1 dy \int_0^1 d\tilde{x} \frac{y^{-1+\epsilon}}{[\tilde{x}+1]^{2-\epsilon}}. \tag{3.46}$$

The procedure also works for overlapping singularities of more than 2 variables. For instance the overlapping singularity in $\frac{1}{x+y+z}$ can be decomposed by cutting the integration region into 3 sectors, each characterized by one variable being the largest one and rescaling the others back to $[0,1]$, i.e. $y = x\tilde{y}$, $z = x\tilde{z}$ etc.

$$\begin{aligned}\int_0^1 dxdydz \frac{1}{x+y+z} &= \int_0^1 dx \int_0^1 dy \int_0^1 dz \frac{1}{x+y+z} \left[\theta(x>y,z) + \theta(y>x,z) + \theta(z>x,y)\right] \\ &= \int_0^1 dx \int_0^1 d\tilde{y} \int_0^1 d\tilde{z} \frac{x}{1+\tilde{y}+\tilde{z}} + (x \leftrightarrow y) + (x \leftrightarrow z).\end{aligned}$$

More generally we have to consider integrals of the form

$$\int_0^1 d\vec{x} \, [p_1(\vec{x})]^{r_1+s_1\epsilon} \cdots [p_k(\vec{x})]^{r_k+s_k\epsilon}, \tag{3.47}$$

where $p_i(\vec{x})$ are polynomials in the Feynman parameters. In practice the exponents r_i and s_i are integers with arbitrary signs. Let us agree on the name "denominators" for the set of those $p_i(\vec{x})$, that come with $r_i < 0$.

$$\text{denoms}(\vec{x}) := \{p_i(\vec{x}) | i \text{ with } r_i < 0\} \tag{3.48}$$

Our integral has a singularity (more precisely an endpoint singularity) in the Feynman parameters $S = \{x_{s_1}, \ldots, x_{s_n}\}$ at $\{\sigma_{s_1}, \ldots, \sigma_{s_n}\} \in \{0,1\}^n$ if there is a vanishing denominator for

$$\{x_{s_1}, \ldots, x_{s_n}\} = \{\sigma_{s_1}, \ldots, \sigma_{s_n}\} \tag{3.49}$$

and S is minimal in the sense, that fixing only a proper subset of S to the given values is not sufficient to cause the vanishing. If we have an overlapping singularity at the origin, i.e. the vanishing happens if all involved variables are set to 0 rather than a collection of 0 and 1, we can again decompose it by cutting the the domain of S, the hypercube $[0,1]^n$ into n sectors, each with one variable dominating all the others in S and rescaling everything back to $[0,1]$. This results in making n copies of the original integral, one for each $x_i \in S$, and replacing

$$d\vec{x} \to d\vec{x}\, x_i^{n-1} \tag{3.50}$$

$$x_j \to x_i x_j \qquad \forall x_j \in S \setminus \{x_i\}. \tag{3.51}$$

After decomposing an overlapping singularity as just described, the resulting n integrals may still contain further singularities. Thus the decomposition step has to be applied recursively until all overlapping singularities are decomposed. However, attention has to be paid to the issues discussed in the next two sections.

3.3.2 Singularities at $x = 1$ and Splitting of Variables

First we have to consider singularities, that involve some variable, say x, set to 1 rather than 0. We can try to flip these variables, $x \to 1 - x$, in order to move the singularity to the origin, and then decompose it. Clearly, flipping a variable x is not a good idea, if there is already an isolated singularity at $x = 0$, as the latter would be converted into an isolated singularity at $x = 1$, and so we would not move towards our goal of having only isolated singularities at 0. In this case, we are forced to split the integration domain $[0,1]$ into $[0, \frac{1}{2}]$ and $[\frac{1}{2}, 1]$ and rescale each of them back to $[0,1]$. That amounts to making two copies of the integral and replacing

$$x_i \to \tfrac{1}{2} x_i \tag{3.52}$$

$$d\vec{x} \to \tfrac{1}{2} d\vec{x} \tag{3.53}$$

and

$$x_i \to \tfrac{1}{2}(x_i + 1) \tag{3.54}$$

$$d\vec{x} \to \tfrac{1}{2} d\vec{x} \tag{3.55}$$

respectively. With no isolated singularity in the way, flipping variables is indeed sufficient, as we will see below.

3.3.3 Ordering Singularities or Avoiding Infinite Loops

If an integral contains more than one overlapping singularity, it makes a difference, which one is decomposed first. This can be seen from the simple example

$$\int_0^1 dx dy dz \frac{1}{x^2 + y^2 z}. \tag{3.56}$$

Obviously there is a singularity, when x and y simultaneously approach zero, but also if x and z do so. Decomposing (x, y) does a good job. Suppressing the integral we get

$$\frac{1}{x^2 + y^2 z} \xrightarrow{(x,y)} \frac{1}{x(1 + y^2 z)} + \frac{1}{y(x^2 + z)}. \tag{3.57}$$

The first term is already decomposed completely, the singularity is caught at $x \to 0$. The second one has an isolated singularity at $y \to 0$ but also an overlapping one at $(x, z) \to (0, 0)$. The latter will need two more (x, z) decomposition steps. This way the original decomposes into four sectors each one having an isolated singularity in either x or y. On the other hand, decomposing the (x, z) singularity in the first place does not help at all:

$$\frac{1}{x^2 + y^2 z} \xrightarrow{(x,z)} \frac{1}{x + y^2 z} + \frac{1}{x^2 z + y^2}. \tag{3.58}$$

The second term is exactly the same as the original one, except for $x \leftrightarrow y$. So the problem has not simplified and if our program then decided to decompose (y, z) in the second term, it would even reproduce the original expression verbatim and thus contain an infinite loop. One might wonder, how it is possible that the decomposition reproduces the original expression plus additional pieces, which are all positive. But this is just an artefact of dealing with divergent integrals. In presence of a regulator, say if the denominator is raised to the power $1+\epsilon$, we do not reproduce the original expression verbatim, but the mechanics of denominators and thus the infinite loop remain unchanged. Note, that also decomposing the non minimal set of variables (x, y, z) is not helpful here, as the rescaling $(x, y) \to (zx, zy)$ immeaditely reproduces the original expression.

So what is the right strategy for choosing which singularity to decompose? This is a difficult question. We implemented a strategy, that avoids the above problem. This strategy has worked, i.e. the decomposition terminated, in all examples considered so far. However, we lack prove, that it always will.

1. First we order singularities according to the number of variables involved. That is first come isolated singularities, then overlapping singularities involving two variables etc. (Isolated singularities do not require decomposition, of course, but it will be convenient to have an ordered list of singularities also including the isolated ones.)

2. The singularities involving the minimum number of variables are further ordered according to their degree. Let

   $$\{x_{s_1}, \ldots, x_{s_n}\} = \{\sigma_{s_1}, \ldots, \sigma_{s_n}\} \tag{3.59}$$

   be such a singularity, i.e. a denominator $p_k(\vec{x})$ vanishes at these values and fixing only a subset of the variables does not cause any denominator to vanish. We define the singularity's degree as the power, with which the $p_k(\vec{x})$ vanishes, when the Feynman parameters approach the singular values. Thus if the substituted denominator

   $$p_k(\vec{x})\Big|_{\substack{x_{s_i} \to \lambda x_{s_i} & \text{for } \sigma_{s_i} = 0 \\ x_{s_i} \to 1 - \lambda x_{s_i} & \text{for } \sigma_{s_i} = 1}} \tag{3.60}$$

   behaves like $\sim \lambda^m$ for $\lambda \to 0$, the degree of the singularity is m. The degree of a

singularity counts, how many powers of Feynman parameters can be factored out from $p_k(\vec{x})$ after decomposing the singularity. It is understood, that for singularities involving $\sigma_{s_i} = 1$, x_{s_i} are flipped first. Substituting $x_{s_i} \to \lambda x_{s_i}$ and $x_{s_i} \to 1 - \lambda x_{s_i}$, respectively, rather than just $x_{s_i} \to \lambda$ and $x_{s_i} \to 1 - \lambda$, respectively prevents failure on indefinite expressions[3] like $x_1 - x_2$. If there is more than one vanishing denominator $p_k(\vec{x})$, we pick the one, that gives the maximum degree. Note that our definition of the degree is blind to the powers r_i in eq. (3.47). So in

$$\frac{1}{[x+y]\,[x+z]^2}, \tag{3.61}$$

(x, z) and (x, y) both have degree 1 and there is no preference, whereas in

$$\frac{1}{[x^2+y^2z]}, \tag{3.62}$$

(x, y) has degree 2 and will thus be favored over (x, z) having degree 1.

3. Last, singularities of equal degree are put in ascending order with respect to the signature $\{\sigma_{s_1}, \ldots, \sigma_{s_n}\}$ understood as a binary number. Note that a position in the signature can correspond to different variables for different singularities.

We mention that the problem of choosing the right singularity for decomposition was analyzed in [64]. The authors could map the problem to a known problem in algebraic geometry and thus come up with three strategies, for which the algorithm is guaranteed to terminate. However, they also in noticed, that a forth strategy, for which they could not prove the algorithm always terminates, performs much better than the first three in the sense, that it produced a much lower amount of sectors for practical problems considered. This strategy is very similar to ours. They just compute the degree based on the whole denominator

$$\prod_i p_i(\vec{x})^{r_i}, \tag{3.63}$$

rather than for individual factors $p_i(\vec{x})$. For two-loop integral parametrized according to the "sunset" strategy, we can see from the representation eq. (3.15) that apart from the common denominator containing the kinematics, the there are only trivial denominators of the form x^r and, after integrating out the delta functions, $(1-x)^r$. In this case, the two strategies are equivalent.

Another comment is on order here: It is often said, that a serious problem of sector decomposition is the proliferation of terms. The problem seems to be more pronounced, if many massless propagators are present. When discussing this question, one should note, however, that the occurrence of many sectors is not a problem *a priori*. To be more precise, the fact that an integrand gets decomposed into two integrands does not necessarily mean, that integration is twice as much work. One can even imagine to shrink the two resulting integration domains to half their volume and glue them together to form a single hypercube again. Numerical integration means sampling all important features of the integrand and sector decomposition is just a change of variables, that rescales and tends to smooth out these features. In the end, due to the rescalings, the algebraic complexity of the integrand

[3] In Feynman parametrized loop integrals, factors free of kinematic invariants always have a definite sign.

does actually grow with sector decomposition. But the growth is not as bad as file sizes suggest, as this is also due the fact, that we ended up with a piecewisely defined integrand. In extreme cases memory can become a problem. However, explicit calculations of cross-sections through next-to-next-to-leading order have shown, that realistic problems are manageable [6, 7, 8, 9, 10, 11].

3.3.4 Some Implementation Details

First, a Feynman diagram has to be brought into a form suitable for sector decomposition. For a two-loop diagram this might look as follows:

1. We introduce Feynman parameters as shown in eq. (3.15). Feynman parameters living on simplices are mapped to the hypercube. In the numerator function $\mathcal{N}(k,\ell)$, k and ℓ are expressed in terms of the new integration momenta K and L according to eq. (3.18).

2. Products appearing in the numerator function $\mathcal{N}$ are multiplied out. Then, dot products linear in K are eliminated according to eq. (3.24). This step is repeated for the second loop momentum L.

3. In the numerator function, terms with the same powers of loop momenta $(K,K)^{m/2}(L,L)^{n/2}$ are collected and the momentum integrals are carried out by using eq. (3.8) twice.

4. Every Feynman parameter integral obtained this way is split into a tensor part originating from terms in $\mathcal{N}$ and a scalar part. Note that for tensor parts originating from terms proportional to $K^m L^n$, the scalar part corresponds to the Feynman diagram with $\mathcal{N}$ set to 1, but evaluated in $d+m+n$ instead of d dimensions.

5. Finally, if polynomials in Feynman parameters raised to negative powers appear in the tensor parts, these are factored out and moved to the scalar part. Such negative powers occur, when expressing k and ℓ through K and L, as can be seen from eq. (3.18).

After these steps, our Feynman diagram is written as a sum of integrals of the form

$$C(\epsilon)\int_0^1 d\vec{x}\ \mathrm{tensor}(\vec{x},\epsilon)\ [p_1(\vec{x})-i0]^{r_1+s_1\epsilon}[p_2(\vec{x})]^{r_2+s_2\epsilon}\dots[p_n(\vec{x})]^{r_n+s_n\epsilon}. \tag{3.64}$$

Out of the polynomials p_i only p_1 depends on kinematical invariants[4]. It stems of course from the combined denominator produced by Feynman parametrization. For physical values of the kinematical invariants, this polynomial can change sign inside the integration region. At such points, the $i0$ then tells the integration contour how to dodge via the complex domain. All other $p_i(\vec{x})$ are pure combinations of Feynman parameters, that is, the polynomial's coefficients are just numbers. Actually these polynomials are positive semidefinite. They can vanish only at the border of the integration domain. If their vanishing leads to a singularity, this is related to the UV or IR behavior of the diagram. $C(\epsilon)$ is a prefactor, usually containing Γ functions, that can be singular for $\epsilon\to 0$. On the other hand, $\mathrm{tensor}(\vec{x},\epsilon)$ is finite for $\epsilon\to 0$. It can be expanded in a Taylor series in ϵ. As expressions raised to negative powers have been moved to the scalar part, the coefficients of this expansion are polynomials in the

[4]If we treat a factorizable diagram as a whole, a product $[p_1(\vec{x})-i0]^{r_1+s_1\epsilon}[p_2(\vec{x})-i0]^{r_2+s_2\epsilon}$ of terms depending on kinematics arises. But in this case $p_1(\vec{x})$ and $p_2(\vec{x})$ depend on disjunct sets of Feynman parameters. This will be important for finding an integration contour.

Feynman parameters. Thus tensor$(\vec{x},\epsilon)$ does not give raise to singularities[5] and it is therefore sufficient, apply sector decomposition to the scalar part only. Of course we have to keep track of all transformations of variables, so we can evaluate tensor$(\vec{x},\epsilon)$ in the correct region afterwards. For instance, if an overlapping singularity in (x_1,x_2) gets decomposed in the scalar part, the two sectors in the end get combined with tensor(x_1,x_1x_2,ϵ) and tensor(x_2x_1,x_2,ϵ), respectively. But as tensor$(\vec{x},\epsilon)$ can be a pretty large expressions, it is good, that the sector decomposition algorithm does not search them for nonexistent singularities in every step. And even more important, aiming for fast numerical evaluation, we do not want to make the tensor expressions even more complicated by algebraically substituting in all rescalings. It is better to compute the values of the original variables, $(x_1^{\text{orig}},x_2^{\text{orig}}) = (x_1,x_1x_2)$ and $(x_1^{\text{orig}},x_2^{\text{orig}}) = (x_2x_1,x_2)$ respectively, in the above example, numerically and to substitute these values into tensor$(\cdot,\epsilon)$. Integrals of the form eq. (3.64) can be submitted to the sector decomposition algorithm, which will perform the following preparation steps:

- The expression tensor$(\vec{x},\epsilon)$ is replaced by a dummy function jet$[\mathtt{x_1},\ldots,\mathtt{x_n},\epsilon]$. The latter is just a bookkeeping device, that will keep track of all changes of variables.
- Powers $[p_i(\vec{x})]^{r_i+s_i\epsilon}$ are rewritten using a private symbol

  $$\mathtt{fac}[\mathtt{p_i}[\mathtt{x_1},\ldots,\mathtt{x_n}],\mathtt{r_i}+\mathtt{s_i}\epsilon].$$

  This prevents uncontrolled application of built in rules by Mathematica. We only equip the symbol `fac` with the following simple rules for dealing with trivial arguments and combining powers of the same expression

  ```
  fac[x_, 0] := 1
  fac[a_, b_] := a^b /; NumericQ[a]
  Times[fac[a_, e_], fac[a_, f_]]^ := fac[a, e + f]
  ```

  Additionally, a factorization routine can be applied to an expression containing `fac` symbols. This routine tries to factorize expressions, that are free of kinematical invariants out of `fac`. For instance

  $$\mathtt{fac}[-\mathtt{x}(1-\mathtt{x})\mathtt{s}+(1-\mathtt{x})\mathtt{m}^2,\mathtt{e}] \to \mathtt{fac}[(1-\mathtt{x}),\mathtt{e}]\mathtt{fac}[-\mathtt{xs}+\mathtt{m}^2,\mathtt{e}]. \tag{3.65}$$

  The routine assumes, these factors cannot change sign and, under this assumption, pulls them out with positive sign. I.e. in the above example, $1-x$ is pulled out rather than $x-1$. The sign is tested by substituting random values for the Feynman parameters. This factorization routine is applied at the beginning and and after every decomposition step.

After this preparation, the actual decomposition algorithm is invoked. Work is done mainly by the follwong functions:

`findFirstSing[expr_]` finds the first singularity according to the ordering discussed in section 3.3.3. It returns an object of the form

$$\mathtt{SingDescr}[\mathtt{vars},\mathtt{signature},\mathtt{degree}].$$

[5] On the other hand, tensor$(\vec{x},\epsilon)$ could sometimes cancel singularities. For instance, if the scalar part contains a factor $x_1^{-1+\epsilon}$ while an overall x_1 could be factored out of tensor$(\vec{x},\epsilon)$, doing so we could avoid the generation of an unnecessary subtraction. We did not implement this, however.

For instance

$$\texttt{SingDescr}[\{\texttt{x}_1, \texttt{x}_5\}, \{1, 0\}, 2]$$

means, that the singularity to be composed lies at $x_1 \to 1 \wedge x_5 \to 0$ and has degree 2.

`decompose[expr_, vars_List]` performs one sector decomposition step on `expr`, decomposing an overlapping singularity at the origin in the variables `vars`. It uses the factorization routine mentioned above to pull generated common factors out of `fac` symbols. A list of `Length[var]` sectors is returned.

`splitVar[expr_, var_]` splits the integration along `var` into two ranges $[0, \frac{1}{2}]$ and $[\frac{1}{2}, 1]$, rescales them back to $[0, 1]$ and returns the two sectors.

The integrand expression is put into a `todo` queue and the algorithm works according to the flowchart depicted in figure 3.3. Some explanations are on order:

- The main working step takes an expression out of the `todo` queue, finds the first singularity to be decomposed, and goes, answering always no, straight down to the decomposition step. Thus the singularity is decomposed and the resulting sectors are put back into the queue.

- Alternatively the algorithm may find, that the discovered singularity is an isolated one at zero. That means, the expression under consideration contains a factor $x_i^{-m+n\epsilon}$ with $m > 0$. In this case, the algorithm just tags this singularity by replacing

  $$\texttt{fac}[\texttt{x}_\texttt{i}, -\texttt{m} + \texttt{n}\epsilon] \to \texttt{ISfac}[\texttt{x}_\texttt{i}, -\texttt{m} + \texttt{n}\epsilon]$$

  and puts it back to the queue. The `findFirstSing` function is blind to the special symbol `ISfac` and thus won't ask to deal with this singularity any more.

- Another possibility is, that the signature of the singularity under consideration contains ones, i.e. the singularity involves variables fixed to 1. Then the algorithm takes the first variable, that is fixed to 1 and checks, whether the expression already contains an `ISfac` in this very variable.

  - If this is the case, the `ISfac` is released, `splitVar` is called and the resulting sectors go back to the queue. Releasing the `ISfac` means replacing it by an ordinary `fac`. This prevents us from ending up with a spurious, nonsingular `ISfac` in $[\frac{1}{2}, 1]$ part. Note, that the `ISfac` in $[0, \frac{1}{2}]$ part is not restored. The sector simply goes back to the queue and the isolated singularity will again be detected in the next step.
  - If there is no `ISfac` in the way, the variable under consideration is simply flipped, and the sector goes back to the queue. Note, that due to the third criterion of ordering singularities, the fact, that we are dealing with a singularity, that involves ones means, that the sector has no singularities (of equal number of variables and degree) involving only zeros. Flipping turns the first 1 in the signature into a 0 and thus moves the singularity forward by at least one bin in the ordering. Other singularities can move backwards or forward, even more than the one under consideration. In any case at least one singularity is moved forward by at least one bin. Therefore, after a finite number of steps, some singularity arrives at bin zero

and gets decomposed. An infinite loop flipping variables back and forward cannot occur[6].

- Eventually, all singularities will be decomposed into isolated singularities and we are almost finished. There is only one left complication. While we have decomposed singularities like $(x_1+x_2)^{-1-\epsilon}$ even though they are integrable, terms like $(x_1+x_2)^{-\epsilon}$ might have survived. When expanding in ϵ, these give rise to logarithms. While $\log(x)$ has only an integrable singularity at 0, we run into trouble with expressions like

$$x_1^{-1-\epsilon} x_2^{-1-\epsilon} (x_1+x_2)^{-\epsilon}, \tag{3.66}$$

as they eventually lead to a singular double subtraction term

$$x_1^{-1-\epsilon} x_2^{-1-\epsilon} (0+0)^{-\epsilon}. \tag{3.67}$$

As long as there is only one isolated singularity, this problem cannot occur, as $x_1^{-1-\epsilon}\, x_1^{-\epsilon}$ is simply $x_1^{-1-2\epsilon}$. But if there is a product of isolated singularities

$$\texttt{ISfac}[\texttt{x}_{\texttt{s}_1}, \texttt{e}_{\texttt{s}_1}] \ldots \texttt{ISfac}[\texttt{x}_{\texttt{s}_k}, \texttt{e}_{\texttt{s}_k}] \tag{3.68}$$

together with a factor

$$\texttt{fac}[\texttt{p}[\texttt{x}_1, \ldots, \texttt{x}_\texttt{n}], \texttt{r} + \texttt{s}\epsilon] \tag{3.69}$$

with $s \neq 0$ and $p[x_1, \ldots, x_n]$ vanishes, if a subset of the variables

$$\{x_{s_1}, \ldots, x_{s_k}\}$$

is set to zero, then this subset needs to be decomposed, even for positive[7] r.

The outcome of the algorithm is a bunch of integrals of the form

$$C(\epsilon) \int_0^1 d\vec{x} \left[\prod_i x_i^{-\alpha_i+\beta_i\epsilon}\right] \left[\prod_j [P_j(\vec{x})]^{\eta_j+\xi_j\epsilon}\right] \frac{\mathrm{jet}(\vec{x}^{\,\mathrm{orig}}(\vec{x}), \epsilon)}{[\Lambda(\vec{x}) - i0]^{\alpha+n_L\epsilon}}. \tag{3.70}$$

$P_i(\vec{x})$ are polynomials in the Feynman parameters, which do not lead to singularities[8]. $\Lambda(\vec{x})$ is the polynomial containing the kinematics. We have given it a special name just to ease further discussion. Just as the $P_i(\vec{x})$, it is decomposed such, that it does not give rise to endpoint singularities. But in contrast to the $P_i(\vec{x})$, the kinematic polynomial $\Lambda(\vec{x})$, stemming from $p_1(\vec{x})$ in eq. (3.64), can change sign inside the integration domain. Therefore the integral would not be well defined, if the $-i0$ prescription was omitted. Note, that the evolution from $p_1(\vec{x})$

[6] In [8] a simpler and less entangled solution is proposed. The idea is to detect at the very beginning, which variables are involved in singularities with both, their 0 and 1 limits. Such variables are split immediately. Then variables which show singularities at 1 are flipped. This way, sector decomposition is invoked only after all singularities have been moved to the origin.

[7] In the case $r = 0$, decomposition is clearly unavoidable. For positive r it can sometimes be avoided. However, care has to be taken, as, depending on the exponents e_{s_i}, subtractions will involve derivatives. Also, special treatment of $x \log x$ like expressions is necessary.

[8] In principle, one could apply sector decomposition until all polynomials are of the form $1 + p(\vec{x})$ with $p(\vec{x}) = 0$. However, as we have tried to avoid unnecessary decomposition of unproblematic factors, we make a weaker statement here.

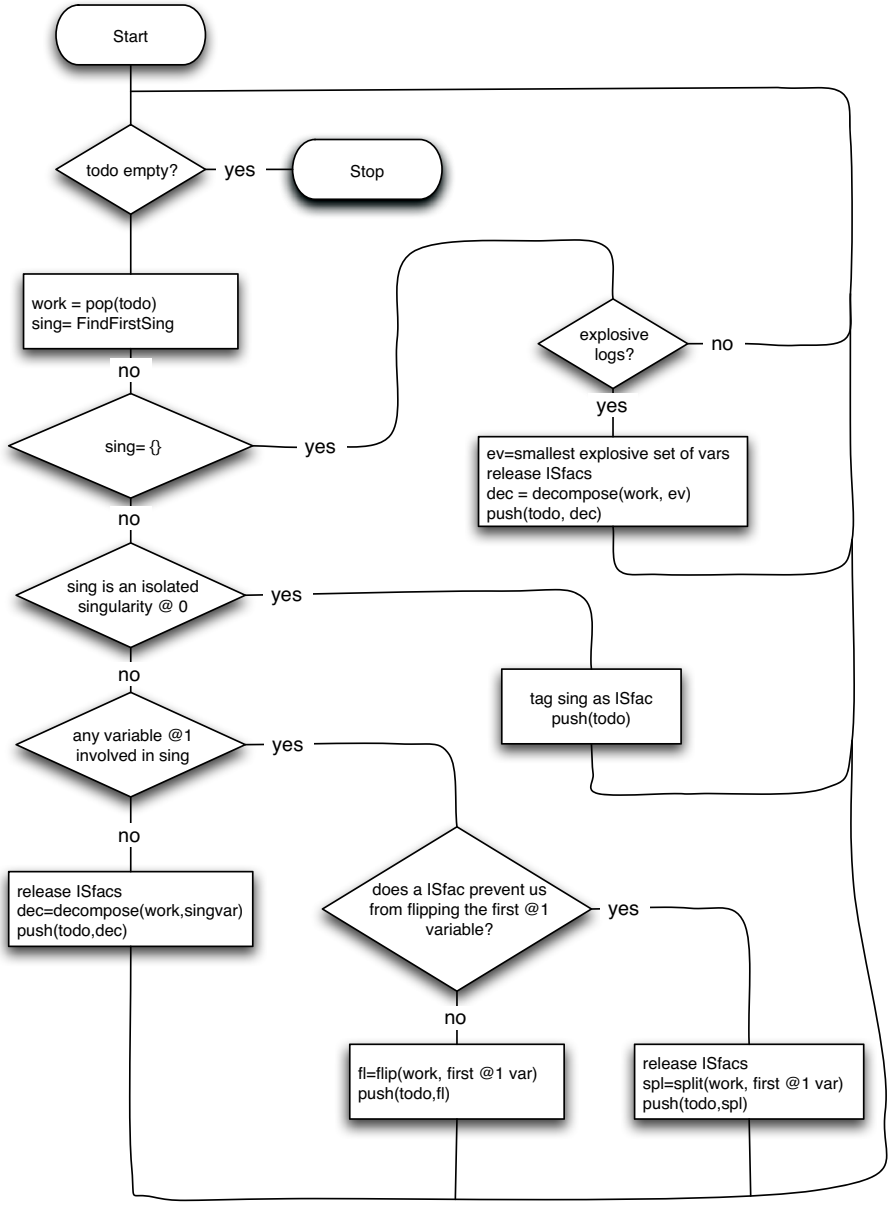

Figure 3.3: sector decomposition

to $\Lambda(\vec{x})$ includes not just changes of variables. In addition, we might have pulled out common positive semidefinite factors. Pulling out factors with positive sign only makes sure, that the $-i0$ prescription in eq. (3.64) actually stays $-i0$ throughout the decomposition process. Negative exponents α_i lead to endpoint singularities and thus ϵ poles. They can be extracted by application of eq. (3.40). However, as it will become clear in the next section, it is important to postpone this step until we have put the $-i0$ prescription into a form that is operative in numerical integration. Note that the exponent n_L corresponds to the number of loops. It is clear, that eventually, we will have to reinstall the proper numerator function tensor$(\cdot, \epsilon)$. But we also postpone this step and go one with the bookkeeping device jet$(\vec{x}^{\text{orig}}(\vec{x}), \epsilon)$, which remembers which bit of the original hypercube integration domain corresponds to a given value of the rescaled variables $\vec{x}$.

3.4 Contour Deformation

3.4.1 General Idea

We now address the problem of implementing the $-i0$ prescription in a way that holds for numerical integration. Nagy and Soper found a simple but very effective way of doing so. It works as follows. Consider a Feynman parameter integral

$$\int_0^1 d\vec{x} \frac{\mathcal{F}(\vec{x})}{[\Lambda(\vec{x}) - i0]^\sigma} \tag{3.71}$$

with kinematical invariants chosen such that $\Lambda(\vec{x})$ vanishes somewhere inside the integration region. Away from singularities, the integrand is a holomorphic function. The integration over each Feynman parameter can be deformed away from the the real line segment $[0, 1]$ into the complex domain. By Cauchy's theorem, this does not change the value of the integral, as long as we keep the end points fixed at 0 and 1, respectively, and no singularities are crossed in going from $[0, 1]$ to the complex contour.

$$\int_0^1 d\vec{x} \frac{\mathcal{F}(\vec{x})}{[\Lambda(\vec{x}) - i0]^\sigma} = \int_C d\vec{z} \frac{\mathcal{F}(\vec{z})}{[\Lambda(\vec{z})]^\sigma} \tag{3.72}$$

Obviously, the poles of the integrand are the zeros of $\Lambda(\vec{z})$. For non-integer σ, as they arise in dimensional regularization, we have to make sure $\Lambda(\vec{z})$ does not cross the cut of the logarithm extending over the whole negative real axis. But that is just what the $-i0$ prescription means: Choose an integration contour, such that $\Lambda(\vec{z})$ always has a negative imaginary part. Remarkably, that is easy to achieve. Let $\vec{z} = \vec{x} + i\vec{y}$ and Taylor expand $\Lambda(\vec{z})$ around $\vec{x}$,

$$\Lambda(\vec{x} + i\vec{y}) = \Lambda(\vec{x}) + i \sum_j y_j \frac{\partial \Lambda(\vec{x})}{\partial x_j} + \mathcal{O}(y^2). \tag{3.73}$$

Therefore, choosing the imaginary parts of Feynman parameters as[9]

$$y_j = -i\lambda x_j (1 - x_j) \frac{\partial \Lambda(\vec{x})}{\partial x_j} \tag{3.74}$$

[9] In [57, 58] Nagy and Soper give a slightly different formula, as they use Feynman parameters on the simplex.

gives

$$\Lambda(\vec{z}) = \Lambda(\vec{x}) - i\lambda \sum_j x_j(1-x_j) \left(\frac{\partial \Lambda(\vec{x})}{\partial x_j} \right)^2 + \mathcal{O}(\lambda^2). \tag{3.75}$$

The positive parameter λ controls the size of the deformation. Clearly, for λ small enough so that higher orders do not spoil the picture, $\Lambda(\vec{z})$ acquires a negative imaginary part. The factors $x_j(1-x_j)$ enforce the vanishing of the deformation at the endpoints of integration. Varying λ continuously deforms the integration contour from the original $[0,1]^n = C(0)$ into a $C(\lambda)$ that usually provides a negative imaginary part of $\Lambda(\vec{z})$ large enough to allow stable numerical integration. A few things should be noted here.

1. For λ small enough we have $\operatorname{Im}\Lambda(\vec{z}) \leq 0$, so the cut of the logarithm along the negative real axis is never crossed. Inside the integration region, the equality $\operatorname{Im}\Lambda(\vec{z}) = 0$ occurs only if all first derivatives of $\Lambda(\vec{x})$ vanish simultaneously. Such vanishing does no harm, unless it coincides with the vanishing of $\Lambda(\vec{x})$ itself. This happens only for special values of the kinematical invariants, generally corresponding to thresholds. At such points, the deformation actually has to fail and allow for divergences.

2. The λ^2 term neglected in eq. (3.75) cannot spoil the sign of the imaginary part, as it is purely real. So it is only the $\mathcal{O}(\lambda^3)$ terms we have to worry about. It is possible to modify the deformation eq. (3.74) in order to control higher order terms. However, this leads to huge expressions and in practice just keeping λ small enough seems to be the better solution.

3. Directly computing the maximal value for λ is not feasible. However, during the actual integration, it is trivial to detect, whether we have chosen λ to large. We just have to check if $\operatorname{Im}\Lambda(\vec{z}) \leq 0$ in every evaluation of the integrand. In practice, the criterion for failure should be $\operatorname{Im}\Lambda(\vec{z}) > \varepsilon$ using an $\varepsilon = 10^{-10}$ or so, to avoid false alarms due to rounding errors.

It is instructive to work out the deformation for the simple case of a equal mass scalar bubble.

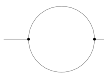

$$= \Gamma(\epsilon) \int_0^1 dx \frac{1}{[-x(1-x)s + m^2 - i0]^\epsilon} \tag{3.76}$$

Strictly speaking, in this example, deformation is not really necessary. As the denominator is raised to the power ϵ only, expanding in ϵ only gives logarithms of the denominator. Therefore, the vanishing of the denominator leads to a integrable singularity only. It would be sufficient to integrate without deformation and use a logarithm function that treats negative real arguments as if they came with $-i0$, i.e. opposite to the usual convention. But this should not prevent us from discussing the deformation, which would become necessary, if one of the propagators was squared, for instance. For simplicity, lets set $m^2 = 1$. The denominator polynomial is then

$$\Lambda(x) - i0 = -x(1-x)s + 1 - i\delta. \tag{3.77}$$

The poles are located at

$$x = \tfrac{1}{2}(1 \pm \sqrt{1 - 4/s}). \tag{3.78}$$

The location of the poles in x for a few special values of s is shown in fig. 3.4. For the unphysical negative values of s the poles lie on the real axis, but outside the interval $[0,1]$.

When s becomes positive, they jump to $0.5 \pm i\infty$. With s approaching the threshold value $s = 4$ from below, the poles move towards 0.5 from the top and the bottom, pinching the the integration contour at 0.5 for $s = 4$. Above threshold, the poles spread out just above the real interval, allowing for a deformation to the lower half plane. From

$$\Lambda'(x) = -s(1 - 2x) \tag{3.79}$$

we get the deformation

$$y(x) = \lambda x(1 - x)s(1 - 2x). \tag{3.80}$$

Figure 3.5 shows the undeformed $\Lambda(x)$ together with $y(x)$, as well as real and imaginary part of $\Lambda(x + iy)$ for $s = 5$, that is above threshold. The top left panel shows the parabola $\Lambda(x)$ with its two zeros, which lead to poles the deformation has to avoid. For s below threshold, the parabola would lie above the x-axis, for $s = 4$ it would just touch it. The bottom left panel is the deformation of the Feynman parameter, $y(x)$. It changes sign where $\Lambda'(x)$ does to give a definite sign to the linear term in the Taylor expansion eq. (3.73). The right panel shows real and imaginary part of the deformed $\Lambda(x + iy)$. The deformation does a good job: The imaginary part jumps in where the real part vanishes. Note that the zeros of the real part are shifted compared to the undeformed case. This is due to the real $\mathcal{O}(\lambda^2)$ contribution. At $x = 0.5$ we have $\operatorname{Im}\Lambda(z) = 0$ and $\operatorname{Re}\Lambda(z)$ equals $\Lambda(x)$ as the deformation vanishes there. This is harmless, as $\Lambda(x)$ is is nonzero there. However, if we go to the threshold $s = 4$, the minimum of the parabola $\Lambda(x)$ hits the x-axis, causing vanishing exactly where the deformation cannot help. For increased denominator powers, this would lead to a singular integral. Three more things should be noted

1. Looking only at the $s = 4 - \varepsilon$ case in fig. 3.4 one could get the wrong impression, that λ has to be kept very small in order not to hit the pole sitting very close to the real axes. But the deformation is exactly zero at $x = 0.5$ due to the vanishing of $\Lambda'(0.5)$, so the pole cannot be hit by making the deformation large. However, passing the poles at short distance still gives a peaked integrand.

2. Also from the fact, that $\Lambda(x)$ is only quadratic in this example it follows, that $\Lambda(z)$ has no $\mathcal{O}(\lambda^3)$ that could spoil the sign of the imaginary part. Thus λ can be made arbitrarily large. Feynman parametrizing one-loop integral usually leads to this situation. However the rescalings occurring during sector decomposition can lead to higher powers.

3. Figure 3.4 shows, that for large s, the poles approach the endpoints of the integration domain. This is unpleasant. The deformation will be small at the location of the poles, as it has to vanish at the endpoints. This problem generally occurs for very disparate values of the kinematic invariants and we shall address it later.

3.4.2 Integrals with $x^{-\alpha+\beta\epsilon}$ Singularities

In the last section, did not specify the numerator function $\mathcal{F}(\vec{x})$. Now it is time to have a special look at integrands, that contain singularities like $x_i^{-\alpha_i+\beta_i\epsilon}$. In presence of such singularities we could first extract the ϵ-poles by application of the subtraction formula (3.40) and expand in ϵ and then deform the individual pieces according to their denominator. For

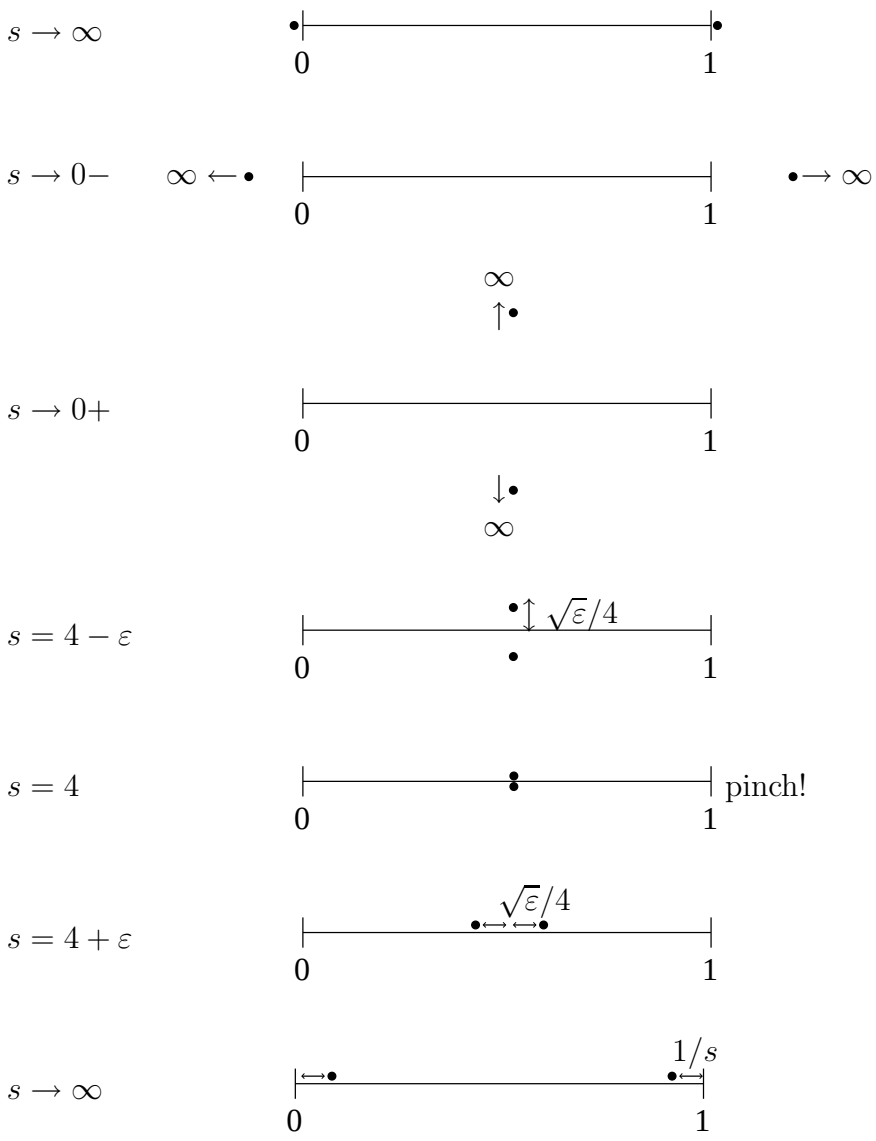

Figure 3.4: Location of poles in the Feynman parametrization of the scalar equal mass bubble. The mass has been set to $m^2 = 1$, several special values of s are shown.

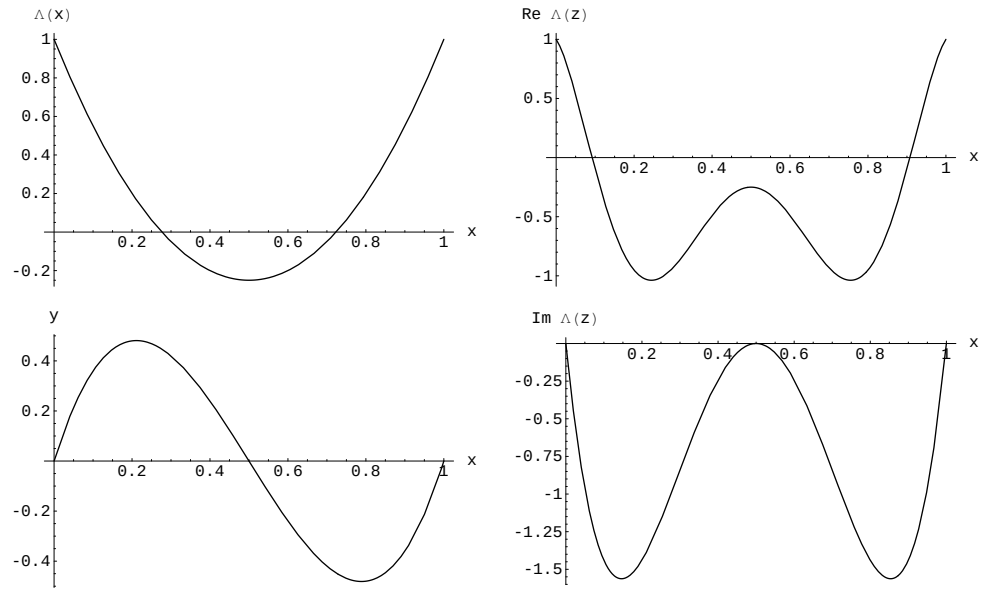

Figure 3.5: Some details of contour deformation for the scalar equal mass bubble. We have set $m^2 = 1$, $s = 5$ and $\lambda = 1$. The top left panel shows the undeformed denominator function $\Lambda(x)$. Below, the deformation of the Feynman parameter $y(x)$ is given. The right hand side shows real and imaginary part of the deformed denominator function $\Lambda(z)$.

instance in a simple one-dimensional case we would write

$$\int_0^1 dx \frac{x^{-1+\epsilon}}{[\Lambda(x) - i0]^\sigma} = \int_0^1 dx \left\{ \frac{x^{-1}}{[\Lambda(x) - i0]^\sigma} - \frac{x^{-1}}{[\Lambda(0) - i0]^\sigma} \right\} + \frac{1}{\epsilon} \frac{1}{[\Lambda(0)]^\sigma} + \mathcal{O}(\epsilon), \tag{3.81}$$

and then introduce deformations generated by $\Lambda(x)$ and $\Lambda(0)$. Of course, there is nothing to deform in $\Lambda(0)$, but in a more complicated case with two variables, we would have $\Lambda(x_1, x_2)$ and $\Lambda(0, x_2)$ and the second term would still require deformation of x_2. However, this is not a good idea. The problem is the unequal manipulation of the two individually divergent pieces of the integral. As we will see below, this manipulation is okay only if the deformation vanishes faster than linear as $x \to 0$. Thus we would have to change our deformation to

$$y_j = -i\lambda x_j^\eta (1 - x_j) \frac{\partial \Lambda(\vec{x})}{\partial x_j} \tag{3.82}$$

with $\eta > 1$, what is again bad for numerical stability. A better solution is to perform the subtraction and expansion only after deforming the integral. Actually, this is also easier to implement, as one does not have to deal with different deformations. We deform the integral

$$I = \int_0^1 d\vec{x} \left[\prod_j x_j^{-\alpha_j + \beta_j \epsilon} \right] \frac{\mathcal{F}(\vec{x}, \epsilon)}{[\Lambda(\vec{x}) - i0]^\sigma} = \int_0^1 d\vec{x} \left[\prod_j z_j^{-\alpha_j + \beta_j \epsilon} \right] J(\vec{x}) \frac{\mathcal{F}(\vec{z}(\vec{x}), \epsilon)}{[\Lambda(\vec{z}(\vec{x}))]^\sigma}, \tag{3.83}$$

where $\mathcal{F}(\vec{x},\epsilon)$ is a regular numerator function and

$$J(\vec{x}) = \det\left[\frac{\partial z_k}{\partial x_l}\right] \tag{3.84}$$

is the jacobian that arises when parametrizing the complex contour with the original Feynman parameters, $\vec{z} = \vec{z}(\vec{x})$. Now we exploit the fact, that y_j contains one power of x_j. We write $z_j = x_j(1+\rho_j)$, where

$$\rho_j(\vec{x}) = -i\lambda(1-x_j)\frac{\partial\Lambda(\vec{x})}{\partial x_k} \tag{3.85}$$

is polynomial. Rewriting

$$[z_j(\vec{x})]^{-\alpha_j+\beta_j\epsilon} = x_j^{-\alpha_j+\beta_j\epsilon}\,[1+\rho_j(\vec{x})]^{-\alpha_j+\beta_j\epsilon} \tag{3.86}$$

makes explicit, that the singularities are located in the real Feynman parameters only. The $[1+\rho_j]^{-\alpha_j+\beta_j\epsilon}$ pieces are nonsingular contributions which we can put together with the nonsingular $\mathcal{F}(\vec{z}(\vec{x}),\epsilon)$. Actually, we can just collect everything but the singularities in a big regular function

$$f_{\mathrm{reg}}(\vec{x},\epsilon) = \left[\prod_j [1+\rho_j(\vec{x})]^{-\alpha_j+\beta_j\epsilon}\right]\; J(\vec{x})\;\frac{\mathcal{F}(\vec{z}(\vec{x}),\epsilon)}{[\Lambda(\vec{z}(\vec{x}))]^\sigma}. \tag{3.87}$$

Our integral then reads

$$I = \int_0^1 d\vec{x}\;\left[\prod_j x_j^{-\alpha_j+\beta_j\epsilon}\right]\; f_{\mathrm{reg}}(\vec{x},\epsilon). \tag{3.88}$$

At this point we can use the subtraction formula (3.40) and expand in ϵ.

Just for illustration, we spell out, what happens inside f_{reg} in a simple two-dimensional example. Consider the integral and its deformation

$$\int_0^1 dx_1dx_2\; x_1^{-1+\epsilon}\frac{1}{[\Lambda(\vec{x})-i0]^\sigma} = \int_0^1 dx_1dx_2\; J(\vec{x})\; x_1^{-1+\epsilon}[1+\rho_1(\vec{x})]^{-1+\epsilon}\frac{1}{[\Lambda(\vec{z}(\vec{x}))]^\sigma}. \tag{3.89}$$

The subtraction formula then leads to

$$\begin{aligned}\int_0^1 dx_1dx_2\; x_1^{-1+\epsilon}\left\{\frac{J(x_1,x_2)[1+\rho_1(x_1,x_2)]^{-1+\epsilon}}{[\Lambda(z_1(x_1,x_2),z_2(x_1,x_2))]^\sigma} - \frac{J(0,x_2)[1+\rho_1(0,x_2)]^{-1+\epsilon}}{[\Lambda(z_1(0,x_2),z_2(0,x_2))]^\sigma}\right\}\\ + \frac{1}{\epsilon}\int_0^1 dx_2\;\frac{J(0,x_2)[1+\rho_1(0,x_2)]^{-1+\epsilon}}{[\Lambda(z_1(0,x_2),z_2(0,x_2))]^\sigma}.\end{aligned} \tag{3.90}$$

We should note a few things

- The deformation guarantees that $\mathrm{Im}\,\Lambda(\vec{z}(\vec{x})) \le 0 \quad \forall\vec{x}$. This includes the case, that some of the x_j are set to zero. Therefore, the deformation produces an imaginary part with the correct sign also for the subtraction terms. One may ask, if the deformation can possibly give a vanishing imaginary part for a subtraction in a case, where subtracting first and deforming the subtraction individually, as we intended at the beginning, would

give a nonzero deformation. The answer is no. The two contours are actually identical, as

$$\left(\frac{\partial}{\partial x_2}\Lambda(x_1,x_2)\right)\Big|_{x_1=0} = \frac{\partial}{\partial x_2}\Lambda(0,x_2). \tag{3.91}$$

- If stronger singularities $x_j^{-\alpha_k+\beta_j\epsilon}$ with $\alpha_j > 1$ are present, the subtraction formula produces x_j-derivatives of f_{reg} up to order $\alpha_j - 1$. Therefore, derivatives of Λ, $\mathcal{F}$ and the jacobian J appear. The deformation still does its job in this case. A derivative ∂_{x_j} acting on

$$\frac{1}{[\Lambda(\vec{z}(\vec{x}))]^\sigma} \tag{3.92}$$

just reproduces this term with an increased power $\sigma+1$ together with an inner derivative $\partial_{x_j}\Lambda(\vec{z}(\vec{x}))$. The latter just stays in the numerator. It never goes into denominators or logarithms, so we don't need to worry about the sign of its imaginary part. Symbolically, the derivative eliminates the constant $-i0$ term.

To conclude this section, we illustrate the claim made at the beginning. Subtracting and expanding first and then deforming the emerging terms individually leads to wrong results unless the deformation y_j vanishes faster than linear when $x_j \to 0$. Simply deforming each of the individually divergent terms according to its denominator in the right hand side of (3.81) gives

$$I_{\text{wrong}} = \frac{1}{\epsilon}\frac{1}{[\Lambda(0)]^\sigma} + \int_0^1 dx\, x^{-1}\left\{\frac{J(x)[1+\rho(x)]^{-1}}{[\Lambda(z(x))]^\sigma} - \frac{1}{[\Lambda(0)]^\sigma}\right\} + \mathcal{O}(\epsilon). \tag{3.93}$$

Here actually only the first term inside the brace got deformed, as the denominator of the subtraction is constant. We have rewritten z as $x[1+\rho(x)]$ and factored the common x^{-1} out of the brace. On the other hand, we can take the safe route of deforming first and expanding afterwards, avoiding the manipulation of divergent integrals.

$$\begin{aligned} I = \int_0^1 dx \frac{x^{-1+\epsilon}}{[\Lambda(x)-i0]^\sigma} = \int_0^1 dx \frac{J(x)z(x)^{-1+\epsilon}}{[\Lambda(z(x))]^\sigma} = \frac{1}{\epsilon}\frac{J(0)[1+\rho(0)]^{-1+\epsilon}}{[\Lambda(z(0))]^\sigma} + \\ \int_0^1 dx\, x^{-1}\left\{\frac{J(x)[1+\rho(x)]^{-1}}{[\Lambda(z(x))]^\sigma} - \frac{J(0)[1+\rho(0)]^{-1}}{[\Lambda(z(0))]^\sigma}\right\} + \mathcal{O}(\epsilon). \end{aligned} \tag{3.94}$$

From the definition of the deformation it follows. that $1+\rho(x) = z/x$ and $J(x) = \partial z/\partial x$ are equal at $x = 0$. Together with $z(0) = 0$ this means, that the terms inside the brace are equal to the corresponding terms in the expression for I_{wrong}. However, in the pole term, we have

$$\frac{1}{\epsilon}\frac{J(0)[1+\rho(0)]^{-1+\epsilon}}{[\Lambda(z(0))]^\sigma} = \frac{1}{\epsilon}\frac{[1+\rho(0)]^\epsilon}{[\Lambda(0)]^\sigma} = \frac{1}{\epsilon}\frac{1}{[\Lambda(0)]^\sigma} + \frac{\log(1+\rho(0))}{[\Lambda(0)]^\sigma} + \mathcal{O}(\epsilon). \tag{3.95}$$

In I_{wrong} we obviously missed the $\log(1+\rho(0))$ term, which vanishes only if $y(x)$ vanishes faster than linear. Clearly, for higher order terms in ϵ, a similar discrepancy occurs also in the subtracted integral.

We could of course subtract the integral, but postpone the ϵ-expansion. This way, the integral remains regulated and so the deformation step does not manipulate divergent integrals.

Deforming each term according to their denominator then produces

$$I = \int_0^1 dx \frac{x^{-1+\epsilon}}{[\Lambda(x) - i0]^\sigma} = \frac{1}{\epsilon}\frac{1}{[\Lambda(0)]^\sigma} + \int_0^1 dx \left\{ \frac{J(x)z(x)^{-1+\epsilon}}{[\Lambda(x)]^\sigma} - \frac{x^{-1+\epsilon}}{[\Lambda(0)]^\sigma} \right\}. \tag{3.96}$$

The problem appears when we try to ϵ-expand the subtracted integral on the right hand side. The $\epsilon \to 0$ limit is not interchangeable with the integration, unless the imaginary part $y(x)$ vanishes faster than linear as $x \to 0$. Computing the limit using a subtraction means deforming first and subtracting afterwards. Blindly interchanging limit and integration directly gives the expression I_{wrong}. This picture generalises to the multidimensional case, where subtractions generally have nontrivial residual deformations, just the jacobians become more involved. We are not going to spell this out. There is no good reason for deforming subtractions separately and using fastly vanishing deformations.

3.4.3 Tuning the Deformation

Using the deformation discussed so far, we were able to evaluate numerically many Feynman diagrams from practical calculations in the physical region. We usually chose to factor out one kinematical invariant from the polynomial $\Lambda(\vec{x})$. This renders $\Lambda(\vec{x})$ dimensionless and for kinematical invariants of comparable size, the coefficients of the polynomial become of order one.

The parameter λ, which controls the size of the deformation an important role. Clearly, too small values of λ do not distance the contour well enough from the poles on the real axis. But due to the uncontrolled $\mathcal{O}(\lambda^3)$ terms, too large values of λ again degrade the quality of the deformation, even to the extent, that $\operatorname{Im}\Lambda$ changes sign, i.e. singularities are crossed. Actually, even in the absence of $\mathcal{O}(\lambda^3)$ terms, exaggerated values for λ usually degrade convergence. In most cases, we found that there is a good range of the parameter λ, that gives good convergence. As a rule of thumb $\lambda = 0.1$ is good starting point.

However, very disparate values for the kinematical invariants sometimes lead to deformation y_i of disparate sizes for different Feynman parameter. It happens, that some y_i should be scaled up in order to circumvent a singularity at a sizeable distance, but cranking up λ would lead to an invalid contour, as some other Feynman parameters are already strongly deformed. That is easy to fix. Nothing prevents us from choosing a separate λ_i for every Feynman parameter x_i. With many parameters λ_i, we need a way of finding good values for them. A simple way of choosing λ_i proved very useful: We perform a small sample integration run using a small[10] common value for all directions, $\lambda_i = \lambda_{\text{test}}$. While discarding result of this integration, for each Feynman parameter x_i we record the maximal $|y_i|$ sample occurring

[10] Our program aborts if an a wrong sign of $\operatorname{Im}\Lambda(\vec{z})$ is detected. Thus λ_{test} has to be chosen small enough to give a valid contour. Unfortunately, our program cannot automatically reduce a λ chosen to large. As we use a third party integration package, the check of $\operatorname{Im}\Lambda(\vec{z}) < 0$ has to be performed by the integrand itself. If the integrand, called by the integration package, detects an invalid deformation, it would have to pass control back to the code that invoked the integration package. An elegant way of doing so would be via the exception handling capability of C++. But as our integration package was compiled using a C rather than a C++ compiler, its stack is not prepared for exception handling. Thus exceptions cannot be thrown through the integration routine.

during integration[11] . Then we simply set

$$\lambda_i = \lambda \cdot \frac{\lambda_{\text{test}}}{\max_{\text{samples}} |y_i|}. \tag{3.97}$$

For the MSSM calculation described in chapter 4, we evaluated Feynman integrals containing particles with masses as disparate as $m_1^2/m_2^2 = 10^4$. Without the above trick, some of these integrals did not converge at all. Also for less problematic diagrams we observed a significant speedup.

At this point, we should recall a comment made at the very beginning of this chapter. While our integrals

$$\int_0^1 d\vec{x}\; J(\vec{x})\; \mathcal{I}(\vec{z}(\vec{x})) \tag{3.98}$$

do not depend on the contour and thus on the parameters λ_i, the same is not true for the integrals of the modulus of the integrand

$$\int_0^1 d\vec{x}\; |\operatorname{Re} J(\vec{x})\; \mathcal{I}(\vec{z}(\vec{x}))| \quad \text{and} \quad \int_0^1 d\vec{x}\; |\operatorname{Im} J(\vec{x})\; \mathcal{I}(\vec{z}(\vec{x}))|, \tag{3.99}$$

as the modulus is not an analytic function. Above threshold, the value of a Feynman integral arises as the difference between positive and negative contributions. The fact, that the integral of the modulus depends on the contour, tells us, that by tuning the contour, we have a handle on the amount of cancellation occurring in the calculation of the integral. In the limit, where the deformation is switched off, the cancellation becomes infinitely large and the integral is defined as a kind of principle value only. But also trading an adequate common value for λ for good values of λ_i can sometimes reduce the amount of cancellation by a factor of ten. This of course leads to a huge speedup, especially when using stochastic integration, where the number of evaluations scales badly with the relative precision required. We have not implemented an automatic optimization for finding values λ_i that minimize cancellations. We just have a switch for inserting a modulus around the integrand and the possibility to hand-tune the λ_i given by eq. (3.97) if everything else fails.

Discussing the deformation for the equal mass bubble we already noticed, that disparate values for kinematical invariants can squeeze the zeros of $\Lambda(x)$ to the boarder of the integration region. In figure 3.4 we can see, that for $s \to \infty$, the zeros are located at $\frac{1}{s}$ and $1 - \frac{1}{s}$. The deformation is weak at these points. We should set $\lambda \sim 1/s$ in order to get a deformation of size $y \sim 1$. But due to the factor $x(1-x)$ enforcing the required vanishing of the deformation at the endpoints, at the zero of $\Lambda(x)$, $x_0 \sim 1/s$ where the deformation is really needed, it gets degraded to $y(x_0) \sim 1/s$. Choosing setting $\lambda \sim 1$, so $y \sim s$ and $y(1/s) \sim 1$ is not an option, since it makes $\Lambda(x+iy)$ grow faster. An interesting detail is, that the growing y does not even bring us as far away from the pole as it seems at first sight. The deformation also modifies the real part of Λ

$$\operatorname{Re} \Lambda(x+iy) = \Lambda(x) - y^2 \Lambda''(x) \xrightarrow{x \to 0} 1 - xs - x^2\lambda^2 s^3. \tag{3.100}$$

The last term becomes sizeable for $x \sim 1/(\lambda s^{\frac{3}{2}})$. So depending on the scaling of λ it can grow

[11] We actually took the maximum over all sectors originating from a given diagram.

faster than xs. If we set $\lambda = 1/s^\alpha$ the zero of $\mathrm{Re}\,\Lambda(z(x))$ will lie roughly at

$$x_0 \sim \begin{cases} s^{-1} & \text{for} \quad \alpha \geq \frac{1}{2} \\ s^{\alpha-3/2} & \text{for} \quad \alpha < \frac{1}{2} \end{cases} \quad . \tag{3.101}$$

Obviously, blowing up the deformation such that $y(1/s) \sim 1$ has the side effect of squeezing the zero of $\mathrm{Re}\,\Lambda(z(x))$ from s^{-1} to $s^{-3/2}$.

The situation can be improved by a change of variables, that stretches the region close to the border. An function that does the job is

$$x(t) = \begin{cases} 2^{n-1}\, t^n & \text{for} \quad t \leq 2 \\ 1 - 2^{n-1}\, (1-t)^n & \text{for} \quad t > 2 \end{cases} \tag{3.102}$$

with the jacobian

$$\frac{\partial x}{\partial t} = \begin{cases} 2^{n-1} n\, t^{n-1} & \text{for} \quad t \leq 2 \\ 2^{n-1} n\, (1-t)^{n-1} & \text{for} \quad t > 2 \end{cases} \quad . \tag{3.103}$$

It is crucial to apply this transformation to the deformed integrand, rather than deforming the transformed integrand. For small x, the deformed integrand is roughly

$$\frac{1}{[\Lambda(x) - ix\mu]^\sigma}, \tag{3.104}$$

where $\mu = \lambda[\Lambda'(0)]^2$ is the slope of the deformation close 0. At the zero $\Lambda(x)$, we have a deformation of the size $x_0\mu$ or $t_0^n\mu$ in the new variable. At this point, the jacobian nt_0^{n-1} tames the size of the integrand. Absorbing the jacobian into the denominator and reexpressing everything in terms of x shows us, what we have gained at x_0. The imaginary part preventing the denominator from vanishing at x_0 has changed

$$-ix_0\mu \longrightarrow -in^{-\sigma}\, x_0^{1-\frac{1}{\sigma}(1-\frac{1}{n})}\, \mu. \tag{3.105}$$

So choosing a mild $n = 2$, for $\sigma = 1$, the small factor x_0 is replaced by $\sqrt{x_0}$. For larger powers σ, the transformation is less effective.

Applying the transformation (3.103) prior to deforming of course gives the same jacobian. But also the deformation gets degraded to

$$-i\lambda t(1-t) \left(\frac{\partial \Lambda}{\partial x}\right)^2 \left(\frac{\partial x}{\partial t}\right)^2. \tag{3.106}$$

Expressing t_0 in terms of x_0 roughly kills one power of $(\partial x/\partial t)$, as $x \sim (\partial x/\partial t)t$. But a factor $n(\partial x/\partial t) = n^2 t^{n-1}$ remains and decreases the deformation at x_0. For $\sigma = 1$ the jacobian cancels this factor up one n. So the scaling of the imaginary part for $x_0 \to 0$ is not improved. For larger σ it is even degraded.

Finally we should mention a weak point of our method, which we have not addressed. Numerical integration gets more difficult, as the denominator power σ increases. For scalar integrals $\sigma = N_{\text{propagators}} - 2N_{\text{loops}}$. Loop momenta in the numerator produce terms with lower σ, but tensors generally contain a part consisting of external momenta only. Singularities $x^{-\alpha+\beta\epsilon}$ with $\alpha > 1$ lead to subtractions containing derivatives ∂_x. This way values of

σ higher than suggested by power counting can appear. It is not clear, whether some clever transformation or a representation of integrals different from ordinary Feynman parametrization can eliminate the problem of large exponents σ.

3.4.4 Comments on Implementation

We mention some issues related to practical implementation of our method.

1. To eliminate prohibitive growth of expressions, it is important not to substitute algebraic expressions into each other wherever this can be avoided. Thus we introduce a symbol $\texttt{poly}_\texttt{i}[\texttt{x}_1, \ldots, \texttt{x}_\texttt{n}]$ for each polynomial p_i occurring in a factor $\texttt{fac}[\texttt{p}_\texttt{i}, \texttt{e}_\texttt{i}]$. The deformation step then only replaces every Feynman parameter $\texttt{x}_\texttt{i}$ occurring as an argument of such a polynomial or in the argument expressions of the bookkeeping function $\texttt{jet}[\cdot, \ldots, \cdot, \epsilon]$ by a new symbol $\texttt{z}_\texttt{i}[\texttt{x}_1, \ldots, \texttt{x}_\texttt{n}]$. Recall, that the slots of `jet` represented by dots contain polynomials in Feynman parameters remembering the rescalings occurring during sector decomposition. Note that It further inserts a symbol for the jacobian $\texttt{jac}[\texttt{x}_1, \ldots, \texttt{x}_\texttt{n}]$. Next, subtraction and ϵ-expansion takes place. This introduces several new objects

   (a) Deformed Feynman parameters and jacobians with some Feynman parameters set to zero e.g. $\texttt{z}_1[\texttt{x}_1, 0]$ and $\texttt{jac}[\texttt{x}_1, 0]$.

   (b) With singularities $x_i^{-\alpha_i+\beta_i\epsilon}$ with $\alpha_i > 1$, the ∂x_i derivative occurring in subtractions leads to derivatives of deformed Feynman parameters, jacobians, polynomials and the bookkeeping function `jet`, e.g.

   $$\texttt{Derivative}[0,1][\texttt{z}_1][\texttt{x}_1, 0]$$
   $$\texttt{Derivative}[0,1][\texttt{jac}][\texttt{x}_1, 0]$$
   $$\texttt{Derivative}[0,1][\texttt{poly}_\texttt{i}][\texttt{z}_1[\texttt{x}_1, 0], \texttt{z}_2[\texttt{x}_1, 0]]$$
   $$\texttt{Derivative}[0,1,0][\texttt{jet}][\cdot, \ldots, \cdot, \epsilon = 0]$$

   Note, that `Derivative` stands for derivatives with respect to slots of the function under consideration. In the last two examples, the slots contain more complicated expressions than just undeformed Feynman parameters $\texttt{x}_\texttt{i}$, so these expressions are always accompanied by the corresponding inner derivatives.

   (c) Derivatives of the bookkeeping function `jet` with respect to ϵ, e.g. $\texttt{Derivative}[0, \ldots, 0, 2][\texttt{jet}][\cdot, \ldots, \cdot, \epsilon = 0]$. As these arise from expanding around $\epsilon = 0$, they are always evaluated at $\epsilon = 0$.

   After introducing all these symbols, it is useful to clean up the our expression by eliminating symbols that vanish identically. For this, we have to dig out all polynomials $\texttt{poly}_\texttt{i}$ and the original tensor we masked by `jet`, compute the necessary derivatives and insert all arguments occurring in our expression, taking into account that $x_i = 0 \Rightarrow z_i = 0$.

2. After deforming and ϵ-expanding taking care of the issues mentioned above, our Mathematica code produces C++ codes of all the deformed integrands. A separate source file is produced for every sector. Further a file containing all required derivatives of the tensor function is produced.

   The integrands step by step evaluate all symbols numerically. I.e. first all deformed Feynman parameters and their derivatives are computed, then these numbers are substituted into polynomials and tensor functions. Thereby each sector integrand calls the

tensor functions with the proper arguments as remembered by the bookkeeping functions `jet`. To simplify the code generation, we use a single large array to store all symbols. We put

$$\mathtt{z}[\mathtt{1}] = \mathtt{z}_\mathtt{1}[\mathtt{x}_\mathtt{1}, \ldots \mathtt{x}_\mathtt{n}]$$

$$\vdots$$

$$\mathtt{z}[\mathtt{n}] = \mathtt{z}_\mathtt{n}[\mathtt{x}_\mathtt{1}, \ldots \mathtt{x}_\mathtt{n}].$$

At higher indices $\mathtt{n}+\mathtt{1}$ etc. we store objects like

$$\mathtt{z}_\mathtt{2}[\mathtt{0}, \mathtt{x}_\mathtt{2}, \ldots \mathtt{x}_\mathtt{n}],$$
$$\mathtt{Derivative}[\mathtt{1}, \mathtt{0}, \ldots, \mathtt{0}][\mathtt{z}_\mathtt{2}][\mathtt{0}, \mathtt{x}_\mathtt{2}, \ldots \mathtt{x}_\mathtt{n}]$$

if they occur and finally all instances of polynomials and jacobians.

The actual C++ files are written using the the `Splice` process of Mathematica. Thereby, Mathematica expressions are converted to C syntax using the `CAssign` function provided by Mark Sofroniou's package `Format.m` [65]. `CAssign` can optimize expressions by introducing a hierarchy of intermediate variables for subexpressions occurring repeatedly. While we have tried to do this by hand at the level of deforming and expanding, the automatic optimization is still very important for the tensor functions and for the complicated sector decomposed polynomials $\Lambda(\vec{x})$. Optimization not only reduces complexity in terms of numbers of operations. It also reduces the size of the code and thus may make it small enough for caching.

3. In the above illustration we have suppressed the treatment of the jacobians, that arise, when the complex contour is parametrized in terms of the real Feynman parameters. We have just represented them as a symbol $\mathtt{jac}[\mathtt{x}_\mathtt{1}, \ldots \mathtt{x}_\mathtt{n}]$, and, as mentioned above, subtraction and ϵ-expansion may have produced derivatives of this symbol, as well as set some of their arguments to zero. For our numerical code, we have to implement the expressions hiding behind all these symbols. So let us spell out a simple example, to see, what they actually mean:

$$\mathtt{jac}[\mathtt{0}, \mathtt{x}_\mathtt{2}] = \det \begin{bmatrix} \mathtt{Derivative}[\mathtt{1},\mathtt{0}][\mathtt{z}_\mathtt{1}][\mathtt{0}, \mathtt{x}_\mathtt{2}] & \mathtt{Derivative}[\mathtt{1},\mathtt{0}][\mathtt{z}_\mathtt{2}][\mathtt{0}, \mathtt{x}_\mathtt{2}] \\ \mathtt{Derivative}[\mathtt{0},\mathtt{1}][\mathtt{z}_\mathtt{1}][\mathtt{0}, \mathtt{x}_\mathtt{2}] & \mathtt{Derivative}[\mathtt{0},\mathtt{1}][\mathtt{z}_\mathtt{2}][\mathtt{0}, \mathtt{x}_\mathtt{2}] \end{bmatrix}. \tag{3.107}$$

In reality we will have more than two Feynman parameters and so the determinant should be computed numerically. For this our Mathematica code will output something like

$$\mathtt{detfun}[\mathtt{z}[\mathtt{47}], \mathtt{z}[\mathtt{48}], \mathtt{z}[\mathtt{63}], \mathtt{z}[\mathtt{64}]], \tag{3.108}$$

collecting the array elements that will store the numerical values of the derivatives occurring in the jacobian matrix. The C function `detfun` will compute the determinant using the LU factorization algorithm provided by the GSL library [66]. Note that jacobians generally contain derivatives of deformed Feynman parameters, that do not occur in the rest of the integrand. Thus these are not explicit, when jacobians represented as symbols only.

Derivatives of determinants can be rewritten using the formula

$$\frac{\partial}{\partial x_i} \det[\vec{v}_1, \dots \vec{v}_n] = \sum_{j=1}^{n} \det[\vec{v}_1, \dots, \frac{\partial \vec{v}_j}{\partial x_i}, \dots, \vec{v}_n], \tag{3.109}$$

that follows from the multi-linearity of the determinant. The $\vec{v}_j$ are column vectors of the matrix under consideration.

4. We mention, that subtractions may lack deformation due to Feynman parameters fixed at 0. The simplest example is a bubble diagram with one massive and one massless particle in the loop. After factoring out a common x, which leads to an IR singularity, the combined denominator is

$$\Lambda(x) = -(1-x)s + m^2. \tag{3.110}$$

Clearly, in the subtraction we ge $\Lambda(0) = -s + m^2$, lacking deformation, as there is no Feynman parameter left. For the $1/\Lambda(0)$ term, this is no problem, but we have to make sure we get the correct imaginary part in $\log(\Lambda(0))$. With our choice of signs Λ always comes with a $-i0$. Therefore it is sufficient to use a logarithm function, that treats negative real arguments as if they came with a $-i0$, i.e. opposite to the usual convention. As easy the fix, as nasty is the bug if one is not aware of the problem.

5. For the actual integration our program invokes the VEGAS, DIVONNE or CUHRE algorithm from the CUBA library by Thomas Hahn [67]. DIVONNE, a Monte Carlo algorithm using advanced methods for variance reduction usually gives the best results. We found, that it tends to underestimate the integration error in difficult situations, though. VEGAS is the classical adaptive Monte Carlo algorithm. While very robust, it is often significantly slower than DIVONNE. Moreover, we found that the implementation in CUBA 1.4. is buggy. In difficult situations it suddenly left the hypercube $[0,1]^n$ and started to sample the integrand at negative values of the integration variables. Values were such, that they did not occur due to rounding errors for sure. We suspect some overflow in the subdivision code. CUHRE is a deterministic algorithm. In situations with 5 or 6 Feynman parameters, one would expect it could still beat Monte Carlo methods. We found, that in many situations, it performed much better than DIVONNE. Unfortunately for some integrals it failed, giving NaN as a result. For others, it gave excellent values, but overestimated the integration error by a two orders of magnitude. The reasons for those issues have not become clear.

3.4.5 Examples

As an illustration, we present result for the two master integrals shown in figure 3.6. It is understood, that here we are dealing with the scalar parts only, i.e. the diagrams stand for their propagators only. Diagrams with a nontrivial tensor structure will show up in chapter 4. Diagram 3.6a is the last master integral contributing to $gg \to h$, computed analytically in chapter 2. In figure 3.7 we compare our numerical result to the analytic expression. On the left panel, we plot the real part of the order ϵ^0 piece of the diagram as a function of $\tau = s/(4m^2)$, normalized to $m^2 = 1$. The inset plot gives a more detailed view of the threshold region, where the numerical integration is most difficult, superimposed with the analytic result. The

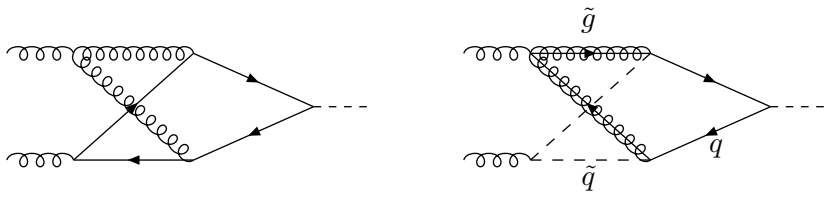

(a) (b)

Figure 3.6: (a) Master integral contributing to $gg \to h$ with a heavy quark loop. (b) Master integral arising in the calculation of $gg \to h$ in the MSSM.

plot on the right panel shows the difference between the numerical and analytical results, normalized to the analytic value. The gray band shows the integration error, obtained by adding in quadrature the errors quoted by the integration routine for each sector. We obtain similar results for the imaginary part of the order ϵ^0 piece and also for real and imaginary part of the single pole coefficient.

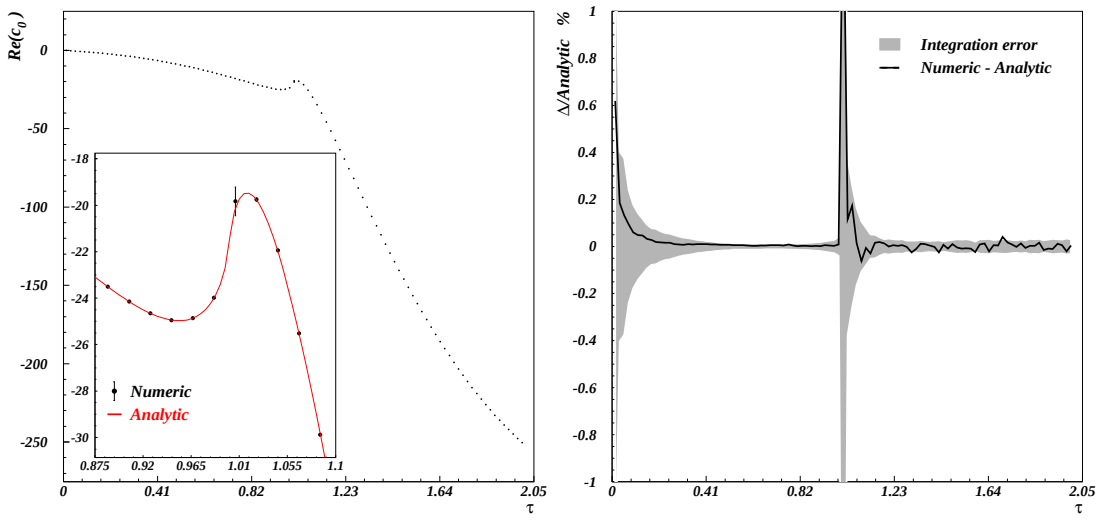

Figure 3.7: Results for the real part of the finite piece ($\mathrm{Re}(c_0)$) of the Feynman diagram in Fig. 3.6a. The left panel shows the results of the numerical integration as black dots with error bars. The inset plot zooms in on the threshold region, the red line corresponds to the evaluation of the analytic result of chapter 2. The right panel shows the difference in percent of the numerical evaluation and the analytic one, normalized to the latter. The gray bands correspond to the integration error. At threshold this error is 3%.

Diagram 3.6b is a master integral arising in the calculation of $gg \to h$ in the MSSM. It involves a massive quark, a massive scalar quark and a massive gluino. Due to the presence of three different masses, it cannot be computed using the analytical method described in chapter 2 and no analytic result is known. For the numerical method, the masses do not pose a problem. On the contrary, due to the absence of massless propagators, the numerical evaluation turns out to be substantially faster than for diagram Diagram 3.6a. Our results

are displayed in figure 3.8 as a function of $\tau = s/(4m_q^2)$ for fixed values of $m_{\tilde{g}}^2 = 400/175\, m_q^2$ and $m_{\tilde{q}}^2 = 600/175\, m_q^2$ with $m_q = 1$.

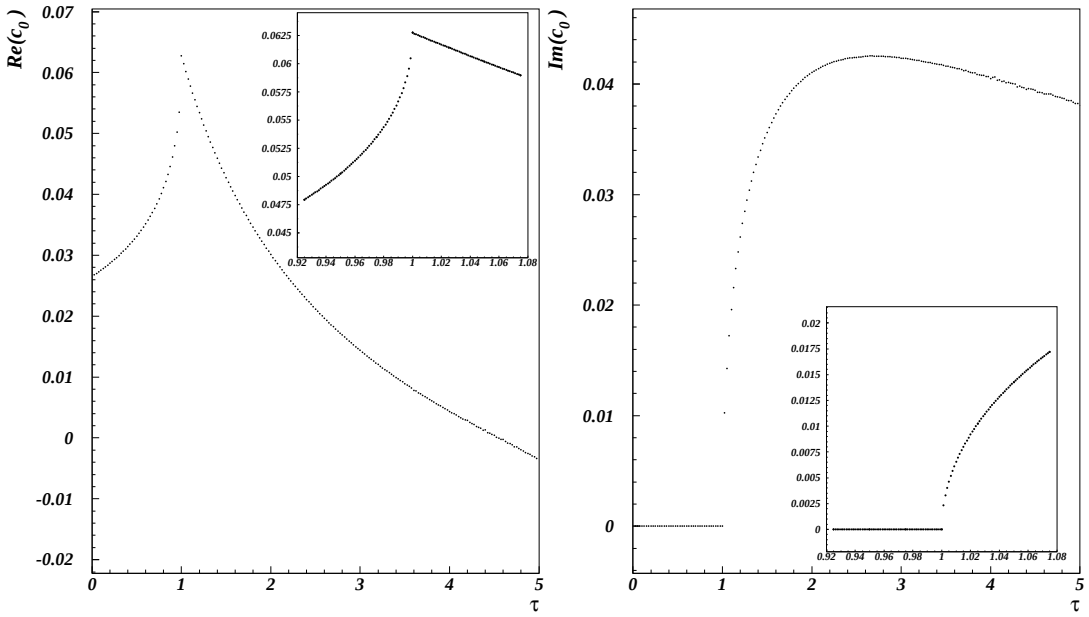

Figure 3.8: Results for the scalar integral corresponding to the Feynman diagram in figure 3.6b as a function of $\tau = s/(4m_q^2)$ for fixed values of $m_{\tilde{g}}^2 = 400/175\, m_q^2$ and $m_{\tilde{q}}^2 = 600/175\, m_q^2$. The inset plots zoom in the threshold region. The estimated relative accuracy of the points is better that 1 per mille.

Chapter 4

Application to $gg \to h, H$ in the MSSM

In this chapter we compute the virtual supersymmetric QCD contributions to $gg \to h, H$ up to two-loop order.

4.1 Overview of the MSSM

4.1.1 Particle Content and Interactions

The matter content of the MSSM is summarized in table 4.1. It essentially arises by taking all Standard Model particles and including a superpartner with opposite statistics for each of them. However, unlike in Standard Model, where masses for both up- and down-type quarks can be generated using a single Higgs doublet, in a supersymmetric model two doublets H_u and H_d are required for this. Two doublets with opposite hypercharge also make sure, that the higgsinos do not spoil the gauge anomaly cancellation. The necessary gauge supermultiplets are listed in table 4.2.

Names		spin 0	spin 1/2	$SU(3)_C$, $SU(2)_L$, $U(1)_Y$
squarks, quarks	Q	$(\widetilde{u}_L \quad \widetilde{d}_L)$	$(u_L \quad d_L)$	$(\mathbf{3}, \mathbf{2}, \frac{1}{6})$
($\times$3 families)	$\overline{u}$	$\widetilde{u}_R^*$	$u_R^\dagger$	$(\overline{\mathbf{3}}, \mathbf{1}, -\frac{2}{3})$
	$\overline{d}$	$\widetilde{d}_R^*$	$d_R^\dagger$	$(\overline{\mathbf{3}}, \mathbf{1}, \frac{1}{3})$
sleptons, leptons	L	$(\widetilde{\nu} \quad \widetilde{e}_L)$	$(\nu \quad e_L)$	$(\mathbf{1}, \mathbf{2}, -\frac{1}{2})$
($\times$3 families)	$\overline{e}$	$\widetilde{e}_R^*$	$e_R^\dagger$	$(\mathbf{1}, \mathbf{1}, 1)$
Higgs, higgsinos	H_u	$(H_u^+ \quad H_u^0)$	$(\widetilde{H}_u^+ \quad \widetilde{H}_u^0)$	$(\mathbf{1}, \mathbf{2}, +\frac{1}{2})$
	H_d	$(H_d^0 \quad H_d^-)$	$(\widetilde{H}_d^0 \quad \widetilde{H}_d^-)$	$(\mathbf{1}, \mathbf{2}, -\frac{1}{2})$

Table 4.1: Chiral supermultiplets in the Minimal Supersymmetric Standard Model. The spin-0 fields are complex scalars, and the spin-1/2 fields are left-handed two-component Weyl fermions.

Names	spin 1/2	spin 1	$SU(3)_C$, $SU(2)_L$, $U(1)_Y$
gluino, gluon	$\widetilde{g}$	g	(**8**, **1** , 0)
winos, W bosons	$\widetilde{W}^{\pm}$ $\widetilde{W}^0$	$W^{\pm}$ W^0	(**1**, **3** , 0)
bino, B boson	$\widetilde{B}^0$	B^0	(**1**, **1** , 0)

Table 4.2: Gauge supermultiplets in the Minimal Supersymmetric Standard Model.

In a renormalizable supersymmetric field theory, masses and interactions of all particles are either fixed by the gauge structure or by the interactions of chiral multiplets

$$\mathcal{L}_{\rm int} = -\frac{1}{2}\frac{\delta^2 W}{\delta\phi_i \delta\phi_j}\psi_i\psi_j + \frac{\delta W}{\delta\phi_i}F_i + c.c.\ , \tag{4.1}$$

parametrized by the superpotential

$$W = L^i\phi_i + \frac{1}{2}M^{ij}\phi_i\phi_j + \frac{1}{6}y^{ijk}\phi_i\phi_j\phi_k. \tag{4.2}$$

Here M^{ij} give rise to masses for fermions, whereas y^{ijk} is a Yukawa coupling[1] of a scalar ϕ_k and two fermions $\psi_i\psi_j$. The superpotential W is an analytic function of the complex scalar fields ϕ_i; it does not depend on the complex conjugates ϕ_i^*. Note, that not all terms in eq. (4.2) are necessarily allowed by gauge invariance.

In the superfield formulation, W is a function of superfields Φ_i, rather than the scalars ϕ_i. Even though we avoid superfields here, we shall use this notation in eq. (4.6), as it is standard and saves some tildes. In any case, the superpotential is just an efficient way of encoding terms of the Lagrangian.

As gauge fields are parts of gauge supermultiplets, coupling them to matter also introduces couplings of gauginos λ^a and the auxiliary fields D^a to matter through the vertices

$$g\,(\phi^* T^a \psi)\lambda^a, \qquad g\,\lambda^{\dagger a}(\psi^\dagger T^a \phi) \qquad \text{and} \qquad g\,(\phi^* T^a \phi)D^a. \tag{4.3}$$

The last term combines with the $D^aD^a/2$ term in the free gauge Lagrangian to give the equation of motion $D^a = -g(\phi^* T^a \phi)$. Substituting this back into the Lagrangian then leads to $-\frac{1}{2}D^aD^a$, which is a quartic potential for the scalar fields. Another contribution to this potential arises from $\mathcal{L}_{\rm int}$: The last term of eq. (4.1), its complex conjugate and the F_iF^{*i} term from the Lagrangian of the free chiral multiplets sum up to $F_iF^{*i} + W^iF_i + W_i^*F^{*i}$, where we have introduced the shorthand $W^i = \delta W/\delta\phi_i$. Using the trivial equations of motion $F_i = -W_i^*$ and $F^{*i} = -W^i$, we arrive at a total $-W^iW_i^*$ or $-F^{*i}F_i$ term in the Lagrangian.

[1]The origin of this notation $\frac{1}{6}y^{ijk}\phi_i\phi_j\phi_k$ is is the following: Requiring, that $\mathcal{L}_{\rm int} = -\frac{1}{2}W^{ij}\psi_i\psi_j + W^i + c.c$ is invariant under SUSY, one gets the condition, that $\frac{\delta W^{ij}}{\delta\phi_k^*}$ vanishes $\forall i,j,k$ and $\frac{\delta W^{ij}}{\delta\phi_k}$ has to by totally symmetric in ijk. Keeping only renormalisable interactions, W^{ij} can only be a polynomial of degree 1 in the scalar fields ϕ_i, so $W^{ij} = M^{ij} + y^{ijk}\phi_k$ with y^{ijk} totally symmetric. Therefore it is convenient to write $W^{ij} = \frac{\delta^2 W}{\delta\phi_i\delta\phi_k}$ with $W = L^i\phi_i + \frac{1}{2}M^{ij}\phi_i\phi_j + \frac{1}{6}y^{ijk}\phi_i\phi_j\phi_k$. Here it is of course pointless to talk about symmetry of y^{ijk}. We have just a Yukawa for every triple of fields, as in eq. (4.6).

Therefore, the full scalar potential is

$$V(\phi,\phi^*) = F^{*i}F_i + \frac{1}{2}D^aD^a = W_i^*W^i + \frac{1}{2}g_a^2(\phi^*T^a\phi)^2. \tag{4.4}$$

V is nonnegative, as it is a sum of squares. Interestingly, it is completely determined by the other interactions of the theory; the D-terms by the gauge interactions and the F-terms by fermion mass terms and Yukawa couplings specified by the superpotential W.

In a realistic phenomenological Model, supersymmetry has to be spontaneously broken. I.e. supersymmetry should only be broken by a non supersymmetric vacuum state, rather than in the Lagrangian. This way, supersymmetry can be hidden at low energies very much like the electroweak symmetry in the Standard Model.

We do not discuss possible mechanisms of supersymmetry breaking here, but just parametrize their low energy effects by including an effective Lagrangian, which explicitly breaks supersymmetry. The breaking terms have to be soft, i.e. they should have positive mass dimensions, in order not to introduce quadratically divergent radiative corrections to scalar masses. The possible terms are in general

$$\mathcal{L}_{\text{soft}} = -\left(\frac{1}{2}M_a\lambda^a\lambda^a + \frac{1}{6}a^{ijk}\phi_i\phi_j\phi_k + \frac{1}{2}b^{ij}\phi_i\phi_j + t_i\phi_i\right) + c.c. - (m^2)^i_j\phi^{j*}\phi_i. \tag{4.5}$$

These are

- Gaugino masses M_a for each gauge group. Unlike gauge boson masses, these terms are not forbidden by gauge symmetry.
- Scalar masses $(m^2)^i_j$. These are allowed, if ϕ_i and ϕ^{j*} transform in complex conjugate representations of each other. As this is always the case for $i = j$, every scalar can acquire a mass this way.
- Trilinear, bilinear and tadpole scalar couplings. These terms have the same form as the terms of the superpotential. They are allowed by gauge invariance if and only if a corresponding term in the superpotential is allowed.

The superpotential in the MSSM is

$$W_{\text{MSSM}} = \overline{u}\mathbf{y_u}QH_u - \overline{d}\mathbf{y_d}QH_d - \overline{e}\mathbf{y_e}LH_d + \mu H_uH_d\ , \tag{4.6}$$

where H_u, H_d, Q, L, $\overline{u}$, $\overline{d}$ and $\overline{e}$ can be seen either as chiral superfields or just as the scalar field from the corresponding chiral multiplet, on which we have suppressed the tildes. It is understood, that the $SU(3)$ color and $SU(2)_L$ indices are implicit here. The Yukawa couplings $\mathbf{y_u}$, $\mathbf{y_d}$ and $\mathbf{y_e}$ are 3×3 matrices in family space. The superpotential (4.6) does not contain all terms allowed by the $SU(3)\times SU(2)\times U(1)_Y$ gauge structure and the matter content from table 4.1. It is rather the minimum necessary to build a sensible model. The same superpotential is obtained by writing the most general superpotential, that does not lead to violation of baryon and lepton number conservation. Also, the interactions generated by this superpotential, just as the gauge interactions, conserve R–parity, under which the SM particles are even, while their superpartners are odd. Within the MSSM field content, but not in general supersymmetric theories, it is also true, that R–parity conservation implies baryon and lepton number conservation.

The Yukawa couplings $\mathbf{y_u}$, $\mathbf{y_d}$, $\mathbf{y_e}$ determine masses and CKM matrices of the SM quarks and leptons after the neutral components of H_u and H_d get VEVs. It is often useful to make the approximation, that only the $(3,3)$ family components are really important,

$$\mathbf{y_u} \approx \begin{pmatrix} 0 & 0 & 0 \\ 0 & 0 & 0 \\ 0 & 0 & y_t \end{pmatrix}, \qquad \mathbf{y_d} \approx \begin{pmatrix} 0 & 0 & 0 \\ 0 & 0 & 0 \\ 0 & 0 & y_b \end{pmatrix}, \qquad \mathbf{y_e} \approx \begin{pmatrix} 0 & 0 & 0 \\ 0 & 0 & 0 \\ 0 & 0 & y_\tau \end{pmatrix}. \tag{4.7}$$

In this approximation, and spelling out the weak isospin doublets $Q_3 = (t\, b)$, $L_3 = (\nu_\tau\, \tau)$, $H_u = (H_u^+\, H_u^0)$, $H_d = (H_d^0\, H_d^-)$, $\overline{u}_3 = \overline{t}$, $\overline{d}_3 = \overline{b}$, $\overline{e}_3 = \overline{\tau}$, the superpotential reads

$$\begin{aligned} W_{\text{MSSM}} \quad &\approx \quad y_t(\overline{t}tH_u^0 - \overline{t}bH_u^+) - y_b(\overline{b}tH_d^- - \overline{b}bH_d^0) - y_\tau(\overline{\tau}\nu_\tau H_d^- - \overline{\tau}\tau H_d^0) \\ &\quad + \mu(H_u^+ H_d^- - H_u^0 H_d^0) \end{aligned} \tag{4.8}$$

The signs in (4.6) are chosen such, that the terms $\mathbf{y}\overline{f}fH^0$, that become fermion masses, when the Higgs bosons acquire VEVs, appear with positive signs. Recall, that a superpotential term $\mathbf{y}\Phi_i\Phi_j\Phi_k$ involving three chiral multiplets gives rise to interactions

$$-\tfrac{1}{2}\mathbf{y}\phi_i\psi_j\psi_k \qquad + \text{ all permutations of } ijk, \tag{4.9}$$

so the quark-quark-higgs coupling, for which the superpotential notation is suggestive, as the supermultiplets are carry the name of their SM component, arises together with a higgsino-squark-quark coupling and so on. As we have already seen in eq. (4.4), the superpotential also produces various scalar quartic interactions, which are proportional to $\mathbf{y}^2$. However, the dimensionless interactions given by the superpotential are usually not the most important ones for phenomenology. Production and decay processes of superpartners in the MSSM are usually dominated by gauge interactions. In this work, the only relevant interactions arising through the dimensionless Yukawa couplings in the superpotential are the higgs-quark-quark and the higgs-squark-squark couplings. All other vertices appearing are strong interactions proportional to g_s or g_s^2. This includes the g_s^2 quartic squark coupling, coming from the D-term in eq. (4.4).

The most general soft breaking terms respecting R-parity in the MSSM are

$$\begin{aligned} \mathcal{L}_{\text{soft}}^{\text{MSSM}} \quad &= \quad -\frac{1}{2}\left(M_3\widetilde{g}\widetilde{g} + M_2\widetilde{W}\widetilde{W} + M_1\widetilde{B}\widetilde{B} + c.c.\right) \\ &\quad - \left(\widetilde{\overline{u}}\,\mathbf{a_u}\,\widetilde{Q}H_u - \widetilde{\overline{d}}\,\mathbf{a_d}\,\widetilde{Q}H_d - \widetilde{\overline{e}}\,\mathbf{a_e}\,\widetilde{L}H_d + c.c.\right) \\ &\quad - \widetilde{Q}^\dagger\,\mathbf{m_Q^2}\,\widetilde{Q} - \widetilde{L}^\dagger\,\mathbf{m_L^2}\,\widetilde{L} - \widetilde{\overline{u}}\,\mathbf{m_{\overline{u}}^2}\,\widetilde{\overline{u}}^\dagger - \widetilde{\overline{d}}\,\mathbf{m_{\overline{d}}^2}\,\widetilde{\overline{d}}^\dagger - \widetilde{\overline{e}}\,\mathbf{m_{\overline{e}}^2}\,\widetilde{\overline{e}}^\dagger \\ &\quad - m_{H_u}^2 H_u^* H_u - m_{H_d}^2 H_d^* H_d - (bH_uH_d + c.c.) \end{aligned} \tag{4.10}$$

The first line consist of gaugino masses for the superpartners of all SM gauge bosons. The second line and the $-bH_uH_d$ term are trilinear and bilinear scalar couplings which have the same form like the $\mathbf{y_u}$, $\mathbf{y_d}$, $\mathbf{y_e}$ and μ terms in the superpotential eq. (4.6). All remaining terms are scalar masses of the $(m^2)_i^j$ type. All bold quantities are of course 3×3 matrices in family space. Note, that while there are two matrices $\mathbf{m_{\overline{u}}^2}$ and $\mathbf{m_{\overline{d}}^2}$ for the right handed squarks, $SU(2)_L$ symmetry only allows a single $\mathbf{m_Q^2}$ left-handed squarks.

Contrary to the sypersymmetric part of the Lagrangian, which parametrizes a large number of interactions in terms of very few parameters , the soft breaking terms introduce a huge number of parameters not present in the Standard Model. It is known, that there are actually 105 parameters, that cannot be rotated away and have no counterpart in the Standard Model.

However, the majority of these parameters leads to flavor-changing or CP-violating effects, which are highly restricted by experiment. In phenomenological studies it is often assumed, that the squark and slepton mass matrices are proportional to the identity matrix, e.g. $\mathbf{m_Q^2} = m_Q^2\mathbf{1}$, the trilinear terms are proportional to the corresponding Yukawa coupling,

$$\mathbf{a_u} = A_u\mathbf{y_u}, \qquad \mathbf{a_d} = A_d\mathbf{y_d}, \qquad \mathbf{a_e} = A_e\mathbf{y_e}, \tag{4.11}$$

and thus small for the first two generations, and finally that M_1, M_2, M_3, A_u, A_d and A_e are real. For our purpose, it is further safe to make the approximation eq. (4.8).

4.1.2 Squark Masses and Mixing

The mass matrix for stops and sbottoms is

$$\mathcal{M}_{\tilde{q}} = \begin{pmatrix} m^2_{\tilde{q}_L} & x_q\, m_q \\ x_q\, m_q & m^2_{\tilde{q}_R} \end{pmatrix} = \mathcal{R}^{q\dagger} \begin{pmatrix} m^2_{\tilde{q}_1} & 0 \\ 0 & m^2_{\tilde{q}_2} \end{pmatrix} \mathcal{R}^q \tag{4.12}$$

with

$$\begin{aligned} m^2_{\tilde{q}_L} &= M^2_{\tilde{Q}} + m_q^2 + m_Z^2\, \cos 2\beta\, \left(I^q_{3L} - Q_q\, \sin^2\theta_W\right)\,, & (4.13)\\ m^2_{\tilde{q}_R} &= M^2_{\{\tilde{U},\tilde{D}\}} + m_q^2 + Q_q\, m_Z^2\, \cos 2\beta\, \sin^2\theta_W\,, & (4.14)\\ x_q &= A_q - \mu\,\{\cot\beta, \tan\beta\}\,, \quad q = \{t, b\} & (4.15) \end{aligned}$$

and the mixing matrix

$$\mathcal{R}^q = \begin{pmatrix} \cos\theta_{\tilde{q}} & \sin\theta_{\tilde{q}} \\ -\sin\theta_{\tilde{q}} & \cos\theta_{\tilde{q}} \end{pmatrix}\,, \tag{4.16}$$

which rotates the from the gauge basis $\tilde{q}_L$, $\tilde{q}_R$ to the mass eigenstates $\tilde{q}_1$, $\tilde{q}_2$. The diagonal elements $m_{\tilde{q}_L}$ and $m_{\tilde{q}_R}$ contain the squark masses $M^2_{\tilde{Q}}$ and $M^2_{\{\tilde{U},\tilde{D}\}}$ from the soft breaking terms, m_q^2 arising from the F-terms of the scalar potential, when the Higgs fields acquire VEVs $[m_t = y_t v \sin\beta, m_d = y_b v\cos\beta]$, and finally contributions from the $SU(2)_L$ and $U(1)_Y$ terms in the scalar potential[2]. The off diagonal entries $m_q x_q$ receive contributions from soft breaking and from F-terms. We treat the mixing angle $\theta_{\tilde{q}}$ rather than the soft breaking parameter A_q as an independent parameter. The relation is

$$A_q = -\frac{\Delta m^2_{\tilde{q}}}{2m_q}\sin 2\theta_{\tilde{q}} + \mu\{\cot\beta, \tan\beta\}, \qquad q = \{t, b\}, \tag{4.17}$$

where $\Delta m^2_{\tilde{q}} = m^2_{\tilde{q}_2} - m^2_{\tilde{q}_1}$.

[2]This part is often denoted $\Delta_\phi = (I^\phi_{3L} g^2 - Y^\phi g'^2)(v_d^2 - v_u^2) = (I^\phi_{3L} - Q^\phi \sin^2\theta_W) m_Z^2 \cos 2\beta$. To understand the sign in eq. (4.14), note that we deal with left and right-handed quarks and their superpartners by giving names to the left-handed and the conjugate of the right-handed particles.

If we consider a complete $SU(2)_L$ multiplet, i.e. (s)tops and (s)bottoms, we have to pay attention to the fact, that left-handed stops and sbottoms share a common soft-breaking parameter $M_{\tilde{Q}}^2$. This is easy to forget once one has moved to the mass eigenstates. Equating $M_{\tilde{Q}}^2$ expressed in terms of (s)top and (s)bottom parameters gives the relation

$$\cos^2\theta_{\tilde{b}} m_{\tilde{b}_1}^2 + \sin^2\theta_{\tilde{b}} m_{\tilde{b}_2}^2 = \cos^2\theta_{\tilde{t}} m_{\tilde{t}_1}^2 + \sin^2\theta_{\tilde{t}} m_{\tilde{t}_2}^2 + m_b^2 - m_t^2 - M_W^2\cos(2\beta). \tag{4.18}$$

In the following, we take $m_{\tilde{b}_1}^2$ as the dependent quantity.

4.1.3 Higgs Couplings

The tree level, the the Yukawa couplings between the Higgs bosons and quarks are simply related to quark masses. The couplings to the squarks are a bit more involved, similar to the situation of squark masses. We are only interested in the couplings of top and bottom quarks and their scalar partners to the two CP even neutral Higgs bosons. The corresponding vertices are

$$\begin{aligned}\mathcal{L}_{Hhtb} = \quad & -\sum_{q=t,b}\left\{\frac{m_q}{v}\,h_{\mathrm{f}}(q)\,h^0\,\bar{q}\,q + \frac{m_q}{v}\,H_{\mathrm{f}}(q)\,H^0\,\bar{q}\,q\right\} \\ & -\sum_{q=t,b}\sum_{i,j=1,2}\left\{\frac{m_q^2}{v}\,h_{\mathrm{s}}(q,i,j)\,h^0\,\tilde{q}_i^*\,\tilde{q}_j + \frac{m_q^2}{v}\,H_{\mathrm{s}}(q,i,j)\,H^0\,\tilde{q}_i^*\,\tilde{q}_j\right\},\end{aligned} \tag{4.19}$$

with the dimensionless couplings

$$h_{\mathrm{f}}(b) = -\frac{\sin\alpha}{\cos\beta}, \qquad h_{\mathrm{f}}(t) = \frac{\cos\alpha}{\sin\beta}, \tag{4.20}$$

where α is the mixing angle in the CP even neutral Higgs sector and β controls the ratio of the VEVs for H_u^0 and H_d^0, $\tan\beta = v_u/v_d$. The corresponding couplings to the heavy Higgs, H^0, can be obtained from the ones above by the replacement $\alpha \to \alpha - \pi/2$.

For the squark couplings we have

$$m_q^2\,h_s(q,i,j) \quad = \quad \left(\mathcal{R}^q \begin{pmatrix} h_{LL}^q & h_{LR}^q \\ h_{RL}^q & h_{RR}^q \end{pmatrix} \mathcal{R}^{q\dagger}\right)_{ij}. \tag{4.21}$$

where h^q_{ij} for $q = t, b$ are given by

$$
\begin{aligned}
h^t_{LL} &= 2\,\frac{\cos\alpha}{\sin\beta}\,m_t^2 + m_Z^2\,\frac{4\,s_W^2 - 3}{3}\,\sin(\alpha+\beta) && (4.22)\\
h^t_{LR} &= h^t_{RL} = m_t\,\frac{A_t\,\cos\alpha + \mu\sin\alpha}{\sin\beta} && (4.23)\\
h^t_{RR} &= 2\,\frac{\cos\alpha}{\sin\beta}\,m_t^2 - m_Z^2\,\frac{4\,s_W^2}{3}\,\sin(\alpha+\beta) && (4.24)\\
h^b_{LL} &= -2\,\frac{\sin\alpha}{\cos\beta}\,m_b^2 + m_Z^2\,\frac{3 - 2\,s_W^2}{3}\,\sin(\alpha+\beta) && (4.25)\\
h^b_{LR} &= h^b_{RL} = -m_b\,\frac{A_b\,\sin\alpha + \mu\cos\alpha}{\cos\beta} && (4.26)\\
h^b_{RR} &= -2\,\frac{\sin\alpha}{\cos\beta}\,m_b^2 + m_Z^2\,\frac{2\,s_W^2}{3}\,\sin(\alpha+\beta)\,. && (4.27)
\end{aligned}
$$

Again the corresponding couplings to H^0 are obtained by replacing $\alpha \to \alpha - \pi/2$ above. A more detailed discussion of the MSSM targeted towards phenomenology can be found in [71].

4.2 Feynman Diagrams

We generate all Feynman diagrams using FeynArts, which has the full MSSM Feynman rules built in. We extract the unintegrated amplitude and project out the form factor $\mathcal{A}$ exactly as in the case of the Standard Model contribution in chapter 2. Also, the integrands were again checked against those obtained using QGRAF and private implementations of the Feynman rules. We continue to use conventional dimensional regularization (DREG) even though this regulator breaks supersymmetry. The necessary supersymmetry restoring counterterm is discussed in the section on renormalization.

The Born level amplitude consists of five one-loop diagrams. The two-loop corrections count 135 diagrams. We count "generic" diagrams only. "Generic" means we use squarks with variable sfermion indices, which can take two values, rather than drawing separate diagrams for all possible values of the sfermion indices. Also quarks can be tops or bottoms in each diagram[3]. No flavor mixing occurs, so we just have to do the same calculation twice, once for the top and once for the bottom sector[4]. We neglect the contributions of the first two generations due to the smallness of their masses.

4.2.1 One-Loop Diagrams

The Born amplitude we have already computed. The five Feynman diagrams are solely those from chapter 2, the three independent ones are shown in figure 2.1. In the scalar contribution,

[3] In FeynArts terminology, our diagrams are essentially *class diagrams*. The only difference is, that at class level, FeynArts distinguishes up-type and down-type quarks. We do not have to make this distinction, as tops and bottoms do not mix in our problem. We can just work with generic quarks and insert the right masses and couplings for each flavor. Note that in FeynArts, *generic diagrams* means that fields are only classified as scalars, fermions, vector bosons or ghosts.

[4] Note however, that the masses of the two stops and the two sbottoms are parametrized by only three independent parameters in the Lagrangian. This also dictates a relation among the corresponding counterterms, when it comes to renormalization.

the particle running in the loop can be either a $\tilde{q}_1$ or a $\tilde{q}_2$, but since the gluon-squark vertex does not mix the two squarks, each diagram can contain only one squark type. Thus each Born level diagram contains only a single type of massive particles and we can just recycle the results from chapter 2. We define new versions $\mathcal{C}_q^{(0)}$ and $\mathcal{C}_{\tilde{q}_i}^{(0)}$ of the expansion coefficients $\mathcal{C}_{\mathrm{f}}^{(0)}$ and $\mathcal{C}_{\mathrm{s}}^{(0)}$ using the MSSM couplings,

$$\mathcal{C}_q^{(0)} = \frac{h_{\mathrm{f}}(q)}{v} \frac{1}{m_q^{2\epsilon}} c_{\mathrm{f}}^{(0)}(x_q) \tag{4.28}$$

$$\mathcal{C}_{\tilde{q}_i}^{(0)} = \frac{h_{\mathrm{s}}(q,i,i)}{v} \left[\frac{m_q}{m_{\tilde{q}_i}}\right]^2 \frac{1}{m_{\tilde{q}_i}^{2\epsilon}} c_{\mathrm{s}}^{(0)}(x_{\tilde{q}_i}). \tag{4.29}$$

Here v denotes the VEV of the Higgs boson and $h_{\mathrm{f}}(q)$ and $h_{\mathrm{s}}(q,i,i)$ are the dimensionless couplings given in eq. (4.20) and eq. (4.21). We have put subscripts q and $\tilde{q}_i$ on the dimensionless variables x as a reminder, that they are based on different masses. The factor $(m_q/m_{\tilde{q}_i})^2$ appears, because the higgs-squark coupling $\mathcal{L} \supset -\frac{m_q^2}{v} h_{\mathrm{s}}(q,i,j)\, h\tilde{q}_i^*\tilde{q}_j$ is proportional to m_q^2 rather than to the squared squark mass, whereas $c_{\mathrm{s}}^{(0)}(x_{\tilde{q}_i})$ has built in a factor $m_{\tilde{q}_i}^2$, suitable in the case of a general scalar particle and mandatory as we want $c_{\mathrm{s}}^{(0)}$ to depend on x only.

4.2.2 Two-Loop Diagrams

In the two-loop contribution it is useful to distinguish the following groups of diagrams:

1. SM and SM-like diagrams. These are the 21 + 56 diagrams shown in in appendix A.2.1 and A.2.2. The diagrams have only gluons and either quarks or squarks (without $\tilde{q}\tilde{q}\tilde{q}\tilde{q}$-interaction) running in the loops. Again all squarks are of the same type, as they all line up to form a single closed squark loop radiating only gluons and one single Higgs boson. Thus we can again reuse the analytic results from chapter 2 just as for the Born level,

$$\mathcal{C}_q^{(1)} = \frac{h_{\mathrm{f}}(q)}{v} \frac{1}{m_q^{4\epsilon}} c_{\mathrm{f}}^{(1)}(x_q) \tag{4.30}$$

$$\mathcal{C}_{\tilde{q}_i}^{(1)} = \frac{h_{\mathrm{s}}(q,i,i)}{v} \left[\frac{m_q}{m_{\tilde{q}_i}}\right]^2 \frac{1}{m_{\tilde{q}_i}^{4\epsilon}} c_{\mathrm{s}}^{(1)}(x_{\tilde{q}_i}). \tag{4.31}$$

   These relations differ from the born case only by the exponents 4ϵ instead of 2ϵ.

2. SUSY-QCD diagrams containing gluinos. These are the most complicated diagrams and their evaluation is the main task of this computation. We distinguish the 21 GQ diagrams shown in appendix A.2.3 in which the Higgs couples to a quark line and the 22 GSQ diagrams in appendix A.2.4, where the Higgs couples to squark line. Also in presence of the quark-squark-gluino-vertex with its γ_5 it remains true, that diagrams related by reversion of arrows on (s)quark lines are equal. This reduces the number of independent diagrams to eight for GQ as well as for GSQ. These are shown in figure 4.1 and 4.2, respectively.

   The GQ diagrams contain only a single squark type, as they contain either a single squark or two squarks meeting at at $g\tilde{q}\tilde{q}$ or $gg\tilde{q}\tilde{q}$-vertex. Therefore they have three

different mass parameters in the loops, $m_{\tilde{g}}, m_q$ and $m_{\tilde{q}_i}$, and we have to evaluate them for the $\tilde{q}_1$ and the $\tilde{q}_2$ case.

The GSQ diagrams contain 2, 3 or 4 squarks, but there are always exactly two independent sfermion indices s_1 and s_2, one for the lines before and one for the lines after the Higgs vertex. So there are three or four different mass parameters in the loops and we have to evaluate each diagram for four different choices of s_1, s_2.

Clearly, the presence of up to five kinematical invariants in two-loop diagrams makes their analytic integration a Herculean task. For mortals the numerical approach from chapter 3 is more promising.

3. SUSY-QCD diagrams containing the $\tilde{q}\tilde{q}\tilde{q}\tilde{q}$-vertex. The 15 diagrams of this type are shown in appendix A.2.5. After dropping four vanishing diagrams and merging equivalent ones we are left with the five diagrams shown in figure 4.3. The diagrams factorize into two simple one-loop diagrams, that should be treatable analytically. Here we just evaluate them numerically for convenience. Note, that due to the presence of the $\tilde{q}\tilde{q}\tilde{q}\tilde{q}$- and the $\tilde{q}\tilde{q}h$-vertex, these diagrams come with three independent sfermion indices $s_1,\ s_2,\ s_3$ and thus eight different combinations of squark masses are possible.

   The $\tilde{q}\tilde{q}\tilde{q}\tilde{q}$-vertex contains family mixing terms. However, in the nonzero diagrams, the four squark lines of the vertex are connected such, that no color flows from one loop to the other through the $\tilde{q}\tilde{q}\tilde{q}\tilde{q}$-vertex. In this configuration, the contribution of the family mixing terms is zero.

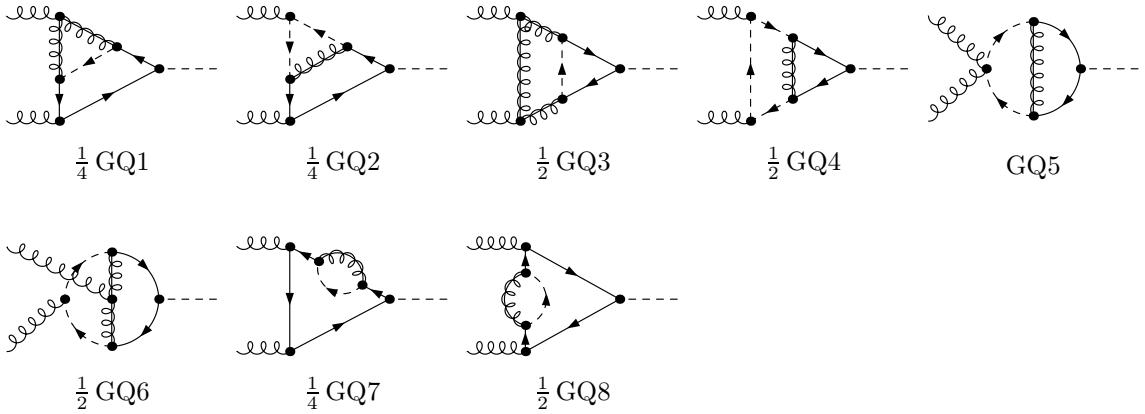

Figure 4.1: SUSY-QCD contributions to $gg \to h, H$ containing gluinos and the quark-quark-higgs coupling.

4.3 Renormalization

4.3.1 Regularization Scheme

As already mentioned, we perform the calculation DREG [49] with modified minimal subtraction for the strong coupling constant, conventionally abbreviated $\overline{\text{MS}}$. This is the standard regularization scheme for QCD calculations, since it preserves gauge symmetry and is technically easy to use. Quark and squark masses, as well as the mixing angle $\theta_{\tilde{q}}$, we renormalize

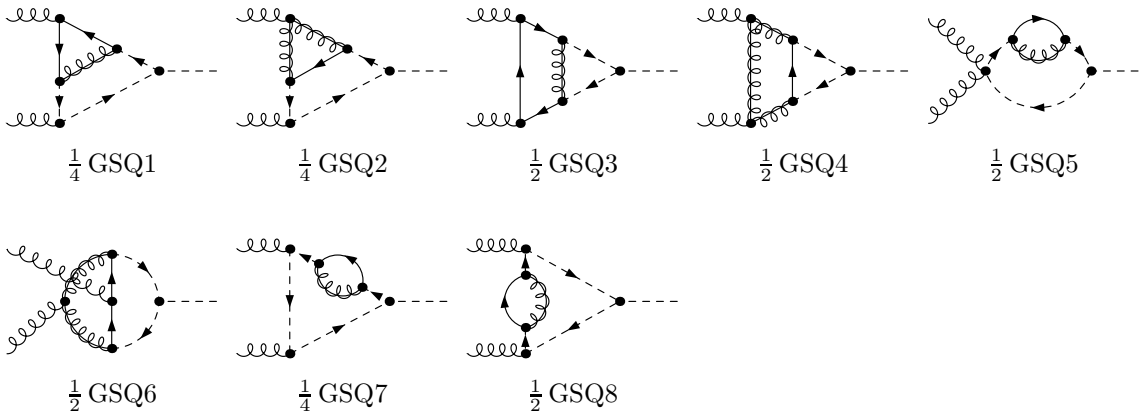

Figure 4.2: SUSY-QCD contributions to $gg \to h, H$ containing gluinos and the squark-squark-higgs coupling.

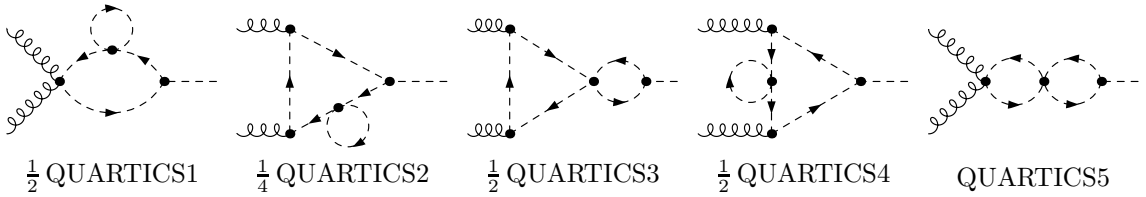

Figure 4.3: SUSY-QCD contributions to $gg \to h, H$ containing a quartic squark interaction.

on-shell. In DREG momenta and also polarizations are continued to $d = 4 - 2\epsilon$ dimensions. UV and IR divergences show up as poles for integer values of d. The Dirac matrices are a set of d matrices satisfying

$$\{\gamma^\mu, \gamma^\nu\} = 2g^{\mu\nu}\mathbf{1}, \qquad \mathrm{tr}[\mathbf{1}] = 4. \tag{4.32}$$

The problem with DREG is, that it breaks supersymmetry. The reason for this is the mismatch between bosonic and fermionic degrees of freedom. The d dimensional gauge bosons have $d-2$ physical degrees of freedom, while a Majorana spinor has two on-shell degrees of freedom.

Supersymmetry requires relations among various pieces of the Lagrangian. Many interactions are controlled by a few parameters only. Apart from the couplings to the Higgs bosons, all vertices entering our calculation are of strength g_s or g_s^2, for instance. For the first six vertices in appendix E, coupling one or two gluons to a particle pair, the equality is also required by just by gauge invariance: Once we introduce a gluon and couple it to a colored quark, also the gluon self-interactions are fixed. To write a kinetic term for the next colored particle, we are then forced to use the same coupling constant. However, the gluino-squark-quark vertices, which are supersymmetrizations of thegluon-quark-quark vertex, and the four squark vertex, which is a D-term, are of strength g_s by virtue of supersymmetry. If supersymmetry is broken by the regulator, in loop corrections these vertices can "get their own life" and renormalize individually. Unrelated parameters of the Lagrangian renormalize differently, even if we assign them equal values at some point. In general one has to include counterterms, that correct for wrong running caused by the regulator. Luckily, in our calculation the gluino as well as the four squark vertex only enter at two-loop level. The corrections to them therefore become important at three loops only.

There are two more vertices to worry about. The higgs-quark coupling is related to the quark mass and this relation is preserved by DREG to all orders. But for the higgs-squark vertex, we have to face the fact, that its one-loop correction is not just that obtained by substituting δm_q, $\delta m_{\tilde{q}_i}$ and $\delta\theta_{\tilde{q}}$ into the tree-level expression for $m_q^2 h_{\rm s}(q,i,j)$. There is an additional shift due to the SUSY breaking caused by DREG. We will compute this shift in section sec:sqsqhrenorm.

Alternatively it is possible to perform the calculation using dimensional reduction, DRED [50, 51], as a regulator. In this scheme, the transition from 4 to $d = 4 - 2\epsilon$ with $d < 4$ dimensions is made by a compactification or reduction. Thus space-time is taken to by d dimensional, but the number of field components remains unchanged. Therefore, unlike in DREG, the anticommutator of Dirac matrices, $\{\gamma^\mu, \gamma^\nu\} = 2g^{\mu\nu}\mathbf{1}$, produces a four dimensional[5] $g^{\mu\nu}$. Also gauge bosons have four components and thus two physical degrees of freedom, avoiding the mismatch with fermions occurring in DREG. In practice one splits the four dimensional $g^{\mu\nu}$ and also gauge bosons A_μ^a and their polarization vectors into a d-dimensional and a 2ϵ-dimensional part. The d-dimensional part of A_μ^a then behaves just as in DREG. However, there is an additional piece $A_{2\epsilon}^a$. Whereas gauge bosons transform under gauge transformations like

$$A_\mu^a \to A_\mu^a + \frac{1}{g}\partial_\mu \alpha^a + f^{abc} A_\mu^b \alpha^c, \tag{4.34}$$

there is no $\partial_{2\epsilon}$ term in the transformation law of $A_{2\epsilon}^a$, since fields depend on d-dimensional momenta only. Therefore the $A_{2\epsilon}^a$ transform just like scalars in the adjoint representation. A similar thing happens when extra-dimensional theories are compactified.The $A_{2\epsilon}^a$ are often called ϵ-scalars.

It was shown in [52], that DRED can be formulated in a mathematically consistent way. The question, to what extent it really preserves supersymmetry is not answered completely, but for our calculation it should be safe. However, while at first sight DRED might look like the ideal scheme for our purpose, its use is indeed highly non-trivial.Care has to be taken about the mass term for the ϵ-scalars. Further, if either (softly broken) supersymmetry or $SU(2)_L$ are absent a direct coupling between two ϵ-scalars and the Higgs boson,

$$\mathcal{L}_{h\epsilon} = \frac{\Lambda_\epsilon}{v} h A_{2\epsilon}^a A_{2\epsilon}^a \tag{4.35}$$

emerges radiatively and should therefore be included in the Lagrangian from the very beginning. The DRED calculation was accomplished in parallel with this thesis and fully agrees with the DREG result [53]

4.3.2 Coupling Constant Renormalization

In SUSY-QCD, the renormalization of α_s involves not only QCD particles, but also the heavy squarks and gluinos. These heavy particles, as well as the top quark, can be decoupled, so that they do not contribute to the running of α_s. The corresponding large logarithms are explicitly left in the amplitudes, rather than being resummed into the running of the coupling constant. This is achieved by introducing a bare coupling in both, the full theory and the

[5]Note, that the relation

$$\not{p}\not{p} = \frac{1}{2} p_\mu p_\nu \{\gamma^\mu, \gamma^\nu\} = p_\mu p_\nu g^{\mu\nu} = p^2 \tag{4.33}$$

holds for d dimensional momenta, since $d < 4$.

theory without the heavy particles, related by [25]

$$\alpha_s^0 = (\zeta_g)^2\, \tilde{\alpha}_s^0. \tag{4.36}$$

Here α_s^0 is the coupling without the heavy particles, i.e. in five-flavor QCD and $\tilde{\alpha}_s^0$ is the coupling in the full theory. The decoupling constant is the inverse of contributions from the heavy particles to the gluon self energy correction at zero momentum. In expressions for amplitudes, diagrams with self energy corrections from heavy particles on external gluons will exactly cancel the contribution of the decoupling constant. In other words, if we do not include self energy corrections to external gluons, we can forget the decoupling constant and just keep in mind, the running of α_s is given solely by the contributions of light particles to the β function. Therefore we have

$$S_\epsilon\, \alpha_s^0 = \alpha_s^{\overline{\rm MS}}(\mu)\, \mu^{2\epsilon} \left[1 - \alpha_s^{\overline{\rm MS}}(\mu) \frac{\beta_0}{4\pi\epsilon}\right], \tag{4.37}$$

$$S_\epsilon\, \alpha_s^0 = \alpha_s^{\overline{\rm MS}}(\mu)\, \mu^{2\epsilon} + \delta\alpha_s^{\overline{\rm MS}} \qquad \text{with} \qquad \delta\alpha_s^{\overline{\rm MS}} = -\left[\alpha_s^{\overline{\rm MS}}(\mu)\right]^2 \mu^{2\epsilon} \frac{\beta_0}{4\pi\epsilon} \tag{4.38}$$

with

$$\beta_0 = 11 - \frac{2}{3}\, n_{\rm light}, \tag{4.39}$$

where $n_{\rm light} = 5$.

The one-loop running of α_s is obtained by differentiating eq. (4.37) with respect to μ, solving for $\mu\frac{\partial}{\partial\mu}\alpha_s$, expanding to order $\mathcal{O}(\alpha_s^2)$ and sending $\epsilon \to 0$. The result is

$$\mu\frac{\partial}{\partial\mu}\alpha_s(\mu) = -\alpha_s^2(\mu)\frac{\beta_0}{2\pi}\ , \tag{4.40}$$

where the right hand side is the well known one-loop QCD β-function.

4.3.3 Renormalization of Masses and Mixing Angles

We use the pole mass scheme to renormalize both the quark and squark masses. Denoting the one-particle irreducible two-point function by $i\Sigma$ we can write

$$\delta m_{\tilde{q}_i}^2 = (m_{\tilde{q}_i}^0)^2 - m_{\tilde{q}_i}^2 = \mathrm{Re}\left(\Sigma_{\tilde{q}_i\tilde{q}_i}(m_{\tilde{q}_i}^2)\right)\ , \tag{4.41}$$

where $m_{\tilde{q}_i}$ are the pole masses of the squarks. For the quark case

$$\delta m_q = \frac{1}{2}\,\mathrm{Re}\, m_q \left[\Sigma_{q_L}(m_q^2) + \Sigma_{q_R}(m_q^2) + 2\Sigma_{q_S}(m_q^2)\right], \tag{4.42}$$

using the Lorentz decomposition[6]

$$\Sigma_q(p) = \not{p}\,\omega_-\Sigma_{q_L}(p^2) + \not{p}\,\omega_+\Sigma_{q_R}(p^2) + m_q\Sigma_{q_S}(p^2). \tag{4.43}$$

[6]Often the sloppy notation $\Sigma(m_q)$ is used. This can be confusing in cases, where γ^5 appears in Σ, as it is the case here due to the quark-squak-gluino vertex. Setting $\not{p} = m$ removes a γ matrix and it then makes a difference, whether the Dirac algebra is performed before or after setting $\not{p} = m$. It is thus safer to view m_q^2 as the value of p^2, at which the inverse propagator *applied to a spinor* $u(p)$ vanishes.

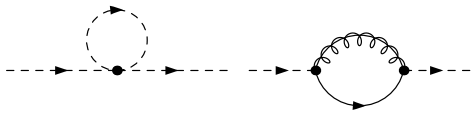

Figure 4.4: SUSY contributions to the squark self-energy. Both diagrams mix the two sfermion types. The flavor mixing parts of the $\tilde{q}\tilde{q}\tilde{q}\tilde{q}$-vertex does not contribute due to the color structure.

Apart from the QCD contribution corresponding to emission and reabsorbtion of a gluon, the squark self energy gets contributions form the diagrams For the quark, the only SUSY contribution comes from a diagram like the second one in figure 4.4, but with quarks and squarks interchanged. We find

$$\begin{aligned}
\delta m_q = \quad & -\frac{\alpha_s^0}{4\,\pi}\,C_F\,\mathrm{Re}\Big\{2\,m_q\,\left(B_0(m_q^2,0,m_q^2) - B_1(m_q^2,0,m_q^2)\,\left(1-\epsilon\,\delta m_q^{\mathrm{SD}}\right)\right) \\
& +m_q\,\left(B_1(m_q^2,m_{\tilde{g}}^2,m_{\tilde{q}_1}^2) + B_1(m_q^2,m_{\tilde{g}}^2,m_{\tilde{q}_2}^2)\right) \\
& +m_{\tilde{g}}\,\sin 2\theta_{\tilde{q}}\,\left(B_0(m_q^2,m_{\tilde{g}}^2,m_{\tilde{q}_1}^2) - B_0(m_q^2,m_{\tilde{g}}^2,m_{\tilde{q}_2}^2)\right)\Big\}\,, \qquad (4.44) \\
\delta m_{\tilde{q}_1}^2 = \quad & -\frac{\alpha_s^0}{4\,\pi}\,C_F\,\mathrm{Re}\Big\{2\,A_0(m_{\tilde{g}}^2) + 2\,A_0(m_q^2) - A_0(m_{\tilde{q}_1}^2)\,(1+\cos^2 2\theta_{\tilde{q}}) - A_0(m_{\tilde{q}_2}^2)\,\sin^2 2\theta_{\tilde{q}} \\
& +2\,(m_{\tilde{g}}^2 + m_q^2 - m_{\tilde{q}_1}^2 - 2m_{\tilde{g}}\,m_q\,\sin 2\theta_{\tilde{q}})\,B_0(m_{\tilde{q}_1}^2,m_{\tilde{g}}^2,m_q^2) \\
& +4\,m_{\tilde{q}_1}^2\,B_0(m_{\tilde{q}_1}^2,0,m_{\tilde{q}_1}^2)\Big\}\,, \qquad (4.45) \\
\delta m_{\tilde{q}_2}^2 = \quad & -\frac{\alpha_s^0}{4\,\pi}\,C_F\,\mathrm{Re}\Big\{2\,A_0(m_{\tilde{g}}^2) + 2\,A_0(m_q^2) - A_0(m_{\tilde{q}_2}^2)\,(1+\cos^2 2\theta_{\tilde{q}}) - A_0(m_{\tilde{q}_1}^2)\,\sin^2 2\theta_{\tilde{q}} \\
& +2\,(m_{\tilde{g}}^2 + m_q^2 - m_{\tilde{q}_2}^2 + 2m_{\tilde{g}}\,m_q\,\sin 2\theta_{\tilde{q}})\,B_0(m_{\tilde{q}_2}^2,m_{\tilde{g}}^2,m_q^2) \\
& +4\,m_{\tilde{q}_2}^2\,B_0(m_{\tilde{q}_2}^2,0,m_{\tilde{q}_2}^2)\Big\}\,. \qquad (4.46)
\end{aligned}$$

Since we are computing in bare perturbation theory, we have explicitly put the bare coupling constant α_s^0. No factor of $\mu^{2\epsilon}$ appears.

The quark pole mass dependence on the bare mass is scheme dependent, the constant δm_q^{SD} is given by $\delta m_q^{\mathrm{SD}} = 1$ for DREG and $\delta m_q^{\mathrm{SD}} = 0$ for DRED. The difference comes from the contribution of the gluon loop only. We have

$$\delta m_q^{\mathrm{DREG}} - \delta m_q^{\mathrm{DRED}} = \frac{\alpha_s^0}{4\,\pi}\,C_F\,m_q + \mathcal{O}(\epsilon) \qquad (4.47)$$

The scalar integrals A_0 and B_0 are defined as

$$A_0(m^2) = \int \frac{d^dk}{i\pi^{d/2}}\frac{1}{[k^2-m^2]} \qquad (4.48)$$

$$B_0(p^2, m_1^2, m_2^2) = \int \frac{d^d k}{i\pi^{d/2}} \frac{1}{[k^2 - m_1^2][(k+p)^2 - m_2^2]} \tag{4.49}$$

and B_1 is defined such, that

$$p^\mu B_1(p^2, m_1^2, m_2^2) = \int \frac{d^d k}{i\pi^{d/2}} \frac{q^\mu}{[k^2 - m_1^2][(k+p)^2 - m_2^2]}. \tag{4.50}$$

The normalization is the same as the one used in LoopTools up to the fact, that we do not include the factor $\mu^{2\epsilon}$, since we are working in bare perturbation theory.

The function B_1 is reducible,

$$B_1(p^2, m_1^2, m_2^2) = \frac{1}{2p^2}\left[A_0(m_1^2) - A_0(m_2^2) + (m_2^2 - m_1^2 - p^2) B_0(p^2, m_1^2, m_2^2)\right]. \tag{4.51}$$

Note, that B_0 is symmetric under exchange of m_1^2 and m_2^2, but B_1 is not.

It is useful to split the mass shifts into two pieces, corresponding to the pure QCD and SUSY corrections respectively,

$$\begin{aligned}
\delta m_q^{\rm QCD} = \quad & -\frac{\alpha_s^0}{4\pi} C_F \, 2 m_q \, \mathrm{Re}\left\{ B_0(m_q^2, 0, m_q^2) - B_1(m_q^2, 0, m_q^2) \, \left(1 - \epsilon \, \delta m_q^{\rm SD}\right) \right\}, && (4.52)\\
\delta m_q^{\rm SUSY} = \quad & -\frac{\alpha_s^0}{4\pi} C_F \, \mathrm{Re}\Big\{ m_q \, \left(B_1(m_q^2, m_{\tilde{q}_1}^2, m_{\tilde{g}}^2) + B_1(m_q^2, m_{\tilde{q}_2}^2, m_{\tilde{g}}^2) \right) \\
& + m_{\tilde{g}} \, \sin 2\theta_{\tilde{q}} \, \left(B_0(m_q^2, m_{\tilde{q}_1}^2, m_{\tilde{g}}^2) - B_0(m_q^2, m_{\tilde{q}_2}^2, m_{\tilde{g}}^2) \right) \Big\}, && (4.53)\\
(\delta m_{\tilde{q}_1}^2)^{\rm QCD} = \quad & -\frac{\alpha_s^0}{4\pi} C_F \, \mathrm{Re}\left\{ 4 m_{\tilde{q}_1}^2 \, B_0(m_{\tilde{q}_1}^2, 0, m_{\tilde{q}_1}^2) - A_0(m_{\tilde{q}_1}^2) \right\}, && (4.54)\\
(\delta m_{\tilde{q}_1}^2)^{\rm SUSY} = \quad & -\frac{\alpha_s^0}{4\pi} C_F \, \mathrm{Re}\Big\{ 2 \, A_0(m_{\tilde{g}}^2) + 2 \, A_0(m_q^2) - A_0(m_{\tilde{q}_1}^2) \, \cos^2 2\theta_{\tilde{q}} - A_0(m_{\tilde{q}_2}^2) \, \sin^2 2\theta_{\tilde{q}} \\
& + 2 \left(m_{\tilde{g}}^2 + m_q^2 - m_{\tilde{q}_1}^2 - 2 m_{\tilde{g}} \, m_q \, \sin 2\theta_{\tilde{q}} \right) B_0(m_{\tilde{q}_1}^2, m_{\tilde{g}}^2, m_q^2) \Big\}, && (4.55)\\
(\delta m_{\tilde{q}_2}^2)^{\rm QCD} = \quad & -\frac{\alpha_s^0}{4\pi} C_F \, \mathrm{Re}\left\{ 4 m_{\tilde{q}_2}^2 \, B_0(m_{\tilde{q}_2}^2, 0, m_{\tilde{q}_2}^2) - A_0(m_{\tilde{q}_2}^2) \right\}. && (4.56)\\
(\delta m_{\tilde{q}_2}^2)^{\rm SUSY} = \quad & -\frac{\alpha_s^0}{4\pi} C_F \, \mathrm{Re}\Big\{ 2 \, A_0(m_{\tilde{g}}^2) + 2 \, A_0(m_q^2) - A_0(m_{\tilde{q}_2}^2) \, \cos^2 2\theta_{\tilde{q}} - A_0(m_{\tilde{q}_1}^2) \, \sin^2 2\theta_{\tilde{q}} \\
& + 2 \left(m_{\tilde{g}}^2 + m_q^2 - m_{\tilde{q}_2}^2 + 2 m_{\tilde{g}} \, m_q \, \sin 2\theta_{\tilde{q}} \right) B_0(m_{\tilde{q}_2}^2, m_{\tilde{g}}^2, m_q^2) \Big\}. && (4.57)
\end{aligned}$$

The shift in the squark mixing angle, $\delta\theta_{\tilde{q}}$ arises from the off diagonal pieces of the squark self energy. We use the scheme proposed in [69], used also in [25], where the whole off-diagonal wave function correction is canceled at a given scale by renormalization of the mixing angle. Explicitly,

$$\delta\theta_{\tilde{q}} = -\frac{\mathrm{Re}\, \Sigma_{\tilde{q}_1 \tilde{q}_2}(Q^2)}{m_{\tilde{q}_2}^2 - m_{\tilde{q}_1}^2}, \tag{4.58}$$

with

$$\begin{aligned}
\Sigma_{\tilde{q}_1 \tilde{q}_2}(p^2) = \Sigma_{\tilde{q}_2 \tilde{q}_1}(p^2) = \quad & \frac{\alpha_s^0}{4\pi} C_F \, \frac{1}{2} \Big\{ \sin 4\theta_{\tilde{q}} \left(A_0(m_{\tilde{q}_2}^2) - A_0(m_{\tilde{q}_1}^2) \right) \\
& + 8 \, m_{\tilde{g}} \, m_q \, \cos 2\theta_{\tilde{q}} \, B_0(p^2, m_q^2, m_{\tilde{g}}^2) \Big\}. && (4.59)
\end{aligned}$$

4.3.4 Renormalization of the $\tilde{q}\tilde{q}h$-Vertex

As discussed in section 4.3.1, the use of the supersymmetry breaking DREG regulator leads to an unwanted shift in the squark-squark-higgs vertex, which we have to correct for. Instead of inspecting the Ward identities, we can compute this shift from comparing the one-loop corrections to Higgs decay into two squarks in both, DREG and DRED, which does not break supersymmetry. The relevant one-loop diagrams are shown in figure 4.5. Differences

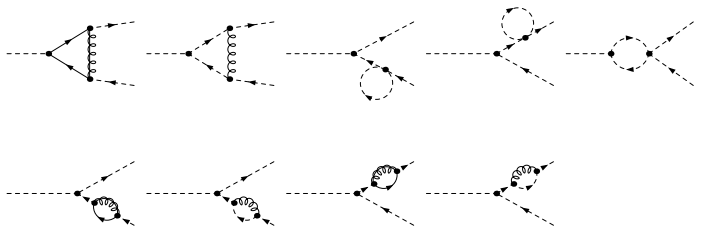

Figure 4.5: One loop corrections to the $h \to \tilde{q}\tilde{q}^*$ decay

between the two schemes can only arise from diagrams containing gluons, which have the additional ϵ-scalar component in DRED. Note that the schemes in principal also differ by the fact, that the indices of gamma matrices either run from 1 to d or from 1 to 4. However, in the absence of gluons the only gamma matrices are those occurring in fermion propagators. As these are always contracted with a $d < 4$ dimensional momentum, there is nobody to see the additional components in DRED. In figure 4.5 there are two diagrams containing a gluon. But in both cases, the gluon couples to a squark line, and thus contracts with a momentum rather than a gamma matrix. Since momenta are d dimensional also in DRED, the diagram, where the gluon is an ϵ-scalar does not contribute. Thus – before renormalization – the contribution is equal in DREG and DRED. The picture changes with renormalization, since there are diagrams containing quarks and, as we saw in the last section, δm_q^{DREG} and δm_q^{DRED} differ by a finite amount. Let us write the $\mathcal{O}(\alpha_s)$ matrix element as

$$M(\alpha_s^0, m^0) = C_0(m^0) + \alpha_s^0 C_1(m^0), \tag{4.60}$$

where m^0 collectively stands for all masses involved. The statement made above now means, that and C_1 has the same functional form in DREG and DRED. The same is of course trivially true for C_0. Renormalization just means writing the bare quantities as $\alpha_s^0 = \alpha_s^{\overline{\text{MS}},\overline{\text{DR}}} + \delta\alpha_s^{\overline{\text{MS}},\overline{\text{DR}}}$ and $m^0 = m + \delta m^{\text{DREG,DRED}}$, where m is the pole mass and thus the same with both regulators. So the renormalized amplitude is

$$M^{\text{DREG,DRED}} = C_0(m) + \alpha_s^{\overline{\text{MS}},\overline{\text{DR}}} C_1(m) + \frac{\partial C_0(m)}{\partial m}\delta m^{\text{DREG,DRED}}. \tag{4.61}$$

The shifts δm^{DREG} and δm^{DRED} contain $\alpha_s^{\overline{\text{MS}}}$ and $\alpha_s^{\overline{\text{DR}}}$, respectively. Obviously no renormalization of the coupling constant happens at this order. The coupling constants are related by

$$\alpha_s^{\overline{\text{MS}}}(\mu) = \alpha_s^{\overline{\text{DR}}}(\mu)\left(1 - \frac{\alpha_s^{\overline{\text{DR}}}(\mu)}{\pi}\frac{C_A}{12}\right), \tag{4.62}$$

there is no difference at order $\mathcal{O}(\alpha_s)$. The two amplitudes thus differ only in in the mass counterterms. Since the Higgs decay width into squarks is a physical quantity, the shift in $m_q^2 h_{\rm s}(q, s_1, s_2)$ has to remedy the difference and we get

$$\delta(m_q^2 h_{\rm s}(q, s_1, s_2))^{\rm FIX} = -\frac{\partial m_q^2 h_{\rm s}(q, s_1, s_2))}{\partial m_q}(\delta m_q^{\rm DREG} - \delta m_q^{\rm DRED}). \tag{4.63}$$

If we were using a regulator, which does not break supersymmetry, $m_q^2 h_{\rm s}(q, s_1, s_2)$ would not renormalize independently, but just the way induced by the parameters it depends on. These the masses m_q, $m_{\tilde{q}_i}^2$ and the mixing angle $\theta_{\tilde{q}}$, which entered in trade for the soft breaking parameter A_q. The supersymmetric Higgs mass parameter μ also enters $h_{\rm s}$, but since it does not renormalize, we do not have to consider it here. Therefore we could compute $\delta(m_q^2 h_{\rm s}(q, s_1, s_2))$ just by Taylor expanding $m_q^2 h_{\rm s}(q, s_1, s_2)$ given in eq. (4.21) up to the first order in these parameters. After some algebra this leads to

$$\begin{aligned}
\delta(m_q^2\, h_s(q,1,1)) = \quad & \frac{h_f(q)}{4}\Bigg\{ \left[16 m_q^2 + \Delta m_{\tilde{q}}^2\,(1-\cos 4\theta_{\tilde{q}})\right]\,\frac{\delta m_q}{m_q} - 2\,\sin^2 2\theta_{\tilde{q}}\,\Delta\delta m_{\tilde{q}}^2 \\
& -2\,\Delta m_{\tilde{q}}^2\,\sin 4\theta_{\tilde{q}}\,\delta\theta_{\tilde{q}}\Bigg\} + \frac{m_q^2}{2}\,(h_s(q,1,1) - h_s(q,2,2))\,\sin^2 2\theta_{\tilde{q}}\,\frac{\delta m_q}{m_q} \\
& + \frac{m_q^2}{2}\,h_s(q,1,2)\,\sin 4\theta_{\tilde{q}}\,\frac{\delta m_q}{m_q} + 2\,m_q^2\,h_s(q,1,2)\,\delta\theta_{\tilde{q}}\,, \qquad (4.64) \\
\delta(m_q^2\, h_s(q,2,2)) = \quad & -\delta(m_q^2\, h_s(q,1,1)) + 8\,h_f(q)\,m_q\,\delta m_q\,.
\end{aligned}$$

The off-diagonal terms we do not need, since in our amplitude $m_q^2 h_{\rm s}(q, 1, 2)$ only appears in two-loop diagrams. Taking δm_q, $\delta m_{\tilde{q}_i}^2$ and $\delta\theta_{\tilde{q}}$ to be the corresponding DRED expressions, this formula tells us how $m_q^2 h_{\rm s}(q, s_1, s_1)$ renormalizes in the presence of soft-breaking terms in DRED. However, taking δm_q, $\delta m_{\tilde{q}_i}^2$ and $\delta\theta_{\tilde{q}}$ to be in DREG does not tell us, how $m_q^2 h_{\rm s}(q, s_1, s_1)$ renormalizes in DREG. The supersymmetry breaking of DREG causes, that in DREG, $\delta(m_q^2 h_{\rm s}(q, s_1, s_2))$ gets an additional contribution, namely $\delta(m_q^2 h_{\rm s}(q, s_1, s_2))^{\rm FIX}$. Clearly, including $\delta(m_q^2 h_{\rm s}(q, s_1, s_2))^{\rm FIX}$ has the same effect as replacing $\delta m_q^{\rm DREG}$ by $\delta m_q^{\rm DRED}$. As the DREG expressions for $\delta m_{\tilde{q}_i}^2$ and $\delta\theta_{\tilde{q}}$ are equal to those in DRED, we can say, that the renormalization of $\delta(m_q^2 h_{\rm s}(q, s_1, s_2))$ in DREG is given by eq. (4.64) with all counterterms set to their DRED values.

The expressions for the heavy Higgs are obtained by replacing $h_{\rm f,s}$ by $H_{\rm f,s}$ everywhere.

4.3.5 Renormalization of the Amplitude

Having computed all necessary counterterms, we are now ready to renormalize the amplitude, or equivalently the formfactor $\mathcal{A}$. For the moment we suppress subscripts q, and $\tilde{q}_i$ identifying the various contributions. Recall, that we have computed $\mathcal{A}$ in bare perturbation theory

$$\mathcal{A}(\alpha_s^0 S_\epsilon, M^0) = \left(\frac{\alpha_s^0 S_\epsilon}{4\pi}\right)\,\mathcal{C}^{(0)}(M^0) + \left(\frac{\alpha_s^0 S_\epsilon}{4\pi}\right)^2\,\mathcal{C}^{(1)}(M^0) + \mathcal{O}\left((\alpha_s^0)^3\right), \tag{4.65}$$

To keep the notation simple, we we only write a collective symbol M, standing for m_q, $m^2_{\tilde{q}_1}$, $m^2_{\tilde{q}_2}$ and also the mixing angle $\theta_{\tilde{q}}$. Of course $\mathcal{A}$ also depends on the Higgs mass $s = m_h^2$ and on the gluino mass $m_{\tilde{g}}$, but this is of no concern here; m_h does not renormalize, since we do not compute electroweak corrections and $m_{\tilde{g}}$ only enters $\mathcal{C}^{(1)}$ but not $\mathcal{C}^{(0)}$.

We renormalize $\mathcal{A}$ by expressing all bare quantities in terms of renormalized quantities plus counterterms, so $S_\epsilon \alpha_s^0 = \alpha_s + \delta\alpha_s$ and $M^0 = M + \delta M$,

$$\mathcal{A}(\alpha_s + \delta\alpha_s, M + \delta M) = \mathcal{A}(\alpha_s, M) + \frac{\partial \mathcal{A}}{\partial \alpha_s}(\alpha_s, M)\,\delta\alpha_s + \frac{\partial \mathcal{A}}{\partial M}(\alpha_s, M)\,\delta M + \mathcal{O}\left(\alpha_s^3\right) \tag{4.66}$$

or in terms of the loop expansion coefficients $\mathcal{C}^i$,

$$\begin{aligned}\mathcal{A} &= \mathcal{A}(S_\epsilon \alpha_s^0, M^0) = \mathcal{A}(\alpha_s + \delta\alpha_s, M + \delta M) \\ &= \left(\frac{\alpha_s}{4\pi}\right)\mu^{2\epsilon}\,\mathcal{C}^{(0)} + \left(\frac{\alpha_s}{4\pi}\right)^2\left[\mu^{4\epsilon}\,\mathcal{C}^{(1)} - \mu^{2\epsilon}\,\frac{\beta_0}{\epsilon}\mathcal{C}^{(0)}\right] + \left(\frac{\alpha_s}{4\pi}\right)\mu^{2\epsilon}\left(\frac{\partial \mathcal{C}^{(0)}}{\partial M}\right)_s \delta M + \mathcal{O}\left(\alpha_s^3\right).\end{aligned} \tag{4.67}$$

We have to remember, that $\mathcal{A}$ and thus $\mathcal{C}^{(0)}$ are functions of M and, even though not explicitly written, $s = m_h^2$. As our analytic expressions for $\mathcal{C}^{(0)}$ are written in terms of M^2 and x, we use a notation borrowed from thermodynamics for the partial derivative. The necessary mass counterterms δM we computed in section 4.3.3. However, we have to pay attention to the fact, that our expressions for δm_q, $\delta m^2_{\tilde{q}_i}$ and $\delta\theta_{\tilde{q}}$ were computed in bare perturbation theory and contain the bare coupling α_s^0, which we have to express in terms of the renormalized coupling α_s. This is relevant, because already at leading order we have $\alpha_s^0 = S_\epsilon^{-1}\mu^{2\epsilon}\alpha_s$. To make the bookkeeping safer, we write factor $\left[\frac{4\pi}{\alpha^0}\right]$ wherever a mass counterterm appears in expressions for renormalized amplitudes. This factor cancels the $\left[\frac{\alpha^0}{4\pi}\right]$ in the definitions of the various δM and all powers of α_s, S_ϵ and μ^ϵ are exposed explicitly, rather than being partially hidden inside the counterterms. Note, that the factor S_ϵ^{-1} multiplying the mass renormalization appears, because we factored out powers of $\frac{S_\epsilon \alpha_s^0}{4\pi}$ from $\mathcal{C}^{(0)}$ and $\mathcal{C}^{(1)}$ but sticked to the standard definitions for the mass shifts δM.

$$\mathcal{A} = \left(\frac{\alpha_s}{4\pi}\right)\mu^{2\epsilon}\,\mathcal{C}^{(0)} + \left(\frac{\alpha_s}{4\pi}\right)^2\mu^{4\epsilon}\left[\mathcal{C}^{(1)} - \mu^{-2\epsilon}\,\frac{\beta_0}{\epsilon}\mathcal{C}^{(0)} + \left(\frac{\partial \mathcal{C}^{(0)}}{\partial M}\right)_s S_\epsilon^{-1}\,\left[\tfrac{4\pi}{\alpha^0}\right]\delta M\right] + \mathcal{O}\left(\alpha_s^3\right). \tag{4.68}$$

Now we could essentially put this formula into use by just duplicating it for the various contributions, was it not that supersymmetry had still prepared some gymnastics for us. For the fermionic case, there are no complications. Our generic M stands for m_q only, since that is the only mass $\mathcal{C}_q^{(0)}$ depends on. We can put the derivative into a more explicit form

$$\left(\frac{\partial \mathcal{C}_q^{(0)}}{\partial M}\right)_s = \frac{d}{dM}\left[\frac{h_{\mathrm{f}}(q)}{v} M^{-2\epsilon} c_f^{(0)}(x(M,s))\right] = \frac{h_{\mathrm{f}}(q)}{v}\frac{1}{M^{1+2\epsilon}}\left[-2\epsilon c_{\mathrm{f}}^{(0)}(x) + M\frac{\partial x}{\partial M}\frac{\partial c_{\mathrm{f}}^{(0)}(x)}{\partial x}\right], \tag{4.69}$$

$$M\frac{\partial x}{\partial M} = 2x\,\frac{1-x}{1+x}, \tag{4.70}$$

and combine it with the δm_q to a $\delta\mathcal{C}_q^{(0)}$

$$\left(\delta\mathcal{C}_q^{(0)}\right)^{\text{QCD,SUSY}} = \frac{h_\text{f}(q)}{v}\frac{1}{m_q^{1+2\epsilon}}\left[-2\epsilon\, c_\text{f}^{(0)}(x) + 2x\,\frac{1-x}{1+x}\, c_\text{f}^{(0)\prime}(x)\right]_{x=x_q} \delta m_q^{\text{QCD,SUSY}}. \quad (4.71)$$

The prime on the second $c_\text{f}^{(0)}$ of course denotes a derivative. Note, that we have defined two parts here, $\left(\delta\mathcal{C}_q^{(0)}\right)^{\text{QCD}}$ and $\left(\delta\mathcal{C}_q^{(0)}\right)^{\text{SUSY}}$, depending on which which contribution to the mass counterterm δm_q, they contain. The reason is, that we want to renormalize the Standard Model contribution $\mathcal{A}_q$ containining only quarks and gluons, the SM-like contribution $\mathcal{A}_{\tilde{q}}$, and the genuine supersymmetric part $\mathcal{A}_\text{SUSY}$ separately. The mass renormalization for $\mathcal{A}_q$ clearly includes only that part of $\delta\mathcal{C}_q^{(0)}$, that is proportional to δm_q^{QCD}, the contribution from radiating and reabsorbing a gluon. In the full SUSY amplitude there is an additional term, where the derivative of the SM contribution $\mathcal{C}_q^{(0)}$ multiplies the remaining piece of δm_q, namely δm_q^{SUSY}, arising from a squark-gluino loop. This term provides mass renormalization for the genuine supersymmetric contribution $\mathcal{A}_\text{SUSY}$, consisting of all diagrams containing gluinos or the four-squark vertex. Note that only two-loop diagrams contribute to the bare $\mathcal{A}_\text{SUSY}$, there is no such object as $\mathcal{C}_\text{SUSY}^{(0)}$. Therefore $\mathcal{A}_\text{SUSY}$ does not receive coupling constant renormalization and only mass renormalization "left over" from $\mathcal{C}_\text{q}^{(0)}$ and $\mathcal{C}_{\tilde{\text{q}}}^{(0)}$. With this, we have discussed in detail all terms entering the the renormalized Standard Model contribution

$$\mathcal{A}_q = \left(\frac{\alpha_s}{4\pi}\right)\mu^{2\epsilon}\,\mathcal{C}_q^{(0)} + \left(\frac{\alpha_s}{4\pi}\right)^2\mu^{4\epsilon}\left[\mathcal{C}_q^{(1)} - \mu^{-2\epsilon}\,\frac{\beta_0}{\epsilon}\mathcal{C}_q^{(0)} + S_\epsilon^{-1}\,\left[\tfrac{4\pi}{\alpha^0}\right]\left(\delta\mathcal{C}_q^{(0)}\right)^{\text{QCD}}\right] + \mathcal{O}\left(\alpha_s^3\right). \quad (4.72)$$

The squark contribution is a bit more involved due to the peculiarity of the coupling. For the mass renormalization we copy the one-loop contribution from eq. (4.29) and regroup the factors to

$$\mathcal{C}_{\tilde{q}_i}^{(0)} = \frac{1}{v}(m_q^2 h_\text{s}(q,i,i))\,\left[(m_{\tilde{q}_i}^2)^{-1-\epsilon}\, c_\text{s}^{(0)}(x_{\tilde{q}_i})\right]. \quad (4.73)$$

Now it is easy to compute the mass renormalization. We can use the product rule to compute $\delta\mathcal{C}_{\tilde{q}_i}^{(0)}$. The bracket only gets a variation from $\delta m_{\tilde{q}_i}^2$ and $\delta(m_q^2 h_\text{s}(q,i,i))$ we have already computed. However, in this representation it is hard to tell, what part of the expression provides counterterms for $\mathcal{A}_{\tilde{q}_i}$ and what part belongs to $\mathcal{A}_\text{SUSY}$. Since we aim to separate the various pieces, some more work is needed.

For a general scalar with mass m, coupling to the Higgs with strength $\frac{1}{v}m^2 h$, the one-loop amplitude is

$$\mathcal{C}_\text{s}^{(0)} = \frac{1}{v}h\left[m^{-2\epsilon}\, c_\text{s}^{(0)}(x)\right]. \quad (4.74)$$

Notice, that the factor m^2 from the coupling has been absorbed into the bracket here. The mass renormalization is simply

$$\delta\mathcal{C}_\text{s}^{(0)} = \frac{1}{v}\,h\,\frac{d}{dm^2}[m^{-2\epsilon}c_s(x)]\,\delta m^2. \quad (4.75)$$

To renormalize the squark part of our amplitude, we need precisely this expression with the

coupling constant

$$h = h_{\rm s}(q,i,i)\,\frac{m_q^2}{m_{\tilde{q}_i}^2}, \tag{4.76}$$

$m = m_{\tilde{q}_i}$ and δm^2 taken to be the QCD part of the mass shift, $(\delta m^2_{\tilde{q}_i})^{\rm QCD}$. The dimensionless coupling constant is a complicated function of m_q, $m_{\tilde{q}_i}$ and $\theta_{\tilde{q}}$ and its variation produces additional contributions to $\delta\mathcal{C}^{(0)}_{\tilde{q}_i}$, but these are counterterms for $\mathcal{A}_{\rm SUSY}$. Using the product rule,

$$\frac{1}{m^2}\frac{d}{dm^2}\left[(m^2)^{-\epsilon}c_s^{(0)}(x)\right] = \frac{d}{dm^2}\left[(m^2)^{-1-\epsilon}c_s^{(0)}(x)\right] + \frac{1}{m^2}\left[(m^2)^{-1-\epsilon}c_s^{(0)}(x)\right], \tag{4.77}$$

we can therefore write

$$(\delta\mathcal{C}^{(0)}_{\tilde{q}_i})^{\rm QCD} = \frac{1}{v}m_q^2 h_{\rm s}(q,i,i)\left[\frac{d}{dm^2_{\tilde{q}_i}}\left[(m^2_{\tilde{q}_i})^{-1-\epsilon}c_s^{(0)}(x_{\tilde{q}_i})\right] + \frac{1}{m^2_{\tilde{q}_i}}\left[(m^2_{\tilde{q}_i})^{-1-\epsilon}c_s^{(0)}(x_{\tilde{q}_i})\right]\right](\delta m^2_{\tilde{q}_i})^{\rm QCD}. \tag{4.78}$$

Comparing this to the full $\delta\mathcal{C}^{(0)}_{\tilde{q}_i}$, i.e. the variation of eq. (4.73), we can see, that it makes sense to define

$$\delta(m_q^2 h_{\rm s}(q,i,i))^{\rm QCD} := m_q^2 h_{\rm s}(q,i,i)\frac{(\delta m^2_{\tilde{q}_i})^{\rm QCD}}{m^2_{\tilde{q}_i}} \tag{4.79}$$

and

$$\delta(m_q^2 h_{\rm s}(q,i,i))^{\rm SUSY} := \delta(m_q^2 h_{\rm s}(q,i,i)) - \delta(m_q^2 h_{\rm s}(q,i,i))^{\rm QCD}. \tag{4.80}$$

With this notation we can write

$$(\delta\mathcal{C}^{(0)}_{\tilde{q}_i})^{\rm QCD} = \frac{1}{v}m_q^2 h_{\rm s}(q,i,i)\,\frac{1}{(m^2_{\tilde{q}_i})^{2+\epsilon}}\left[(-1-\epsilon)c_s^{(0)}(x) + x\frac{1-x}{1+x}\,c_s^{(0)\prime}(x)\right]_{x=x_{\tilde{q}_i}}(\delta m^2_{\tilde{q}_i})^{\rm QCD} + \frac{1}{v}\delta(m_q^2 h_{\rm s}(q,i,i))^{\rm QCD}\left[(m^2_{\tilde{q}_i})^{-1-\epsilon}c_s^{(0)}(x_{\tilde{q}_i})\right], \tag{4.81}$$

$$(\delta\mathcal{C}^{(0)}_{\tilde{q}_i})^{\rm SUSY} = \frac{1}{v}m_q^2 h_{\rm s}(q,i,i)\,\frac{1}{(m^2_{\tilde{q}_i})^{2+\epsilon}}\left[(-1-\epsilon)c_s^{(0)}(x) + x\frac{1-x}{1+x}\,c_s^{(0)\prime}(x)\right]_{x=x_{\tilde{q}_i}}(\delta m^2_{\tilde{q}_i})^{\rm SUSY} + \frac{1}{v}\delta(m_q^2 h_{\rm s}(q,i,i))^{\rm SUSY}\left[(m^2_{\tilde{q}_i})^{-1-\epsilon}c_s^{(0)}(x_{\tilde{q}_i})\right], \tag{4.82}$$

where we have also spelled out the mass derivative. The two formulae are identical up to the QCD and SUSY superscripts.

Finally we can write down the renormalized expressions for the remaining two contributions

$$\mathcal{A}_{\tilde{q}_i} = \left(\frac{\alpha_s}{4\pi}\right)\mu^{2\epsilon}\,\mathcal{C}_q^{(0)} + \left(\frac{\alpha_s}{4\pi}\right)^2\mu^{4\epsilon}\left[\mathcal{C}_q^{(1)} - \mu^{-2\epsilon}\,\frac{\beta_0}{\epsilon}\mathcal{C}_q^{(0)} + S_\epsilon^{-1}\,\left[\tfrac{4\pi}{\alpha^0}\right](\delta\mathcal{C}^{(0)}_{\tilde{q}_i})^{\rm QCD}\right] + \mathcal{O}\left(\alpha_s^3\right), \tag{4.83}$$

$$\mathcal{A}_{\text{SUSY}} = \left(\frac{\alpha_s}{4\pi}\right)^2 \mu^{4\epsilon} \left[\mathcal{C}^{(1)}_{\text{SUSY}} + S_\epsilon^{-1} \left[\tfrac{4\pi}{\alpha^0}\right] \left[(\delta\mathcal{C}_q^{(0)})^{\text{SUSY}} + (\delta\mathcal{C}_{\tilde{q}_1}^{(0)})^{\text{SUSY}} + (\delta\mathcal{C}_{\tilde{q}_2}^{(0)})^{\text{SUSY}}\right]\right] + \mathcal{O}\left(\alpha_s^3\right). \tag{4.84}$$

Note, that no field-strength renormalization takes place. Self-energy corrections on the Higgs line are absent, since we do not include electroweak corrections. Self-energy corrections on the external gluon lines from top quarks and SUSY particles must not be included, since we have decoupled these heavy particles. In principle, self-energy corrections from bottom quarks should be included, but this contribution is negligible due to the smallness of m_b.

4.3.6 Renormalization of the Redundant Parameter $m_{\tilde{b}_1}$

Recall, that our masses are not independent. The bare parameters are related by eq. (4.18). So far, we have completely ignored this fact and our amplitude depends on the full, dependent set of mass parameters.

Solving eq. (4.18) for the $m^2_{\tilde{b}_1}$, which we take as the dependent quantity gives

$$m^2_{\tilde{b}_1} = \frac{1}{\cos^2\theta_{\tilde{b}}} \left(-\sin^2\theta_{\tilde{b}} m^2_{\tilde{b}_2} + \cos^2\theta_{\tilde{t}} m^2_{\tilde{t}_1} + \sin^2\theta_{\tilde{t}} m^2_{\tilde{t}_2} + m_b^2 - m_t^2 - M_W^2\cos(2\beta)\right)\Bigg|_{\text{bare}}. \tag{4.85}$$

Let us for a moment abbreviate this relation as

$$m^0 = B(M^0), \tag{4.86}$$

where m^0 stands for the bare $m^2_{\tilde{b}_1}$ and M^0 collectively denotes all independent bare quantities on the right hand side of eq. (4.85).

We can mimic the situation, where the dependent m^0 has been eliminated at the very beginning, say in the Lagrangian, writing $B(M^0)$ instead of m^0 in unrenormalized quantities like eq. (4.65). We then renormalize by writing $M^0 = M + \delta M$, and thus implicitly

$$m^0 = B(M^0) = B(M + \delta M) = B(M) + \delta B \tag{4.87}$$

instead of $m^0 = m + \delta m$, where m is the pole mass and δm the counterterm in the pole scheme. Series expansion in the coupling then also leads to expansion of the coefficient functions $\mathcal{C}^{(0)}$ and $\mathcal{C}^{(1)}$ around $B(M)$ rather than m. Consequently the correct renormalized expression can be obtained from our renormalized expression where we have treated all masses as if they were independentjust by replacing

$$m \to B(M) \tag{4.88}$$

$$\delta m \to \delta B. \tag{4.89}$$

While this mimics exactly what would happen, if m^0 was eliminated from the beginning, arguably it is not a very natural thing to do. Since m_0 has *not* been eliminated from the Lagrangian, our results depend on the parameter m just as they depend on all other masses M. There is nothing special about m. But the above mimicking procedure obviously corresponds to renormalizing m using a weird scheme $m^0 = B(M) + \delta B$ for the dependent sbottom mass, while we have renormalized all other masses on shell. We can fix this by expressing the input

parameter $B(M)$ in terms of the pole mass m,

$$B(M) = m + \delta m - \delta B. \tag{4.90}$$

Substituting this into our expression is easy. In all $\mathcal{O}(\alpha_s^2)$ terms, the $\mathcal{O}(\alpha_s)$ shift $\delta m - \delta B$ is irrelevant, so $B(M)$ simply gets replaced by m. In the Born contribution the shift matters and its net effect is simply, that in the mass renormalization δB gets replaced by δm again. So we are back home again, all masses are renormalized on-shell and our final result does not need any modification. We just have to compute the dependent mass in the pole scheme,

$$m = B(M) + \delta B - \delta m \tag{4.91}$$

or spelled out

$$\begin{aligned} m^2_{\tilde{b}_1} = \frac{1}{\cos^2\theta_{\tilde{b}}}\Big(&-\sin^2\theta_{\tilde{b}} m^2_{\tilde{b}_2} + \cos^2\theta_{\tilde{t}} m^2_{\tilde{t}_1} + \sin^2\theta_{\tilde{t}} m^2_{\tilde{t}_2} + m_b^2 - m_t^2 - M_W^2\cos(2\beta)\Big) + \\ \frac{1}{\cos^2\theta_{\tilde{b}}}\Big(&\cos^2\theta_{\tilde{t}}\,\delta m^2_{\tilde{t}_1} + \sin^2\theta_{\tilde{t}}\,\delta m^2_{\tilde{t}_2} - \sin^2\theta_{\tilde{b}}\,\delta m^2_{\tilde{b}_2} - \sin 2\theta_{\tilde{t}}(m^2_{\tilde{t}_1} - m^2_{\tilde{t}_2})\delta\theta_{\tilde{t}} \\ &+ \sin 2\theta_{\tilde{b}}(m^2_{\tilde{b}_1} - m^2_{\tilde{b}_2})\delta\theta_{\tilde{b}} - 2m_t\delta m_t + 2m_b\delta m_b\Big) - \delta m^2_{\tilde{b}_1}. \end{aligned} \tag{4.92}$$

Clearly what has happened here is, that we have just computed the $\mathcal{O}(\alpha_s)$ correction to the tree-level relation eq. (4.85). The last two lines are the correction $\delta B - \delta m$. As it stands, this expression is not explicit, as $m^2_{\tilde{b}_1}$ also appears on the right hand side through various shifts and end even explicitly. But as usual it is sufficient to insert the leading order value given by the first line only.

A careful discussion of the impact of various renormalization schemes can be found in [70].

4.3.7 Infrared Counterterms

Since we do not consider real radiation processes here, we subtract the infrared counterterm of [62]. This amounts to *adding* the following expressions to the two-loop contributions $\mathcal{C}^{(1)}$

$$\mathcal{C}_q^{\rm IR} = \left(\frac{1}{-s}\right)^{\epsilon} \frac{e^{\epsilon\gamma_E}}{\Gamma(1-\epsilon)}\left(\frac{6}{\epsilon^2} + \frac{\beta_0}{\epsilon}\right)\mathcal{C}_q^{(0)}, \tag{4.93}$$

$$\mathcal{C}_{\tilde{q}_i}^{\rm IR} = \left(\frac{1}{-s}\right)^{\epsilon} \frac{e^{\epsilon\gamma_E}}{\Gamma(1-\epsilon)}\left(\frac{6}{\epsilon^2} + \frac{\beta_0}{\epsilon}\right)\mathcal{C}_{\tilde{q}_i}^{(0)}. \tag{4.94}$$

The SUSY contribution $\mathcal{C}^{(1)}_{\rm SUSY}$ is infrared finite.

4.4 Numerical Evaluation of the SUSY Diagrams

To finalize our amplitude, we still have to compute the missing piece $\mathcal{C}^{(1)}_{\rm SUSY}$, consisting of the factorizable diagrams QUARTICS and mainly the challenging diagrams containing gluions, GQ and GSQ, which contain up to five of the invariants $s = m_h^2$, m_q, $m_{\tilde{q}_1}$, $m_{\tilde{q}_2}$ and $m_{\tilde{g}}$. We accomplish this using the numerical method described in chapter 3. We briefly recall the main steps here.

1. The integrand of each diagram is projected onto the form factor $\mathcal{A}$. Therefore, all numerators are written entirely in term of dot products.

2. Feynman parameters are introduced. We parametrize the non-factorizable two-loop diagrams GQ and GSQ according to the strategy "sunset" described in section 3.2.2. Feynman parameters on simplices are mapped to the hypercube using the simple rescaling given in section 3.2.4. This is sufficient, as only low-dimensional simplices appear by virtue of the "sunset" parametrization. Dot products in numerators are treated as described in section 3.2.3. The now trivial integrations over loop momenta are carried out by applying eq. (3.8) twice.

3. Sector decomposition, contour deformation and ϵ-expansion up to $\mathcal{O}(\epsilon^0)$ are performed and C++ programs, that evaluate the individual diagrams are generated. Very few sectors per diagram emerge, as all diagrams are IR finite and UV singularities are already factorized in the "sunset" parametrization.

To compute $\mathcal{C}^{(1)}_{\text{SUSY}}$ we have to evaluate each diagram for to (s)top and the (s)bottom case and in each case for all possible combinations of sfermion indices s_i. We perform the numerical evaluation for integrands with couplings and mixing matrices stripped off and "dress" the results afterwards with these quantities. This has the advantage, that only masses enter the numerical code. We gain the flexibility to change couplings and mixing angles without rerunning. Stripping off the higgs-quark and higgs-squark couplings $h_{\text{f}}(q)$ and $h_{\text{s}}(q, s_1, s_2)$ is straightforward. Also the mixing matrices

$$\mathcal{S}^q = \begin{pmatrix} \cos 2\theta_{\tilde{q}} & -\sin 2\theta_{\tilde{q}} \\ -\sin 2\theta_{\tilde{q}} & -\cos 2\theta_{\tilde{q}} \end{pmatrix} . \tag{4.95}$$

appearing in the QUARTICS factor out trivially. The dependence of the GQ and GSQ diagrams on the mixing angle is more involved, here we have to compute the coefficients of the two mixing matrices (see appendix E)

$$\mathcal{R}^q_+ = 2 \begin{pmatrix} 1 & 0 \\ 0 & 1 \end{pmatrix} , \qquad \mathcal{R}^q_- = 2 \begin{pmatrix} \sin 2\theta_{\tilde{q}} & \cos 2\theta_{\tilde{q}} \\ \cos 2\theta_{\tilde{q}} & -\sin 2\theta_{\tilde{q}} \end{pmatrix} \tag{4.96}$$

for each diagram. We do not actually generate two different codes for the two coefficients, but rather keep input parameters `RRplus` and `RRminus`, which we set to 1 or 0 in order to select the desired part. Due to the different tensor structures of the $\mathcal{R}^q_+$ and $\mathcal{R}^q_-$ coefficients, this does not produce optimal code; there are usually some sectors[7], which only contribute to one of the coefficients and thus always evaluate to zero, when we compute the other coefficient. While this may look peculiar it does no real harm.

In the individual groups of diagrams, sfermion indices, mixing matrices and couplings appear as follows.

[7]We use the term "sector" as a synonym for "individual integral contributing to a diagram" here. The splitting of diagrams into sectors does not come from sector decomposition only, but also from the treatment of numerators, which have to be split into pieces according to how many powers of the loop momenta they contain.

GQ The Higgs couples to a quark line, squark propagators are separated only by gluon vertices. So there is a single sfermion index s_1 and so there are two versions of these diagrams. The coupling is $h_{\mathrm{f}}(q, s_1, s_1)$, the mixing matrices $(\mathcal{R}^q_+)_{s_1,s_1}$ and $(\mathcal{R}^q_-)_{s_1,s_1}$ appear.

GSQ The Higgs couples to a squark line. Two sfermion indices s_1 and s_2 appear, belonging to squark propagators before and after the Higgs vertex. Four versions of each diagram have to by computed. Note that the diagrams are not necessarily symmetric under $s_1 \leftrightarrow s_2$. The coupling is $h_{\mathrm{s}}(q, s_1, s_2)$, the mixing matrices $(\mathcal{R}^q_+)_{s_1,s_2}$ and $(\mathcal{R}^q_-)_{s_1,s_2}$ appear.

QUARTICS The Higgs again couples to a squark line and there is an additional squark line "on the other side of the $\tilde{q}\tilde{q}\tilde{q}\tilde{q}$-vertex". Thus there are three sfermion indices s_1, s_2, s_3 and we choose them such, that s_3 always belongs to the squark line, which does not interact with the Higgs. Then the coupling is always $h_{\mathrm{s}}(q, s_1, s_2)$ and the mixing matrices are $(\mathcal{S}^q)_{s_1,s_3}(\mathcal{S}^q)_{s_2,s_3}$. Clearly, eight versions of each diagram have to be computed.

Note, that similar to the treatment of $(\mathcal{R}^q_+)$ and $(\mathcal{R}^q_-)$, we actually do not really factor out the mixing matrices $\mathcal{S}^q$ and the couplings, we just set the corresponding input parameters to 1. It is also possible to perform the sum over sfermion indices before code generation. This means, that a separate code is generated for each combination of sfermion indices. This way only the masses `m_sq1` and `m_sq2` remain as input parameters, rather than `m_sq_Sfe1`, `m_sq_Sfe2`, `m_sq_Sfe3`, and also the entries of the mixing matrices can be substituted in immediately, leaving only `cos2theta` and `sin2theta` as input parameters. While not overly elegant, this is very useful for testing purposes, as it leaves less room for mistakes. For the production run we proceed as described above, performing sums over sfermion indices by running the same code several times for all combinations of masses and dressing the results with couplings and mixing matrices afterwards. We perform all runs for the (s)top and (s)bottom case for both, the light and the heavy Higgs boson. The four cases differ only in the input values for masses, mixing angles and couplings.

4.5 Results

In this section we present numerical results for the MSSM two-loop amplitudes $gg \to h, H$. We neglect here the Higgs couplings to quarks and squarks other than the ones in the third generation. The two-loop amplitudes are infrared divergent with poles up to second order in the regularisation parameter ϵ. The singular part is universal and cancels against other universal contributions at the same order in α_s from real radiation processes. We present here the finite part after UV renormalization in the $\overline{\mathrm{MS}}$ scheme and subtracting the infrared counter-term of Ref. [62], displayed in eq. (4.93) and (4.94). A complete phenomenological analysis would require the inclusion of the non-singular parts from real radiation. Therefore the results displayed here are not physical. They should be seen primarily as a demonstration, that our method is capable of handling the most difficult diagrams one can expect in NLO $gg \to h$ calculations beyond the Standard Model. Nevertheless some useful conclusions may also be inferred from solely the two-loop amplitudes, which include all diagrams with more than one massive internal particle. These are the diagrams which had not been computed earlier in the literature [44, 45, 46, 47]. They form a subset which is infrared finite.

In Figure 4.6 we present our results for the production of a light Higgs in gluon fusion in the MSSM. The MSSM parameters have been chosen to represent a section through the golden region of the MSSM, discussed in [74]. The first stop has a relatively small mass of $m_{\tilde{t}_1} = 150\,\text{GeV}$, while $m_{\tilde{t}_2}$ is varied from $400 - 580\,\text{GeV}$. Note, that due to the constraint eq. (4.92) it is not possible to keep fixed all of $m_{\tilde{b}_1}, m_{\tilde{b}_2}, \theta_{\tilde{t}}$ and $\theta_{\tilde{b}}$ while varying $m_{\tilde{t}_2}$. The values of all fixed parameters are listed in tab. 4.3, those varied in the $m_{\tilde{t}_2}$ scan are shown in tab. 4.4. The renormalization scale was set to $\mu = m_h$.

$\alpha_s^{\overline{\text{MS}}}(m_Z)$	0.1176
m_t	172.5 GeV
m_b	5 GeV
m_Z	91.187 GeV
$\sin^2\theta$	0.223
m_h	115 GeV
α	0.0524
$\tan\beta$	20
μ_{SUSY}	300 GeV
$m_{\tilde{g}}$	500 GeV
$m_{\tilde{t}_1}$	150 GeV
$\theta_{\tilde{t}}$	$\pi/4$
μ_θ	200 GeV

Table 4.3: Input parameters not varied throughout the mass scan.

The displayed quantity is the K-factor, i.e. the ratio of the squared amplitude through $\mathcal{O}(\alpha_s^3)$ divided by the $\mathcal{O}(\alpha_s^2)$ result,

$$\text{K} = \frac{\left(\frac{\alpha_s^{\text{NLO}}}{4\pi}\right)^2 \mu^{4\epsilon}\, \mathcal{C}^{(0)*}\mathcal{C}^{(0)} + \left(\frac{\alpha_s^{\text{NLO}}}{4\pi}\right)^3 \mu^{6\epsilon}\, 2\,\text{Re}\,\mathcal{C}^{(0)*}\left[\mathcal{C}^{(1)} + \mathcal{C}^{(\text{UV})} + \mathcal{C}^{(\text{IR})}\right]}{\left(\frac{\alpha_s^{\text{LO}}}{4\pi}\right)^2 \mu^{4\epsilon}\, \mathcal{C}^{(0)*}\mathcal{C}^{(0)}}. \tag{4.97}$$

Here all $\mathcal{C}^{(i)}$ of course denote the sums over quark, squark and SUSY contributions from the bottom as well as from the top sector. $\mathcal{C}^{(\text{UV})}$ includes mass and coupling constant renormalization. Note that the coupling constant in the numerator, α_s^{NLO}, runs with the two-loop β-function, whereas the denominator is the leading order result and thus contains α_s^{LO}, running with the one-loop β-function only. In addition to the MSSM result we include K-factors obtained in various approximations of the full result: The curve labeled "No SUSY vertices" discards diagrams containing gluinos or quartic squark couplings and thus consists of SM and SM-like contributions only, which are computable analytically. This is obviously a poor approximation of the full result, demonstrating the importance of the true SUSY diagrams. Their contribution to the squared amplitude is negative and grows in absolute value with growing $m_{\tilde{t}_2}$. Also the contributions from the bottom sector can be sizeable, as can be read off the corresponding curve. The result neglecting the bottom sector can be approximated using the the effective theory calculation of Ref. [25]. The corresponding curve was computed using the published program `evalcsusy`. With the mass splitting growing, the effective field theory deviates more and more from the result neglecting the bottom sector but accounting

$m_{\tilde{t}_2}$	$m_{\tilde{b}_1}$	$m_{\tilde{b}_2}$	$\theta_{\tilde{b}}$
400.000	265.457	504.092	0.138
410.000	273.032	504.172	0.141
420.000	280.572	504.257	0.144
430.000	288.077	504.349	0.148
440.000	295.551	504.448	0.152
450.000	302.993	504.554	0.156
460.000	310.406	504.669	0.161
470.000	317.790	504.793	0.166
480.000	325.145	504.928	0.171
490.000	332.472	505.075	0.177
500.000	339.769	505.235	0.183
510.000	347.038	505.411	0.190
520.000	354.276	505.603	0.197
530.000	361.483	505.816	0.205
540.000	368.656	506.051	0.215
550.000	375.793	506.312	0.225
560.000	382.891	506.604	0.236
570.000	389.944	506.932	0.248
580.000	396.948	507.302	0.262

Table 4.4: Mass scan through the golden region of the MSSM.

for the full mass dependence in the top sector. Ironically, for large $m_{\tilde{t}_2}$, this deviation brings the effective field theory result closer to the full MSSM result. This is purely accidental, however.

In Figure 4.7 we show the corresponding results for the production of a heavy Higgs. Here the mass of the heavy Higgs boson m_H is varied from $280 - 455\,\text{GeV}$ and the renormalization scale is set to $\mu = m_H$. All other parameters are chosen like in the first point of the light Higgs calculation, i.e. $m_{\tilde{t}_1} = 150\,\text{GeV}$, $m_{\tilde{t}_2} = 400\,\text{GeV}$, $m_{\tilde{b}_1} = 265.457\,\text{GeV}$, $m_{\tilde{b}_2} = 504.092\,\text{GeV}$, $\theta_{\tilde{b}} = 0.138$ and the values given in tab. 4.3. A threshold occurs at $m_H = 2\,m_{\tilde{t}_1} = 300\,\text{GeV}$, where an on-shell stop1 pair can be produced. As the perturbative calculation diverges at the threshold, we have whitewashed a window of $5\,\text{GeV}$ around the threshold. The numerical method has no problems approximating the threshold from below, whereas approximating it from above leads to increasing errors due to large cancellations. As in the light Higgs case contributions from diagrams with gluinos and quartic squark couplings are substantial in the top as well as in the bottom sector. Due to the missing mass hierarchy an effective field theory calculation is meaningless in the case of a heavy Higgs boson.

4.6 Numerical Stability

In the (s)top contribution to the light Higgs case, the heavy particles cannot go on-shell. Accordingly numerical integration is extremely fast. All other contributions are more demanding. The most difficult cases are the diagrams GQ7 and GQ8 in the bottom case. Power counting shows, that the combined denominator is raised to the second power here and set-

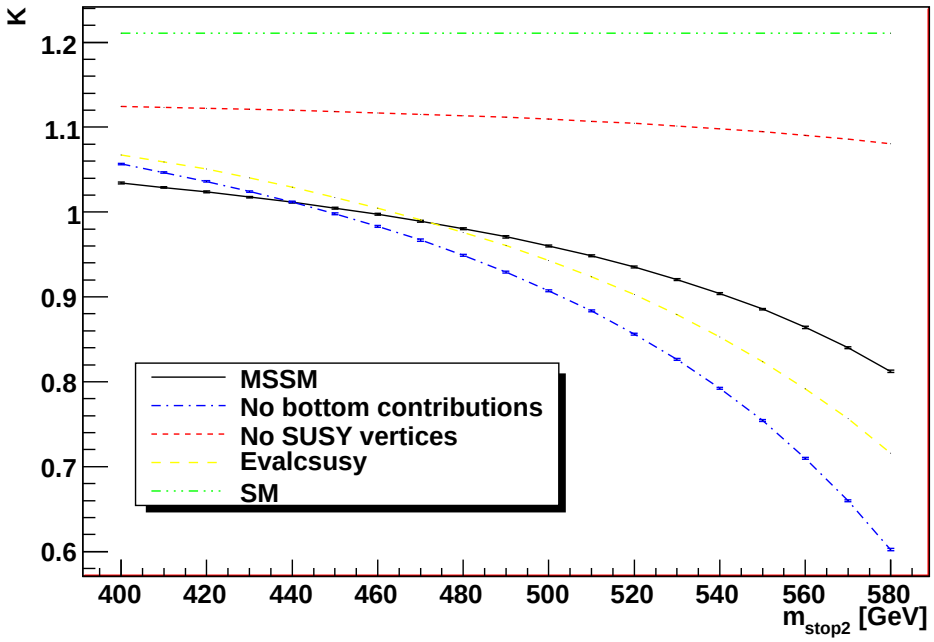

Figure 4.6: NLO K-factor for the production of a light Higgs boson.

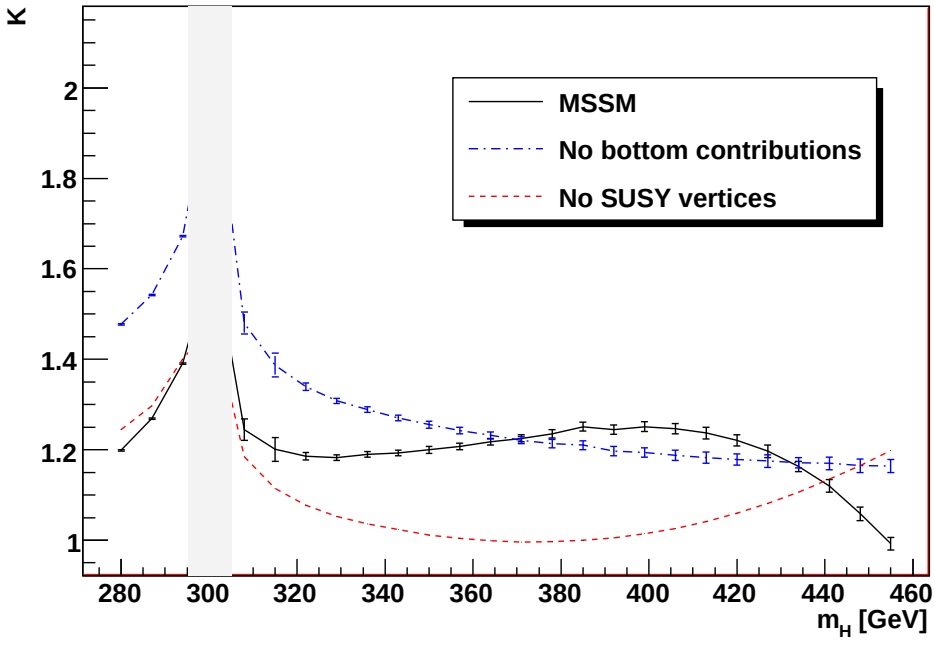

Figure 4.7: NLO K-factor for the production of a heavy neutral Higgs boson.

ting $m_b = 5\,\text{GeV}$ and $m_{\tilde{g}} = 500\,\text{GeV}$ means having ratios of squared masses of the order 10^4. To evaluate these integrands it was necessary to adjust the deformation of each Feynman parameter individually by using separate λ_i as described in section 3.4.3. Alternatively these diagrams could be evaluated using a Feynman parametrization similar to [8]. This parameterization casts diagrams with bubble subgraphs as a sum of two terms. One of them corresponds to a one-loop integral and matches the counter-term for mass renormalization. The second term corresponds to a two-loop integral which can be evaluated without a specially tuned contour deformation. Here we do not discuss this option further.

The numerical behavior of the $\mathcal{R}^q_+$-coefficient of diagram GQ8 in the bottom case for the heavy Higgs is illustrated in figure 4.8. Runs using the Divonne and the Cuhre integrator from the Cuba library are shown. Here the code chose the parameter values for the parameters λ_i controlling the size of the deformation as described in section 3.4.3. For some runs, the λ_i chosen this way were corrected by hand, in order to obtain smaller cancellations between positive and negative contributions, and thus a better deformation. Unfortunately, this is not visible in the figure. All λ_i were then multiplied by an overall scaling factor `laR`. The idea is to vary the overall size of the deformation to check stability, after a suitable direction and order of magnitude of $\vec{\lambda}$ have been found. Also the rescaling power from eq. (3.102), called here r, was set to 1 and 2. No clear preference is visible here, but the possibility to change an additional parameter is still useful in cases like this, where the range of possible values for `laR` is obviously pretty limited.

Clearly integration is a delicate issue in this extreme case. While reasonably small errors can be a achieved by tuning the parameters (run 21 shows relative errors of 1.4 and 4.4 per mill with only 3.4 million evaluations), without tuning, results can be much worse. It is unsatisfactory, that none of the integrators really performs well here. Cuhre seems to give very precise results here even with relatively few integrand evaluations, but constantly overestimates errors by more than an order of magnitude. This often causes, that Cuhre only stops, when it reaches the specified maximal number of evaluations. We have no clue, what causes this behavior. Also in some cases Cuhre fails completely, returning `NaN`. On the other hand Divonne often stops after a low number of evaluations, but underestimates the integration error by a factor of 2 or 3, sometimes even by more than an order of magnitude. An inconvenient feature of Divonne is also, that it is necessary to specify a ϵ_{border} in order to prevent it from sampling on the border of the integration domain, where the integrand is often not well defined. With extremely disparate kinematic invariants it is necessary to watch this parameter, as features of the integrand can be squeezed to the border. Here we set[8] $\epsilon_{\text{border}} = 10^{-9}$.

[8]Our code automatically rescales the ϵ_{border} specified in the parameter file, such that the same region of the original integrand is sampled for different values of the rescaling exponent r.

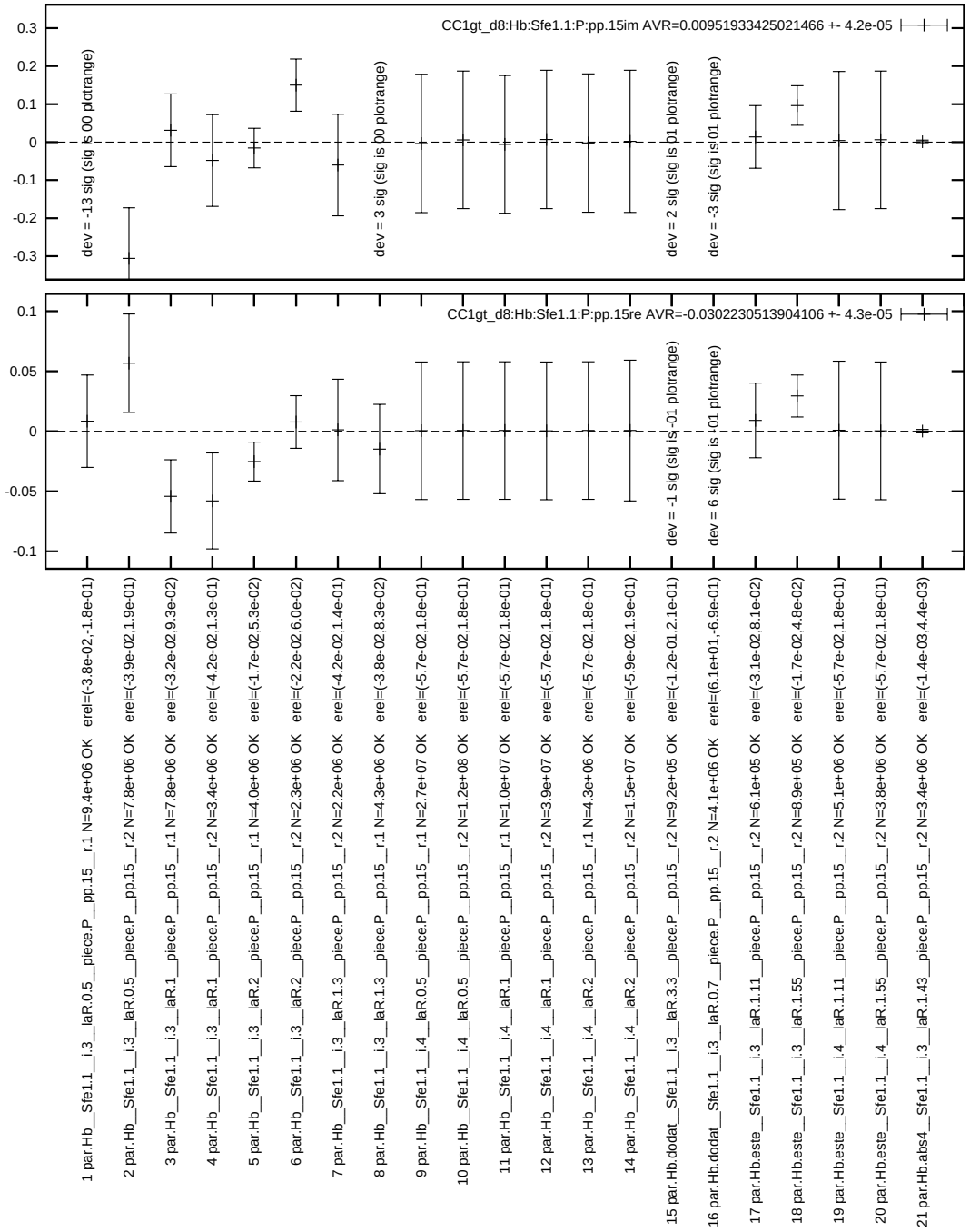

Figure 4.8: Comparison of different integration runs for the $\mathcal{R}^q_+$-coefficient of diagram GQ8 in the bottom case for the heavy Higgs. The lower and upper panel correspond to real and imaginary parts. The central values show the deviation of each run from the weighted average of all runs normalized to the weighted average. The lengths of the error-bars show the error quoted by the integrator. Outliers are given in words only to prevent blow up the scale of the plot. The labels show again the relative errors quoted by the integrator, the cumulative number of evaluations for all sectors N, and the name of the input parameter file, revealing the integrator [i.3 = Divonne, i.4 = Cuhre], the overall rescaling of λ_i, laR, as well as the exponent r for rescaling Feynman parameters close to 0 and 1.

Chapter 5

Conclusions

The production of a Higgs boson via gluon fusion, $gg \to h$, is a fundamental LHC process. It is the most important production channel for the yet undiscovered Higgs boson, the last missing particle predicted by the extremely successful Standard Model of strong and electroweak interactions. In scenarios, where a Higgs boson exists, but the Standard Model is incomplete, the $gg \to h$ process is very sensitive to so-called physics beyond the Standard Model. Via quantum effects unknown new particles will generally give rise to sizeable contributions, even if they should be to heavy to be produced in a collider experiment. Since the gluon fusion process cannot occur directly through tree-level interactions, the next-to-leading order corrections, indispensable in QCD, already contain two loops.

In this thesis, we have computed the full two-loop SUSY QCD amplitude for the $gg \to h, H$ process in the Minimal Supersymmetric Standard Model, a complicated extension of the Standard Model. This is the first complete result for a two-loop three-point Green's function in the MSSM. We achieve this using two complementary approaches.

Modern analytic computation technology for multi-loop processes is well suited for those partial contributions with simple mass patterns. We identify a complete set of 17 two-loop master integrals for the $gg \to h$ process in the Standard Model. We write these master integrals as Laurent series in ϵ and compute their coefficients in terms of harmonic polylogarithms. Contributions to $gg \to h$ in arbitrary models can be reduced to these master integrals in an automated manner, as long as only a single mass parameter appears in the loops. We give the result for the Standard Model case, as well as for the SM-like case, where a heavy scalar instead of a fermion is running in the loops. The former represents the first independent check of the calculation by Spira, Djouadi, Graudenz and Zerwas from 1993. The latter is a new result. With adequate couplings, they both form partial contributions to $gg \to h, H$ in the MSSM.

The two-loop contributions to $gg \to h, H$ containing gluinos contain up to five kinematic invariants, clearly hinting towards numerical integration. We show how to use contour deformation for treating thresholds in the context of sector decomposition. This yields a method, allowing for the first time direct numerical evaluation of multi-loop Feynman diagrams containing UV, IR and threshold singularities. For one-loop multi-leg amplitudes, this might not be the method of choice. Approaches based on reduction present strong competition, especially if they manage to avoid Feynman diagrams at the loop level [72, 73]. However, at the time of this writing, our method is the only viable way of evaluating two-loop diagrams containing several mass parameters in the physical region. In our calculation we encounter

the numerically challenging case of diagrams, that simultaneously contain bottom quarks and heavy SUSY particles. Ratios of squared masses of the order of 10^4 present a real stress test for the numerical method.

While we do not expect to find the MSSM at LHC, we see it as an archetype model exposing the computational difficulties one might encounter in computing the $gg \to h$ amplitude in beyond the Standard Model scenarios: Multi-loop diagrams containing many masses conspiring with a mass spectrum, that does not allow the application of effective theories.

Our calculation demonstrates, that our numerical method is not just a handy device for checking analytic calculations. It can be used as a computation method for important processes, that were not tractable before. Many applications are conceivable and the limitations of our method have not yet been explored thoroughly. For the $gg \to h$ process it is certainly realistic to hope, that our method will allow the evaluation of the two-loop contributions in any model physicists might propose, if LHC will force us to revise the Standard Model.

Appendix A

SUSY-QCD Diagrams for $gg \to h, H$ in the MSSM

Here we give the complete set of (generic) Feynman diagrams contributing to $gg \to h, H$ in the MSSM up to the two-loop level. Diagrams, that evaluate to zero for various reasons are not suppressed and also all diagrams related by Bose symmetry and/or reversion of arrows are spelled out. All diagram names include an "o" for "original" in order to distinguish them from the "collective" diagrams used in the main part, e.g. $\frac{1}{2}$BORN1 = BORNo1 = BORNo2. In each diagram, the (s)quarks can be (s)tops or (s)bottoms. Further squarks can be squark1 or squark2. The GQ diagrams always have one, the GSQ diagrams two and the QUARTICS three independent squark indices. All further diagrams with squarks have one independent squark index.

A.1 Born Level Diagrams

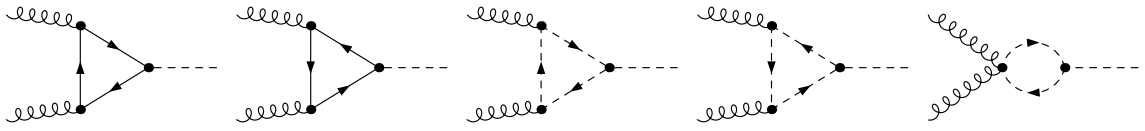

BORNo1 BORNo2 BORNo3 BORNo4 BORNo5

A.2 NLO Diagrams

A.2.1 SM Diagrams

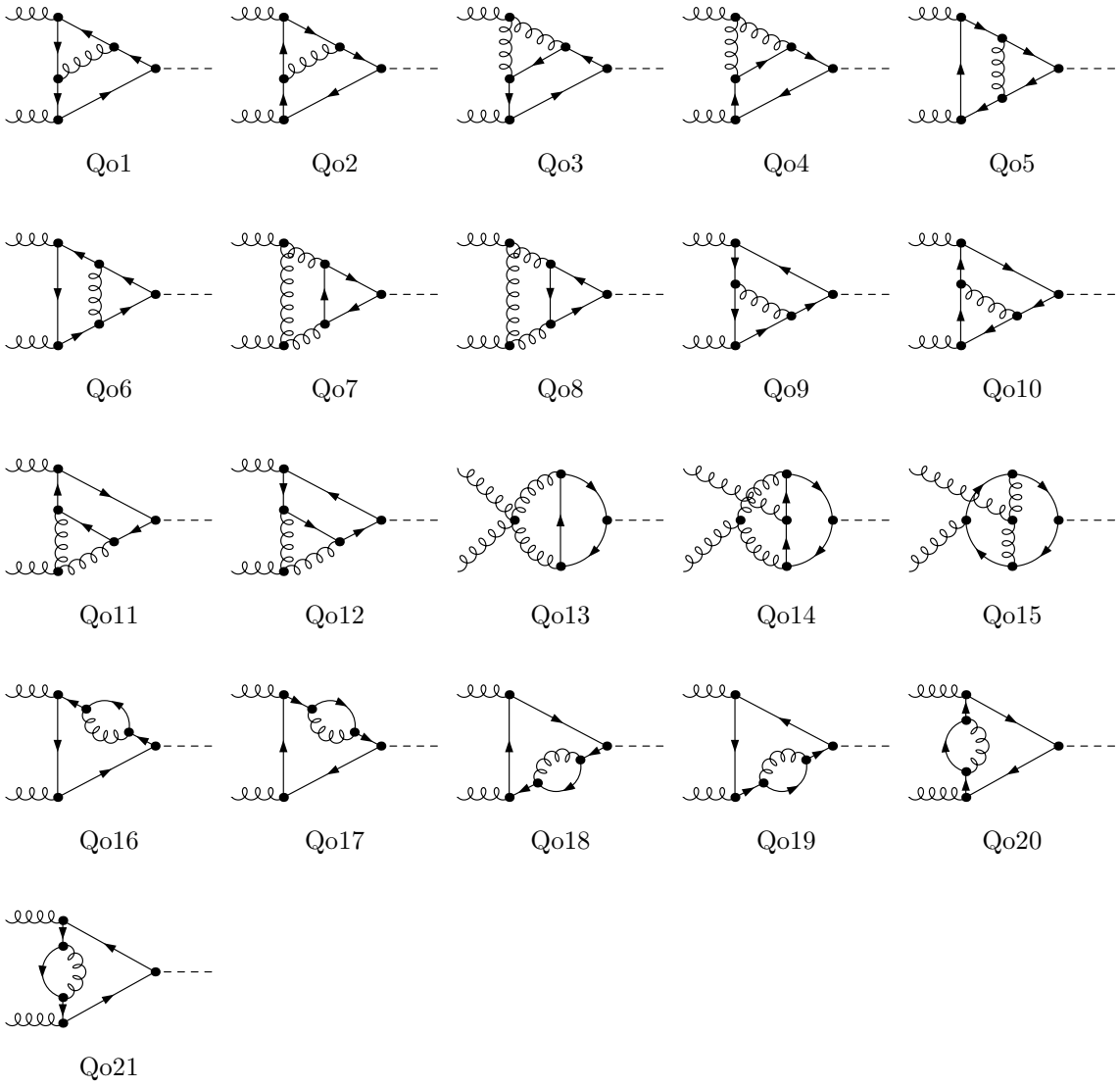

A.2.2 SM-like Diagrams Containing Scalars

There are 56 two-loop contributions to the ggh-interaction mediated by a single massive scalar. In the MSSM context, the scalar is a scalar quark, coming with a sfermion index $i \in 1, 2$. While the interaction with the Higgs mixes the two sfermion types, the $\tilde{q}\tilde{q}g$-vertex

is diagonal. For this reason, all sfermions occurring in a diagram of this class are of the same type. So only a single mass parameter is present.

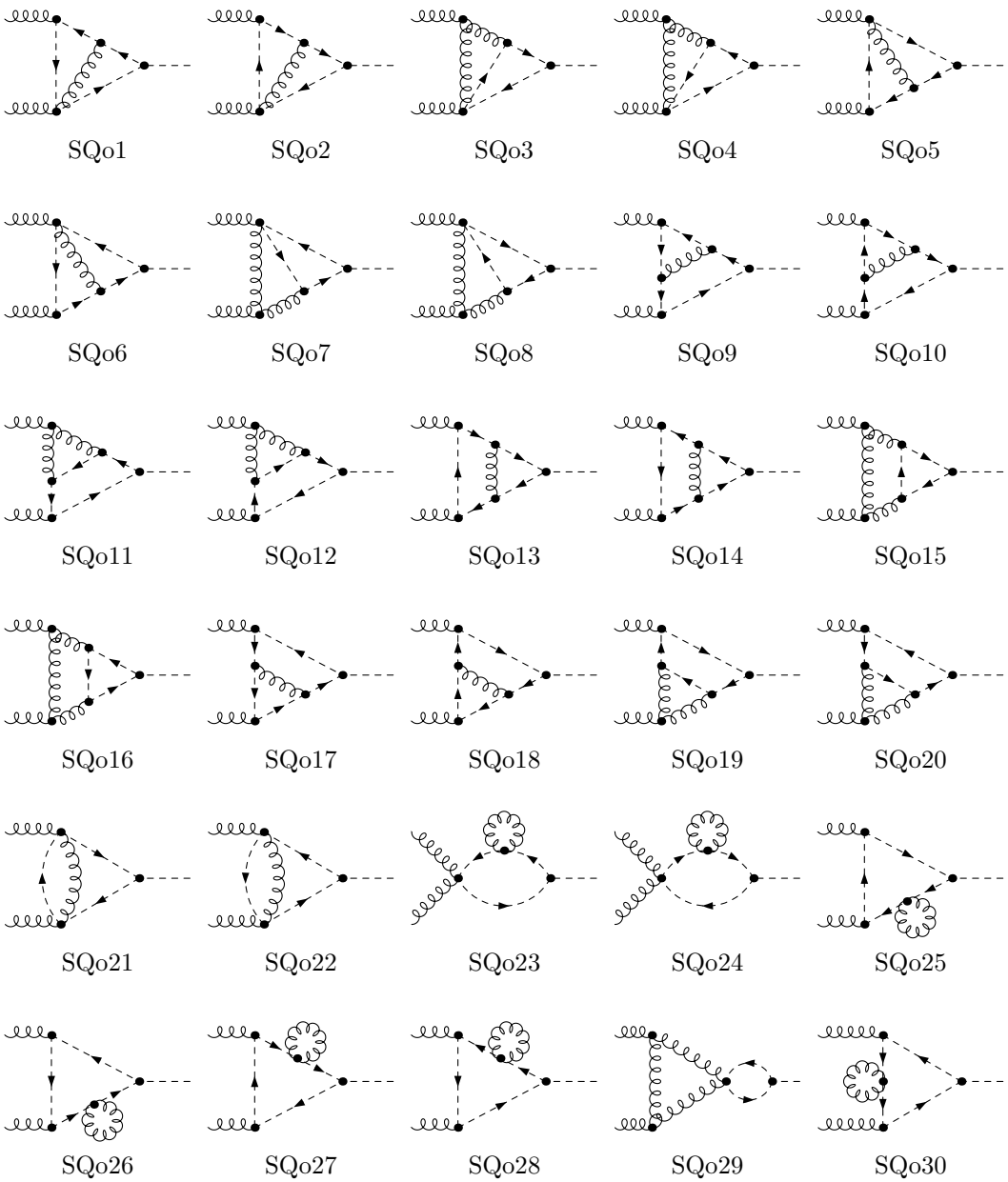

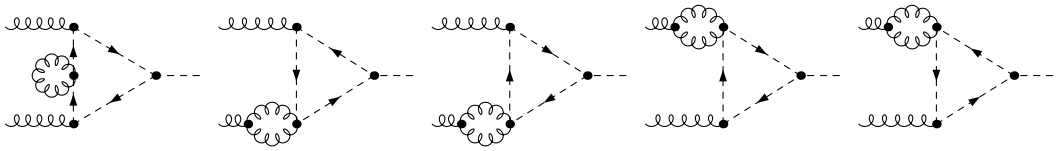

SQo31 SQo32 SQo33 SQo34 SQo35

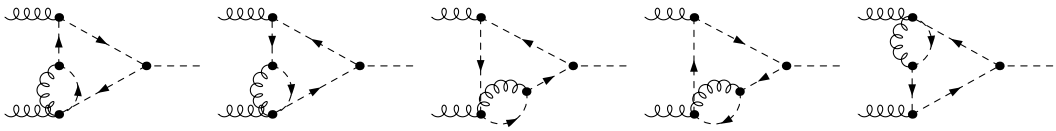

SQo36 SQo37 SQo38 SQo39 SQo40

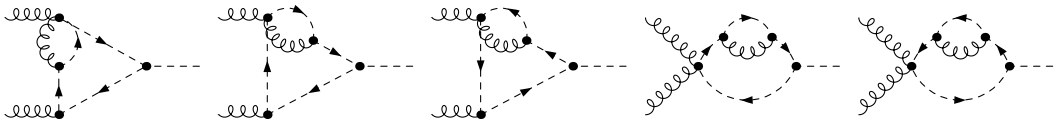

SQo41 SQo42 SQo43 SQo44 SQo45

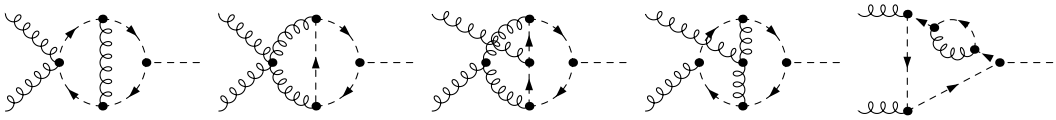

SQo46 SQo47 SQo48 SQo49 SQo50

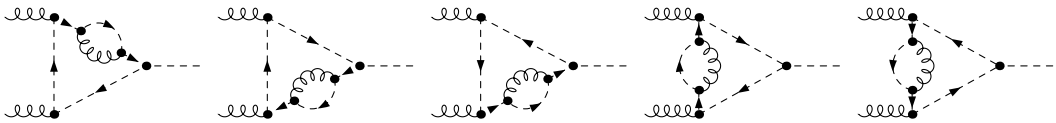

SQo51 SQo52 SQo53 SQo54 SQo55

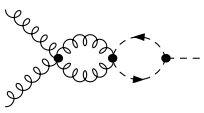

SQo56

A.2.3 Diagrams Containing Gluinos and the qqh-Vertex

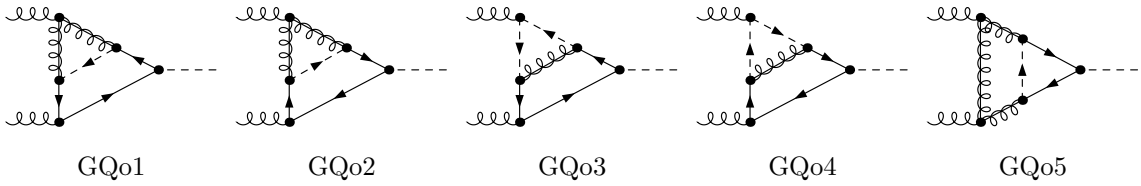

GQo1 GQo2 GQo3 GQo4 GQo5

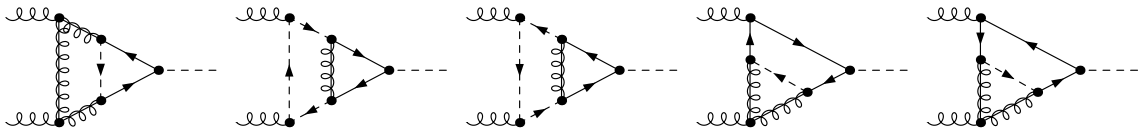

GQo6 GQo7 GQo8 GQo9 GQo10

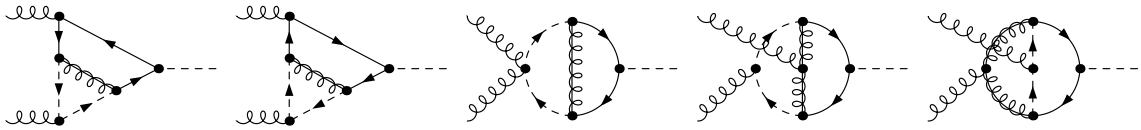

GQo11 GQo12 GQo13 GQo14 GQo15

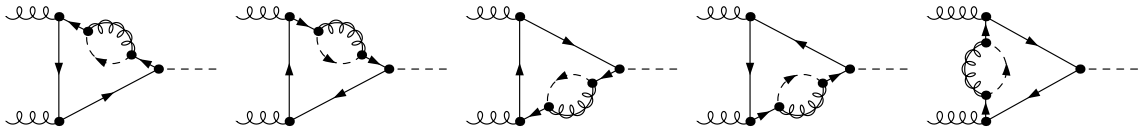

GQo16 GQo17 GQo18 GQo19 GQo20

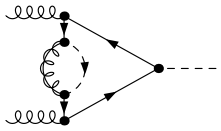

GQo21

A.2.4 Diagrams Containing Gluinos and the $\tilde{q}\tilde{q}h$-Vertex

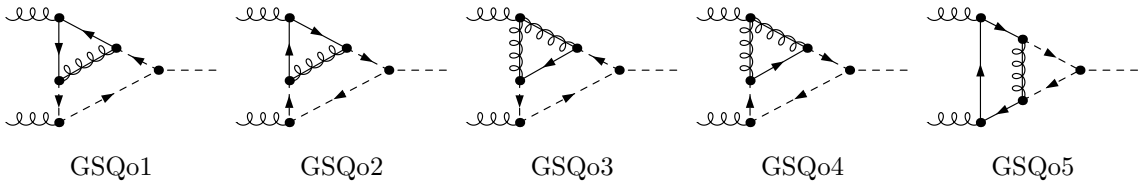

GSQo1 GSQo2 GSQo3 GSQo4 GSQo5

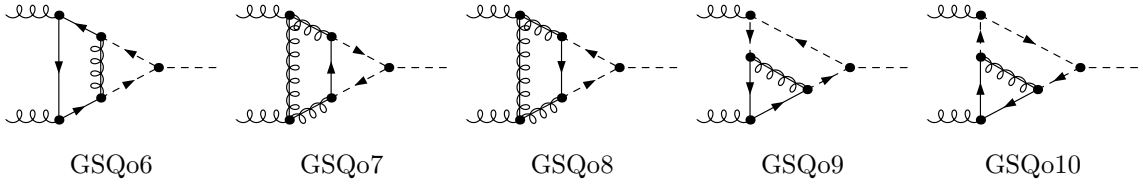

GSQo6 GSQo7 GSQo8 GSQo9 GSQo10

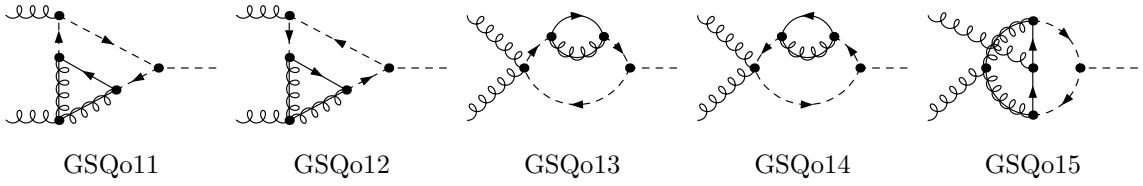

GSQo11 GSQo12 GSQo13 GSQo14 GSQo15

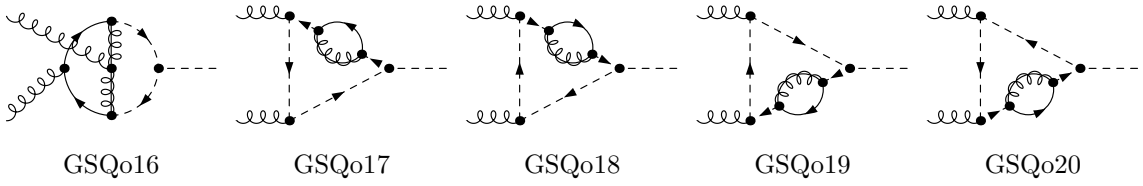

GSQo16 GSQo17 GSQo18 GSQo19 GSQo20

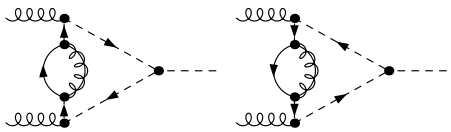

GSQo21 GSQo22

A.2.5 Factorizable Diagrams Containing a $\tilde{q}\tilde{q}\tilde{q}\tilde{q}$-Vertex

The diagrams 11–14 vanish: Due to the Lorentz-structure of the $g\tilde{q}\tilde{q}$-vertex, their bubble part is proportional to the external momentum flowing in and thus vanishes when contracted with the polarization vector or the projector $P_s^{\mu\nu}$. In all other diagrams, the legs of the $\tilde{q}\tilde{q}\tilde{q}\tilde{q}$-vertex are connected such, that no color is flowing from one loop to the other through this vertex. In this configuration, the color factors of the family mixing terms evaluate to zero.

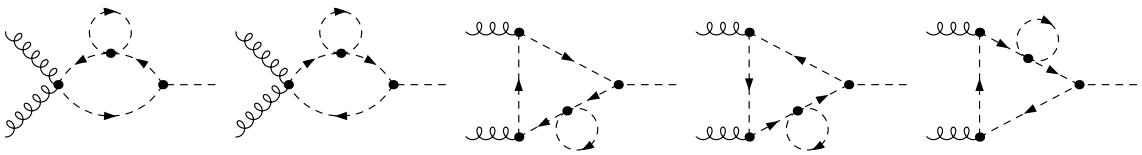

QUARTICSo1 QUARTICSo2 QUARTICSo3 QUARTICSo4 QUARTICSo5

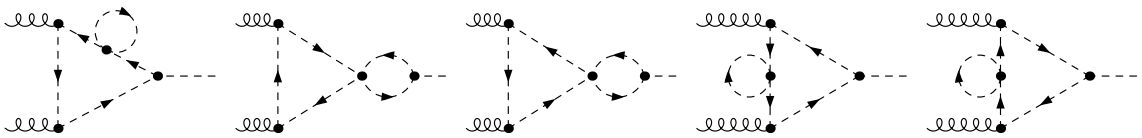

QUARTICSo6 QUARTICSo7 QUARTICSo8 QUARTICSo9 QUARTICSo10

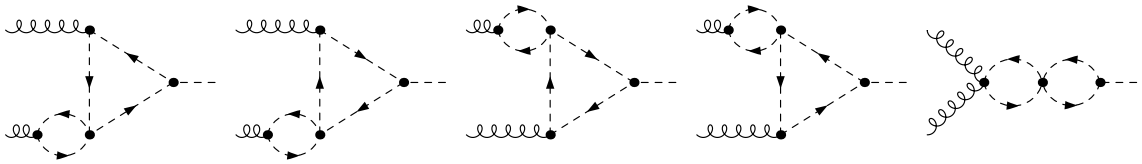

QUARTICSo11 QUARTICSo12 QUARTICSo13 QUARTICSo14 QUARTICSo15

Appendix B

NLO Amplitudes in terms of Master Integrals

The expansion coefficients $c_{\rm f}^{(1)}$ and $c_{\rm s}^{(1)}$, i.e. the NLO versions of eq. (2.21) and (2.22) are given by

$$
\begin{aligned}
c_{\rm f}^{(1)}(x) = e^{2\gamma_E\epsilon} m^{4\epsilon} \Bigg\{ \Bigg\{ & \frac{N}{\epsilon\, s^2\, x^2} \Big[-24\, x\, (1+x)^2 - \epsilon\, (1 + 56\, x + 238\, x^2 + 56\, x^3 + x^4) \\
& + \epsilon^2\, (9 - 360\, x - 994\, x^2 - 360\, x^3 + 9\, x^4) + 2\, \epsilon^3\, (19 - 900\, x - 2014\, x^2 - 900\, x^3 + 19\, x^4) \Big] \\
& + \frac{C_F}{s^2\, x^2\, (1+x)^2} \Big[4\, (1 - 12\, x - 25\, x^2 + 8\, x^3 - 25\, x^4 - 12\, x^5 + x^6) \\
& - 8\, \epsilon\, (1 + 10\, x + 51\, x^2 + 36\, x^3 + 51\, x^4 + 10\, x^5 + x^6) \\
& - 8\, \epsilon^2\, (5 + 37\, x + 203\, x^2 + 214\, x^3 + 203\, x^4 + 37\, x^5 + 5\, x^6) \Big] \Bigg\} \\
& + \Bigg\{ \frac{N}{s\, (1-x)^2} \Big[24\, (1+x)^2 + 20\, \epsilon^2\, (17 + 46\, x + 17\, x^2) + 4\, \epsilon\, (23 + 42\, x + 23\, x^2) \Big] \\
& + \frac{C_F}{s\, (1-x)^2\, (1+x)^2} \Big[8\, (1-x)^2\, (1 - 6\, x + x^2) + 8\, \epsilon\, (9 - 8\, x + 30\, x^2 - 8\, x^3 + 9\, x^4) \\
& + 8\, \epsilon^2\, (21 + 8\, x + 102\, x^2 + 8\, x^3 + 21\, x^4) \Big] \Bigg\} \\
& + \frac{N}{(1-x)^2} \Big[16\, x - 16\, \epsilon\, x - 16\, \epsilon^2\, x \Big]
\end{aligned}
$$

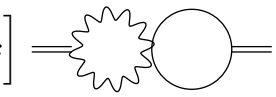

$$+\left\{\frac{N}{\epsilon^2\,(1-x)^4}\left[4\,s\,x\,(1+x)^2+2\,\epsilon\,s\,x\,(3+x)\,(1+3\,x)+\epsilon^2\,s\,(1+2\,x+122\,x^2+2\,x^3+x^4)\right]\right.$$

$$\left.+\frac{C_F}{\epsilon\,(1-x)^4}\left[8\,s\,x\,(1+x)^2-4\,\epsilon\,s\,(1-8\,x-10\,x^2-8\,x^3+x^4)\right]\right\}$$

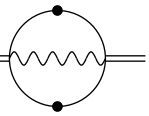

$$+\left\{\frac{N}{(1-x)^4}\left[4\,\epsilon\,s\,(1+x)^2\,(1-26\,x+x^2)\right]+\frac{C_F}{(1-x)^2}\left[-16\,\epsilon\,s\,(1+x)^2\right]\right\}$$

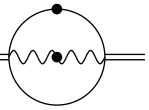

$$+\left\{\frac{N}{\epsilon\,(1-x)^4}\left[-24\,(1+x)^2\,(1-4\,x+x^2)-4\,\epsilon\,(1-4\,x+x^2)\,(7+26\,x+7\,x^2)\right.\right.$$

$$\left.-4\,\epsilon^2\,(43-46\,x-442\,x^2-46\,x^3+43\,x^4)-4\,\epsilon^3\,(1-4\,x+x^2)\,(201+550\,x+201\,x^2)\right]$$

$$+\frac{C_F}{(1-x)^4}\left[-16\,(1+x)^2\,(1-4\,x+x^2)-8\,\epsilon\,(7-16\,x-30\,x^2-16\,x^3+7\,x^4)\right.$$

$$\left.\left.-16\,\epsilon^2\,(10-19\,x-70\,x^2-19\,x^3+10\,x^4)\right]\right\}$$

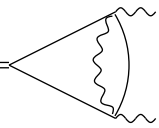

$$+\left\{\frac{N}{\epsilon^2\,(1-x)^6}\left[-32\,s^2\,x^2\,(1+x)^2-16\,\epsilon\,s^2\,x^2\,(5+14\,x+5\,x^2)-8\,\epsilon^2\,s^2\,x^2\,(41+118\,x+41\,x^2)\right]\right.$$

$$\left.+\frac{C_F}{\epsilon\,(1-x)^6}\left[-16\,s^2\,x^2\,(1+x)^2-32\,\epsilon\,s^2\,x^2\,(3+4\,x+3\,x^2)\right]\right\}$$

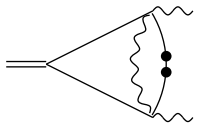

$$+\left\{\frac{N}{\epsilon\,(1-x)^4}\left[-8\,s\,x\,(1+x)^2+16\,\epsilon\,s\,x\,(1+x^2)\right]\right\}$$

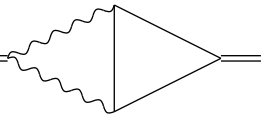

$$+\left\{\frac{N}{(1-x)^2}\left[32\,\epsilon\,(1+x)^2+4\,(1+6\,x+x^2)\right]\right.$$

$$\left.-\frac{C_F}{(1-x)^2}\left[8\,(1+14\,x+x^2)+96\,\epsilon\,x\right]\right\}$$

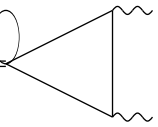

$$+\left\{\frac{N}{(1-x)^2}\left[-80\,\epsilon^2\,(1+x)^2+2\,(1-18\,x+x^2)-16\,\epsilon\,(1+4\,x+x^2)\right]\right.$$

$$+\frac{C_F}{(1-x)^2}\Big[-8\,(1-6\,x+x^2)+8\,\epsilon\,(1+6\,x+x^2)+8\,\epsilon^2\,(5+6\,x+5\,x^2)\Big]\Bigg\}$$ 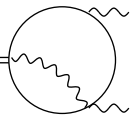

$$+\quad\frac{C_F}{(1-x)^2\,(1+x)^2}\Big[-32\,\epsilon^2\,x^2+16\,x\,(1+x^2)-16\,\epsilon\,x\,(1+4\,x+x^2)\Big]$$ 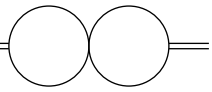

$$+\left\{\frac{N}{(1-x)^4}\Big[8\,s\,x\,(1+x)^2+24\,\epsilon\,s\,x\,(1+x)^2\Big]\right.$$

$$\left.+\frac{C_F}{(1-x)^4}\Big[-16\,\epsilon\,s\,(1-x)^2\,x+8\,s\,x\,(1+x)^2\Big]\right\}$$ 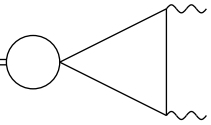

$$+\frac{C_F}{(1-x)^6}\Big[-8\,s^2\,x\,(1+x)^2\,(1+x^2)\Big]$$ 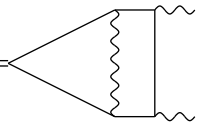

$$+\left\{\frac{N}{(1-x)^4}\Big[-4\,s^2\,x\,(1+x)^2-2\,\epsilon\,s^2\,x\,(3+x)\,(1+3\,x)\Big]\right\}$$ 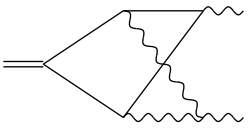

$$+\left\{\frac{N}{\epsilon\,s\,(1-x)^2}\Big[-96\,(1+x)^2-32\,\epsilon\,(5+16\,x+5\,x^2)\right.$$

$$\left.-8\,\epsilon^2\,(105+326\,x+105\,x^2)-24\,\epsilon^3\,(161+446\,x+161\,x^2)\Big]\right.$$

$$\left.-\frac{16\,C_F}{s\,(1-x)^2}\Big[4\,(1+x)^2+8\,\epsilon\,(2+3\,x+2\,x^2)\right.$$

$$\left.+3\,\epsilon^2\,(17+38\,x+17\,x^2)\Big]\right\}$$ 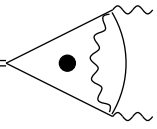

$$\left.+\mathcal{O}(\epsilon)\right\}. \tag{B.1}$$

$$c_{\rm s}^{(1)}(x)=m^{4\epsilon}e^{2\gamma_E\epsilon}\left\{\left\{\frac{N}{\epsilon\,s^2\,x}\Big[24\,x-4\,\epsilon^2\,(1-108\,x+x^2)-4\,\epsilon\,(1-24\,x+x^2)+4\,\epsilon^3\,(5+462\,x+5\,x^2)\Big]\right.\right.$$

$$\left.+\frac{C_F}{s^2\,x\,(1+x)^2}\Big[4\,x\,(9-2\,x+9\,x^2)+4\,\epsilon\,(1+23\,x+32\,x^2+23\,x^3+x^4)\right.$$

$$+ 8\,\epsilon^2\,(1 + 48\,x + 78\,x^2 + 48\,x^3 + x^4)\Big]\Big\}$$ 

$$+ \left\{ \frac{N}{s\,(1-x)^2}\Big[- 24\,x - 88\,\epsilon\,x - 400\,\epsilon^2\,x\Big] \right.$$

$$+ \frac{C_F}{s\,(1-x)^2\,(1+x)^2}\Big[- 4\,(1-x)^2\,(2 - 3\,x + 2\,x^2) - 8\,\epsilon\,(1 + 3\,x + 3\,x^3 + x^4)$$

$$\left. - 16\,\epsilon^2\,(1+x)^2\,(1 + 3\,x + x^2)\Big]\right\}$$ 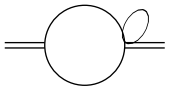

$$+ \frac{N}{(1-x)^2}\Big[- 4\,x + 4\,\epsilon\,x + 4\,\epsilon^2\,x\Big]$$ 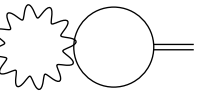

$$+ \left\{ \frac{N}{\epsilon^2\,(1-x)^4}\Big[- 4\,s\,x^2 - 8\,\epsilon\,s\,x^2 + 4\,\epsilon^2\,s\,x\,(1 - 10\,x + x^2)\Big]\right.$$

$$\left. + \frac{C_F}{\epsilon\,(1-x)^4}\Big[- 8\,s\,x^2 - 24\,\epsilon\,s\,x^2\Big]\right\}$$ 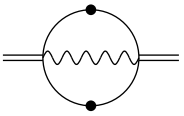

$$+ \frac{N}{(1-x)^4}\Big[24\,\epsilon\,s\,x\,(1+x)^2\Big]$$ 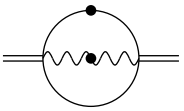

$$+ \left\{ \frac{N}{\epsilon\,(1-x)^4}\Big[24\,x\,(1 - 4\,x + x^2) + 40\,\epsilon\,x\,(1 - 4\,x + x^2) + 8\,\epsilon^2\,x\,(27 - 110\,x + 27\,x^2)\right.$$

$$\left. + 952\,\epsilon^3\,x\,(1 - 4\,x + x^2)\Big]\right.$$

$$\left. + \frac{C_F}{(1-x)^4}\Big[16\,x\,(1 - 4\,x + x^2) + 8\,\epsilon\,x\,(5 - 22\,x + 5\,x^2)\right.$$

$$\left. + 8\,\epsilon^2\,x\,(21 - 86\,x + 21\,x^2)\Big]\right\}$$ 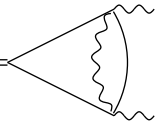

$$+ \left\{ \frac{N}{\epsilon^2\,(1-x)^6}\Big[32\,s^2\,x^3 + 96\,\epsilon\,s^2\,x^3 + 400\,\epsilon^2\,s^2\,x^3\Big]\right.$$

$$+\frac{C_F}{\epsilon\,(1-x)^6}\Big[16\,s^2\,x^3+80\,\epsilon\,s^2\,x^3\Big]\Bigg\}$$ 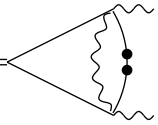

$$+\frac{N}{\epsilon\,(1-x)^4}\Big[8\,s\,x^2-8\,\epsilon\,s\,x^2\Big]$$ 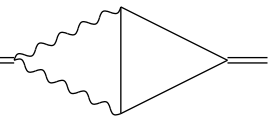

$$+\Bigg\{\frac{N}{(1-x)^2}\Big[-8\,x-32\,\epsilon\,x\Big]+\frac{C_F}{(1-x)^2}\Big[20\,x+32\,\epsilon\,x\Big]\Bigg\}$$ 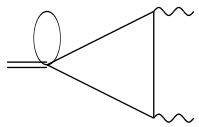

$$+\Bigg\{\frac{N}{(1-x)^2}\Big[8\,x+24\,\epsilon\,x+80\,\epsilon^2\,x\Big]+\frac{C_F}{(1-x)^2}\Big[-8\,x-16\,\epsilon\,x-32\,\epsilon^2\,x\Big]\Bigg\}$$ 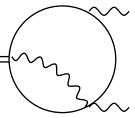

$$+\frac{C_F}{(1-x)^2\,(1+x)^2}\Big[2\,\epsilon\,(1-x)^2\,x+2\,\epsilon^2\,(1-x)^2\,x-4\,x\,(1+x^2)\Big]$$ 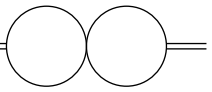

$$+\Bigg\{\frac{N}{(1-x)^4}\Big[-8\,s\,x^2-24\,\epsilon\,s\,x^2\Big]$$

$$+\frac{C_F}{(1-x)^4}\Big[4\,s\,x^2+4\,\epsilon\,s\,x^2\Big]\Bigg\}$$ 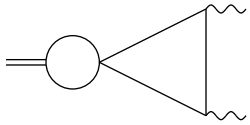

$$+\frac{C_F}{(1-x)^6}\Big[8\,s^2\,x^2\,(1+x^2)\Big]$$ 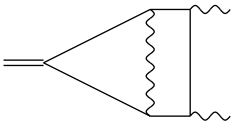

$$+\Bigg\{\frac{N}{(1-x)^4}\Big[s\,x^2\Big]+\frac{C_F}{(1-x)^4}\Big[-4\,s\,x^2\Big]\Bigg\}$$ 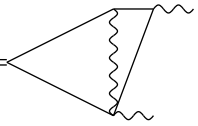

$$+\frac{N}{(1-x)^4}\Big[4\,s^2\,x^2+8\,\epsilon\,s^2\,x^2\Big]$$ 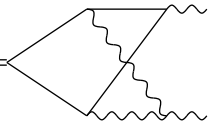

$$+\left\{\frac{N}{\epsilon\, s\,(1-x)^2}\left[96\,x+208\,\epsilon\,x+1072\,\epsilon^2\,x+4608\,\epsilon^3\,x\right]\right.$$

$$\left.+\frac{C_F}{s\,(1-x)^2}\left[64\,x+224\,\epsilon\,x+864\,\epsilon^2\,x\right]\right\} \Longrightarrow \quad + \mathcal{O}(\epsilon)\Bigg\}, \tag{B.2}$$

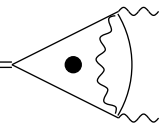

Some benchmark points for checks are

below threshold: $m = 1,\ s = 0.5,\ x = 0.75 + 0.661438I$
$\mathcal{C}_{\rm f}^{(0)} = \Lambda_{\rm f}[-1.37435 - 0.0421235\epsilon - 1.13149\epsilon^2 + \mathcal{O}(\epsilon^3)]$
$\mathcal{C}_{\rm s}^{(0)} = \Lambda_{\rm s}[-0.178758 - 0.0126135\epsilon - 0.147561\epsilon^2 + \mathcal{O}(\epsilon^3)]$
$\mathcal{C}_{\rm f}^{(1)} = \Lambda_{\rm f}[8.24607\epsilon^{-2} + (6.31478 + 25.9058I)\epsilon^{-1} + (-42.1955 + 18.7505I) + \mathcal{O}(\epsilon)]$
$\mathcal{C}_{\rm s}^{(1)} = \Lambda_{\rm s}[1.07255\epsilon^{-2} + (0.871793 + 3.36952I)\epsilon^{-1} + (-7.42416 + 2.57333I) + \mathcal{O}(\epsilon)]$,
where one can already see, that the results approach the "heavy top limit",

and above threshold: $m = 2.1,\ s = 28.1,\ x = -0.242146$
$\mathcal{C}_{\rm f}^{(0)} = \Lambda_{\rm f}[(-2.17367 - 1.04114I) + (2.91528 - 0.402908I)\epsilon - (2.56232 - 0.147077I)\epsilon^2 + \mathcal{O}(\epsilon^3)]$
$\mathcal{C}_{\rm s}^{(0)} = \Lambda_{\rm s}[(-0.0732197 - 0.438951I) + (0.737994 + 0.267139I)\epsilon - (0.520376 - 0.217928I)\epsilon^2 + \mathcal{O}(\epsilon^3)]$
$\mathcal{C}_{\rm f}^{(1)} = \Lambda_{\rm f}[(13.042 + 6.24684I)\epsilon^{-2} - (89.9695 - 37.8954I)\epsilon^{-1} + (109.005 - 241.958I) + \mathcal{O}(\epsilon)]$
$\mathcal{C}_{\rm s}^{(1)} = \Lambda_{\rm s}[(0.439318 + 2.63371I)\epsilon^{-2} - (16.9248 + 10.4905I)\epsilon^{-1} + (57.7865 - 26.6481I) + \mathcal{O}(\epsilon)]$

Appendix C

Harmonic Polylogarithms

Harmonic polylogarithms (HPLs) [29] are a generalization of the usual polylogarithms and the Nielsen polylogarithms. HPLs have been implemented for the algebraic manipulation system `FORM` [30, 31, 32] and in the C++ framework GiNaC [40, 41]. A FORTRAN code for numerical evaluation is also available [27]. An implementation of the algebraic analytic properties of HPLs for `Mathematica` is provided by the package `HPL`, [39]. This package can also perform numerical evaluation of HPLs for arbitrary complex arguments, although not competitive in terms of speed. Here we only list the definition and some basic properties.

HPLs are functions of a single variable, labeled by a vector of indices, $\mathrm{HPL}(a_1, \ldots, a_k; x)$. They are defined through recursive integration against kernels $g_a(x)$. The number of indices k is called the weight of the HPL. The kernels are defined as

$$g_0(x) = \frac{1}{x} \tag{C.1}$$

$$g_{-1}(x) = \frac{1}{1+x} \tag{C.2}$$

$$g_1(x) = \frac{1}{1-x}\,. \tag{C.3}$$

The definition then reads

$$\mathrm{HPL}(0; x) = \log(x) \tag{C.4}$$

$$\mathrm{HPL}(-1; x) = \int_0^x g_{-1}(t)dt = \int_0^x \frac{1}{1+t}(t) = \log(1+x) \tag{C.5}$$

$$\mathrm{HPL}(1; x) = \int_0^x g_1(t)dt = \int_0^x \frac{1}{1-t}(t) = -\log(1-x), \tag{C.6}$$

and for higher weights

$$\mathrm{HPL}({}^n0; x) = \frac{1}{n!}\log^n(x) \tag{C.7}$$

$$\mathrm{HPL}(a, a_1, \ldots, a_k; x) = \int_0^x g_a(t)\,\mathrm{HPL}(a_1, \ldots, a_k; t)dt, \tag{C.8}$$

where ${}^n0$ denotes a series of n zeros. For derivatives of HPL, the above definition immediately

gives

$$\frac{d}{dx}\,\mathrm{HPL}(a,a_1,\ldots,a_k;x) = g_a(x)\,\mathrm{HPL}(a_1,\ldots,a_k;x). \tag{C.9}$$

Products of HPLs of weight w_1 and w_2 can be written as a linear combination of HPLs of weight $w = w_1 + w_2$ according to

$$\mathrm{HPL}(\vec{p};x)\;\mathrm{HPL}(\vec{q};x) = \sum_{\vec{r}\in\vec{p}\uplus\vec{q}} \mathrm{HPL}(\vec{r};x) \tag{C.10}$$

where $\vec{p}\uplus\vec{q}$ is the set of all arrangements of the elements of $\vec{p}$ and $\vec{q}$ such that the internal order of the elements of $\vec{p}$ and $\vec{q}$ is kept. For instance for $\vec{p}=(a,b)$ and $\vec{q}=(x,y)$ this means

$$\begin{aligned}\mathrm{HPL}(a,b;x)\,\mathrm{HPL}(y,z;x) \;=\;& \mathrm{HPL}(a,b,y,z;x) + \mathrm{HPL}(a,y,b,z;x)\\ &+ \mathrm{HPL}(a,y,z,b;x) + \mathrm{HPL}(y,a,b,z;x)\\ &+ \mathrm{HPL}(y,a,z,b;x) + \mathrm{HPL}(y,z,a,b;x).\end{aligned} \tag{C.11}$$

This relation can be used to extract the logarithmic singularities from HPLs of higher weight as shown in eq. (2.42).

Appendix D

Master Integrals for $gg \to h$ in the Standard Model

Here we give solutions for those master integrals not displayed in section 2.2.3. Unfortunately, the expressions are rather lengthy. All solutions are written as

$$(m^2)^{2n_L - n_P - n_L\epsilon}\,\mathrm{mi}(x), \tag{D.1}$$

where n_P is the number of propagators and n_L the number of loops. The variable x is defined as

$$x = \frac{\sqrt{1-\tau}-1}{\sqrt{1-\tau}+1} + i0 \qquad \text{where} \qquad \tau = \frac{4m^2}{s} \tag{D.2}$$

and $\mathrm{mi}(x)$ is given in terms of HPLs with argument x. Therefore without worrying about analytic continuation, they can be evaluated for $x \in [0,1]$, what corresponds to the Euclidean region.

Note, that the form (D.1), while suitable for the method of differential equations, is not adequate for representing the massless bubble. The latter is essentially $(-s)^{-\epsilon}$ and s gets expressed in terms of x and the mass m^2, which is absent in the massless bubble. But using s instead of m^2 as the dimensionful variable is no better, it just moves the awkwardness from the massless bubble to the massive tadpole diagram.

One loop integrals

$$= \int \frac{d^dk}{i\pi^{d/2}} \frac{1}{k^2 - m^2 + i\varepsilon} = \frac{\Gamma(1+\epsilon)}{1-\epsilon}\,(m^2)^{-\epsilon+1} \cdot \frac{1}{\epsilon} \tag{D.3}$$

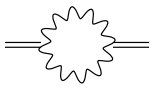

$$= \int \frac{d^dk}{i\pi^{d/2}} \frac{1}{D_{11}D_{13}} = \frac{\Gamma(1+\epsilon)}{1-\epsilon}\,(m^2)^{-\epsilon} \cdot \frac{1}{\epsilon} \frac{\Gamma(2-\epsilon)\Gamma(1-\epsilon)}{\Gamma(2-2\epsilon)} \left(\frac{(1-x)^2}{x} - i\varepsilon\right)^{-\epsilon} \tag{D.4}$$

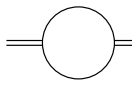

$$= \int \frac{d^dk}{i\pi^{d/2}} \frac{1}{D_{21}D_{23}} = \frac{\Gamma(1+\epsilon)}{1-\epsilon} (m^2)^{-\epsilon} \sum_{i=-1}^{3} \epsilon^i F^i_{\rm mbub}(x) + \mathcal{O}(\epsilon^4) \tag{D.5}$$

$$F^{-1}_{\rm mbub}(x) = 1 \tag{D.6}$$

$$F^{0}_{\rm mbub}(x) = \frac{1}{1-x}\Big\{ -x + (x+1)H(0;x) + 1 \Big\} \tag{D.7}$$

$$\begin{aligned} F^{1}_{\rm mbub}(x) = {} & \frac{1}{1-x}\Big\{ \frac{1}{6}\left(-\pi^2 x - 12x - \pi^2 + 12\right) + (x+1)H(0;x) - 2(x+1)H(-1,0;x) \\ & + (x+1)H(0,0;x) \Big\} \end{aligned} \tag{D.8}$$

$$\begin{aligned} F^{2}_{\rm mbub}(x) = {} & \frac{1}{1-x}\Big\{ -\frac{1}{6}\pi^2(x+1) - 2((2+\zeta(3))x + \zeta(3) - 2) \\ & + \frac{1}{3}\pi^2(x+1)H(-1;x) - \frac{1}{6}\left(-12+\pi^2\right)(x+1)H(0;x) \\ & - 2(x+1)H(0,-1,0;x) - 2(x+1)H(-1,0;x) + (x+1)H(0,0;x) \\ & + 4(x+1)H(-1,-1,0;x) - 2(x+1)H(-1,0,0;x) + (x+1)H(0,0,0;x) \Big\} \end{aligned} \tag{D.9}$$

$$\begin{aligned} F^{3}_{\rm mbub}(x) = {} & \frac{1}{1-x}\Big\{ -\frac{1}{40}\pi^4(x+1) - \frac{1}{3}\pi^2(x+1) - 2((4+\zeta(3))x + \zeta(3) - 4) \\ & + \frac{1}{3}\pi^2(x+1)H(0,-1;x) + \frac{1}{3}(x+1)H(-1;x)\left(\pi^2 + 12\zeta(3)\right) \\ & - \frac{1}{6}(x+1)\left(\pi^2 + 12(-2+\zeta(3))\right)H(0;x) - 2(x+1)H(0,0,-1,0;x) \\ & - 2(x+1)H(0,-1,0;x) - \frac{2}{3}\pi^2(x+1)H(-1,-1;x) \\ & + \frac{1}{3}\left(-12+\pi^2\right)(x+1)H(-1,0;x) - \frac{1}{6}\left(-12+\pi^2\right)(x+1)H(0,0;x) \\ & + 4(x+1)H(0,-1,-1,0;x) - 2(x+1)H(0,-1,0,0;x) + 4(x+1)H(-1,0,-1,0;x) \\ & + 4(x+1)H(-1,-1,0;x) - 2(x+1)H(-1,0,0;x) + (x+1)H(0,0,0;x) \\ & + 4(x+1)H(-1,-1,0,0;x) - 8(x+1)H(-1,-1,-1,0;x) \\ & + (x+1)H(0,0,0,0;x) - 2(x+1)H(-1,0,0,0;x) \Big\} \end{aligned} \tag{D.10}$$

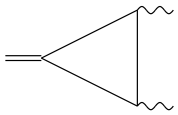

$$= \int \frac{d^dk}{i\pi^{d/2}} \frac{1}{D_{21}D_{22}D_{23}} = \frac{\Gamma(1+\epsilon)}{1-\epsilon} (m^2)^{-\epsilon-1} \sum_{i=0}^{2} \epsilon^i F^i_{\rm mtri}(x) + \mathcal{O}(\epsilon^3) \tag{D.11}$$

$$F^{0}_{\rm mtri}(x) = -\frac{xH(0,0;x)}{(x-1)^2} \tag{D.12}$$

$$F^{1}_{\rm mtri}(x) = \frac{x}{(1-x)^2}\Big\{ \frac{1}{6}\pi^2 H(0;x) + 2H(0,-1,0;x) + H(0,0;x) + 3\zeta(3)$$

$$- H(0,0,0;x)\Big\} \tag{D.13}$$

$$\begin{aligned} F^2_{\rm mtri}(x) &= \frac{x}{(1-x)^2}\Big\{ -\frac{1}{3}\pi^2 H(0,-1;x) + H(0;x)\left(-\frac{\pi^2}{6}+2\zeta(3)\right) - 3\zeta(3) + \frac{\pi^4}{72} \\ &\quad + 2H(0,0,-1,0;x) - 2H(0,-1,0;x) + \frac{1}{6}\pi^2 H(0,0;x) - 4H(0,-1,-1,0;x) \\ &\quad + 2H(0,-1,0,0;x) + H(0,0,0;x) - H(0,0,0,0;x)\Big\} \end{aligned} \tag{D.14}$$

Factorizable integrals

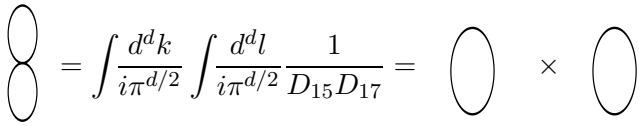

$$= \int \frac{d^dk}{i\pi^{d/2}} \int \frac{d^dl}{i\pi^{d/2}} \frac{1}{D_{15}D_{17}} = \times \tag{D.15}$$

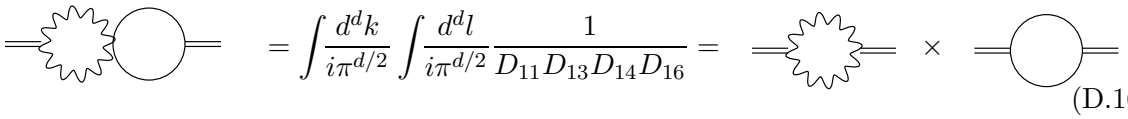

$$= \int \frac{d^dk}{i\pi^{d/2}} \int \frac{d^dl}{i\pi^{d/2}} \frac{1}{D_{11}D_{13}D_{14}D_{16}} = \times \tag{D.16}$$

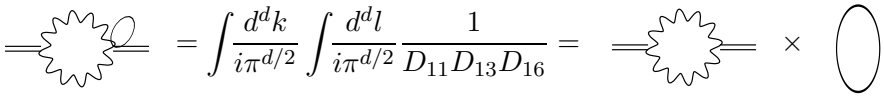

$$= \int \frac{d^dk}{i\pi^{d/2}} \int \frac{d^dl}{i\pi^{d/2}} \frac{1}{D_{11}D_{13}D_{16}} = \times \tag{D.17}$$

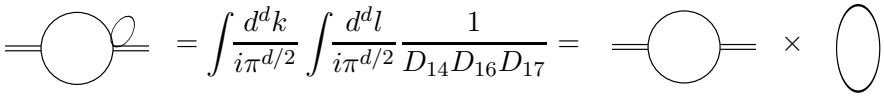

$$= \int \frac{d^dk}{i\pi^{d/2}} \int \frac{d^dl}{i\pi^{d/2}} \frac{1}{D_{14}D_{16}D_{17}} = \times \tag{D.18}$$

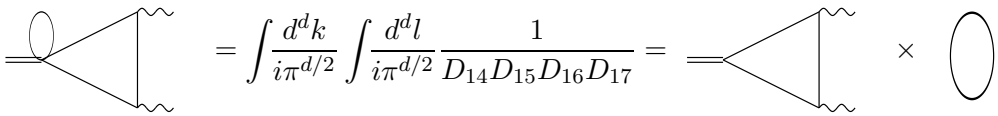

$$= \int \frac{d^dk}{i\pi^{d/2}} \int \frac{d^dl}{i\pi^{d/2}} \frac{1}{D_{14}D_{15}D_{16}D_{17}} = \times \tag{D.19}$$

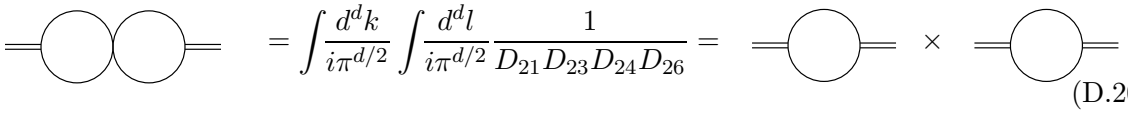

$$= \int \frac{d^dk}{i\pi^{d/2}} \int \frac{d^dl}{i\pi^{d/2}} \frac{1}{D_{21}D_{23}D_{24}D_{26}} = \times \tag{D.20}$$

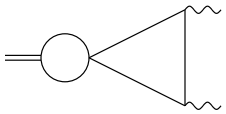

$$= \int \frac{d^dk}{i\pi^{d/2}} \int \frac{d^dl}{i\pi^{d/2}} \frac{1}{D_{21}D_{23}D_{24}D_{25}D_{26}} =$$

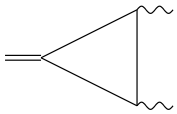

$\times$

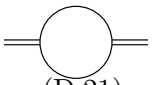

(D.21)

Three propagator integrals

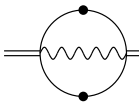

$$= \int \frac{d^dk}{i\pi^{d/2}} \int \frac{d^dl}{i\pi^{d/2}} \frac{1}{D_{11}D_{14}^2D_{17}^2}$$
$$= \left(\frac{\Gamma(1+\epsilon)}{1-\epsilon}\right)^2 (m^2)^{-2\epsilon-1} \sum_{i=0}^{2} \epsilon^i F_1^i(x) + \mathcal{O}(\epsilon^3) \qquad \text{(D.22)}$$

$$F_1^0(x) = -\frac{2xH(0,0;x)}{(x-1)^2} \qquad \text{(D.23)}$$

$$F_1^1(x) = \frac{x}{(1-x)^2}\Big\{\frac{1}{3}\pi^2 H(0;x) + 12H(0,-1,0;x) + 4H(0,0;x) + 6\zeta(3)$$
$$- 4H(0,1,0;x) - 6H(0,0,0;x) + 4H(1,0,0;x)\Big\} \qquad \text{(D.24)}$$

$$F_1^2(x) = \frac{x}{(1-x)^2}\Big\{ - 2\pi^2 H(0,-1;x) - 12\zeta(3) + \frac{13\pi^4}{180}$$
$$+ \left(-\frac{2\pi^2}{3} + 16\zeta(3)\right) H(0;x) + \frac{2}{3}\pi^2 H(0,1;x) - 12H(1;x)\zeta(3)$$
$$+ 36H(0,0,-1,0;x) - 24H(0,-1,0;x) + \left(-2+\pi^2\right) H(0,0;x) - \frac{2}{3}\pi^2 H(1,0;x)$$
$$+ 8H(0,1,0;x) - 12H(0,0,1,0;x) - 72H(0,-1,-1,0;x) + 48H(0,-1,0,0;x)$$
$$+ 24H(0,-1,1,0;x) + 12H(0,0,0;x) - 24H(1,0,-1,0;x) - 8H(1,0,0;x)$$
$$+ 8H(1,0,1,0;x) + 24H(0,1,-1,0;x) - 20H(0,1,0,0;x) - 8H(0,1,1,0;x)$$
$$- 14H(0,0,0,0;x) + 12H(1,0,0,0;x) - 8H(1,1,0,0;x)\Big\} \qquad \text{(D.25)}$$

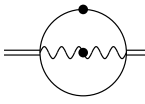

$$= \int \frac{d^dk}{i\pi^{d/2}} \int \frac{d^dl}{i\pi^{d/2}} \frac{1}{D_{11}^2D_{14}^2D_{17}}$$
$$= \left(\frac{\Gamma(1+\epsilon)}{1-\epsilon}\right)^2 (m^2)^{-2\epsilon-1} \sum_{i=-1}^{2} \epsilon^i F_2^i(x) + \mathcal{O}(\epsilon^3) \qquad \text{(D.26)}$$

$$F_2^{-1}(x) = \frac{xH(0;x)}{x^2-1} \tag{D.27}$$

$$\begin{aligned}
F_2^0(x) = {} & \frac{x}{(x-1)^3(x+1)}\Big\{ -2H(0;x)(x-1)^2 - \frac{1}{6}\pi^2(x-1)^2 \\
& + (x-1)(5x-3)H(0,0;x) - 6(x-1)^2H(-1,0;x) \\
& + 2(x-1)^2H(1,0;x)\Big\}
\end{aligned} \tag{D.28}$$

$$\begin{aligned}
F_2^1(x) = {} & \frac{x}{(x-1)^3(x+1)}\Big\{\frac{1}{3}(x-1)\left(6\zeta(3)(4-7x)+\pi^2(x-1)\right) \\
& + \pi^2(x-1)^2H(-1;x) - \frac{1}{6}(x-1)\left(-6x+\pi^2(5x-3)+6\right)H(0;x) \\
& - \frac{1}{3}\pi^2H(1;x)(x-1)^2 - 6(5x-3)H(0,-1,0;x)(x-1) \\
& + 12(x-1)^2H(-1,0;x) - 2(x-1)(5x-3)H(0,0;x) \\
& + 2(x-1)(5x-3)H(0,1,0;x) - 4(x-1)^2H(1,0;x) \\
& + 36(x-1)^2H(-1,-1,0;x) - 24(x-1)^2H(-1,0,0;x) \\
& + (x-1)(13x-7)H(0,0,0;x) - 12(x-1)^2H(-1,1,0;x) \\
& + 2(x-1)(3x-5)H(1,0,0;x) - 12(x-1)^2H(1,-1,0;x) \\
& + 4(x-1)^2H(1,1,0;x)\Big\}
\end{aligned} \tag{D.29}$$

$$\begin{aligned}
F_2^2(x) = {} & \frac{x}{(x-1)^3(x+1)}\Big\{ -\frac{1}{360}(x-1)\left(60\pi^2(x-1)+\pi^4(61x-35)-1440(7x-4)\zeta(3)\right) \\
& + \pi^2(x-1)(5x-3)H(0,-1;x) - 2(x-1)^2H(-1;x)\left(\pi^2-33\zeta(3)\right) \\
& + \frac{1}{3}(x-1)H(0;x)\left(6\zeta(3)(9-17x)+\pi^2(5x-3)\right) \\
& + \frac{2}{3}(x-1)H(1;x)\left(6\zeta(3)(7-4x)+\pi^2(x-1)\right) \\
& - \frac{1}{3}\pi^2(x-1)(5x-3)H(0,1;x) - 6(x-1)(13x-7)H(0,0,-1,0;x) \\
& + 12(x-1)(5x-3)H(0,-1,0;x) - 6\pi^2(x-1)^2H(-1,-1;x) \\
& + 2\left(-3+2\pi^2\right)H(-1,0;x)(x-1)^2 + 2\pi^2H(-1,1;x)(x-1)^2 \\
& - \frac{1}{6}(x-1)\left(-30x+\pi^2(13x-7)+18\right)H(0,0;x) \\
& + 2\pi^2(x-1)^2H(1,-1;x) - \frac{1}{3}(x-1)\left(-6x+\pi^2(3x-5)+6\right)H(1,0;x) \\
& - \frac{2}{3}\pi^2H(1,1;x)(x-1)^2 - 4(5x-3)H(0,1,0;x)(x-1) \\
& + 2(x-1)(13x-7)H(0,0,1,0;x) + 36(x-1)(5x-3)H(0,-1,-1,0;x) \\
& - 24(x-1)(5x-3)H(0,-1,0,0;x) - 12(x-1)(5x-3)H(0,-1,1,0;x) \\
& + 144(x-1)^2H(-1,0,-1,0;x) - 72(x-1)^2H(-1,-1,0;x) \\
& + 48H(-1,0,0;x)(x-1)^2 + 24H(-1,1,0;x)(x-1)^2 \\
& - 48H(-1,0,1,0;x)(x-1)^2 - 2(13x-7)H(0,0,0;x)(x-1) \\
& + 24(x-1)^2H(1,-1,0;x) - 12(x-1)(3x-5)H(1,0,-1,0;x)
\end{aligned}$$

$$
\begin{aligned}
&- 8H(1,1,0;x)(x-1)^2 - 4(3x-5)H(1,0,0;x)(x-1) \\
&+ 4(x-1)(3x-5)H(1,0,1,0;x) - 12(x-1)(5x-3)H(0,1,-1,0;x) \\
&+ 2(x-1)(27x-17)H(0,1,0,0;x) + 4(x-1)(5x-3)H(0,1,1,0;x) \\
&+ 144(x-1)^2H(-1,-1,0,0;x) - 216(x-1)^2H(-1,-1,-1,0;x) \\
&+ 72(x-1)^2H(-1,-1,1,0;x) - 60(x-1)^2H(-1,0,0,0;x) \\
&+ 72(x-1)^2H(-1,1,-1,0;x) - 48(x-1)^2H(-1,1,0,0;x) \\
&+ (x-1)(29x-15)H(0,0,0,0;x) - 24(x-1)^2H(-1,1,1,0;x) \\
&+ 72(x-1)^2H(1,-1,-1,0;x) - 48(x-1)^2H(1,-1,0,0;x) \\
&+ 2(x-1)(7x-13)H(1,0,0,0;x) - 24(x-1)^2H(1,-1,1,0;x) \\
&+ 4(x-1)(5x-3)H(1,1,0,0;x) - 24(x-1)^2H(1,1,-1,0;x) \\
&+ 8(x-1)^2H(1,1,1,0;x)\Big\}
\end{aligned} \tag{D.30}
$$

Four propagator integrals

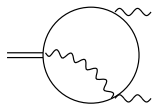

$$
\begin{aligned}
&= \int \frac{d^dk}{i\pi^{d/2}} \int \frac{d^dl}{i\pi^{d/2}} \frac{1}{D_{11}D_{14}D_{15}D_{17}} \\
&= \left(\frac{\Gamma(1+\epsilon)}{1-\epsilon}\right)^2 (m^2)^{-2\epsilon} \sum_{i=-2}^{1} \epsilon^i F_3^i(x) + \mathcal{O}(\epsilon^2)
\end{aligned} \tag{D.31}
$$

$$
F_3^{-2}(x) = \frac{1}{2} \tag{D.32}
$$

$$
F_3^{-1}(x) = -\frac{1}{2} \tag{D.33}
$$

$$
\begin{aligned}
F_3^0(x) = \frac{1}{(1-x)^2}\Big\{ &- 3x^2 + (6 - 4\zeta(3))x + 2\left(x^2-1\right)H(0;x) - 3 \\
&- H(0,0;x)(x-1)^2 + 2xH(0,0,0;x) + 4xH(1,0,0;x)\Big\}
\end{aligned} \tag{D.34}
$$

$$
\begin{aligned}
F_3^1(x) = \frac{1}{(1-x)^2}\Big\{ &3(-4+\zeta(3))x^2 - 2(-12+\zeta(3))x + \frac{2\pi^4 x}{45} - \frac{1}{3}\pi^2\left(x^2-1\right) + 3(-4+\zeta(3)) \\
&+ \frac{1}{6}H(0;x)\left(\pi^2(x-1)^2 + 12\left(4x^2 - 3\zeta(3)x - 4\right)\right) - 12xH(1;x)\zeta(3) \\
&+ 6H(0,-1,0;x)(x-1)^2 - 12xH(0,0,-1,0;x) - 12\left(x^2-1\right)H(-1,0;x) \\
&+ \left(11x^2 - \frac{1}{3}\left(6+\pi^2\right)x - 5\right)H(0,0;x) + \left(4x^2 - \frac{2\pi^2 x}{3} - 4\right)H(1,0;x) \\
&- 2H(0,1,0;x)(x-1)^2 + 4xH(0,0,1,0;x) + \left(-3x^2+4x-3\right)H(0,0,0;x) \\
&- 24xH(1,0,-1,0;x) + 2\left(x^2-4x+1\right)H(1,0,0;x) + 8xH(1,0,1,0;x) \\
&- 4xH(0,1,0,0;x) + 6xH(0,0,0,0;x) + 12xH(1,0,0,0;x) \\
&- 8xH(1,1,0,0;x)\Big\}
\end{aligned} \tag{D.35}
$$

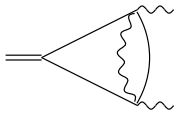

$$= \int \frac{d^dk}{i\pi^{d/2}} \int \frac{d^dl}{i\pi^{d/2}} \frac{1}{D_{12}D_{14}D_{16}D_{17}}$$
$$= \left(\frac{\Gamma(1+\epsilon)}{1-\epsilon}\right)^2 (m^2)^{-2\epsilon} \sum_{i=-2}^{1} \epsilon^i F_4^i(x) + \mathcal{O}(\epsilon^2) \tag{D.36}$$

$$F_4^{-2}(x) = \frac{1}{2} \tag{D.37}$$

$$F_4^{-1}(x) = \frac{1}{(1-x)^2}\left\{\frac{3}{2}(x-1)^2 + \left(1-x^2\right) H(0;x)\right\} \tag{D.38}$$

$$\begin{aligned} F_4^0(x) = {} & \frac{1}{(1-x)^2}\Big\{5x^2 + 2(-5+2\zeta(3))x + \left(-3x^2 + \frac{\pi^2 x}{3} + 3\right) H(0;x) + 5 \\ & + 2\left(x^2-1\right) H(-1,0;x) - (x-1)(x+2)H(0,0;x) + \left(1-x^2\right) H(1,0;x) \\ & + 2xH(0,1,0;x) + xH(0,0,0;x)\Big\} \end{aligned} \tag{D.39}$$

$$\begin{aligned} F_4^1(x) = {} & \frac{1}{(1-x)^2}\Big\{ -(-16+\zeta(3))x^2 + \left(-32 - \frac{11\pi^4}{90} + \zeta(3)\right) x - 4(-4+\zeta(3)) \\ & + H(0;x)\left(-10x^2 - \frac{1}{6}\pi^2(x+1)x - 3\zeta(3)x + 10\right) - \frac{2}{3}\pi^2 xH(0,-1;x) \\ & + \frac{1}{3}\pi^2 xH(0,1;x) + \frac{1}{6}H(1;x)\left(-48\zeta(3)x - \pi^2\left(x^2-1\right)\right) \\ & - 2xH(0,0,-1,0;x) + 2(x-1)(x+2)H(0,-1,0;x) + 6\left(x^2-1\right) H(-1,0;x) \\ & + \left(-3x^2 + \frac{1}{6}\left(-18+\pi^2\right)x + 6\right) H(0,0;x) + \left(-3x^2 - \frac{2\pi^2 x}{3} + 3\right) H(1,0;x) \\ & - 2\left(x^2+x-1\right) H(0,1,0;x) + 2xH(0,0,1,0;x) - 2xH(0,-1,0,0;x) \\ & - 4xH(0,-1,1,0;x) + \left(4-4x^2\right) H(-1,-1,0;x) + 3\left(x^2-1\right) H(-1,0,0;x) \\ & + 2\left(x^2-1\right) H(-1,1,0;x) + \left(-2x^2-3x+4\right) H(0,0,0;x) \\ & + 2\left(x^2-1\right) H(1,-1,0;x) + \left(-x^2-2x+3\right) H(1,0,0;x) \\ & + \left(2-2x^2\right) H(1,1,0;x) - 4xH(1,0,1,0;x) - 4xH(0,1,-1,0;x) \\ & + 4xH(0,1,0,0;x) + 4xH(0,1,1,0;x) + 3xH(0,0,0,0;x) \\ & - 2xH(1,0,0,0;x)\Big\} \end{aligned} \tag{D.40}$$

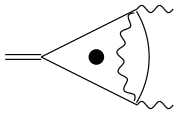

$$= \int \frac{d^dk}{i\pi^{d/2}} \int \frac{d^dl}{i\pi^{d/2}} \frac{(k+p_1)\cdot(l-k)}{D_{12}D_{14}D_{16}D_{17}}$$

$$= \left(\frac{\Gamma(1+\epsilon)}{1-\epsilon}\right)^2 (m^2)^{1-2\epsilon} \sum_{i=-2}^{1} \epsilon^i F_5^i(x) + \mathcal{O}(\epsilon^2) \tag{D.41}$$

$$F_5^{-2}(x) = \frac{(x-1)^2}{8x} \tag{D.42}$$

$$F_5^{-1}(x) = \frac{1}{(1-x)^2 x}\Big\{\frac{5}{16}(x-1)^4 + \left(-\frac{x^4}{4} + x^3 - x + \frac{1}{4}\right) H(0;x)\Big\} \tag{D.43}$$

$$\begin{aligned}
F_5^0(x) = {} & \frac{1}{(1-x)^2 x}\Big\{\frac{1}{32}\left(31x^4 - 140x^3 + (218 - 64\zeta(3))x^2 - 140x + 31\right) \\
& + \frac{1}{24}\left(-15x^4 + 54x^3 - 4\pi^2 x^2 - 54x + 15\right) H(0;x) \\
& + \frac{1}{2}\left(x^4 - 4x^3 + 4x - 1\right) H(-1,0;x) \\
& + \frac{1}{4}\left(-x^4 + 4x^3 + 3x^2 - 8x + 2\right) H(0,0;x) + \left(-\frac{x^4}{4} + x^3 - x + \frac{1}{4}\right) H(1,0;x) \\
& - H(0,1,0;x)x^2 - \frac{1}{2}H(0,0,0;x)x^2\Big\}
\end{aligned} \tag{D.44}$$

$$\begin{aligned}
F_5^1(x) = {} & \frac{1}{(1-x)^2 x}\Big\{\left(\frac{189}{64} - \frac{\zeta(3)}{4}\right)x^4 + \left(-\frac{233}{16} + \frac{\pi^2}{24} + \zeta(3)\right)x^3 + \left(\frac{743}{32} + \frac{11\pi^4}{180} - \frac{3\zeta(3)}{4}\right)x^2 \\
& - \frac{1}{48}\left(699 + 2\pi^2 - 192\zeta(3)\right)x - \zeta(3) + \frac{189}{64} + \frac{1}{3}\pi^2 x^2 H(0,-1;x) \\
& + \frac{1}{48}H(0;x)\left(-\left(93 + 2\pi^2\right)x^4 + \left(342 + 8\pi^2\right)x^3 + 6\left(\pi^2 + 12\zeta(3)\right)x^2 - 342x + 93\right) \\
& + \frac{1}{24}H(1;x)\left(96x^2\zeta(3) - \pi^2\left(x^4 - 4x^3 + 4x - 1\right)\right) \\
& + x^2 H(0,0,-1,0;x) - \frac{1}{6}\pi^2 x^2 H(0,1;x) \\
& + \frac{1}{2}\left(x^4 - 4x^3 - 3x^2 + 8x - 2\right) H(0,-1,0;x) \\
& + \frac{1}{4}\left(5x^4 - 18x^3 + 18x - 5\right) H(-1,0;x) \\
& + \left(-\frac{5x^4}{8} + 2x^3 - \frac{1}{24}\left(-57 + 2\pi^2\right)x^2 - 5x + \frac{5}{4}\right) H(0,0;x) \\
& + \frac{1}{24}\left(-15x^4 + 60x^3 + 8\pi^2 x^2 - 60x + 15\right) H(1,0;x) \\
& + \frac{1}{2}\left(-x^4 + 4x^3 + 3x^2 - 4x + 1\right) H(0,1,0;x) - x^2 H(0,0,1,0;x) \\
& + H(0,-1,0,0;x)x^2 + 2H(0,-1,1,0;x)x^2 + \left(-x^4 + 4x^3 - 4x + 1\right) H(-1,-1,0;x) \\
& + \frac{3}{4}\left(x^4 - 4x^3 + 4x - 1\right) H(-1,0,0;x) \\
& + \frac{1}{2}\left(x^4 - 4x^3 + 4x - 1\right) H(-1,1,0;x) \\
& + \left(-\frac{x^4}{2} + 2x^3 + \frac{9x^2}{4} - 4x + 1\right) H(0,0,0;x)
\end{aligned}$$

$$
\begin{aligned}
&+\frac{1}{2}\left(x^4-4x^3+4x-1\right)H(1,-1,0;x)\\
&+\left(-\frac{x^4}{4}+x^3+\frac{3x^2}{2}-3x+\frac{3}{4}\right)H(1,0,0;x)\\
&+2H(1,0,1,0;x)x^2+\frac{1}{2}\left(-x^4+4x^3-4x+1\right)H(1,1,0;x)\\
&+2H(0,1,-1,0;x)x^2-2H(0,1,0,0;x)x^2-2H(0,1,1,0;x)x^2\\
&+x^2H(1,0,0,0;x)-\frac{3}{2}x^2H(0,0,0,0;x)\Big\} \qquad \text{(D.45)}
\end{aligned}
$$

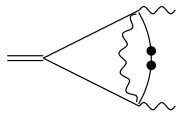

$$
\begin{aligned}
&=\int\frac{d^dk}{i\pi^{d/2}}\int\frac{d^dl}{i\pi^{d/2}}\frac{1}{D_{12}D_{14}D_{16}D_{17}^3}\\
&=\left(\frac{\Gamma(1+\epsilon)}{1-\epsilon}\right)^2(m^2)^{-2\epsilon-2}\sum_{i=0}^{2}\epsilon^iF_6^i(x)+\mathcal{O}(\epsilon^3) \qquad \text{(D.46)}
\end{aligned}
$$

$$
F_6^0(x) = \frac{xH(0,0;x)}{2(x-1)^2} \qquad \text{(D.47)}
$$

$$
\begin{aligned}
F_6^1(x) &= \frac{x}{(1-x)^2}\Big\{-\frac{1}{4}\pi^2H(0;x)-H(0,-1,0;x)-H(0,0;x)-\frac{9\zeta(3)}{2}\\
&\quad -H(0,1,0;x)+\frac{1}{2}H(0,0,0;x)+H(1,0,0;x)\Big\} \qquad \text{(D.48)}
\end{aligned}
$$

$$
\begin{aligned}
F_6^2(x) &= \frac{x}{(1-x)^2}\Big\{\frac{1}{2}\pi^2H(0,-1;x)+\frac{1}{2}\pi^2H(0;x)+9\zeta(3)+\frac{11\pi^4}{144}\\
&\quad +3\zeta(3)H(1;x)-\frac{1}{6}\pi^2H(0,1;x)-H(0,0,-1,0;x)+2H(0,-1,0;x)\\
&\quad +\frac{1}{12}\left(6-\pi^2\right)H(0,0;x)+\frac{1}{2}\pi^2H(1,0;x)+2H(0,1,0;x)\\
&\quad +2H(0,-1,-1,0;x)+2H(0,-1,1,0;x)-H(0,0,0;x)-2H(1,0,-1,0;x)\\
&\quad -2H(1,0,0;x)+4H(1,0,1,0;x)+2H(0,1,-1,0;x)-H(0,1,0,0;x)\\
&\quad -2H(0,1,1,0;x)+\frac{1}{2}H(0,0,0,0;x)+4H(1,0,0,0;x)+2H(1,1,0,0;x)\Big\} \qquad \text{(D.49)}
\end{aligned}
$$

Five propagator integrals

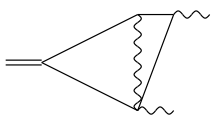

$$
\begin{aligned}
&=\int\frac{d^dk}{i\pi^{d/2}}\int\frac{d^dl}{i\pi^{d/2}}\frac{1}{D_{22}D_{23}D_{24}D_{26}D_{27}}\\
&=\left(\frac{\Gamma(1+\epsilon)}{1-\epsilon}\right)^2(m^2)^{-2\epsilon-1}F_7^0(x)+\mathcal{O}(\epsilon^1) \qquad \text{(D.50)}
\end{aligned}
$$

$$
\begin{aligned}
F_7^0(x) &= \frac{1}{(1-x)^2}\Big\{ -\frac{1}{6}\pi^2 H(0,0;x)x - \frac{1}{3}\pi^2 H(1,0;x)x - \frac{\pi^4 x}{36} \\
&\quad - xH(0,0,1,0;x) - 2xH(1,0,1,0;x) - 2xH(0,1,0,0;x) - 3xH(1,0,0,0;x) \\
&\quad - 4xH(1,1,0,0;x)\Big\} \qquad \text{(D.51)}
\end{aligned}
$$

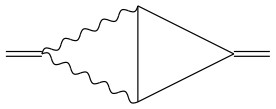

$$
\begin{aligned}
&= \int \frac{d^dk}{i\pi^{d/2}} \int \frac{d^dl}{i\pi^{d/2}} \frac{1}{D_{11}D_{13}D_{14}D_{16}D_{17}} \\
&= \left(\frac{\Gamma(1+\epsilon)}{1-\epsilon}\right)^2 (m^2)^{-2\epsilon-1} \sum_{i=0}^{1} \epsilon^i F_8^i(x) + \mathcal{O}(\epsilon^2) \qquad \text{(D.52)}
\end{aligned}
$$

$$
F_8^0(x) = \frac{x}{(1-x)^2}\Big\{ -2H(0,0,1;x) - 2H(0,1,0;x) + 4H(1,0,0;x) - 6\zeta(3)\Big\} \qquad \text{(D.53)}
$$

$$
\begin{aligned}
F_8^1(x) &= \frac{x}{(1-x)^2}\Big\{ -12\zeta(3)H(0;x) + \frac{1}{3}\pi^2 H(0,1;x) - 24H(1;x)\zeta(3) - \frac{\pi^4}{10} \\
&\quad - 8H(0,0,0,1;x) - 10H(0,0,-1,0;x) + 4H(0,-1,0,1;x) - \frac{2}{3}\pi^2 H(1,0;x) \\
&\quad - 4H(1,0,0,1;x) - 4H(0,1,0,1;x) - 4H(0,0,1,0;x) - 4H(0,0,1,1;x) + 4H(0,-1,0,0;x) \\
&\quad + 4H(0,-1,1,0;x) - 24H(1,0,-1,0;x) + 4H(1,0,1,0;x) + 4H(0,1,-1,0;x) \\
&\quad - 6H(0,1,0,0;x) - 4H(0,1,1,0;x) + 12H(1,0,0,0;x)\Big\} \qquad \text{(D.54)}
\end{aligned}
$$

Six propagator integrals

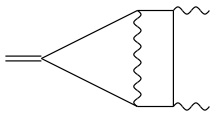

$$
\begin{aligned}
&= \int \frac{d^dk}{i\pi^{d/2}} \int \frac{d^dl}{i\pi^{d/2}} \frac{1}{D_{21}D_{23}D_{24}D_{25}D_{26}D_{27}} \\
&= \left(\frac{\Gamma(1+\epsilon)}{1-\epsilon}\right)^2 (m^2)^{-2\epsilon-2} F_9^0(x) + \mathcal{O}(\epsilon^1) \qquad \text{(D.55)}
\end{aligned}
$$

$$
\begin{aligned}
F_9^0(x) &= \frac{x^2}{(1-x)^3(x+1)}\Big\{ 8\zeta(3)H(0;x) + 16H(0,0,-1,0;x) + \frac{\pi^4}{10} \\
&\quad + \frac{2}{3}\pi^2 H(0,0;x) - 4H(0,0,1,0;x) - 8H(0,-1,0,0;x) + 14H(0,1,0,0;x) \\
&\quad + H(0,0,0,0;x)\Big\} \qquad \text{(D.56)}
\end{aligned}
$$

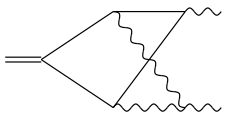

$$= \int \frac{d^dk}{i\pi^{d/2}} \int \frac{d^dl}{i\pi^{d/2}} \frac{1}{D_{31}D_{32}D_{33}D_{34}D_{35}D_{37}}$$
$$= \left(\frac{\Gamma(1+\epsilon)}{1-\epsilon}\right)^2 (m^2)^{-2\epsilon-2} \sum_{i=-1}^{0} \epsilon^i F_{10}^i(x) + \mathcal{O}(\epsilon^1) \qquad \text{(D.57)}$$

$$F_{10}^{-1}(x) = \frac{x^2}{(1-x)^4}\Big\{ -\frac{2}{3}\pi^2 H(0;x) - 8H(0,-1,0;x) + 4H(0,0,0;x) - 12\zeta(3)\Big\} \qquad \text{(D.58)}$$

$$\begin{aligned} F_{10}^{0}(x) = \frac{x^2}{(1-x)^4}\Big\{ & \frac{8}{3}\pi^2 H(0,-1;x) + 24\zeta(3) - \frac{16\pi^4}{45} \\ & + \frac{4}{3}\left(\pi^2 - 33\zeta(3)\right) H(0;x) - \frac{4}{3}\pi^2 H(0,1;x) - 48H(1;x)\zeta(3) \\ & - 56H(0,0,-1,0;x) + 16H(0,-1,0;x) - \frac{10}{3}\pi^2 H(0,0;x) - \frac{8}{3}\pi^2 H(1,0;x) \\ & + 8H(0,0,1,0;x) + 64H(0,-1,-1,0;x) - 40H(0,-1,0,0;x) - 16H(0,-1,1,0;x) \\ & - 8H(0,0,0;x) - 32H(1,0,-1,0;x) - 16H(0,1,-1,0;x) + 8H(0,1,0,0;x) \\ & + 12H(0,0,0,0;x) + 16H(1,0,0,0;x)\Big\} \end{aligned} \qquad \text{(D.59)}$$

Appendix E

Feynman Rules for SUSY QCD

All momenta are incoming.

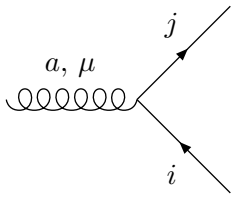

$$-i\,g\,T^a_{ij}\gamma^\mu$$

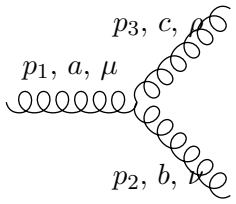

$$-g\,f_{abc}\,[(p_1-p_2)^\rho\,g^{\mu\nu}+(p_2-p_3)^\mu\,g^{\nu\rho}+(p_3-p_1)^\nu\,g^{\rho\mu}]$$

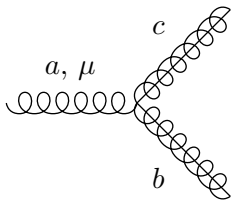

$$-g\,f_{abc}\,\gamma^\mu$$

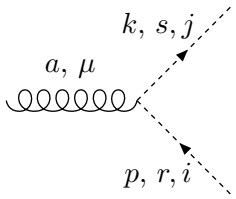

$$-i\,g\,\delta_{rs}\,T^a_{ij}\,(p-k)^\mu$$

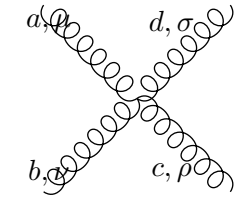

$$-i\,g^2 \quad \Big[\quad f^{eac} f^{ebd} \left(g^{\mu\nu} g^{\rho\sigma} - g^{\mu\sigma} g^{\nu\rho}\right) + f^{ead} f^{ebc} \left(g^{\mu\nu} g^{\rho\sigma} - g^{\mu\rho} g^{\nu\sigma}\right) + f^{eab} f^{ecd} \left(g^{\mu\rho} g^{\nu\sigma} - g^{\mu\sigma} g^{\nu\rho}\right) \Big]$$

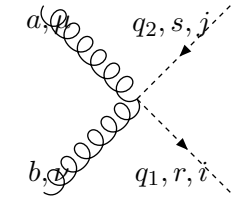

$$i\,g^2\,\delta_{q_1 q_2}\,\delta_{rs}\,\Big(T^a_{ik}\,T^b_{kj} + T^b_{ik}\,T^a_{kj}\Big)\,g^{\mu\nu}$$

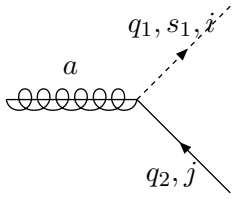

$$i\,\frac{g}{\sqrt{2}}\,\delta_{q_1 q_2}\,T^a_{ij}\;\left(A(q_1,s_1) - B(q_1,s_1)\,\gamma_5\right)$$

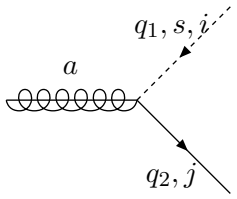

$$i\,\frac{g}{\sqrt{2}}\,\delta_{q_1 q_2}\,T^a_{ij}\;\left(A(q_1,s_1) + B(q_1,s_1)\,\gamma_5\right)$$

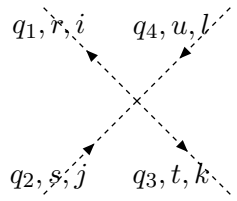

$$-i\,g^2 \quad \Big\{ \quad \delta_{q_1 q_2}\delta_{q_3 q_4}\left[T^a_{ij}T^a_{kl}\,\mathcal{S}^{q_1}_{rs}\mathcal{S}^{q_3}_{tu} + \delta_{q_1 q_3}\,T^a_{il}T^a_{kj}\,\mathcal{S}^{q_1}_{ru}\mathcal{S}^{q_3}_{ts}\right] + \delta_{q_1 q_4}\delta_{q_2 q_3}\left(1 - \delta_{q_1 q_2}\right)\left[T^a_{il}T^a_{kj}\,\mathcal{S}^{q_1}_{ru}\mathcal{S}^{q_3}_{ts} + \delta_{q_1 q_3}\,T^a_{ij}T^a_{kl}\,\mathcal{S}^{q_1}_{rs}\mathcal{S}^{q_3}_{tu}\right] \Big\}$$

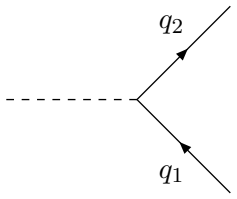

$$-i\,\frac{m_q}{v}\,\delta_{q_1 q_2}\,h_f(q_1)$$

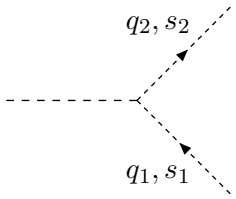

$$-i\,\frac{m_q^2}{v}\,\delta_{q_1 q_2}\,h_s(q_1,s_1,s_2)$$

In the vertices involving a gluino, a quark and a squark, we have introduced:

$$A(q,s) = \mathcal{R}^q_{s,2} - \mathcal{R}^q_{s,1}\,, \tag{E.1}$$
$$B(q,s) = -\mathcal{R}^q_{s,2} - \mathcal{R}^q_{s,1}\,. \tag{E.2}$$

The matrices $\mathcal{R}^q$ and $\mathcal{S}^q$ are the mixing matrices

$$\mathcal{R}^q = \begin{pmatrix} \cos\theta_{\tilde{q}} & \sin\theta_{\tilde{q}} \\ -\sin\theta_{\tilde{q}} & \cos\theta_{\tilde{q}} \end{pmatrix}\,, \tag{E.3}$$

and

$$\mathcal{S}^q_{ij} = \mathcal{R}^q_{i1}\,\mathcal{R}^q_{j1} - \mathcal{R}^q_{i2}\,\mathcal{R}^q_{j2}\,, \tag{E.4}$$

$$\mathcal{S}^q = \begin{pmatrix} \cos 2\theta_{\tilde{q}} & -\sin 2\theta_{\tilde{q}} \\ -\sin 2\theta_{\tilde{q}} & -\cos 2\theta_{\tilde{q}} \end{pmatrix}\,. \tag{E.5}$$

In the diagrams containing a gluino, the combinations $A(q,s_1)\,A(q,s_2)$ and $B(q,s_1)\,B(q,s_2)$ appear. It is convenient to express them in terms of

$$\left(\mathcal{R}^q_{\pm}\right)_{ij} = B(q,i)\,B(q,j) \pm A(q,i)\,A(q,j)\,, \tag{E.6}$$

which have the form

$$\mathcal{R}^q_{+} = 2\begin{pmatrix} 1 & 0 \\ 0 & 1 \end{pmatrix}\,, \qquad \mathcal{R}^q_{-} = 2\begin{pmatrix} \sin 2\theta_{\tilde{q}} & \cos 2\theta_{\tilde{q}} \\ \cos 2\theta_{\tilde{q}} & -\sin 2\theta_{\tilde{q}} \end{pmatrix}\,. \tag{E.7}$$

The vacuum expectation value of the higgs boson, which appears in the higgs-matter couplings is

$$\frac{1}{v} = \frac{1}{\sqrt{v_u^2 + v_d^2}} = \frac{e}{2\,\sin\theta_W\,M_W}\,. \tag{E.8}$$

Bibliography

[1] M. Spira, A. Djouadi, D. Graudenz and P. M. Zerwas, Phys. Lett. B **318**, 347 (1993); M. Spira, A. Djouadi, D. Graudenz and P. M. Zerwas, Nucl. Phys. B **453**, 17 (1995) [arXiv:hep-ph/9504378].

[2] S. Dawson, Nucl. Phys. B **359**, 283 (1991).

[3] T. Gehrmann and E. Remiddi, Nucl. Phys. B **580**, 485 (2000) [arXiv:hep-ph/9912329].

[4] T. Binoth and G. Heinrich, Nucl. Phys. B **585**, 741 (2000) [arXiv:hep-ph/0004013].

[5] T. Binoth and G. Heinrich, Nucl. Phys. B **680**, 375 (2004) [arXiv:hep-ph/0305234].

[6] K. Melnikov and F. Petriello, "Electroweak gauge boson production at hadron colliders through Phys. Rev. D **74**, 114017 (2006) [arXiv:hep-ph/0609070].

[7] K. Melnikov and F. Petriello, Phys. Rev. Lett. **96**, 231803 (2006) [arXiv:hep-ph/0603182].

[8] C. Anastasiou, K. Melnikov and F. Petriello, JHEP **0709**, 014 (2007) [arXiv:hep-ph/0505069].

[9] C. Anastasiou, K. Melnikov and F. Petriello, "Fully differential Higgs boson production and the di-photon signal through Nucl. Phys. B **724**, 197 (2005) [arXiv:hep-ph/0501130].

[10] C. Anastasiou, K. Melnikov and F. Petriello, "Higgs boson production at hadron colliders: Differential cross sections Phys. Rev. Lett. **93**, 262002 (2004) [arXiv:hep-ph/0409088].

[11] C. Anastasiou, K. Melnikov and F. Petriello, Phys. Rev. Lett. **93**, 032002 (2004) [arXiv:hep-ph/0402280].

[12] G. Heinrich, Int. J. Mod. Phys. A **23** (2008) 1457 [arXiv:0803.4177 [hep-ph]].

[13] F. V. Tkachov, Phys. Lett. B **100**, 65 (1981).

[14] K. G. Chetyrkin and F. V. Tkachov, Nucl. Phys. B **192**, 159 (1981).

[15] S. Laporta, Int. J. Mod. Phys. A **15**, 5087 (2000) [arXiv:hep-ph/0102033].

[16] C. Anastasiou and A. Lazopoulos, JHEP **0407**, 046 (2004) [arXiv:hep-ph/0404258].

[17] A. Daleo, unpublished.

[18] R. Bonciani, P. Mastrolia and E. Remiddi, Nucl. Phys. B **661**, 289 (2003) [Erratum-ibid. B **702**, 359 (2004)] [arXiv:hep-ph/0301170].

[19] R. Bonciani, P. Mastrolia and E. Remiddi, Nucl. Phys. B **690**, 138 (2004) [arXiv:hep-ph/0311145].

[20] A. I. Davydychev and M. Y. Kalmykov, Nucl. Phys. B **699**, 3 (2004) [arXiv:hep-th/0303162].

[21] J. Fleischer, O. V. Tarasov and V. O. Tarasov, Phys. Lett. B **584**, 294 (2004) [arXiv:hep-ph/0401090].

[22] A. I. Davydychev and M. Y. Kalmykov, Nucl. Phys. B **605** (2001) 266 [arXiv:hep-th/0012189].

[23] D. J. Broadhurst, J. Fleischer and O. V. Tarasov, r Z. Phys. C **60**, 287 (1993) [arXiv:hep-ph/9304303].

[24] M. Y. Kalmykov and O. Veretin, Phys. Lett. B **483**, 315 (2000) [arXiv:hep-th/0004010].

[25] R. V. Harlander and M. Steinhauser, JHEP **0409** (2004) 066 [arXiv:hep-ph/0409010].

[26] G. Degrassi and P. Slavich, arXiv:0806.1495 [hep-ph].

[27] T. Gehrmann and E. Remiddi, Comput. Phys. Commun. **141**, 296 (2001) [arXiv:hep-ph/0107173].

[28] R. Harlander and P. Kant, "Higgs production and decay: Analytic results at next-to-leading order QCD," JHEP **0512**, 015 (2005) [arXiv:hep-ph/0509189].

[29] E. Remiddi and J. A. M. Vermaseren, Int. J. Mod. Phys. A **15** (2000) 725 [arXiv:hep-ph/9905237].

[30] J. A. M. Vermaseren, arXiv:math-ph/0010025.

[31] J. A. M. Vermaseren, Int. J. Mod. Phys. A **14**, 2037 (1999) [arXiv:hep-ph/9806280].

[32]

[32] http://www.nikhef.nl/ form/maindir/oldversions/FORMdistribution/packages/harmpol

[33] A. V. Kotikov, Phys. Lett. B **254**, 158 (1991).

[34] A. V. Kotikov, Phys. Lett. B **259**, 314 (1991).

[35] A. V. Kotikov, Phys. Lett. B **267**, 123 (1991).

[36] E. Remiddi, Nuovo Cim. A **110**, 1435 (1997) [arXiv:hep-th/9711188].

[37] M. Caffo, H. Czyz, S. Laporta and E. Remiddi, Acta Phys. Polon. B **29**, 2627 (1998) [arXiv:hep-th/9807119]; M. Caffo, H. Czyz, S. Laporta and E. Remiddi, Nuovo Cim. A **111**, 365 (1998) [arXiv:hep-th/9805118].

[38] D. Maitre, Comput. Phys. Commun. **174**, 222 (2006) [arXiv:hep-ph/0507152].

[39] D. Maitre, arXiv:hep-ph/0703052.

[40] C. W. Bauer, A. Frink and R. Kreckel, "Introduction to the GiNaC Framework for Symbolic Computation within the C++ arXiv:cs/0004015.

[41] J. Vollinga and S. Weinzierl, Comput. Phys. Commun. **167** (2005) 177 [arXiv:hep-ph/0410259].

[42] M. Y. Kalmykov, Nucl. Phys. B **718** (2005) 276 [arXiv:hep-ph/0503070].

[43] M. Y. Kalmykov and A. Sheplyakov, "lsjk: A C++ library for arbitrary-precision numeric evaluation of the generalized log-sine functions," Comput. Phys. Commun. **172** (2005) 45 [arXiv:hep-ph/0411100].

[44] C. Anastasiou, S. Beerli, S. Bucherer, A. Daleo and Z. Kunszt, JHEP **0701** (2007) 082 [arXiv:hep-ph/0611236].

[45] U. Aglietti, R. Bonciani, G. Degrassi and A. Vicini, JHEP **0701** (2007) 021 [arXiv:hep-ph/0611266].

[46] M. Muhlleitner and M. Spira, Nucl. Phys. B **790**, 1 (2008).

[47] R. Bonciani, G. Degrassi and A. Vicini, JHEP **0711**, 095 (2007).

[48] A. I. Davydychev, Phys. Lett. B **263** (1991) 107.

[49] G. 't Hooft and M. J. G. Veltman, Nucl. Phys. B **44**, 189 (1972).

[50] W. Siegel, Phys. Lett. B **84**, 193 (1979).

[51] D. M. Capper, D. R. T. Jones and P. van Nieuwenhuizen, Nucl. Phys. B **167**, 479 (1980).

[52] D. Stockinger, JHEP **0503** (2005) 076 [arXiv:hep-ph/0503129].

[53] A. Daleo, private communication

[54] D. E. Soper, Phys. Rev. Lett. **81** (1998) 2638 [arXiv:hep-ph/9804454].

[55] D. E. Soper, "Techniques for QCD calculations by numerical integration," Phys. Rev. D **62** (2000) 014009 [arXiv:hep-ph/9910292].

[56] Z. Nagy and D. E. Soper, "General subtraction method for numerical calculation of one-loop QCD matrix elements," JHEP **0309**, 055 (2003). [arXiv:hep-ph/0308127].

[57] Z. Nagy, private communication

[58] Z. Nagy and D. E. Soper, "Numerical integration of one-loop Feynman diagrams for N-photon amplitudes," Phys. Rev. D **74**, 093006 (2006); [arXiv:hep-ph/0610028].

[59] A. Lazopoulos, T. McElmurry, K. Melnikov and F. Petriello, arXiv:0804.2220 [hep-ph].

[60] A. Lazopoulos, K. Melnikov and F. J. Petriello, Phys. Rev. D **77** (2008) 034021 [arXiv:0709.4044 [hep-ph]].

[61] A. Lazopoulos, K. Melnikov and F. Petriello, Phys. Rev. D **76** (2007) 014001 [arXiv:hep-ph/0703273].

[62] S. Catani, Phys. Lett. B **427** (1998) 161 [arXiv:hep-ph/9802439].

[63] S. Weinzierl, "The art of computing loop integrals," arXiv:hep-ph/0604068.

[64] C. Bogner and S. Weinzierl, Comput. Phys. Commun. **178** (2008) 596 [arXiv:0709.4092 [hep-ph]].

[65] Format.m package by Mark Sofroniou
http://library.wolfram.com/infocenter/MathSource/60/

[66] GNU Scientific library
http://www.gnu.org/software/gsl/

[67] Cuba - a library for multidimensional numerical integration, Version 1.4
http://www.feynarts.de/cuba/

[68] http://www.feynarts.de/

[69] W. Beenakker, R. Hopker, T. Plehn and P. M. Zerwas, Z. Phys. C **75**, 349 (1997) [arXiv:hep-ph/9610313].

[70] S. Heinemeyer, W. Hollik, H. Rzehak and G. Weiglein, "High-precision predictions for the MSSM Higgs sector at O(alpha(b) alpha(s))," Eur. Phys. J. C **39** (2005) 465 [arXiv:hep-ph/0411114].

[71] S. P. Martin, arXiv:hep-ph/9709356.

[72] G. Ossola, C. G. Papadopoulos and R. Pittau, "Reducing full one-loop amplitudes to scalar integrals at the integrand level," arXiv:hep-ph/0609007.

[73] W. T. Giele, Z. Kunszt and K. Melnikov, "Full one-loop amplitudes from tree amplitudes," JHEP **0804** (2008) 049 [arXiv:0801.2237 [hep-ph]].

[74] J. Kasahara, K. Freese and P. Gondolo, Phys. Rev. D **79** (2009) 045020 [arXiv:0805.0999 [hep-ph]].

Acknowledgments

I would like to thank my advisor Prof. Zoltan Kunszt for giving me the opportunity to work in the thrilling field of particle physics. I appreciate very much Zoltan's original insights in and beyond physics, as well as his integer personality and professional style. Zoltan's constructive critisism is priceless.

I am indepted to Prof. Babis Anastasiou for the fruitful collaboration, his patience in giving me a taste of how things are *really* done and also for telling me off from time to time. I could not have done it without you.

Further thanks go to my officemates, I like José's positive mindset and I appreciate Mert's willingness to discuss at increased volume many of my concerns appearing during the writeup.

Finally I owe a lot to the Czechoslovak gang I could always count on, for their support, endless discussions, Saturday morning running and brunches, barbecue at Züriberg and numerous other "akce".

Curriculum Vitae

Personal Data

Name	Stefan Beerli
Date of Birth	11th February 1977
Nationality	Swiss

Education

2004 – 2008	ETH Zürich
	PhD in Theoretical Particle Physics, Group of Prof. Z. Kunszt
2003 – 2004	ETH Zürich
	PhD student in Computational Science, Group of Prof. P. Koumoutsakos
1998 – 2003	ETH Zürich, Diploma in Theoretical Physics
1997 – 1998	Student of Physics, Technical University of Vienna
1993 – 1996	Gymnasium Muttenz, Matura Typus C

Scientific Publications

2008 C. Anastasiou, S. Beerli and A. Daleo,
"The two-loop QCD amplitude $gg \to h, H$
in the Minimal Supersymmetric Standard Model,"
arXiv:0803.3065 [hep-ph].
Accepted in Physical Review Letters.

2007 C. Anastasiou, S. Beerli and A. Daleo,
"Evaluating multi-loop Feynman diagrams with infrared and threshold singularities numerically,"
JHEP **0705** (2007) 071 [arXiv:hep-ph/0703282].

2006 C. Anastasiou, S. Beerli, S. Bucherer, A. Daleo and Z. Kunszt,
"Two-loop amplitudes and master integrals for the production of a Higgs boson via a massive quark and a scalar-quark loop,"
JHEP **0701** (2007) 082 [arXiv:hep-ph/0611236].